
# Effects of aroylated phenylenediamines and mechanical stress on lung epithelial immunity

Iwona Teresa Myszor

**Faculty of Life and Environmental Sciences**
**University of Iceland**
**2021**

# Effects of aroylated phenylenediamines and mechanical stress on lung epithelial immunity

Iwona Teresa Myszor

Dissertation submitted in partial fulfillment of a
*Philosophiae Doctor* degree in Biology

Advisor
Gudmundur Hrafn Gudmundsson, PhD

PhD Committee
Gudmundur Hrafn Gudmundsson, PhD
Thorarinn Gudjonsson, PhD
Sigurbergur Karason, MD, PhD
Margret Helga Ogmundsdottir, PhD

Opponents
Henk P. Haagsman, PhD
Sif Hansdottir, MD, PhD

Faculty of Life and Environmental Sciences
School of Engineering and Natural Sciences
University of Iceland
Reykjavik, February 2021

Effects of aroylated phenylenediamines and mechanical stress on lung epithelial immunity
Short title: Lung innate immunity responses upon challenge
Dissertation submitted in partial fulfillment of a *Philosophiae Doctor* degree in Biology



Faculty of Life and Environmental Sciences
School of Engineering and Natural Sciences
University of Iceland
Askja, Sturlugata 7
101, Reykjavik
Iceland

Telephone: 525 4000

Bibliographic information:
Iwona Teresa Myszor, 2021,
*Effects of aroylated phenylenediamines and mechanical stress on lung epithelial immunity*,
PhD dissertation, Faculty of Life and Environmental Sciences,
University of Iceland, 192 pp.

ISBN 978-9935-9514-9-6

Printing: Haskolaprent ehf.
Reykjavik, Iceland, February 2021

# Abstract

Innate immunity of the lung epithelium provides efficient defenses against pathogens or other stress factors by secretion of antimicrobial peptides, presence of cellular junction proteins and autophagy. Upon activation through epithelial cell receptors the system triggers a defense response. Activation of epithelial immunity can lead to elimination of bacteria, enhanced epithelial integrity and lysosomal degradation. Therefore, modulation of immune signalling for epithelial immunity by specific inducers can serve as a treatment strategy to fight infections. The use of innate immunity modulators is of interest for management of ventilator induced lung injury (VILI), that can lead to acute respiratory distress syndrome (ARDS) in patients.

The aim of this work was to investigate the effect of the aroylated phenylenediamine (APD) inducers HO53 and HO56 and mechanical stress on the innate immunity in the lung epithelium.

The novel compounds HO53 and HO56 induced expression of antimicrobial effectors in bronchial epithelium and reduced bacterial entry. Both APD inducers exhibited a synergistic effect with vitamin D on *CAMP* gene expression and HO53 activated the STAT3 transcription factor. The HO53 compound enhanced epithelial barrier integrity and promoted induction of autophagy in differentiated cells. Treatment with HO53 had broad effect on gene expression, including expression of histone modifying enzymes and stimulated AMPK pathway together with TFEB activation.

Mechanical stress generated by the cyclical pressure air-liquid device (CPAD) affected cell morphology and expression of markers for VILI and ARDS development together with pro-inflammatory genes. A preliminary study indicates that HO53 compound exacerbates pro-inflammatory response induced by mechanical stress.

# Útdráttur

Náttúrulegt ónæmi lungnaþekju myndar virkt varnarkerfi með seytingu örverudrepandi peptíða, myndun þéttitengja og sjálfsáti. Varnarkerfið virkjast með örvun viðtaka í þekjunni og getur leitt til þess að bakteríum er eytt, þéttni þekjunnar aukist og að virkni leysikorna sé örvuð. Með því að hafa áhrif á boðleiðir fyrir náttúrulegt ónæmi með sérhæfðum efnum má örva kerfið til að verjast sýkingum. Notkun á efnum sem örva boðleiðir þekjuvarna eru áhugaverður möguleiki tengt sýkingum en einnig í öndunarvélatengdum lungnaskaða (ÖTL) til að hindra brátt andnauðarheilkenni (BAH) sjúklinga í öndunarvél.
Markmið verkefnisins var að rannsaka áhrif nýrra örvunarefna, aroylated phenylenediamin (APD) efna á náttúrulegt ónæmi og skoða áhrif þrýstings og slitálags á þekjuvarnakerfið.
Ný APD örvunarefni HO53 og HO56 juku tjáningu örverudrepandi efna í lungnaþekju og drógu úr innrás baktería í þekjufrumur. Bæði APD efnin sýndu samverkan með vítamín D fyrir örvun á *CAMP* cathelicidin geninu og HO53 virkjaði STAT3 umritunarþáttinn í þeirri örvun. Meðhöndlun á skautuðum þekjufrumum með HO53 styrkti þekjuna og jók sjálfsát. HO53 hafði víðtæk áhrif á genatjáningu í frumunum sérstaklega tjáningu umbreytiensíma fyrir históna, en örvaði jafnframt AMPK boðleiðina og virkjaði TFEB umritunarþáttinn. Þrýstingsálag í sérhönnuðu tæki CPAD (e. cyclical pressure air-liquid device) hafði áhrif á útlit þekjunnar og tjáningu lífmerkja (e. biomarkers) fyrir ÖTL, BAH og bólgumiðla. Fyrsta athugun sýnir að HO53 efnið eykur á bólguviðbragð sem örvað hafði verið með þrýstingsálagi.

# List of Papers

**Paper I**

Myszor IT, Parveen Z, Ottosson H, Bergman P, Agerberth B, Strömberg R, Gudmundsson GH (2019) Novel aroylated phenylenediamine compounds enhance antimicrobial defense and maintain airway epithelial barrier integrity. *Sci Rep* **9**: 7114.

**Paper II (as a manuscript)**

Myszor IT, Sigurdsson S, Viktorsdottir AR, Agerberth B, Eskelinen E-L, Ogmundsdottir MH, Gudmundsson GH. "Novel inducer of innate immunity HO53 stimulates autophagy in human airway epithelial cells".

**Paper III**

Joelsson JP, Myszor IT, Arason, AJ, Ingthorsson S, Cherek P, Windels GS, Leosson K, Gudmundsson GH, Gudjonsson T and Karason S (2019) Innovative in vitro method to study ventilator induced lung injury. *ALTEX* **36**: 634–642.

**Published article not included in the thesis:**

**Paper IV**

Joelsson JP, Myszor IT, Sigurdsson S, Lehmann F, Page C, Gudmundsson GH, Gudjonsson T and Karason S. Azithromycin has lung barrier protective effects in a cell model mimicking ventilator-induced lung injury. ALTEX 2020 May 19.doi: 10.14573/altex.2001271. Online ahead of print.

# Table of Contents

# List of Figures

# Abbreviations

| | |
|---|---|
| **AJ** | adherens junction |
| **AKT** | protein kinase B (also called PKB) |
| **ALI** | air-liquid interphase |
| **AMPs** | antimicrobial peptides |
| **AMPK** | 5' adenosine monophosphate-activated protein kinase |
| **AMR** | antimicrobial resistance |
| **APDs** | aroylated phenylenediamines |
| **ARDS** | acute respiratory distress syndrome |
| **ATG** | autophagy related protein |
| **CAMP** | cathelicidin antimicrobial peptide |
| **CFTR** | cystic fibrosis transmembrane receptor |
| **CFU** | colony-forming unit |
| **cGAMP** | cyclic guanosine monophosphate–adenosine monophosphate |
| **CLR** | C-type lectin receptor |
| **DFCP1** | zinc finger FYVE domain-containing protein 1 (also called ZFYVE1) |
| **EHMT2** | euchromatic histone lysine methyltransferase 2 |
| **EZH2** | enhancer of zeste homolog 2 |
| **FIP200** | RB1 inducible coiled-coil 1 |
| **GSEA** | Gene Set Enrichment Analysis |
| **HDAC** | histone deacetylase |
| **HIF-1α** | hypoxia-inducible factor 1-α |
| **IFN** | interferon |
| **JAK** | Janus kinase |
| **JAM** | junctional adhesion molecule |
| **LC3B** | microtubule-associated proteins 1A/1B light chain 3B |
| **LGALS** | gene encoding galectin |
| **LPS** | lipopolysaccharide |
| **MDR** | multidrug-resistant strain |
| **MOI** | multiplicity of infection |
| **mTOR** | mammalian target of rapamycin |
| **MV** | mechanical ventilation |
| **NF-κB** | nuclear factor kappa-light-chain-enhancer of activated B cells |
| **NLR** | nucleotide-binding oligomerization domain-like receptor |
| **PAMPs** | pathogen associated molecular patterns |
| **PAO1** | *Pseudomonas aeruginosa* PAO1 |
| **PBA** | 4-phenylbutyrate |
| **PEEP** | positive end-expiratory pressure |
| **PIK3C3** | phosphatidylinositol 3-kinase catalytic subunit type 3 (also called VPS34) |

| | |
|---|---|
| **PIK3R4** | phosphoinositide 3-kinase regulatory subunit 4 (also called VPS15) |
| **PI3P** | phosphatidylinositol 3-phosphate |
| **PRKAA2** | 5' adenosine monophosphate-activated protein kinase catalytic subunit α2 |
| **PRR** | pathogen recognition receptor |
| **p62** | sequestosome 1 (also called SQSTM1) |
| **RLR** | retinoic acid inducible gene-I-like receptor |
| **RNAseq** | RNA sequencing |
| **ROS** | reactive oxygen species |
| **RXR** | retinoic X receptor |
| **SCFA** | short chain fatty acid |
| **STAT3** | signal transducer and activator of transcription 3 |
| **TEER** | trans-epithelial electrical resistance |
| **TEM** | transmission electron microscopy |
| **TFEB** | transcription factor EB |
| **TJs** | tight junctions |
| **TLR** | Toll-like receptor |
| **TNF** | tumor necrosis factor |
| **TSC2** | tuberin |
| **ULK1** | unc-51 like autophagy activating kinase 1 |
| **USP44** | ubiquitin specific peptidase 44 |
| **WIPI2** | WD repeat domain phosphoinositide-interacting protein 2 |
| **VALI/VILI** | ventilator-associated/induced lung injury |
| **VDR** | vitamin D receptor |
| **VDRE** | vitamin D response element |
| **ZO-1** | zonula occludens-1 |

# Declaration of contribution

**Paper I**

In this paper, all experiments were designed by me, Gudmundur Hrafn Gudmundsson and Zahida Parveen. Roger Stromberg and Hakan Ottosson designed and synthesized HO53 and HO56 compounds. I cultured bronchial epithelial cells, in normal and air-liquid interface conditions. I performed and analyzed the following experiments: dose response experiments together with analyses of the LL-37 peptide level in culture medium, cytotoxicity assay, innate immunity and pro-inflammatory genes and protein expression in air-liquid interface cultured cells. I developed and conducted antimicrobial assays with evaluation of the direct bactericidal effect of APDs. I was responsible for the measurement of ROS production and semi-quantitative PCR. Zahida Parveen was responsible for time course and cooperation experiments, analyses of innate immunity and pro-inflammatory genes and protein expression in monolayer cells, cytotoxicity/viability assay, evaluation of barrier integrity and confocal imaging. I statistically analyzed all data, wrote, edited and submitted the manuscript with Gudmundur Hrafn Gudmundsson supervision. I thank Birgitta Agerberth, Peter Bergman and Roger Stromberg for revision of the manuscript and Birigtta Agerberth for providing monoclonal LL-37 antibodies.

**Paper II**

In this paper, I designed all experiments with help of Gudmundur Hrafn Gudmundsson and Margret Helga Ogmundsdottir. All experiments were performed by me with the following exceptions. I thank Alexia Ros Viktorsdottir for conducting under my supervision experiments with VA10 cells and occasional help with maintaining ALI cell cultures. DeCODE genetics performed RNA sequencing. Thanks to Snaevar Sigurdsson for the initial analysis of raw RNA sequencing data by Kallisto/Sleuth software and his support in the continuation of further analyses performed by me. Paulina Cherek embedded and trimmed samples for TEM and image acquisition was performed with assistance of Johann Arnfinnsson. Special thanks to prof. Eeva-Liisa Eskelinen for professional help with identification of autophagy structures in TEM images. I analyzed all data, performed statistical analyses, made figure panels and wrote the manuscript.

**Paper III**

The third article is the effect of collaboration with Jon Petur Joelsson, where I am the second author. In agreement with Jon Petur Jolesson, Gudmundur Hrafn Gudmundsson, Thorarinn Gudjonsson and Sigurbergur Karason, I selected innate immunity and inflammatory gene candidates and performed qPCR analyses of their expression: *HBD2*, *CAMP*, *IL10*, *TNF*, *IL8* and *LCN2* in VA10 and BCi cells. I performed all Western blot experiments assessing YKL-40 protein level in VA10 cells, lipocalin 2 protein level in VA10 and BCi cells and Surfactant Protein B level in VA10 cells. I performed ELISA experiments measuring IL-8 and TNFα protein level in conditioned cell culture media. The leading role in this paper had Jon Petur Joelsson who designed experiments, cultured cells, performed the rest of experiments and with help of Kristjan Leosson, Gabriel Solvi

Windels designed CPAD. Paulina Cherek and Johann Arnfinnsson contributed to TEM analysis. Jon Petur Joelsson statistically analyzed the data, wrote and submitted the manuscript with the contribution of me, Gudmundur Hrafn Gudmundsson, Thorarinn Gudjonsson and Sigurbergur Karason.

# Acknowledgements

All work presented in this thesis was performed at Biomedical Center, Faculty of Life and Environmental Sciences, University of Iceland.

First, I would like to thank Prof. Guðmundur Hrafn Guðmundsson for the supervision and constant support during this project. I would like to thank for all our discussions and critical points. I am grateful to my PhD committee members Þórarinn Guðjónsson and Sigurbergur Kárason for the advice and valid points during my PhD committee meetings. Many thanks to the committee member Margrét Helga Ögmundsdóttir for all autophagy discussions and help with the technical issues I faced during this part of the project. I would like to also extend my deepest gratitude to Birgitta Agerberth for all the scientific and technical support and Peter Bergman for revision of our work. I also wish to thank Roger Strömberg and Håkan Ottosson for the synthesis of APD compounds.

Special thanks to Jón Pétur Jóelsson for the fruitful collaboration on the CPAD project, interesting discussions and always being ready to help me whenever I needed. Alexía Rós Viktorsdóttir for the collaboration on the autophagy project and taking care of my ALI cell cultures during my holidays.

I would like to express my gratitude to DeCODE genetics for RNA sequencing, Snævar Sigurðsson for the initial Kallisto/Sleuth analysis of raw RNA sequencing data and teaching me together with Arnar Pálsson how to further proceed with RNAseq data.

I would like to thank my friend Paulina Cherek and Jóhann Arnfinnsson for their services of TEM core facility. Prof. Eeva-Liisa Eskelinen from University of Turku and University of Helsinki for help with the professional interpretation of TEM images.

I would like to thank all Stem Cell Research Unit members for allowing me to use their equipment and lending me their reagents, especially Bryndís and Jennifer for teaching me how to handle bronchial epithelial cell culture. I would like to thank Skarphéðinn Halldórsson for allowing me to use fluorescence plate reader and all Biomedical Center members.

Many thanks to Marjorie Barrier and Fanney Rut Elínardóttir for fun in the lab. All my friends and colleagues from Læknagarður: Ingunn, Erika, Sophie, Amaranta, Alba, Unnur, Daisy, Juan, Thejus, Kimberly and Fatih. I also wish to thank Lukas and Thibault for all your support and fun we had together in Iceland! I would not make it without having you around! Special thanks to my good friend Andrea from the fifth floor for our “coffee chats” concerning not only autophagy. Many thanks to Zuzana for our conversations and supporting me during difficult times. Thanks to my good friends Gałan and Monika for listening and lifting my spirit during moment of crisis.

At the end I would like to thank my parents and sisters for their support and understanding.

The project was supported by the Icelandic Center for Research (RANNÍS) and University of Iceland research fund. Akthelia Pharmaceuticals holds a patent on APD compounds, Patent No. US 9,957,226 B2 and sponsored synthesis of the compounds.

# 1 Introduction

## 1.1 Human respiratory system

Human respiratory tract is anatomically divided into two parts: the upper respiratory tract beginning from the nasal cavity and the lower respiratory tract, where the gas exchange takes place. In the upper respiratory tract, the inhaled air is warmed up and filtered from contaminants. In pharynx, the respiratory tract intersects with the gastro-intestinal tract and it is protected from the food by the anatomical structure called epiglottis. Further, the air is passed through the larynx, where vocal cords are placed and then to the lower respiratory tract. The lower respiratory tract begins with the trachea and branches to the left and right primary bronchi (main), then into secondary bronchus (lobar), next into tertiary bronchi (segmental), that further branch into bronchioles connected through the alveolar ducts with alveoli, which are responsible for the gas exchange [1].

### 1.1.1 Structure of the lower respiratory tract epithelium

The complete human respiratory tract is covered with epithelial cells of different types depending on the anatomical part of the airway system. In this work, I mainly concentrate on the epithelial cells of the lower respiratory tract, where two histologically different epithelial layers are distinguished: pseudostratified epithelium (***Figure 1***) of the airways and epithelium of the alveoli (***Figure 3***).

Human trachea and airways are covered with pseudostratified epithelium (***Figure 1***) composed of different types of cells, occurring as a single cell layer, where every cell has contact with the basal (basement) membrane. Under the basal membrane, in the stroma, mesenchymal cell types such as airway smooth muscle (ASM) and fibroblasts are placed. Moreover, submucosal glands and cartilages are present in the structure of the human trachea and large airways. In general, the epithelial layer is composed of mature, differentiated cells, protecting basal (progenitor/stem) cells, which can replenish all different type of mature cells during pathological conditions and normal homeostatic turnover of the cells. Among mature, differentiated cells of the airways it is possible to distinguish goblet cells, producing mucus with numerous granules, where the mucus is stored, from ciliated cells responsible for mucus movement and removal of inhaled particles. Furthermore, secretory cells (club cells) and columnar cells of the airway epithelium produce variety of different factors involved in the respiratory host defence and neutralisation of inhaled toxic substances [2]. Apart from these main cell types of the airway epithelium, novel cell types have been described such as brush (tuft) cells with microvilli [3], which recently have been better characterized by increasing accessibility of single cell RNA sequencing. In the mouse airway epithelium, two main subpopulations of tuft cells have been identified, one expressing G protein-coupled receptors and the other responsible for leukotriene biosynthesis [4]. Another rare cell type includes pulmonary neuroendocrine cells (PNECs), occurring as single cells or clustered into neuroendocrine bodies (NEBs). PNECs are the only cells in the airways that are supplied with nerves,

participating in the neurotransmission. They act as sensory cells for the oxygen level in addition to detect and respond to inhaled allergens [5]. By single cell RNAseq the ionocytes have recently been identified and exhibit high expression level of cystic fibrosis transmembrane receptor (CFTR), implying a role in the regulation of the ionic microenvironment in mucus [4]. The submucosal glands (SMGs) contain different group of epithelial cells such as serous and mucous cells, producing mucus and myoepithelial cells responsible for the release of the produced mucus into the luminal space of the airways [2].

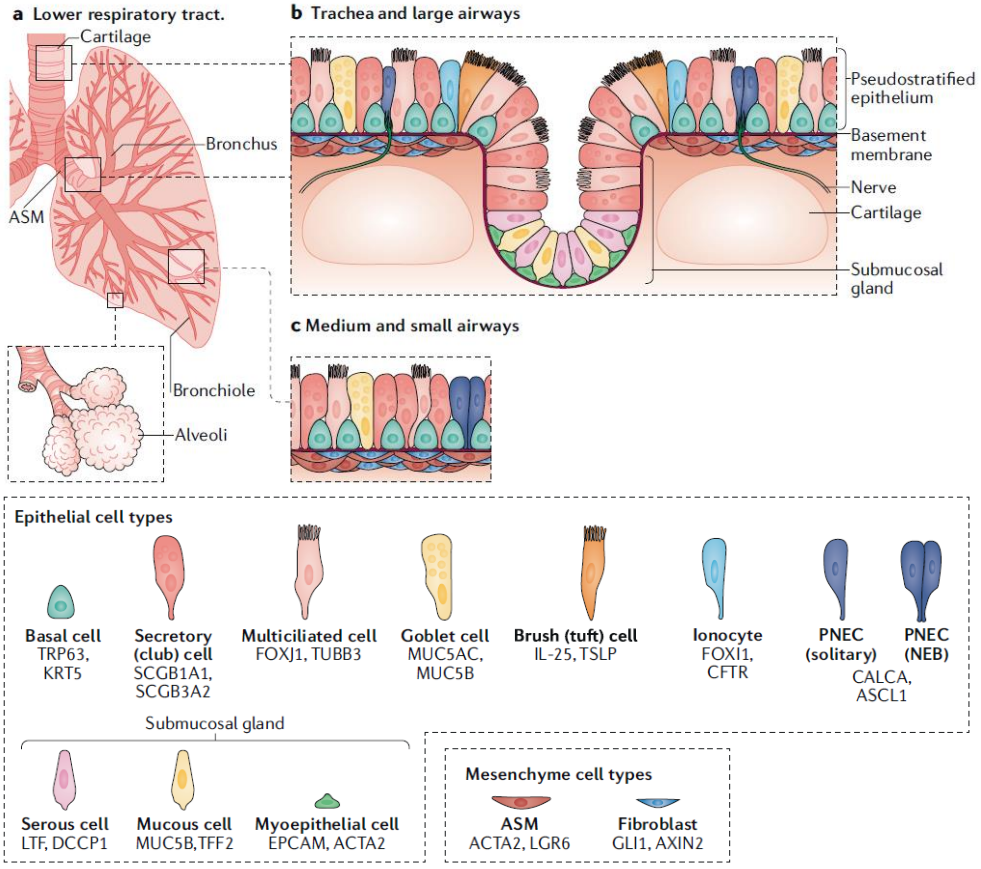


***Figure 1. The structure of the respiratory tract epithelium and epithelial cell types with specific cell type markers.***
***a)*** *Schematic presentation of the human lower respiratory tract with magnification of the alveoli.* ***b)*** *Structure of the airway epithelium in trachea and large airways.* ***c)*** *Structure of the airway epithelium in medium and small airways. The main cell types in the airway epithelium with specific markers are indicated in the lower panel. The image was adapted and modified from Zepp and Morrisey, 2019.*

The human mucus covering apical surface of the respiratory tract is mainly produced by goblet cells and mucous cells of the submucosal gland. It is composed of water (97%), proteins, peptides, lipids and ions (3%). Among the proteins, the mucins are dominant, mainly mucin 5AC and mucin 5B. These glycoproteins have extended glycan side chains that determine gel like properties of the mucus [6]. Apart from mucins, mucus contains additional proteins and peptides, possessing antimicrobial activity such as lysozyme, lactoferrin, lipocalin 2, cathelicidin LL-37 and defensins [7]. Other important components are ions and lipoproteins like surfactant protein A and D, which are found mainly in the alveoli and produced by secretory cells [6,7]. Among ions, the most common are sodium and chloride. Their concentrations are tightly regulated by sodium channels, importing sodium ions and cystic fibrosis transmembrane conductance regulator (CFTR), which together with calcium activated channels export chloride ions [6]. Another structural element of the airway epithelium are tight junctions (TJs) and adherens junctions (AJs) (***Figure 2***). Both junctional complexes occur on the lateral side of the adjacent cells, where TJs are localized closer to the apical side and AJs are placed below them. TJs and AJs are composed of the transmembrane proteins, interacting with the proteins of the intracellular junctional plaque coupled to cytoskeleton proteins. TJs are made by several transmembrane proteins classified into following groups: protein crumb homolog 3 (CRB3) having epidermal growth factor (EGF)-like domain and MARVEL (myelin and lymphocyte (MAL) and related proteins for vesicle trafficking and membrane linkage) domain proteins (e.g., occludin and tricellulin). The most common group of transmembrane proteins are claudins (26 identified) and additional transmembrane proteins are distinguished such as blood vessel epicardial substance (BVES) proteins, junctional adhesion molecules (JAMs) and other immunoglobulin-type adhesion proteins. Further, transmembrane proteins of the AJs complex are divided into the two subgroups of E-cadherin and nectins. All TJs and AJs transmembrane proteins interact with several other proteins, forming the intracellular junctional plaque, containing multiple interaction domains. ZO-1 (zonula occludens-1) is one well-defined protein from the junctional plaque complex and its deletion is lethal in the mouse embryos. ZO-1 contains three binding domains PSD95, DlgA, ZO-1 homology (PDZ) in the N-terminal region that binds to the transmembrane proteins such as claudins and JAM. Other protein-protein binding domains in the N-terminus of ZO-1 are guanylate kinase homology domain (GUK), interacting with transmembrane occludin and SRC homology 3 (SH3) domain binding ZO-1-associated nucleic acid binding protein (ZONAB), which interacts with actin. Direct interaction of ZO-1 with actin is also possible through the C-terminal domain of ZO-1. The examples of AJs intracellular junctional plaque proteins are α-, β- and p120 catenins and afadin (AF6), displaying similar functions as proteins of TJs intracellular junctional plaque [8].

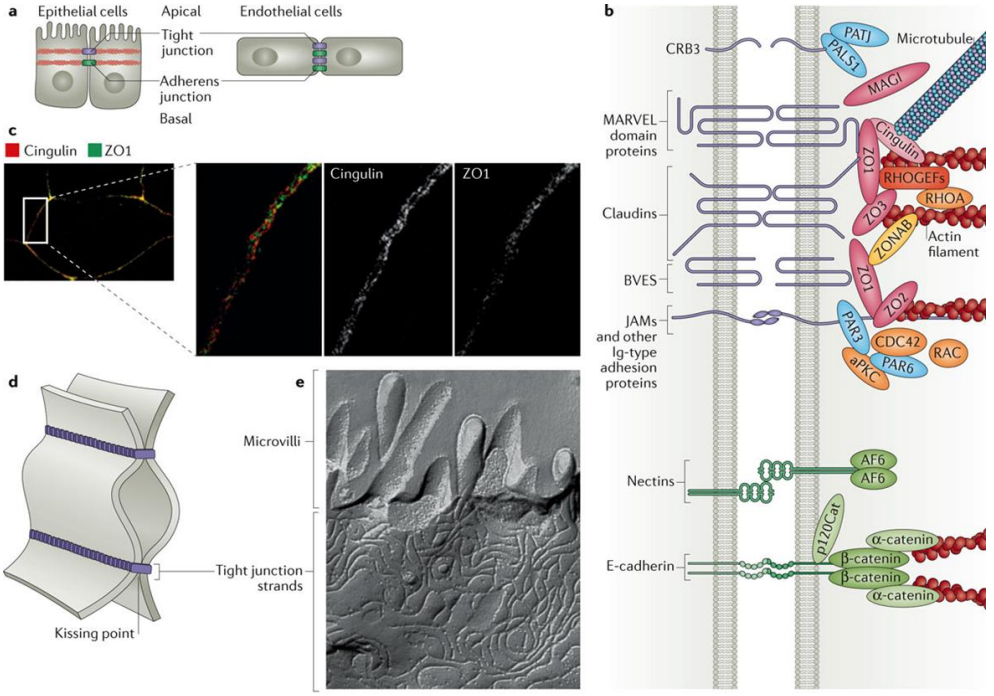


***Figure 2. The structure of the tight and adherens junctions.***
***a)*** *Location of tight (violet) and adherens (green) junctions in epithelial and endothelial cells.* ***b)*** *Different groups of proteins forming junctional plaque of tight (violet) and adherens (green) junctions with few examples of proteins from each group.* ***c)*** *Immunostaining of tight junctional plaque proteins forming regular nets of tight junctions in renal epithelial cells.* ***d)*** *Schematic presentation of cell membranes neighbouring cells with tight junctions strands forming "kissing point".* ***e)*** *Organization of tight junctions in the intestinal epithelial cells analysed by freeze fracture electron microscopy. The image was adapted from Zihni et al., 2016.*

The lower respiratory tract terminates with alveoli composed of the two epithelial cell types, alveolar type 1 cells (AT1; ATI; type I pneumocytes) surrounded by capillaries, where the gas exchange takes place and alveolar type 2 cells (AT2; ATII; type II pneumocytes) responsible for surfactant production [2] (***Figure 3***). Surfactant lines the inner surface of the alveoli and is composed of lipids (90%) and proteins (10%). Among surfactant lipids, the most abundant is phosphatidylcholine and the protein fraction is composed of the surfactant proteins A, B, C and D (SP-A, SP-B, SP-C, SP-D). Surfactant proteins exhibit different properties, SP-B and SP-C are hydrophobic, whereas SP-A and SP-D are hydrophilic and belong to the group of collectins. The synthesis of the surfactants takes place in the endoplasmic reticulum (ER), from there they are transported and modified in the Golgi apparatus. Produced surfactants are stored in lamellar bodies and are released to the alveolar space by exocytosis [9]. Apart from the surfactants, alveolar macrophages, mesenchymal cells and interstitial fibroblasts are present in the alveoli [2].

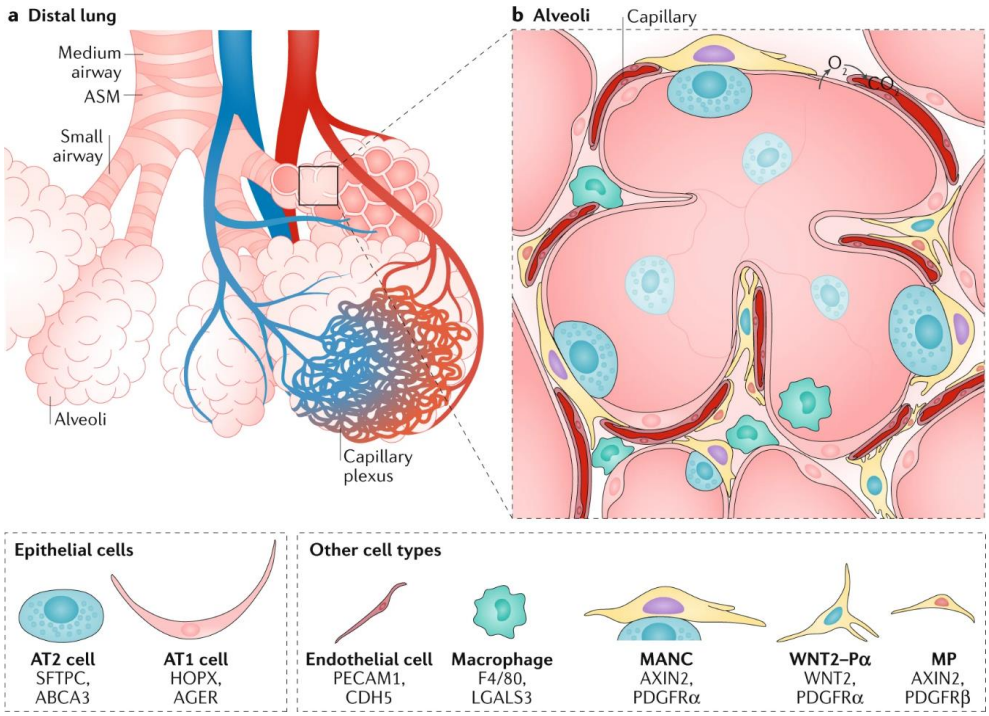


***Figure 3. The structure of the alveolar epithelium with different cell types and their markers.***
***a)*** *Scheme of the distal part of the lower respiratory tract, showing medium airways with airway smooth muscle (ASM) branching to small airways and alveoli surrounded by capillaries.* ***b)*** *Structure of alveoli composed of epithelial cells and other cells of different origin. All cell types occurring in the alveoli are enlisted in the lower panel with indicated specific markers. MANC – mesenchymal alveolar niche cells, WNT2-Pα and MP – interstitial fibroblasts. The image was adapted from Zepp and Morrisey, 2019.*

### 1.1.2 Function of the lower respiratory tract epithelium

The basic function of the lower respiratory tract is to pass air down to the alveoli, where the gas exchange takes place [1]. The important role of the lower respiratory tract epithelium is protection of the tissues by sealing them from environmental factors coming with the inhaled air [1]. A part of the physical barrier between internal tissue and the environment is provided by the tight and adherent junctions between adjacent cells of respiratory tract epithelium. TJs and AJs mediate communication between cells and in addition to regulate paracellular influx of ions, small molecules and microbes [10]. TJs are important for the protection from invading pathogens such as influenza A virus, targeting membrane-associated guanylate kinase (MAGI) proteins [8] and *Pseudomonas aeruginosa* disrupting TJs integrity [11,12]. Additionally, TJs transduce signals, regulating their assembly and also send signals, which regulate gene expression, cell proliferation and differentiation [13]. For instance, in cystic fibrosis, a genetic disease caused by a mutation in the CFTR, the organization of TJs in some patients is altered because of reduced stability of the ZO-1-CFTR complex. This leads to translocation of the ZONAB signalling

proteins from the junctional plaque to the nucleus and stimulation of cyclin D1 expression and cell proliferation [8]. The role of TJ proteins in cell differentiation is exemplified by ZO-1 protein, participating in the cell junction assembly and maturation of polar cells during the differentiation process [8]. The protective function is also provided by the mucus layer present on top of the respiratory tract epithelium. Mucus layer entraps inhaled pathogens and particles that can be harmful for the respiratory system. Next, entrapped molecules are removed by the mucociliary clearance of beating cilia that causes movement of the mucus layer estimated to be 1 mm per minute [6]. The production of mucus components such as mucin 5B is crucial for host defence [14] and it is enhanced upon detection of β-glucan [15] or by pro-inflammatory cytokines present during infection [16]. The production of another component of the mucus, mucin 5AC, can also be stimulated by invading pathogens such as *P. aeruginosa* producing pyocyanine [17], cytokines like IL-13 [18] and by the antimicrobial peptide LL-37, a mucus component [19]. It has been shown that mice with altered mucus composition, lacking mucin 5B ($Muc5b^{-/-}$ mutant mice), accumulated more particles and pathogen *Staphylococcus aureus*, as a result of impaired mucociliary clearance [14]. In addition, these mutant mice showed increased accumulation of macrophages. This indicates the crucial role of the mucus composition in host defence, which was supported by clinical observations of patients suffering from cystic fibrosis, chronic obstructive pulmonary disease (COPD) and asthma [14]. Since it takes time to remove the entrapped particles from the distal part of the respiratory tract the second function of the mucus is neutralisation of the entrapped pathogens and particles by innate immunity effectors present in the mucus layer, e.g. antimicrobial peptides, collectins, lactoferrin and lysozyme [9,20]. Moreover, mucus of the respiratory tract epithelium is also responsible for the hydration of the airway surface. The concentration of sodium chloride is crucial for the maintenance of proper amount of water in the mucus, determining thickness of the mucus layer (7 µm thick in periciliary layer and 0.5-5 µm thickness of the outer layer), which is necessary for efficient mucociliary clearance [6]. Another mechanical protection of the respiratory system involving mucus removal in the situation of impaired mucociliary clearance is cough, very often a symptom of disease [6]. During disease or other pathological conditions causing injury of the airway epithelial layer, the function of the basal cells is regeneration of the epithelial layer by differentiation towards different epithelial cell types [2].

The main function of the terminal part of the lower respiratory tract epithelium is gas exchange in the alveoli. The thin, single cell epithelial layer of the alveoli participate in the $O_2/CO_2$ gas exchange between alveoli and pulmonary capillaries [1]. Both alveolar cell types are responsible for maintenance of the lung fluid balance and removal of the excess fluid from the airspace by vectorial ion transport [21]. Moreover, alveolar type 2 cells produce surfactant lipids necessary for maintaining alveolar tension during the breathing process and to prevent a collapse of the alveoli [2,9]. Apart from gas exchange and maintenance of the alveoli, the alveolar epithelium function is host defence, contributing to protection against invading pathogens and in immunomodulation [9,22]. Moreover, upon stress caused by lung injury or infection, alveolar type 2 cells producing SP-C can self-renew and replace alveolar type 1 cells, and thus display a regenerative function [2,23].

## 1.2 Innate immunity in the airway epithelium

The airway epithelial cells coating all respiratory tract are constantly exposed to environmental factors in the inhaled air. Therefore, the innate immunity of the airway epithelium is crucial for the protection and detection of danger molecules, and after damage for restoration of the healthy state and its maintenance. Without the highly effective innate immunity system in the airway epithelium, the gas exchange, an essential process would not be possible. The innate immunity of the airway epithelium is a complex system composed of many specialized elements necessary for our survival [7] (***Figure 4***).

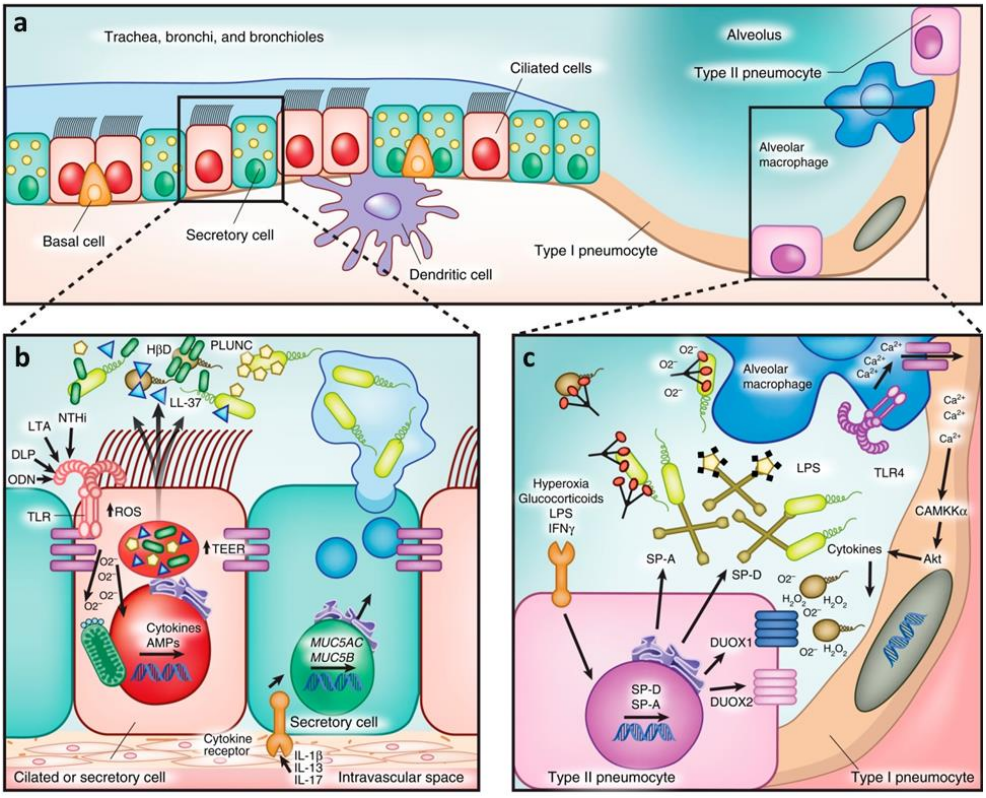


***Figure 4. Innate immunity components of the respiratory tract epithelium.***
***a)*** *Overview on epithelial cells of the lower respiratory tract involved in defence responses highlighting innate immunity components produced by* ***b)*** *bronchial epithelial cells and* ***c)*** *alveolar cells. Abbreviations not mentioned in the introduction text: NTHi, non-typeable Haemophillus influenza*; *LTA, lipotechtoic acid; DLP, diacylated lipopeptides; ODN, oligodeoxynucleotide; HβD, human β-defensin; CAMKKα, $Ca^{2+}$/calmodulin-dependent protein kinase kinase α. The image was adapted from Leiva-Juárez et al., 2018.*

### 1.2.1 Pathogen recognition receptors

One of the initial functions of innate immunity in the airway epithelium is pathogen detection by pathogen recognition receptors (PRRs), recognizing pathogen associated molecular patterns (PAMPs). Upon stimulation PRRs activate signalling cascade leading to inflammation and clearance of pathogens. Among different types of PRRs, present in the airway epithelium are: Toll-like receptors (TLRs), NOD-like receptors (NLRs), RIG-I-like receptors (RLRs) and C-type lectin receptors (CLRs) [7,24].

In the airway epithelium all types of TLRs (TLR2/1, TLR2/6, TLR3, TLR4, TLR5, TLR7, TLR8, TLR9, TLR11) are present, anchored in the cell membrane and in the endosomes. TLRs recognize bacterial lipopeptides, lipopolysaccharide (LPS), flagellin, DNA and RNA by the leucine-rich repeat (LRR) motif that is linked through a single transmembrane domain to the intracellular motif of the Toll/IL-1 receptor (TIR). The activation of the receptor requires binding of the adaptor protein MyD88 or TIR-domain-containing adapter-inducing interferon-β (TRIF) to the TIR domain. MyD88 is an adaptor protein for all TLRs except TLR3 and TRIF is the adaptor protein for TLR3 and TLR4. Additional adaptor proteins such as TIRAP (TIR domain containing adaptor protein), TRAM (translocation associated membrane protein 1), SARM (sterile alpha and TIR motif containing) have been shown involved in the TLR signalling. The stimulation of TLRs initiates downstream signalling of NF-κB and MAPK, leading to induction of pro-inflammatory cytokines and type I interferons [7,25].

Unlike TLRs, apart from cell and endosomal membranes, NLRs occur as soluble receptors in the cytoplasm. Based on the effector domain, NLRs were classified into subgroups that contain caspase recruitment domain (CARD or NLRCs), pyrin domain (PYD or NLRPs) and baculoinhibitor of apoptosis protein domain (NAIP or NLRBs) [7]. In the airway epithelium NLRs with CARD domain are represented by NOD1 and NOD2 receptors, recognizing bacterial peptidoglycans and working in synergy with TLRs towards activation of NF-κB and MAPK pathways [26]. The other types of NLRs, containing PYD and NLRB domains form inflammasome controlling cleavage of IL-1β and IL-18 pro-forms by caspase-1 [7,24]. For instance, in human lung epithelial cells NRLP3 receptor harbouring pyrin domain forms NRLP3 inflammasome responsible for cleavage of IL-1β upon *Candida albicans* or influenza A virus infections [27–29].

Human airway epithelial cells have also cytoplasmic receptors for the detection of nucleic acids from pathogens [7]. Among them are RIG-I-like receptors (RLRs), recognizing viral ss/dsRNA of influenza and paramyxoviruses, causing respiratory diseases, e.g. respiratory syncytial virus (RSV) [30,31]. The group of RLR receptors includes retinoic acid inducible gene-I (RIG-I), melanoma differentiation-associated gene 5 (MDA5) and RIG-I-like receptor dsRNA helicase (LGP2) [24]. With the involvement of the adaptor proteins, e.g. mitochondrial antiviral-signalling protein (MAVS), RIG-I and MDA5 receptors transduce signals, activating NF-κB, IRF3 and IRF7 pathways, leading to production of pro-inflammatory cytokines and interferons [26]. Other cytoplasmic receptors recognize bacterial DNA and bacterial signalling molecules such as cyclic dinucleotides (CDNs) [7]. A prominent member of this family is the stimulator of IFN genes (STING) located on the ER membrane. STING recognizes CDNs and is an adaptor protein for additional cytoplasmic receptors like IFI16, recognizing *Streptococcus pneumoniae* dsDNA [7,32]. Moreover, STING can be activated by cGAMP (cyclic GMP-AMP) that is synthetized by cGAS (cGAMP synthase) in human airway epithelial cells upon detection of

microbial/viral DNA in the cytoplasm but also by self-DNA originated from the nucleus or damaged mitochondria [33].

Another example of PRRs are C-type lectin receptors (CLRs) on airway epithelial cells, recognizing carbohydrates present on the pathogens, activating pro-inflammatory responses [7,24]. The CLRs occur as membrane anchored receptors such as Dectin-1, recognizing *Haemophilus influenza* and *Aspergillus fumigatus* infections [34,35]. The second form of CLRs are soluble collectins, containing C-type lectin domain such as SP-A and SP-D, exhibiting antimicrobial activity through opsonisation of bacterial, viral and fungal pathogens [7].

### 1.2.2 Antimicrobial peptides

Apart from PRRs, antimicrobial effectors produced by the airway epithelial cells are part of the host defence system. There are several known antimicrobial effectors in the lung epithelial cells: antimicrobial peptides (AMPs) and proteins, antiproteases, collectins, plate-lung-nasal-clone (PLUNC) proteins, chemokines, nitric oxide (NO) and reactive oxygen species (ROS) [7]. Among AMPs there are two main families: cathelicidins and defensins [36,37]. Human cathelicidins have one dominant mature peptide LL-37 encoded by the *CAMP* gene and produced as an inactive proform hCAP18 containing the N-terminal cathelin domain [38,39]. Inactive proform hCAP18 is produced by immune cells such as neutrophils and other immune cells like mast cells, monocytes and NK cells but also by epithelial cells including lung epithelium [36,38,39]. The inactive proform is stored in the cells and upon stimuli cleaved to the active LL-37 peptide by serine proteases, e.g. kallikreins and proteinase 3 [36]. The name of LL-37 peptide comes from the first two leucine residues of the peptide and the length of 37 amino acid residues, including several lysines and arginines [39]. The active LL-37 is a cationic peptide with α-helical structure [40]. Of note, LL-37 is considered as the dominant peptide among human cathelicidins but not the only one, since the peptide can be processed in skin to smaller peptides, e.g. RK-31, KS-30, KS-20 [36]. In contrast to cathelicidins, defensins have many members and are divided in α-, β- and θ-defensins [36,37,40]. The first group α-defensins is produced mainly by granulocytes and Paneth cells of the gut epithelium and they are released upon pro-inflammatory stimuli. The second group β-defensins is produced by both, immune and epithelial cells, where β-defensin 1 is produced and released constitutively, while production of β-defensin 2 and β-defensin 3 is inducible. Defensins are also produced as an inactive precursors that undergo further processing to the active forms [36,37]. Interestingly, there is also the third group θ-defensins that was detected in *Rhesus* monkeys and have circular structure of two hemi-α-defensins [40]. In the human genome there are genes encoding θ-defensins, however proteins are not produced as a result of a premature stop codon [41]. AMPs are produced constitutively but can also be induced. Their constitutive expression is enhanced upon stress conditions such as infection or injury. Most of them are stored in cellular granules as a proform and are further released and processed upon occurrence of danger signals [36,37]. The primary studied function of AMPs is their bactericidal effect on both, gram positive and negative bacteria, but they are also effective against viruses and fungi. The common antimicrobial activity of AMPs is associated with their cationic and amphipathic properties. Positively charged AMPs can strongly interact through electrostatic and hydrophobic interactions with negatively charged phospholipids of the bacterial cell membrane. They can also interfere with LPS of gram-negative bacteria or teichoic and lipoteichoic acids of gram-positive bacteria. The interaction of AMPs with

bacterial membranes causes disruption, leakage of intracellular components, leading to bacterial cell death [36,40,42]. Another, less known antimicrobial mechanism of AMPs is translocation of the peptide through the membrane and binding to intracellular components of the bacteria, resulting in bacterial cell death [42]. Furthermore, human β-defensin 3 has been shown to disrupt bacterial cell wall biosynthesis by binding to lipid II, which makes bacteria more vulnerable to damage [43]. Hence, AMPs have different activities against bacteria, but the membrane disruption seems to be of major general importance. The importance of AMPs for the host innate immunity during bacterial infection has been demonstrated in *in vivo* models, showing protective function against skin infection caused by group A *Streptococcus* (GAS) [44] and enteric infection by *Salmonella* [45]. In case of viral infections, AMPs bind and destabilise viral structures like the viral envelope of influenza viruses or RSV, Zika virus and the viral capsid of rhinoviruses, HPV16 and adenoviruses [42]. Similar mechanism takes place during fungal infections, as demonstrated in *C. albicans*, where AMPs permeabilise yeast cell membrane [46].

Of note, at physiological concentrations AMPs do not damage human cell membrane due to its lack of negative charge in the outer leaflet of the membrane and the presence of cholesterol [40]. However, AMPs at higher concentrations, e.g. when granulocytes are recruited to a site of infection with subsequent release of AMPs might damage our cells [47]. A similar aspect has been raised concerning the effect of AMPs on beneficial commensal bacteria [40]. The study by Cullen *et al.* shows that commensal bacteria of the gastrointestinal (GI) tract from phylum *Bacteroidetes* have different composition of LPS, containing less phosphorylated lipid A that increases resistance to AMPs, even in high concentrations such as during inflammation [48,49]. This can indicate microbial adaptation to exposure of AMPs.

Apart from antimicrobial activity, AMPs exhibit immunomodulatory functions [36,37,42]. AMPs display chemoattractant functions towards immune cells, e.g. hBD2 is chemoattractant for mast cells [50] and LL-37 for neutrophils, monocytes and T cells [51]. By enhancing phagocytosis, ROS production and participation in neutrophil extracellular trap (NET) formation, LL-37 contributes to enhancement of bacterial clearance [36,42]. AMPs also indirectly recruit leukocytes to the local site of infection or injury by inducing release of chemokines and cytokines [36,42]. For instance, LL-37 can induce expression of pro-inflammatory IL-8, a chemoattractant for neutrophils in human A549 lung epithelial cells, displaying a pro-inflammatory function [52]. AMPs activate antigen presenting cells (monocytes/macrophages and dendritic cells (DCs)), initiating T cell response, and therefore play a role in the intersection of innate and adaptive immunity [42]. AMPs interfere with cell signalling cascades, while displaying at the same time a dual pro- and anti-inflammatory role, depending on the local environment and the phase of infection. For instance, during infection when NF-κB pathway is activated by bacterial LPS, which binds TLR4 receptor, LL-37 peptide can selectively inhibit the production of pro-inflammatory TNF and ROS, while at the same time stimulate IL-8 production in epithelial cells to attract immune cells [53]. Furthermore, the local environment also affects immunomodulatory function of AMPs, like upon citrullination of LL-37 by peptidyl arginine deaminase, the peptide loses its ability to enhance pro-inflammatory responses in macrophages [54,55]. Another example of pro- and anti-inflammatory effect of AMPs is in the early stage of bacterial infection with *P. aeruginosa*, where LL-37 enhances pro-inflammatory response in airway epithelial cells [56]. Cathelicidins are also able to prevent activation of TLR2 and TLR4 signalling in macrophages by non-viable

bacteria and their products at later stage of infection [57]. The result in reduced production of pro-inflammatory response might protect local tissue from injury [57]. Therefore, AMPs can play a dual role in shaping both pro- and anti-inflammatory responses and maintaining tissue homeostasis.

Apart from AMPs, there are also many antimicrobial proteins such as lysozyme that degrades bacterial peptidoglycans and bacteriostatic lipocalin 2 and lactoferrin [7]. Bacteriostatic effect of lipocalin 2 and lactoferrin are linked to inhibition of iron uptake by bacteria from the local environment, as they bind bacterial iron-chelating molecules. Lipocalin 2 has been shown effective against *E. coli* causing pneumonia [58] and mutant mice lacking lipocalin 2 were more susceptible to *K. pneumoniae* infections [59].

### 1.2.3 Other molecules

Apart from AMPs lung epithelial cells produce additional innate immunity effectors for the host defence. The antiproteases such as secretory leukocyte protease inhibitor (SLPI) and elafin are included in host defence [7]. Both are induced by LPS, TNF and IL-1β [60] and exhibit antimicrobial properties against the pathogens *P. aeruginosa* and *S. aureus* [61,62]. Moreover, they have anti-inflammatory potential, e.g. by inhibition of NF-κB pathway through reducing degradation of IκBα in macrophages and endothelial cells [63]. Additional components of the innate immunity in the lung epithelium are collectins, SP-A and SP-D, produced by alveolar type 2 cells [7]. They are able to opsonize bacteria and to increase phagocytosis by the alveolar macrophages [9]. The immunomodulatory function of collectins can be exemplified by the inhibitory effect of SP-A on the production of IL-8 by eosinophils present during allergic reaction [22]. The antimicrobial and immunomodulatory functions are also displayed by plate-lung-nasal-clone (PLUNC) proteins [7]. SPLUNC1 protein has been shown to have antibacterial effect against *Mycoplasma pneumoniae* and to reduce the production of the pro-inflammatory cytokine IL-8 [64]. Of note, several chemokines like CXCL9 and CXCL11 present in the lung epithelium as a result of IFNγ stimulation have antibacterial functions against *E. coli* and *L. monocytogenes* [65]. Another important element of innate immunity in the lung is the ability of epithelial cells to produce ROS for the elimination of invading pathogens [7]. Dual oxidases (DUOX) are the key enzymes responsible for generation of ROS in the lung epithelium, occurring as superoxide and hydrogen peroxide [66].

### 1.2.4 Physical components of innate immunity

The physical components of innate immunity in the epithelial barrier integrity are partly provided by junctional complexes of the neighbouring cells [7]. They regulate paracellular transport in response to signals from the environment [8]. Junctional complexes are not only self-regulating signalling platform but also intersecting signals from the innate immunity receptors present in the airway epithelium, and hence be considered as a part of innate immunity [7,8]. For instance, activation of Toll-like receptor 2 (TLR2) led to increased expression of claudin-1, a tight junction protein, through atypical protein kinase C zeta, resulting in enhanced epithelial barrier integrity [7,67]. Thus, the junctional complexes are a gateway that control the entrance of signalling molecules such as pathogen associated molecular patterns (PAMPs) and cytokines to the epithelial receptors located in the lateral and basolateral membranes [7].

Another element of innate immunity is the thick (7.5- 12 μm) mucus layer present on the airway epithelium, providing a physical barrier for invading pathogens and inhaled particles [6]. It protects airway tissue from damage by inactivation of entrapped pathogens and the removal by mucociliary clearance [7,20].

## 1.3 Modulation of innate immunity on the epithelial surfaces

AMPs on the epithelial surfaces form a shield, protecting us from invading pathogens and represent an early evolutionary defence mechanism. The initial pathogen recognition by PRRs, signal transduction and signalling are complex mechanisms, initiating fast responses and elimination of the intruders. Despite these potent host defence mechanisms, several pathogens escape as they have developed strategies to subvert host innate immunity responses by production of virulence factors. Molecules produced by pathogens can subvert host innate immune responses even at the initial point of the host-pathogen interaction on the epithelial surfaces [68]. For instance, the pathogen *Streptococcus pyogenes* from Group A *Streptococcus* produces M1 protein, a virulence factor that binds and sequesters LL-37, making the peptide inefficient to kill the pathogen and limit its spreading [69]. Furthermore, *Shigella spp*. can downregulate the expression of LL-37 and β-defensin 1, at early stage of the infection to promote invasion and colonization of the bacteria [70]. Apart from advanced mechanisms allowing for the successful host colonization, pathogens very quickly adapt to the changing environment, including the presence or absence of antibiotics. The misuse of antibiotics for example in treating viral infections and importantly overuse of antibiotics in the animal husbandry as growth factors has led to the selection of antimicrobial resistance (AMR), which is becoming a global problem [71–73]. According to World Health Organization (WHO) antibiotic resistance occurs in every country and many opportunistic pathogens have gained resistance to antibiotics routinely used for the treatment of infections [71]. A prominent example is the group of **ESKAPE** pathogens including ***E****nterococcus faecium*, ***S****taphylococcus aureus*, ***K****lebsiella pneumoniae*, ***A****cinetobacter baumanii*, ***P****seudomonas aeruginosa* and ***E****nterobacter spp*. like adherent-invasive *E. coli* (AIEC), causing hospital acquired and transmitted diseases [74,75]. According to the study by Cassini *et al.*, 63.5% of all infections caused by multidrug-resistant strains were connected to health care [76]. This example presents the scale of the problem of antimicrobial resistance, therefore World Health Organization (WHO) and other institutions undertook a global initiative to reduce the scale of this problem. The following action were undertaken in order to prevent and slow down the spreading of AMR: to reduce general use of antibiotics in animal food production and implement the ban of using colistin, the last resort antibiotic, used in animal husbandry in some countries, better control of spreading nosocomial infections, work on the awareness of the society about the AMR problem and the development of pipelines for new antibiotics [72,73]. After few years of implementation of this programme, the spread of AMR genes in some pathogens has remained on the same level, such as for *S. aureus* and *E. faecium* [72,73]. However, the AMR of ESKAPE pathogens is still a serious problem, even in the high income countries, where the percentage of the antibiotic resistant *E. faecium*, *A. baumanii* and *E. coli* remains relatively high [72,73]. Another obstacle is the development of new antibiotics, that is a long and costly process taking several years until the new drug is introduced to the market.

Recently alternative strategies for treatment of infectious diseases have gained more attention. By deciphering molecular pathways of host innate immunity and infection strategies of pathogens, an opportunity of modulating these mechanisms might result in development of new alternative treatment strategies, limiting and/or reducing the use of antibiotics and thereby reducing the selection of AMR strains.

The utilization of AMPs is one of these alternative treatment and/or preventive strategies in comparison to antibiotics because the development of resistance against the activity of AMPs by pathogens has been claimed limited [40,77]. The development of AMP resistance in laboratory conditions by culturing bacteria through serial passaging with increasing concentration of AMPs or through selection on agar plates is sufficient to generate selective pressure to evolve resistance to AMPs [78]. However, as Lazzaro *et al.* in a recent review claim: "The pharmacodynamics of AMPs reduces the probability of resistance evolution", because AMPs mode of action and elimination from the environment are faster than for antibiotics [77]. In addition, by mathematical modelling accompanied by the experimental study, the authors show that a chance for development of resistance against AMPs is much lower than against antibiotics [77]. Several clinical trials for the treatment of infectious diseases by using AMPs and their analogues have been conducted but mainly concentrate on topical administration. For example, the derivative of LL-37 peptide, OP-145 was tested for treatment of middle ear infections and plant defensins HXP124 for treatment of fungal nail infections [42]. Another therapeutic potential of AMPs, resulting from their effect on proliferation and wound closure, is evaluated in wound healing studies, using the human synthetic LL-37 peptide for the treatment of venous leg ulcers [79]. Among several attempts, only few passed clinical trials and are available on the market. One of them is a peptide (PAC-113) derived from histatine found in saliva that is used for treatment of oral *C. albicans* infections. A second example is intravenously administered semisynthetic lipoglycopeptide, dalbavancin, used in the therapy of acute skin infections [42]. The microbicidal potential of AMPs has also been tested for coating of biomedical devices such as prosthetic joints, catheters and dental implants. The aim of modifying biomedical devices by surface tethering AMPs and incorporating the release of AMPs is to avoid and/or limit biomaterial-associated infections [80]. This approach should be evaluated carefully due to the potential risk of the development of AMP resistance [77]. This risk might be minimized by using biomedical devices with a release system of AMPs, reducing the time of exposure to AMPs and by coating medical devices with a mixture of different peptides instead of using only one peptide [77,80]. Furthermore, approaches using immunomodulatory potential of AMPs have entered preclinical trials that concentrate on e.g. enhancing natural immune responses and controlling chronic inflammatory diseases [42]. Therapeutic potential of boosting natural immune responses can be exemplified by innate defence regulator (IDR) synthetic peptides. These peptides enhance bacterial clearance not by direct interaction with pathogens but by enhancing recruitment of immune cells to the infection site [81]. The immunomodulatory potential of AMPs indicates potential application in the treatment of non-infectious inflammatory diseases. It has been shown, that in the mouse model of *C. difficile* colitis administration of the Cramp peptide (mouse homologue to LL-37 peptide) inhibited intestinal inflammation [82]. The exploitation of the immunomodulatory potential of AMPs has also been shown in the veterinary research, where the chicken embryos received the chicken cathelicidin analogue CATH-2 *in ovo* (in the egg) and later in early life after hatch they were resistant to pneumonia caused by *E. coli* [83]. Instead of using

antibiotics, this approach could be widely utilized in the animal husbandry as an alternative protective strategy, resembling vaccination and would reduce selection of AMR bacteria.

An alternative approach to the direct administration of AMPs and their analogues as an alternative for antibiotics, is the modulation of signalling pathways by different agents leading to stimulation of innate immunity responses by enhanced expression of antimicrobial effectors. This approach might be considered as closer to physiological conditions, where AMP concentration is maintained at the level that allow for protection of the host constantly exposed to environmental factors and in case of infection is rapidly upregulated. Moreover, host-directed therapies inducing expression of endogenous AMPs are within a concept of maintaining minimal risk of the development of AMP resistance [77]. The effectiveness of this approach was shown by Fan *et al.* in the mouse model, where modulation of Cramp expression via activation of Hif-1α transcription factor provided protection from *C. albicans* colonization of the gastrointestinal tract [84]. Several different molecules have been tested to find the best drug candidates for modulation of innate immune responses. Among them are compounds from the natural pharmacopoeia, e.g. inducing production of human β-defensin 3 without affecting inflammatory response in the colon epithelium [85]. Another example is a small molecule, a pyrimidine synthesis inhibitor PALA (*N*-phosphonacetyl-l-aspartate**)** stimulating production of β-defensin 2 and LL-37 in human skin explants for enhancing clearance of bacteria causing skin infections (methicillin-resistant *S. aureus*, *P. aeruginosa* and *A. baumanii*) without showing direct antimicrobial activity [86]. Furthermore, nutrients like lactose in the breast milk was shown to induce *CAMP* gene expression in the gut epithelial cells and macrophages underlining the importance of modulating mucosal innate immunity responses in infants [87]. Also vitamin D, metabolites like short chain fatty acids (SCFAs) and chemicals like Entinostat, together with its derivatives were shown effective in the modulation of innate immunity responses [88–90]. In the chapter below I will concentrate more on these modulators.

### 1.3.1 Vitamin D3

The biologically active form of vitamin D, 1α,25-dihydroxyvitamin D3 (hereafter called vitamin D3; also called calcitriol) is produced from 7-dehydrocholesterol in skin exposed to sunlight and from cholecalciferol provided with the diet. Normally, cholecalciferol is hydroxylated to 25-hydroxyvitamin D3 by CYP2R1 enzyme, mainly in liver, where it can be stored or circulates until it is converted to the active form 1α,25-dihydroxyvitamin D3 (vitamin D3) by CYP27B1 enzyme. At the same time, increased level of vitamin D3 activates expression of CYP24A1 enzyme, that inactivates vitamin D3 creating a self-regulatory negative feedback loop [91,92]. The active form of vitamin D binds to the nuclear vitamin D receptor (VDR) that forms a heterodimer with nuclear receptor partner retinoic X receptor (RXR). Together they bind to vitamin D response elements (VDREs) that are located in the promoter region of vitamin D3 primary target genes, e.g. *CAMP* and *DEFB4* or within the regulatory domain distant from the gene promoter, e.g. *CD14* gene [93–95]. However, Carlberg group suggested that in monocytes vitamin D3 works through other mechanisms, causing broad transcriptional changes. One of these mechanisms might be linked to the expression of secondary target genes, e.g. through enhanced expression of transcription factors such as BCL6, NFE2, POU4F2 and ELF4, which are primary targets of vitamin D3. Moreover, vitamin D3 can induce expression of secondary target genes through epigenetic changes linked to the chromatin opening state by modulating the activity of histone modifying enzymes. This modulation can be the result of direct protein-protein interaction or by induced expression of genes encoding histone modifying enzymes

like histone deacetylases (HDAC) HDAC4 and HDAC6 [93]. The third suggested mechanism for induction of secondary target genes is based on the fact, that VDR binding sites together with vitamin D3 target genes are located within topologically associating domains (TADs), forming loops/anchors flanked with vitamin D3 sensitive multi-zinc finger protein CCCTC-binding factor (CTCF) sites located upstream and downstream of VDR binding sites. TADs organize human genome into transcriptionally active and inactive regions, therefore the authors proposed that administration of vitamin D3 reorganizes three-dimensional chromatin structure by increased binding of CTCF and forming transcriptionally active TAD loops [93,96]. The same group suggested that binding of VDR to genomic DNA is possible without vitamin D3 ligand in limited number of accessible loci. They also proposed that transcription factor PU.1 supports binding of VDR to genomic DNA in monocytes since ChIP-seq analysis revealed the presence of PU.1 in the 2/3 of the detected sites, where VDR is bound to VDRE [96]. This was also seen in the colon epithelial cells HT-29 upon addition of vitamin D3, where PU.1 and VDR were recruited to the *CAMP* promoter [97]. Besides this, another study showed involvement of PU.1 in the vitamin D3 induced response in lung epithelial cells, where PU.1 co-operated with VDR and CCAAT/enhancer-binding protein α (CEBPα) in *CAMP* induction [98]. Thus, vitamin D3 remains a prominent inducer of innate immunity responses by induction of *CAMP* and also *DEFB4* expression in different cell types via binding of VDR to VDREs located in the promoters of these genes for activating transcription [94,95]. Interestingly, stimulation of TLR1/2 receptor in human macrophages induced antimicrobial response by enhanced expression of VDR and CYP27B1 enzyme that converted 25-hydroxyvitamin D3 to active vitamin D3 and consequently induced *CAMP* gene expression responsible for antimicrobial response against *Mycobacterium tuberculosis* (*Mtb*). This study also provided a proof of concept that the level of vitamin D3 is an important innate immunity modulator and that reduced level of 25-hydroxyvitamin D3 in serum increases susceptibility to bacterial infections [99]. The follow-up studies revealed the effective clearance of *Mtb* is a result of vitamin D3 induced innate immunity due to increased LL-37 production [100]. Human cathelicidin LL-37 peptide is known from its stimulatory properties on human lung cells proliferation and migration [101], therefore Gonzalez-Curiel *et al*. evaluated effect of vitamin D3 on wound healing. In the *in vitro* model of keratinocytes derived from diabetic foot ulcers, the authors showed that vitamin D3 promotes expression of *CAMP*, *DEFB4*, *VDR* and increased antimicrobial response against *E. coli*. Moreover, vitamin D3 promoted wound healing, suggesting utilization of immunomodulatory properties of vitamin D3 for the treatment of chronic wounds [102]. By inducing the production of LL-37, vitamin D3 was also effective in the inhibition of rhinovirus replication in primary bronchial cells derived from cystic fibrosis patients, showing immunomodulatory properties against viral infections and therapeutic potential for treatment of infections in cystic fibrosis patients [103]. On the other hand, prolonged treatment of differentiating primary bronchial epithelial cells in air-liquid interphase with vitamin D3 did not reduce replication of the rhinovirus but led to thickening of the cell layer, displaying squamous character [104]. This could be in agreement with the explanation proposed by the Carlberg group, indicating that vitamin D3 can induce different responses, depending on the differentiation status of the cell and time of the treatment [93,96]. Furthermore, vitamin D3 induced expression of antimicrobial effectors in lung cells and showed synergistic effect in the induction of *CAMP* gene expression with the innate immunity modulator phenylbutyrate (PBA) [105]. This observation was supported by clinical trials, showing that supplementation with cholecalciferol and PBA boosted innate immunity responses and improved treatment outcome of *Mtb* infected patients [106,107].

### 1.3.2 SCFAs and derivatives

The natural source of short chain fatty acids (SCFAs) is from fermentation of dietary fibres and carbohydrates by the gut microbiota. Most abundant is acetate, then propionate and the lowest concentration is butyrate produced mainly by *Firmicutes* bacteria [108]. Locally in the gut, SCFAs are the main energy source for the gut epithelial cells and only small portion of SCFAs can be taken up and distributed with the blood [108,109]. The transport of SCFAs takes place mainly through passive diffusion and it is also possible through monocarboxylate transporters (MCTs) and sodium coupled monocarboxylate transporters (SMCTs) [108]. SCFAs in particular butyrate are also signalling molecules through three different G protein coupled receptors (GPCRs) expressed in the gut epithelium and additional cells: GPR41 (free fatty acid receptor 3; FFAR3), GPR43 (free fatty acid receptor 2; FFAR2) and GPR109A (hydroxycarboxylic receptor 2, HCA2) [109]. Apart from the energy source, SCFAs are able to enhance expression of LL-37 peptide in colonocytes, demonstrating the potential to modulate innate immunity responses in the gut [110]. The importance of SCFAs production by balanced gut microbiota and their immunomodulatory properties have mainly been linked to maintaining anti-inflammatory environment in the gut. This has been indicated in studies on inflammatory bowel diseases (IBD) like Crohn´s disease and ulcerative colitis [108], where patients suffering from IBDs had lower level of butyrate in faecal samples and had dysbiosis with decreased proportion of the commensal bacteria *Firmicutes* and *Bacteroidetes* [111,112]. Dysbiosis of the gut microbiota could also be caused by the use of antibiotics, that can lead to secondary infections such as caused by *Clostridium difficile*. In the mouse model of *C. difficile* induced colitis administration of butyrate reduced inflammation and improved intestinal epithelial barrier function, limiting bacterial translocation [113]. This demonstrates, that SCFAs are key compounds in maintaining homeostasis of the gastrointestinal tract and restoring the balance upon damage. Among SCFAs, butyrate is also well-known as a weak histone deacetylase (HDAC) inhibitor and was shown to imprint antimicrobial programme in differentiating macrophages. The imprinted antimicrobial programme in differentiated macrophages was exhibited by increased production of antimicrobial effectors, mainly calprotectin and induction of autophagy for effective clearance of invading pathogens. Interestingly, the effect of butyrate on differentiating macrophages was not mediated by activation of GPCRs but through HDAC3 inhibition, indicating epigenetic mechanisms involved in the regulation of innate immunity [114]. These studies demonstrate immunomodulatory properties of SCFAs in the local environment of the gut epithelium and on recruited monocytes that differentiate towards intestinal macrophages. However, SCFAs concentration in blood is lower than in the gut [108], therefore additional supplementation of SCFAs and the improved, non-scent derivative phenylbutyrate (PBA) could be beneficial to strengthen innate immunity responses. PBA is a drug registered for the treatment of urea cycle disorders (DRUGBANK database; www.drugbank.ca) and like butyrate is an HDAC inhibitor [115]. Treatment with PBA was shown to induce expression of LL-37 in the human lung epithelial cells and was more efficient than butyrate [105]. Moreover, administration of PBA improved outcome of *Shigella* infected rabbits by counteracting bacteria mediated downregulation of AMPs in the gut and lung epithelium [116]. Thus, this *in vivo* study demonstrated immunomodulatory potential of PBA on distant tissues and relevance of PBA for the treatment of infections. In another *in vivo* study immunomodulatory effect of PBA on the gut mucosal tissue was shown in a mouse model of *Salmonella* infection. This study showed immunomodulatory effect of PBA from a different perspective because PBA shifted the mouse microbiota towards higher proportion of *Lactobacillales* and segmented filamentous bacteria. These bacteria are

responsible for enhanced mucosal immunity connected to induction of mucosal Th17 cells, protecting mouse from different enteropathogens [117]. Taken together, SCFAs and their derivatives modulate innate immunity responses in the mucosal tissues and immune cells.

### 1.3.3 Entinostat and APDs

Recently it has been shown that some drugs from the group of histone deacetylase inhibitors (HDACi) display immunomodulatory properties. Among them are pan-HDAC inhibitors like Vorinostat (SAHA - suberanilohydroxamic acid) and more selective inhibitors, targeting defined group of HDACs. One of the selective HDACi, displaying immunomodulatory properties is Entinostat, targeting class I HDACs [89]. It is a cytotoxic compound, showing activity against cancer cells and therefore tested in clinical trials of anti-cancer therapy [118–120].

Entinostat was selected as a potential drug candidate with immunomodulatory properties by activity screening of different HDAC inhibitors using the colonic epithelial cell line HT-29 in a luciferase reporter system for *CAMP* expression [89,121]. Interestingly, Entinostat induced *CAMP* and *DEFB1* gene expression in the cell line through activation of STAT3 signalling pathway. Transcription factor STAT3 did not bind to the promoter of *CAMP* gene but was translocated to the nucleus, indicating more complex signalling cascade, containing activation of HIF-1α transcription factor. In fact, upon administration of Entinostat, HIF-1α was recruited to the *CAMP* gene promoter and expression of HIF-1α was depended on STAT3. Moreover, involvement of STAT3 in induction of the *CAMP* gene expression by Entinostat was demonstrated in macrophages isolated from patients with hyper-IgE syndrome caused by mutation in *STAT3* gene, resulting in impaired STAT3 signalling [89]. Furthermore, Entinostat treatment improved survival of *Shigella* infected rabbits and restored rabbit cathelicidin expression [90]. Despite immunomodulatory properties of Entinostat comparable to PBA and vitamin D3, this compound remains cytotoxic with low solubility. Therefore, based on the structure of Entinostat a new group of less toxic compounds designated aroylated phenylenediamines (APDs) was designed (***Figure 5***) and tested for induction of *CAMP* gene expression. The phenylenediamine moiety of the Entinostat was critical to induce *CAMP* gene expression and by modification of the substituent group, containing hydrophilic groups the solubility was increased [90].

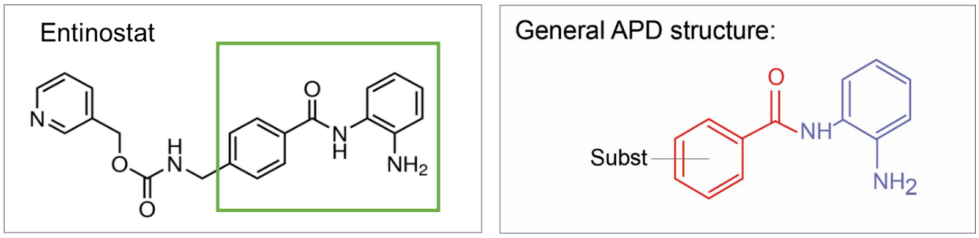


***Figure 5. Structures of Entinostat and its derivative aroylated phenylenediamine (APD).*** *Chemical structure of Entinostat adapted from www.sigmaaldrich.com and general APD structure from Ottosson et al., 2016.*

Based on the screening of several novel APDs for *CAMP* gene expression using the HT-29 luciferase reporter cell line performed at Karolinska Institutet in Sweden (unpublished data), two APDs candidates, exhibiting immunomodulatory properties were selected for further studies and designated as **HO53** and **HO56** (***Figure 6***).

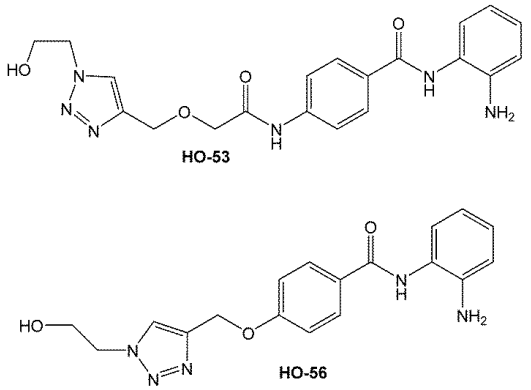


***Figure 6. Chemical structure of HO53 and HO56 compounds.***
*Chemical structures adapted from Myszor et al., 2019.*

## 1.4 Modulation of the epithelial barrier function

Apart from modulation of the innate immunity responses that concentrate on inducting the expression of AMPs by using different molecules, the important aspect of the protective innate immunity is to provide a physical barrier for the pathogens. Therefore, pharmacological modulation of epithelial barrier function, leading to its strengthening and preventing colonization by pathogens gives another opportunity for alternative strategies to fight infections. Vitamin D3 possessing immunomodulatory properties was shown to regulate expression of the claudin-2 tight junction protein and demonstrated the potential to regulate gut epithelial barrier integrity [122]. On the other hand, in the lung epithelial cells administration of vitamin D3 during the differentiation process led to thickening of the epithelial layer, displaying features of squamous metaplasia [104]. This suggest that effect of vitamin D3 on enhancing epithelial barrier might be tissue specific. Another innate immunity inducer, butyrate was also shown to improve intestinal epithelial barrier function in a mouse model of *C. difficile* induced colitis and in a human colon epithelial three-dimensional cell model via activation of HIF-1α pathway. The treatment of human colon epithelial cells with butyrate counteracted the disruptive effect of *C. difficile* conditioned medium and increased expression of TJ proteins claudin-1 and occludin [113]. Similar butyrate effects on the intestinal barrier during LPS-induced inflammation were observed in a porcine intestinal epithelial cell model. Treatment with butyrate increased trans-epithelial electrical resistance (TEER), reduced paracellular permeability and enhanced expression of claudin-3 and -4 but not occludin [123].

Interestingly, the well-known antibiotic azithromycin was shown to strengthen epithelial barrier integrity and this activity of the drug had beneficial effect in the treatment of cystic fibrosis patients [124]. Azithromycin was shown to enhance epithelial barrier integrity by

increasing TEER and to counteract the disruptive effect of *P. aeruginosa* conditioned medium [125]. More recently this study was accompanied by supporting evidences, suggesting azithromycin to work via increased lamellar body formation and affecting epidermal differentiation [126]. However, azithromycin is an antibiotic, therefore prolonged use of azithromycin to strengthen epithelial barrier and to prevent infections is restricted because of the risk for the development of antibiotic resistance. Synthesis of novel compounds that are derivatives of azithromycin without antibiotic properties but retaining the effect on the epithelial barrier function can be beneficial [126]. Moreover, by adding to this combination innate immunity modulatory properties may create a perfect drug candidate to prevent and/or treat infections.

## 1.5 Autophagy as a part of innate immunity

Autophagy is one of the key cellular processes maintaining the balance in cells exposed to constantly changing environment. In general, autophagy is a complex process involving interaction of several different proteins (full names of proteins are included in the list of abbreviations) leading to vesicle formation (***Figure 7***).

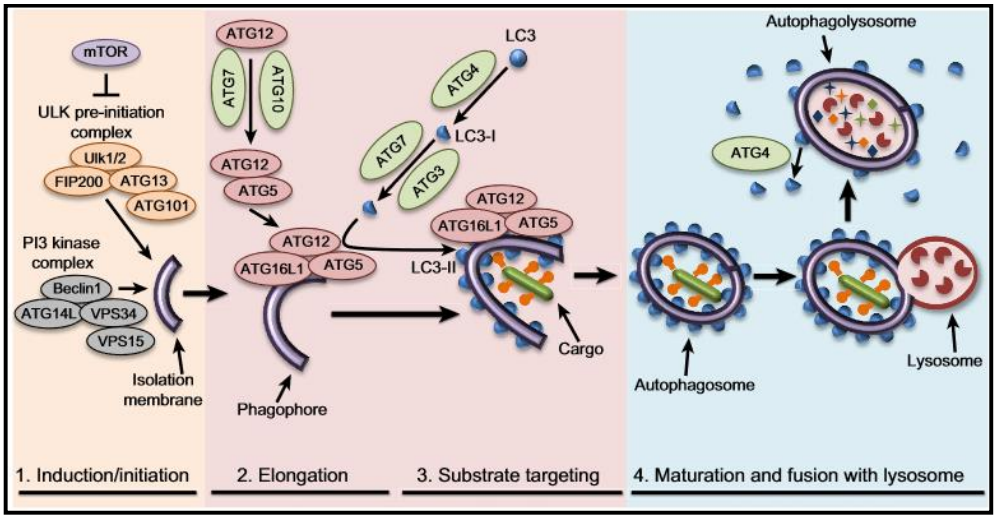


***Figure 7. A schematic illustration of the autophagy process.***
*Autophagy initiation/induction, elongation, substrate targeting, maturation and fusion with lysosome is indicated with representative proteins involved in each step. The image was adapted from Kimmey and Stallings, 2016.*

Autophagy can be activated through pathogen recognition receptors (PRRs), Toll-like receptors (TLRs) and nucleotide-binding oligomerization domain (NOD)-like receptors. Moreover, pro-inflammatory cytokines like IL-1β, interferons and small molecules, e.g. produced by the host such as cyclic-GAMP or even by the pathogen derived cyclic-di-AMP can induce autophagy [127,128]. In response to the stimuli autophagy is initiated by ULK1 complex (composed of ULK1 kinase, ATG13, ATG101 and FIP200 proteins) that phosphorylates PI3KC3 complex I. The PI3KC3 complex (composed of Beclin 1, PIK3C3 also known as VPS34, PIK3R4 or VPS15 and additional proteins) produces PI3P on the membrane of endoplasmic reticulum (ER), leading to the engulfment of the double

membrane structure called phagophore. Next, WIPI2 and DFCP1 proteins bind to the PI3P and the expansion of the phagophore described as the elongation step that further depends on two ubiquitin-like conjugation systems. The first system contains ATG12 activated by ATG7 (E1-like enzyme), transferred to ATG10 (E2-like enzyme) and then bound to ATG5, forming the complex ATG12-ATG5, which binds to WIPI2 through ATG16L1. The second system of the ATG8 family proteins (the name of the group comes from Atg8 protein discovered in yeast) contains several members in mammals, classified into two subfamilies of microtubule-associated proteins 1A/1B light chain 3, referred to as LC3 proteins encoded by *MAP1LC3* genes: LC3A (*MAP1LC3A*), LC3B (*MAP1LC3B*), LC3C (*MAP1LC3C*) and γ-aminobutyric acid receptor-associated proteins (GABARAPs): GABARAP, GABARAPL1, GABARAPL2/GATE-16 conjugated to PE (phosphatidylethanolamine) on the elongating autophagosomal membrane. By using LC3 proteins as an example, the protein pro-LC3 is processed to the cytoplasmic LC3-I by ATG4 and conjugated to PE on the elongating autophagosomal membrane by ATG7 (E1-like enzyme) and ATG3 (E2-like enzyme), forming LC3-II. During the elongation process cargo is sequestered by the elongating autophagosomal membrane. Upon closure, ATG12-ATG5-ATG16L1 dissociate and the external LC3 is removed by ATG4 that facilitates maturation of the autophagosome and the fusion with lysosomes. This leads to the formation of autophagolysosomes and degradation of autophagosomal cargo with further release of degraded molecules to the cytoplasm [128,129]. The rate of autophagic degradation is described as autophagy flux, informing about the amount of substrate degraded by lysosomes [130].

Autophagy plays a major house-keeping function on the cellular level, where it is responsible for the degradation of damaged organelles, unfolded/misfolded proteins and intracellular pathogens [131]. Three different types of autophagy are distinguished: macroautophagy, microautophagy and chaperone mediated autophagy. Macroautophagy is commonly referred to as "autophagy", where the part of the cytoplasm, containing cargo is engulfed by phagophore and further enclosed in the double membrane structure called autophagosome. Macroautophagy was initially recognized as a non-selective process, where the random part of the cytoplasm was engulfed by the phagophore. However, this has changed and macroautophagy is considered more as a selective process, targeting specific substrates, like damaged mitochondria ("mitophagy") or pathogens ("xenophagy"). Microautophagy is the second type of autophagy, where the only part of the cytoplasm is taken up directly by invagination of the lysosomal or late endosomal membrane. The third type is chaperone-mediated autophagy, where chaperones recognize a specific amino acid sequence in proteins designated for degradation. Then the complex is translocated to the lysosomes through binding to the Lamp-2A lysosomal receptor [131]. Autophagy occurs in every cell and the dynamics of the autophagy process varies depending on the cell type. Autophagy process is more rapid in phagocytic cells such as macrophages than in non-phagocytic cells such as bronchial epithelial cells [132].

An important function of the autophagy process in respect to innate immunity is degradation of invading pathogens, when the initial barrier of innate immunity like mucins and AMPs or TJs are not sufficient to halt the pathogen, entering the cells [128]. Some pathogens have developed a variety of different strategies to overcome the first line of defence like *Shigella* spp., downregulating the production of AMPs on the mucosa of infected patients [70] or *Pseudomonas aeruginosa* that disrupts the integrity of tight junctions on airway epithelium [11,12]. Thus, autophagy can be considered as a part of cell

autonomous innate immunity and an intracellular defence mechanism of the last chance for the prevention of pathogen dissemination and progression of infectious diseases [133]. The commonly used cell model to study the role of autophagy in innate immunity are phagocytic professional cells like monocytes/macrophages. However, the importance of autophagy in epithelial cells should be more highlighted due to the vital role of epithelial cells in the first line of host defence. An example underlining the essential role of autophagy in epithelial cells is the study by Benjamin *et al.* showing that gut epithelium recognizes and limits colonization by pathogenic and opportunistic commensal bacteria, like *Salmonella sp.* and *Enterococcus faecalis*, respectively [134]. Another example is airway epithelial cells that can effectively eliminate pathogens like *Pseudomonas aeruginosa* [135,136] or conidia of *Aspergillus fumigatus* [137]. Moreover, the importance of autophagy in human lung is demonstrated in cystic fibrosis patients, where autophagy is impaired due to aggregating Beclin-1. In cell and animal models of cystic fibrosis, this phenotype can be rescued upon Beclin-1 restoration, suggesting a key role of autophagy in lung homeostasis [131,138].

Even though the host innate immunity provides a complex protection from invading pathogens, some of them have evolved and produce virulent factors that enable intracellular survival and growth [127,128]. *Mtb* can serve as an example, which produces variety of virulence factors, e.g. Eis (enhanced intracellular survival) protein, inhibiting autophagy and inflammatory response dependent on ROS generation [139] or PhoP and ESAT-6, which block Rab7-mediated autolysosomal fusion [140]. Another example is *Salmonella enterica* subsp. *enterica* serovar Typhimurium that after translocation to host cells forms *Salmonella* containing vacuole (SCV). Due to the expression of *Salmonella* needle-like Type 3 Secretion System (T3SS-1), SCVs undergo perforation, threatening further bacterial growth. Hence *Salmonella* can repair perforations of the SCVs by utilization of the host autophagic machinery in order to provide intracellular niche for bacterial growth [141]. Furthermore, *Salmonella* can inhibit autophagy by restoring mTOR function through interaction of SCVs with the focal adhesion kinase (FAK) [142]. These are only few examples from the artillery of pathogen virulence factors with known mechanism of action during host-pathogen interaction, affecting autophagy. However, there are more pathogen specific virulence factors with uncharacterized mechanism of action on host cells that needs to be investigated.

The most common treatment methods of infectious diseases are still antibiotics, sometimes used for several months such as in treatment of tuberculosis [143]. With increasing number of infections with multidrug-resistant strains (MDRs) [71], such prolonged treatment will carry a risk of the development of antibiotic resistance [143]. Therefore, alternative therapies, limiting and reducing the time of using antibiotics for treatment of infectious diseases are of interest.

It has been demonstrated that LL-37 has immunomodulatory effect on macrophages infected with *Mtb*, where treatment with synthetic peptide LL-37 led to inhibition of pro-inflammatory responses caused by prolonged infection with *Mtb* [144]. Accordingly, it has been shown that several inducers of LL-37 can also induce autophagy in macrophages. In the study by Yuk *et al.*, it was shown that vitamin D3 induces autophagy by increasing the transcription of Beclin-1 and Atg5 via human cathelicidin stimulated activity of C/EBPβ and MAPK pathways. Moreover, vitamin D3 induced LL-37 expression and its recruitment to the autophagosomes through $Ca^{2+}$/Calmodulin-dependent Protein Kinase Kinase β ($Ca^{2+}$/CaMKK-β) and AMPK pathways that resulted in increased bacterial clearance

[100]. Also the innate immunity inducer PBA induces autophagy through LL-37 mediated activation of the P2X7 receptor present on monocytes/macrophages [145]. A combination of both inducers, vitamin D3 (administered as cholecalciferol) and PBA, have been shown effective in the oral treatment of tuberculosis patients as an adjunctive therapy [106]. Other examples of promising autophagy activating agents to fight *Mtb* infections could be ohmyungsamycins A and B (OMS). Both, are cyclic peptides isolated from the bacteria *Streptomyces sp.*, inducing autophagy through AMPK pathway and reducing pro-inflammatory responses in mouse macrophages. These peptides have been shown efficient in a fruit fly infection model of *Mycobacterium marinum*. However, they also exhibit direct antibacterial activity against *Mtb*, comparable to the antibiotic isoniazid that might lead to selection of resistance [146]. Interestingly, a small molecule called D61 did not exhibit direct activity against *Salmonella sp.*, however it induced autophagy only in macrophages but not in cells of epithelial origin [147]. On the other hand, naturally occurring resveratrol induced autophagy and promoted clearance of *Salmonella sp*. and adherent-invasive *E. coli* (AIEC) in cells of both origin, macrophages as well as epithelial cells. Antibacterial activity of resveratrol was also confirmed in a zebrafish infection model with *Salmonella* [148].

Taken together, autophagy is a key cellular process during physiological and pathological conditions. The basic research on the autophagy process and its regulation during different conditions remain future perspectives for the development of novel strategies in treating infectious diseases.

## 1.6 Innate immunity of airway epithelium in stress conditions caused by mechanical ventilation

Mechanical ventilation (MV) is a life-saving procedure for critically ill patients at intensive care units of hospitals. The need for mechanical ventilation is usually a consequence of the underlying medical conditions, resulting in respiratory failure. In order to provide oxygen and help to remove carbon dioxide, the endotracheal tube connected to the ventilator is placed in the patient´s upper respiratory tract down to the trachea. The ventilator pushes gas, which is a mixture of air and oxygen into the lungs and during expiration it provides positive end expiratory pressure (PEEP) to keep alveoli open and prevent from their collapse [149]. During inspiration, the pressure of the air pushed to the lungs by the ventilator generates positive pressure causing mechanical stress, affecting the airway epithelium of the lower respiratory tract and the alveoli. This may lead to ventilator-induced lung injury (VILI; also known as ventilator-associated lung injury VALI) and in the context of other medical conditions may further exacerbate acute respiratory distress syndrome (ARDS). Respiratory failure caused by acute respiratory distress syndrome is diagnosed based on the Berlin criteria established in 2012, that includes: time of worsening respiratory functions (within a week), origin of the respiratory failure (not connected to the cardiac function), chest radiography or CT scans (presence of lung opacities) and oxygenation level, indicating onset of hypoxaemia. Based on these criteria three levels of ARDS are distinguished: mild, moderate and severe [21]. The development of ARDS usually takes place in the background of other medical conditions, for example sepsis, pneumonia, aspiration, trauma, blood transfusions, pancreatitis and overdose of drugs. Among them, the most common condition is sepsis (32%) and pneumonia (30%) of different origin, either bacterial or viral [150]. The latter is the main global concern in

recent days, due to the global pandemic situation caused by spreading of the new coronavirus SARS-CoV-2, announced in March 2020 by the World Health Organization (WHO) [151]. Infection with SARS-CoV-2 causes disease of the respiratory system named COVID-19, showing main symptoms like dry cough, fever and shortness of breath typical for the other respiratory tract infections [152]. The progression of the disease in several patients, especially from risk groups, causes pneumonia with further respiratory failure, the need of the use of mechanical ventilation and development of ARDS [152,153]. Acute respiratory distress syndrome (***Figure 8***) is developed as a result of increased lung epithelial-endothelial permeability to fluids, proteins and immune cells [21].

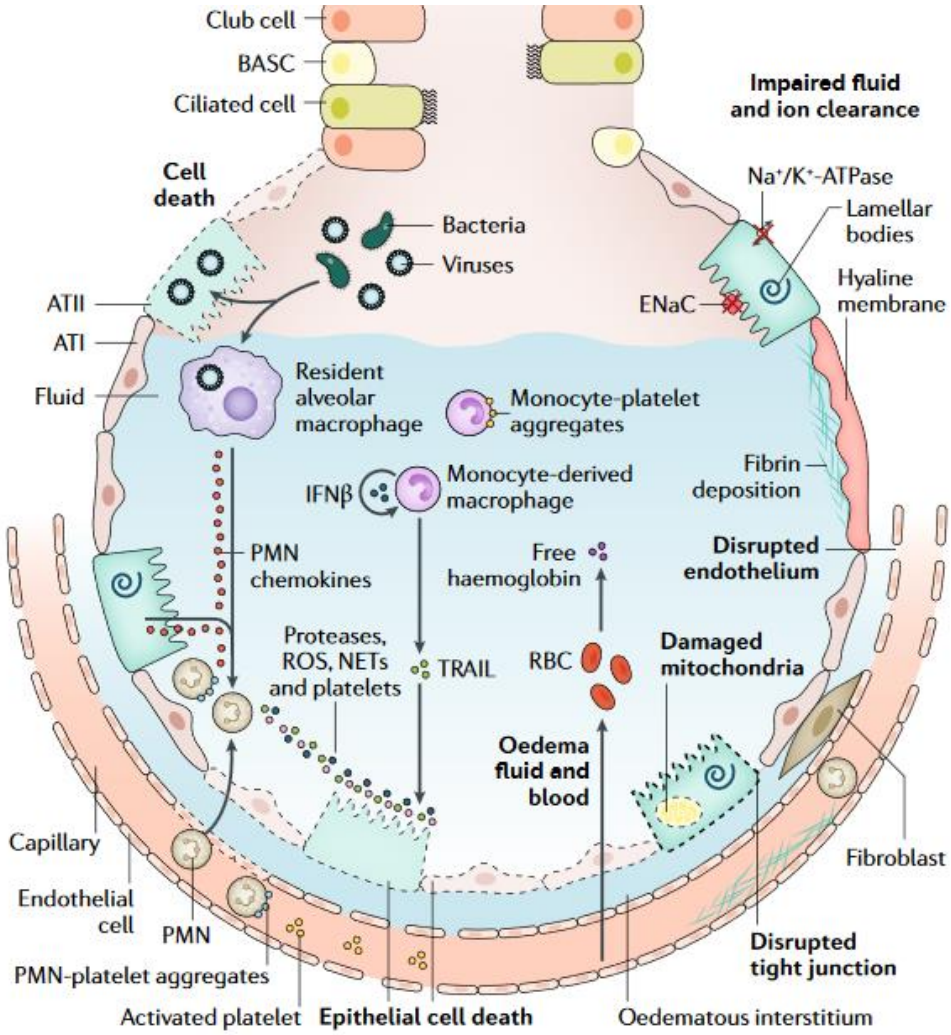


***Figure 8. Alveolar injury in acute respiratory distress syndrome (ARDS).***
*The main events, contributing to the lung tissue injury manifested by disruption of tight junctions and endothelium, epithelial cell death, accumulation of oedematous fluid and blood in the alveolar space with impaired fluid and ion clearance are highlighted in bold. The image was adapted from Matthay et al., 2019.*

The origin of ARDS is the damage of the alveolar epithelium and endothelium followed by activation of alveolar macrophages due to exposition to different factors, e.g. bacteria, viruses, ventilator induced lung injury (VILI) [21]. Then, epithelial cells and pulmonary macrophages release a variety of inflammatory chemokines that contribute to increased endothelial permeability and to recruit neutrophils and monocytes to the alveolar space [21,154]. These events aggravate inflammation because neutrophils release AMPs, proteases, ROS and NETs (neutrophil extracellular traps) to kill pathogens that at the same time cause further epithelial-endothelial barrier damage [154,155]. In addition, monocyte derived macrophages contribute to apoptosis of the alveolar epithelial cells and disruption of the alveolar epithelial barrier integrity through production of IFNβ and subsequently IFNβ-dependent release of TNF-related apoptosis inducing ligand (TRAIL) [21,156]. The inflammatory events in the alveolar space also activate endothelial cells, releasing mediators like angiopoietin 2 and aggregation of neutrophils and platelets, facilitating further endothelial disruption and increased permeability [21,154]. At the same time destabilisation of VE-cadherin by bacterial molecules and inflammatory signals can contribute to increased endothelial permeability [157,158]. The consequence is, oedematous fluid, platelets and erythrocytes accumulation in the lung interstitial space and further translocation to the alveolar space through the disrupted alveolar epithelial layer [21,159]. The release of haemoglobin from erythrocytes causes further destruction of the alveolar epithelium due to oxidative stress [160]. The presence of oedematous fluid and blood cells in the alveoli leads to hypoxaemia that requires mechanical ventilation. Together with the vascular damage, this leads to hypercapnia, an impairment of the removal of $CO_2$, contributing to increased pulmonary dead space, another clinical symptom of ARDS. The respiratory failure due to hypoxaemia and hypercapnia causes further progression of ARDS, leading to impairment of the vectorial ion transport and removal of the excess fluid from the alveoli [21].

Furthermore, mechanical ventilation of patients with ARDS although life-saving may worsen their condition due to VILI. The use of high tidal volumes and airway pressures may generate injury of the alveolar epithelium together with the surrounding endothelium and the distal part of the bronchial epithelium and may increase mortality of patients with ARDS [161]. The paradox of MV in the context of the development of ARDS is that MV is inevitable to rescue life and at the same time may worsen the ARDS due to VILI. This is underlined by the study, where lower tidal volumes and reduced pressure on the airways increase the survival of patients with ARDS, demonstrating clinical importance of VILI [161,162]. Therefore, the main strategy for ventilator treatment of ARDS is to reduce VILI (complete elimination is probably not possible) by using lower tidal volumes to prevent overdistention during inspiration and sufficient PEEP to keep alveoli open during expiration [21,162]. Unfortunately, there are no good monitoring methods to identify these pressure limits for each individual patient, therefore empirical ventilator settings are used [163]. Apart from this, the common approach for treatment of patients with ARDS is based on prone positioning, changing regional distribution of transpulmonary pressure and neuromuscular blockade, limiting patient-ventilator dyssynchronies. In addition to that, fluid management is included to limit fluid filtration from the capillaries to the alveolar space. When these treatments fail, rescue therapies include administration of glucocorticoids [21]. Of note, all these approaches are only recommendations based on empirical observations of clinicians over the years. There is no direct effective pharmacological strategy to treat ARDS, despite of many clinical trials like the one with unsuccessful surfactant replacement therapy [164,165]. Another case is quick diagnosis

and immediate implementation of the therapy when ARDS develops. Usually the diagnosis takes approximately 3 days and the first 7 days from the onset of ARDS is the critical time frame for implementation of the treatment that could limit the time of MV and improve the outcome [21,166,167]. To apply this strategy, the identification of accurate markers for ARDS development is needed. There are several candidates of biomarkers associated with ARDS, among them are: 1) epithelial markers, e.g. receptor for advanced glycation end products (RAGE) and SP-D, 2) endothelial markers, like von Willebrand factor and angiopoietin 2, 3) inflammatory cytokines and chemokines, for instance IL-6, IL-8 and IL-1β, 4) coagulation and fibrinolysis markers, e.g. protein C in plasma, 5) apoptosis markers, like tumor necrosis factor receptor superfamily member 6 (FAS) [21]. However, in practice the use of these markers is limited because before ARDS develops, the underlying clinical conditions such as sepsis and pneumonia, affect the profile of biomarkers and complicates the interpretation of the results. Thus, defining better, more precise markers, allowing prediction of risk for ARDS development and effective pharmacotherapy is urgently needed. Moreover, a limited access to the patient´s lung tissue is a bottle neck for the studies on VILI and ARDS, therefore so much research is performed in animal and *in vitro* models. The latter models are especially common and differentiated lung cells are used to apply static pressure or monolayer lung cells for cyclical stretch [168,169].

# 2 Aims

The main aim of this thesis was to study innate immunity responses in bronchial epithelium upon different stimuli. The first part of this thesis is based on two specific aims, evaluating effect of the novel compounds aroylated phenylenediamines (APDs) on innate immunity responses and barrier function in bronchial epithelium (**Paper I**) and autophagy (**Paper II**). The second part of this thesis concentrated on studying innate immunity responses in mature bronchial epithelial cells subjected to mechanical stress generated by cyclical pressure air-liquid interphase device (CPAD) and mimicking ventilator induced lung injury (VILI) (**Paper III**).

The three projects of this thesis were conducted based on the three following specific aims:

1. Evaluation of aroylated phenylenediamines (APDs) as novel inducers for modulation of innate immunity responses linked to increased expression of antimicrobial effectors and enhanced epithelial barrier integrity (**Paper I**).

2. The effect of aroylated phenylenediamine HO53 on autophagy induction as a part of innate immunity defense system in bronchial epithelium by defining molecular pathways responsible for this effect (**Paper II**).

3. Evaluation of innate immunity responses in mature bronchial epithelial cells subjected to mechanical stress generated by cyclical pressure air-liquid interphase device (CPAD), mimicking ventilator induced lung injury (VILI) (**Paper III**). In addition, influences of the aroylated phenylenediamine HO53 on stressed cells were evaluated.

# 3 Technical consideration of methodology aspects

All reagents and methods used for the preparation of this doctoral dissertation are described in the materials and methods chapter of each article/manuscript included in the thesis, allowing for replication of each experiment. In this chapter, I will present and comment on some of the technical challenges and solutions followed by results included in this thesis. First, I will comment on air-liquid interphase (ALI) culture of bronchial epithelial cells and related to these experiments consideration of biological/technical replicates. Next, I will describe technical considerations connected to detection of the LL-37 peptide by Western blotting. Then, I will briefly mention the discrepancies between Western blotting and confocal imaging of the disruption of tight junctions (TJs). This will be followed by the description of challenges linked to infection studies of human bronchial epithelial cells.

## 3.1 Utilization of air–liquid interphase cultures of human bronchial epithelial cells

Two human bronchial epithelial cell lines BCi-NS1.1 (BCi) and VA10 were utilized for the experiments, verifying the activity of the novel inducers aroylated phenylenediamines (APDs) on antimicrobial responses, maintaining epithelial barrier integrity and induction of autophagy [170,171]. Both cell lines retain basal/stem like character, where BCi cells were immortalized with retrovirus, expressing human telomerase (hTERT) and VA10 with E6/E7 viral oncogene. The differentiation of the human bronchial epithelial cells BCi and VA10 in air-liquid interphase (ALI) culture was performed as previously described [170,171] (***Figure 9***), except for 8% $CO_2$ for the first 5 days of ALI culture of BCi cells. Briefly, monolayer cells were seeded at different densities, $4.5\text{-}5\times10^5$ of BCi (up to passage 21) and $2\text{-}2.5\times10^5$ of VA10 cells (below passage 20) on 12-well trans-well inserts with 0.4 µm porous membranes coated with collagen IV from human placenta for 1 h, mimicking basal membranes. BCi cells were seeded in Dulbecco´s Modified Eagle Medium F-12 Nutrient Mixture (DMEM/F-12) supplemented with 10% FBS and VA10 cells in bronchial/tracheal growth medium (BEGM). Both cell lines were maintained in the presence of the antibiotics penicillin (50 U/ml) and streptomycin (50 µg/ml). The next day medium in BCi culture was replaced with medium supplemented with 2% UltorserG (UG) and after 2-3 days post-seeding ALI culture was established. VA10 cells were maintained in BEGM medium for 2 days and then DMEM/F-12 with 2% UG was added for the next 3-4 days before ALI was established. ALI was established by aspiration of the medium from the upper chamber and exposition of the cell layer to air. Medium in the lower chamber was replaced every 2-3 days.

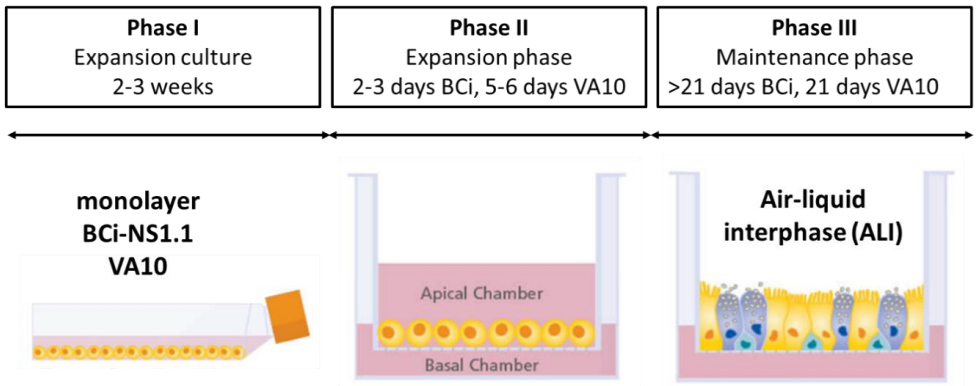


***Figure 9. Schematic presentation of the air-liquid interphase culture of human bronchial epithelial cells.***
*The timeline for BCi and VA10 shows the time needed to obtain differentiated cells for further experiments. Adapted and modified from www.stemcell.com/products/pneumacult-ali-medium.*

One of the markers for the cell differentiation in air-liquid interphase culture is the formation of tight junctions (TJs) between adjacent cells. Along with the cell differentiation, the tight junctions are formed, which results in increase of trans-epithelial electrical resistance (TEER) and this is frequently used as a parameter for the assessment of the differentiation status of the cells. In the original article describing the generation and the differentiation potential of the BCi cells, the ALI culture was maintained up to 40 days and the plateau phase for the TEER was observed at day 31. In my experiments, ALI culture of BCi cells was maintained until the TEER reached 800-1000 $\Omega \times cm^2$ that usually took place between 3-4 weeks of ALI culture and corresponded to the values from the original article by Walters *et al.* [170]. In addition, in the Paper II (as a manuscript; Supplementary figure 1), the MUC5AC (secretory cells) and acetylated α-tubulin (ciliated cells) markers were detected, confirming the differentiated status of the cells. On the contrary, VA10 cells were always maintained 21 days in ALI culture, where TEER values reached approximately 400 $\Omega \times cm^2$, corresponding to TEER values from the original article by Halldorsson *et al.* [171].

Another technical aspect connected to the utilization of ALI cultured cells concerns the experimental study design, whether the separate ALI inserts with differentiated cells should be treated as technical or biological replicates. The population of monolayer cells were seeded on trans-well filters (inserts), which might indicate that a single insert with differentiated cells should be treated as a technical replicate. However, the cells growing in the same ALI culture but on different inserts after the differentiation never reached the same TEER values and the number of the particular cell types, e.g. ratio of ciliated cells versus mucous cells could vary between the inserts. For that reason, we consider the differentiated cells from the same ALI culture but growing on different trans-well inserts as biological replicates. The results presented in the thesis are from at least two independent experiments, otherwise it is indicated in the figure legend and treated as a pilot study.

## 3.2 Detection of LL-37 peptide by Western blotting

Expression of LL-37/pro-LL-37 in cell culture media was investigated by Western blotting and the synthetic peptide (Innovagen) was used as a positive control. Proteins were separated on 4-12% gradient NuPAGE Bis-Tris gels (Invitrogen) in MES buffer (Invitrogen) for 1 h 30 min at 120 V and 275 mA on ice. Next, separated proteins/peptides were blotted on a PVDF membrane and the membrane was incubated in 10% skimmed milk in TBS-T for 1 h at room temperature. To identify LL-37/pro-LL-37 peptide, rabbit polyclonal primary antibodies from Innovagen were incubated overnight at 4 °C in 5% milk in TBS-T. The first Western blotting was successful, showing single pro-LL-37 band with correct molecular weight. Once the experiment was repeated, the molecular weight of specific bands for LL-37 pro-form was doubled in all samples, whereas the synthetic peptide showed correct molecular size, indicating that the protocol for sample preparation has to be optimized to avoid possible dimerization formation. After six months of protocol optimization (testing different loading buffers, temperatures for sample denaturation and electrophoresis) all possibilities for dimer formation were ruled out and only the primary antibodies needed verification. In our laboratory we used rabbit polyclonal antibodies against LL-37 from Innovagen used in previous studies by Kulkarni *et al.* [172] as well as in the first experiment. When the primary antibodies were changed to mouse monoclonal anti-LL-37 described previously by Yoshio *et al.* [173], specific bands had the correct molecular weight in the same sample material as used with the polyclonal antibody. The reason for the doubled sized bands recognized by the rabbit polyclonal antibodies was because of batch-to-batch differences. Polyclonal antibodies recognize different epitopes and represent a mixture of antibodies derived from multiple B-cells as a result of the immune response to the antigen. This is the reason for the vulnerable batch-to-batch differences unlike monoclonal antibodies derived from one parental B-cell clone.

## 3.3 Analysis of occludin disruption upon *Pseudomonas aeruginosa* (PAO1) conditioned medium challenge

In the first article the disruption of TJs integrity was presented as a result of PAO1 conditioned medium challenge and this effect was counteracted by pre-treatment with HO53 (Paper I, Fig. 6). Occludin upon PAO1 conditioned medium challenge was visualized by confocal imaging and showed disorganized, disrupted phenotype at 6 h post challenge. While analysing the occludin level by Western blotting at the same time point, the band corresponding to the main isoform was faintly detected. However, the full-length Western blot (Paper I, Supplementary figure S9) showed degradation/processing products visualized by confocal imaging as a disrupted phenotype. This observation encourages for consideration of the way how Western blots are presented in articles. Presenting of full-length Western blots in articles are often not possible due to graphical limitations but from a technical point of view, the requirement of enclosing full-length Western blots as supplementary figures should be a rule for every journal.

## 3.4 Infection of human bronchial epithelial cells

Undifferentiated BCi cells were pre-treated with HO53 (75 µM) for 24 h and infected with *Pseudomonas aeruginosa* PAO1 (Paper I, Fig.4) using MOI (multiplicity of infection) ~40:1 (***Figure 10***).

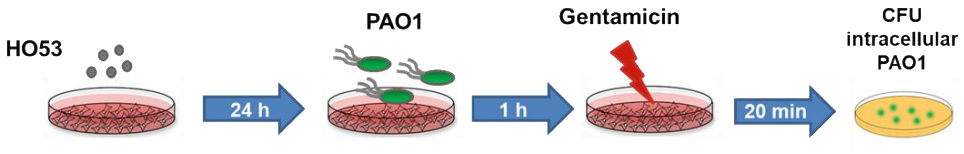


***Figure 10. Schematic presentation of the antimicrobial assay.***
*This method was used for infection of undifferentiated BCi cells with Pseudomonas aeruginosa PAO1.*

The high number of bacteria used for infection in this study was based on the literature, indicating that the MOI should be higher than in the case of infection of phagocytic cells, e.g. MOI with the *P. aeruginosa* strain PAK for macrophages/monocytes was 10:1 [174] to enable the count of intracellular bacteria using serial dilutions. For that reason, the MOI ~40:1 used in these experiments refers to studies using *P. aeruginosa* at: 1) MOI 50:1 for infection of A549 alveolar epithelial cells [175] and CFTE29o$^-$ cells derived from human tracheobronchial epithelium carrying a ΔF508 mutation of CFTR [176] and 2) MOI 30:1 was used for infection of BEAS-2B, normal human bronchial epithelial cells [177]. After 1 h incubation, the remaining extracellular bacteria were eliminated by gentamicin treatment (100 µg/ml) for 20 min. Then, cells were washed three times, lysed in 0.1% Triton X-100/$H_2O$ (v/v) and after serial dilutions plated on LB agar plates for CFU (colony forming units) counting. The selected MOI ~40:1 resulted in experimentally confirmed intracellular bacterial load of ~$1\times10^4$ PAO1.

# 4 Results and discussion

In this chapter I will summarize and discuss results of this PhD project, concentrating on modulation and regulation of innate immunity responses in bronchial epithelium during different conditions. The main scope of this work was to study modulation of innate immunity responses by the novel compounds aroylated phenylenediamines (APDs) (**Paper I**). This part was continued by evaluation of the effect of the selected APD compound HO53 on autophagy induction (**Paper II**). The third part of this PhD project focused on regulation of innate immunity responses in mechanically stressed differentiated (polarized) lung epithelial layers in a newly established cyclical pressure air-liquid device (CPAD) modelling ventilator induced lung injury (VILI), contributing to acute respiratory distress syndrome (ARDS) development (**Paper III**) and creating a drug testing platform for treatment of VILI and ARDS.

**Paper I**

In the first article we studied the effect of the two novel inducers HO53 and HO56 on innate immunity responses and epithelial barrier integrity. Both compounds belong to the group of aroylated phenylenediamines and are derivative of Entinostat, a cytotoxic HDAC inhibitor, tested in cancer therapy [118]. Entinostat was demonstrated to induce *CAMP* gene expression in colon epithelial cells [89] and to improve the outcome of *Shigella* infected rabbits [90]. Cytotoxicity and viability assays showed that the two APD compounds HO53 and HO56 were less toxic than Entinostat (Supplementary Figure S5) and induced *CAMP* gene expression in a dose-dependent manner in bronchial epithelial cells BCi-NS1.1 (BCi) and VA10 (Figure 1, Supplementary Figures S3 and S4). Both cell lines retain basal/stem cells like character and can be utilized for *in vitro* research as monolayer undifferentiated cells and as polarized differentiated in air liquid interphase (ALI) culture cells resembling *in vivo* environment [170,171]. To evaluate the effects of the APDs, we mainly used undifferentiated monolayer BCi cells, and when indicated BCi cells in ALI culture. In respect to cytotoxicity and the lowest concentration that effectively induced *CAMP* gene expression, we selected 75 µM for HO53 and HO56 for further experiments. The highest level of *CAMP* expression was reached after 24 h of treatment BCi cells and lasted until 48 h for both compounds (Figure 1). Interestingly, HO53 and HO56 showed synergistic effect in induction of *CAMP* expression with the previously described inducer vitamin D3 (Figure 1). There was no cooperation in *CAMP* induction with the inducer PBA, which might indicate that PBA and HO53 are activating *CAMP* induction through the same signalling cascade. Consequently, the synergy with vitamin D3 was observed in Western blot analysis of pro-LL-37 secreted to the culture medium after 24 h stimulation (Figure 1). APDs solely increased pro-LL-37 level in the culture medium similar to PBA, which was lower in comparison to vitamin D3 (Figure 1). Normally, cathelicidin antimicrobial peptide LL-37 is produced as an inactive pro-form secreted to the extracellular environment, and undergoes processing by proteases to active LL-37 peptide [39]. As observed in our study, neither BCi, nor previously described VA10 cells [172] process pro-LL-37 to its active form, which is a limitation of this model. However, LL-37 is one of several antimicrobial effectors in our model system, hence, to obtain better insight into induction of antimicrobial activity by APDs, expression of additional

antimicrobial components was analyzed. Interestingly, HO53 and HO56 induced the expression of additional antimicrobial effectors on RNA and protein levels such as lipocalin 2, and β-defensin 1 (Figure 2). This indicates that APDs induce expression of several antimicrobial effectors. Both HO53 and HO56 induced pro-inflammatory responses in undifferentiated BCi cells measured on RNA and protein levels of IL-8 and TNFα. The level of IL-8 was increased in cell culture medium after 24 h and was further accompanied by increase in TNFα level after 48 h (Figure 3). Overall, these experiments suggest that HO53 and HO56 induce the production of antimicrobial effectors and initiate a pro-inflammatory response in undifferentiated BCi cells. Therefore, we evaluated APDs induced responses in an antimicrobial assay designed to measure bacterial translocation to the cytoplasm of the cells (Figure 4). In this experimental setup, time for infection was 1 h and 20 min for elimination of extracellular bacteria by gentamicin and then intracellular bacteria were counted. By using high MOI, we confirmed the intracellular bacterial load to ~$1\times10^4$ PAO1. This approach included minimal risk of influencing bacterial count by other cellular mechanisms like autophagy [128]. Both APDs reduced the number of *Pseudomonas aeruginosa* PAO1, entering BCi cells without displaying any direct microbicidal activity on bacterial viability and growth. This suggested that reduced number of intracellular bacteria was a consequence of antimicrobial effectors produced by the cells and it was not connected to increased production of reactive oxygen species involved in the directed killing of the pathogen (Supplementary Figure S6) [7]. Further, HO53 and HO56 modulated innate immunity responses by enhancing expression of genes encoding cathelicidin, lipocalin 2, β-defensin 1, S100A8 and lysozyme in differentiated BCi cells in ALI culture (Figure 5). Increased expression of S100A8 and lipocalin 2 was also confirmed on protein level. In comparison to monolayer BCi cells, HO53 and HO56 did not induce a pronounced pro-inflammatory response in ALI culture of BCi cells, since only *IL1B* gene expression was increased after treatment with HO53 for 24 h (Supplementary Figure S7). This indicates different responses dependent on the differentiation status of the cells and suggests that the responses to APDs treatment may vary between different tissues. Similarly to the mechanism of vitamin D3 proposed by Carlberg's group [96], this indicates that epigenetic mechanisms may be involved. Transient induction of antimicrobial components and pro-inflammatory responses by APDs has to be tightly controlled in order to fight pathogens and may be beneficial for host-directed therapy. Furthermore, detailed insight into the modulation of especially pro-inflammatory responses would be needed since this might limit APDs application for patients suffering from inflammatory disorders like inflammatory bowel diseases or auto-immune diseases such as psoriasis.

In the continuation we selected the APD compound HO53 to evaluate effects on epithelial barrier integrity by counteracting disruptive effect of PAO1 conditioned medium. This medium containing PAO1 virulence factors is known to disintegrate junctional complexes (Figure 6) [11]. Pre-treatment of ALI BCi cells with HO53 reduced the decrease of TEER mediated by PAO1 conditioned medium and maintained integrity of the tight junction proteins occludin and ZO-1, as visualized by confocal imaging. The counteraction of the disruptive effect was also shown by monitoring the level of the main occludin isoform on Western blot at different time points of the challenge. This effect could be mediated by a broad activity of HO53 that increased the expression of some TJs proteins like occludin. In general, the effect of HO53 on epithelial barrier integrity is resembling the effect of the previously described drug azithromycin [125]. The difference is that azithromycin did not induce expression of tight junction proteins, instead led to their processing and possibly

reorganization [125]. More recently, this was accompanied by a study, showing that azithromycin increased lamellar body formation and affected epidermal differentiation [126]. Despite of using different cell lines in the studies, the second main difference was the time of the compound exposure. Azithromycin was applied for three weeks of differentiation, whereas HO53 was applied only three days before the challenge. Considering the fact that azithromycin is an antibiotic, prolonged use of azithromycin to strengthen epithelial barrier and to prevent infections is limited because of the risk of the development of antibiotic resistance. Therefore, utilization of the HO53 compound, which does not display antibiotic properties and affects the epithelial barrier function could be beneficial. In addition, the innate immunity modulatory properties of HO53 are interesting for drug development and relevant to prevent and/or treat infections.

Similar to Entinostat, the mechanism of *CAMP* induction by HO53 in undifferentiated BCi cells was linked to the STAT3 and HIF-1α transcription factors (Figure 7) [89]. By using the STAT3 inhibitor Stattic, *CAMP* gene expression was reduced in a dose-dependent manner. Treatment with HO53 activated STAT3 by increasing phosphorylation of STAT3 at Tyr705 after 4 to 8 h and by increasing the expression of HIF-1α after 24 h that also have been shown for Entinostat [89]. Although, HO53 did not affect acetylation of STAT3 at Lys685, additional post-translational modifications of STAT3 should be considered. This study present STAT3 as an important transcription factor linked to innate immunity and possibly to the regulation of the epithelial barrier integrity in gut epithelium, where STAT3 has been shown to regulate the expression of ZO-1 and occludin [178].

In summary, APDs could be considered as potential candidates for host-directed therapy of infectious diseases, limiting the development of bacterial resistance to antibiotics. Further studies on the mechanism of modulating the signalling cascades by APDs and *in vivo* tests, evaluating their efficiency for the treatment of infections would be needed.

**Paper II**

The second article presented as a manuscript (in preparation) is a continuation of the work in **Paper I**. After identifying HO53 and HO56 as novel inducers of innate immunity, enhancing epithelial barrier, we evaluated the effect of HO53 on autophagy induction in bronchial epithelium. Autophagy can be considered as a part of innate immunity for effective pathogen elimination when surface defense mechanisms are not sufficient. In case of successful translocation of pathogens to host cells, autophagy is the last defense line, preventing dissemination of pathogens to the local tissues. This is crucial especially for non-phagocytic epithelial cells, forming epithelial surfaces that provide a barrier for pathogens and protect the inner tissues from intruders [133,179]. Several pathogens can effectively escape innate immunity defenses and be translocated to the host cells, inhibiting or impairing the autophagy process by production of different virulence factors. In some cases, this might lead to persistent infections, requiring extended antibiotic treatment. Another problem are infections with multidrug resistant bacteria, since access to effective antibiotics is limited [128]. Therefore, induction of autophagy together with enhancement of innate immunity barrier might be beneficial in the combat against pathogens [180].

In this manuscript, we evaluated induction of autophagy by HO53 and tried to define activated molecular pathways responsible for this effect. We utilized the most common markers to monitor autophagy induction. One of them is the autophagosomal marker LC3B. LC3B is present in the cytosol (referred to as LC3B-I) or lipidated in the

auotphagosomal membrane (referred to as LC3B-II). It is possible to distinguish between LC3B-I and LC3B-II as the proteins migrate at a different speed in a SDS-PAGE gel. Furthermore, LC3B-II can be detected as puncta using fluorescent microscopy, representing autophagosomes. Another marker that we used for autophagy was p62, an adaptor protein, linking cargo to the inner autophagosomal membrane. To monitor the autophagy flux, Bafilomycin A1, an inhibitor of autophagosome-lysosome fusion, was used to evaluate lysosomal degradation of the autophagosomal cargo described as autophagy flux [130].

We analyzed phenotypic changes, indicating autophagy induction by HO53 through monitoring LC3B processing by Western blot, LC3B puncta by confocal imaging and presence of autophagosomes by transmission electron microscopy (TEM) (Figure 1). We observed HO53 dose dependent accumulation of LC3B-II, indicating induction of autophagy in differentiated BCi in ALI culture but not in undifferentiated monolayer cells. Similar phenotype of autophagy induction was observed in VA10 cells, where increased LC3B processing was only observed in differentiated cells (Supplementary Figure 1). To analyze autophagy flux, we utilized Bafilomycin A1, an inhibitor of autophagosome-lysosome fusion and analyzed the effect on LC3B as well as p62. The analysis of p62 degradation did not show active autophagy flux (Supplementary Figure 1), which might be a result of transcriptional and translational regulation of *SQSTM1*/p62 level, respectively. Although p62 is a marker for autophagy flux, different mechanisms within the cell might affect the levels of p62 protein, depending on the conditions and the types of cell or tissue [130]. An example is muscle cells, where *SQSTM1* gene expression is increased during exercise in nutrient deficient conditions, leading to misinterpretation of p62 degradation on the protein level [181]. Next, when comparing HO53 treatment without and in co-treatment with Bafilomycin A1, autophagy flux in ALI BCi cells did not seem to be increased, suggesting that additional triggers might be needed to complete the autophagy clearance. Another possibility is that cells in this model reached the maximum rate of autophagy flux or are lacking some components to complete this process. Further investigation by using an additional method to evaluate autophagy flux such as degradation of long-lived proteins (LLP) would be needed [130]. The presence of fluorescent LC3B puncta is a widely used marker for autophagy induction because LC3B is normally dispersed in the cytoplasm and forms aggregates that are visible as puncta upon autophagy induction [130]. Interestingly, the treatment with HO53 appears to increase the number of LC3B puncta in ALI cells, forming small clusters, making them unable to quantify. Therefore, in the next step we evaluated if the clusters of LC3B puncta possibly occur in specific cell types of differentiated cell layer in ALI. However, clusters of LC3B puncta were not localized in a cell type specific manner and not restricted to the mucous or ciliated cells (Supplementary Figure 1). Next, by using transmission electron microscopy, we investigated whether treatment of BCi cells in ALI with HO53 affects formation of autophagic structures. We confirmed the presence of fully formed autophagosomes, double membrane vesicles identified in co-treatment with Bafilomycin A1, indicating that the treatment with HO53 did not impair this process. Together, these phenotypic changes indicate that HO53 stimulates autophagy through promotion of autophagosome formation, however without further increase in the autophagy flux. The effect of HO53 on autophagy in our model seems to be similar to the mechanism of AMPK, promoting autophagy by priming autophagy kinases upon detection of bacteria-secreted outer membrane vesicles independently on bacterial invasion. This mechanism prepares cells for a fast response in

case of bacterial invasion and facilitates rapid autophagy clearance of invading pathogens [182].

To understand the molecular signalling behind the observed phenotypic changes, indicating autophagy induction, we performed RNA sequencing analysis of HO53 in differentiated BCi cells at 4, 8 and 24 h (Figure 2 and Supplementary Figure 2). We observed a broad effect of HO53 on gene expression over time. Gene set enrichment analysis (GSEA) revealed that HO53 affects many pathways including those directly related to autophagy induction such as reactive oxygen species (ROS), glycolysis, PI3K-AKT-mTOR, mTORC1 and IL6-JAK-STAT3. In differentiated BCi cells we did not observe post-translational modifications of STAT3 (Supplementary Figure 3), a transcription factor known to be also involved in induction of autophagy [183]. Therefore, we concentrated on the verification of other pathways indicated by GSEA, contributing to autophagy induction like mTOR inhibition and further activation of AMPK (Figure 3) [184]. Interestingly, in the RNA sequencing analysis we observed a prominent increase in expression of the catalytic subunit of AMPKα, which was confirmed by qRT-PCR and increased phosphorylation of AMPK, indicating autophagy induction. We also analyzed a downstream target of mTOR and did not detect a significant decrease in the phosphorylation level of S6K1. Recently, it was shown that both pathways might be regulated by galectins as a result of lysosomal membrane damage [185,186]. Interestingly, in our RNA sequencing data we observed and confirmed by qRT-PCR increased expression of *LGALS9* encoding galectin 9. Therefore, our hypothesis was that increased production of galectin 9 in the presence of an uncharacterized trigger (like disruption of endolysosomal membrane) might be responsible for the activation of AMPK pathway and consequently affect mTOR. However, the increase of galectin 9 at the protein level was not confirmed (Supplementary Figure 3).

Furthermore, we analyzed nuclear translocation of TFEB (Figure 4) from the family of MiT/TFE transcription factors known as “a master regulator of lysosomal function and autophagy” [187]. In normal conditions TFEB is phosphorylated mainly by mTORC1 and extracellular signal-regulated kinase 2 (ERK2 also known as MAPK1), resulting in cytoplasmic localization of TFEB. Upon different stimuli such as low nutrient accessibility or lysosomal stress, leading to mTORC1 and ERK2 inhibition, TFEB is dephosphorylated by the calcium activated phosphatase calcineurin. Then, TFEB is translocated to the nucleus, where it activates its own expression and expression of autophagy related and lysosomal genes [187]. In our study, we observed nuclear translocation of TFEB between 8 h and 24 h that might result in induced expression of the selected autophagy related genes *ATG* and *MAP1LC3*, encoding proteins associated with formation of autophagosomes at early phase of autophagy. The complexity of the HO53 mechanism related to activation of TFEB is highlighted by the fact, that TFEB nuclear translocation is a late event (between 8 h and 24 h), while expression of autophagy related genes was also affected at earlier time points. Moreover, no further increase in the autophagy flux might be explained by downregulated expression of some autophagy related genes and negatively correlated with enrichment in autophagy-lysosomal pathway. This also indicates that additional mechanisms, partially interacting with the effect of TFEB might be involved.

Further, the broad effect of HO53 on gene expression observed in RNA sequencing analysis and the fact that HO53 is a derivative of Entinostat, an HDAC inhibitor, suggests that HO53 may promote autophagy induction also on epigenetic level by modulation of chromatin accessibility. Several histone modifying epigenetic enzymes, e.g. G9a, EZH2,

USP44 or CARM1 are important for modulation of autophagy [188]. We observed that HO53 modulates expression of some genes encoding histone modifying epigenetic enzymes such as G9a - H3K9 methyltransferase, EZH2 - H3K27 methyltransferase and USP44 - H2BK120 deubiquitinase (Figure 5). In our BCi cell model in ALI culture, changes in the expression of histone modifying enzymes might contribute to the autophagy induction by decreased H2BK120Ub status as a result of increased *USP44* expression and reduced H3K27me3 status caused by downregulation of *EZH2* expression. The reduced expression of *EZH2* was additionally confirmed by the expression pattern of *TSC2* gene, a downstream target of EZH2 involved in mTOR regulation. We observed decreased H2BK120Ub/total H2B levels at 8 h, indicating autophagy stimulation on the chromatin level followed by increased expression of *USP44* at 24 h.

Despite of changes in expression of *EZH2*, we did not observe any changes in levels of H3K27me3/total H3 (Supplementary Figure 5) that we considered mainly as an inhibitory histone mark [188]. Overall, we showed that HO53 stimulated autophagy on the chromatin level by modulation of histone epigenetic marks. Considering the fact that regulation of the chromatin state is recognized as a dynamic process, reported epigenetic changes of histone modifications and expression of histone modifying enzymes are rather late events in our BCi cell model in ALI culture.

Overall, this work presents a novel effect of the drug candidate HO53, a representative of the APD compounds that could be used to promote autophagy induction in mature bronchial epithelial cells. Characterization of molecular pathways responsible for HO53 triggered autophagy induction underlines involvement of previously well-characterized autophagy regulating pathways like AMPK. It also highlights the epigenetic regulation of the chromatin state that might result in autophagy induction. Together with previously shown properties of HO53 such as enhancing epithelial barrier integrity and induction of AMPs, the use of HO53 might have implications for prevention and/or treatment of infectious diseases, especially caused by pathogens, affecting initiation of autophagosome formation. This can limit the use of antibiotics and help to reduce the selection of antibiotic resistant strains. Furthermore, we are working on the optimization of bacterial infections of ALI cultures as a continuation of this study, to evaluate HO53 as an effective promoter of autophagy induction for pathogen elimination. Unlike monolayer cells, the infection of differentiated in ALI culture polarized bronchial epithelial cells with *Pseudomonas aeruginosa* is a challenge because of the low intracellular bacterial count. Currently, we are considering another pathogen for infection studies for more efficient entrance to the cytoplasm. The count of intracellular bacteria accompanied by confocal imaging of bacteria co-localized with LC3B or lysosomal-associated membrane proteins (LAMPs) would strengthen this work. It is possible that the presence of bacteria could be the trigger needed for autophagy flux after priming with HO53.

**Paper III**

In **Paper III** my main focus was on innate immunity responses in mature bronchial epithelial cells subjected to mechanical stress generated by cyclical pressure air-liquid interphase device (CPAD). The CPAD can mimic ventilator induced lung injury (VILI) by generating cyclical stress on the differentiated lung cells. The combination of both parameters was innovatory for this project because in previously described models only static pressure was applied to differentiated cells in ALI culture [168] and only cyclical stretch on monolayer cells [169]. This was a limitation of the *in vitro* models in

comparison to animal models [189,190]. These, mainly rodent, models do not offer insight into responses in human cells, and differences between species must be taken into consideration. The design and construction of CPAD for mechanical stress of differentiated cells in ALI culture did overcome these limitations and allowed for improved settings relevant to VILI and ARDS. The development of the novel CPAD also allows for defining more accurate markers and hallmarks of VILI and ARDS, analyzing innate immunity responses and can provide a platform for drug testing.

The technical aspect of CPAD construction (Figure 1 and S1) was led by the PhD student Jón Pétur Jóelsson and in collaborative project we concentrated on characterization of responses in human differentiated lung cells in ALI culture subjected to mechanical stress generated by CPAD. The included analysis of phenotypic changes of the cells, VILI/ARDS markers and mechanosensitive biomarkers, innate immunity and pro-inflammatory responses caused by mechanical stress made by CPAD.

The main strategy for treatment of ARDS is to reduce VILI (complete elimination is not possible) by using lower tidal volumes (6 ml/kg) that has to be adjusted individually to avoid peak inspiratory pressure, extending to 30 cm $H_2O$ to prevent tidal overdistention [153,162], and sufficient high PEEP to keep alveoli open during expiration [21]. Based on the clinical data, in this study we used the following parameters: two different peak inspiratory pressure values 22 cm and 27 cm $H_2O$, PEEP 5 cm $H_2O$ and frequency for the cyclical stretch 0.27 Hz (16 beats-per-minute). Two human bronchial epithelial cell lines BCi-NS1.1 (BCi) and VA10 differentiated in ALI culture were utilized to evaluate the effects of mechanical stress generated by CPAD. Apart from alveolar epithelium, distal bronchial epithelium is also affected by mechanical stress during mechanical ventilation (MV) and the shedding of bronchial epithelial cells is observed in the pathogenesis of ARDS [163]. Both cell lines are well-characterized and frequently used by our research group, therefore we decided to use them for the initial studies on CPAD.

Mechanical stress (27 cm $H_2O$) generated by CPAD caused morphological changes in ALI epithelial layers showed as accumulation of actin stress fibres (VA10 cells) and disrupted phenotype of the cell layers visualized in TEM (VA10 and BCi cells) (Figure 2 and S2). Next, we concentrated on the analyses of gene expression for selected VILI/ARDS markers, antimicrobial effectors and pro-inflammatory chemokines/cytokines in differentiated VA10 cells. Among previously described VILI/ARDS markers [21,191,192], we observed significant increase in vascular endothelial growth factor A (*VEGFA*) gene expression for both pressure values and surfactant protein B (SP-B protein encoded by *SFTPB* gene) for 22 cm $H_2O$ (Figure 3) with no clear increase on the protein level as SP-B is mainly produced by alveolar type 2 cells (Figure S6). The *SFTPB* gene was identified as one of the first genetic markers for increased ARDS susceptibility because of a mutation in the *SFTPB* gene that caused neonatal respiratory distress syndrome [191]. The increased protein level of SP-B released from injured alveolar epithelial cells is a biomarker for the exudative phase of ARDS [163,193]. The protein VEGFA is produced by alveolar epithelial cells, macrophages, neutrophils and platelets, regulating endothelial function by increasing microvascular permeability [194]. Increased endothelial permeability is typical for ARDS and hence high level of VEGFA was detected in plasma of ARDS patients [195]. Despite increased level of VEGFA in plasma, indicated as a risk factor for ARDS development [191], low levels of VEGFA were detected in the lung tissue of ARDS patient with high mortality rate [194]. This might explain increased apoptosis of endothelial cells and impaired blood flow in the lung [194]. Moreover, it highlights that the

course of VEGFA level is dynamically changes in the onset and during ARDS. Next, the expression of the receptor for advanced glycation end products (*RAGE*) was observed decreased (Figure 3), which is opposite to the increased serum RAGE levels observed in patients with ARDS caused by direct lung injury [21]. There was no difference in expression of hypoxia inducible 1α (*HIF1A*) (Figure 3), a transcription factor, regulating expression of VEGFA and known to be activated during inflammatory responses and hypoxic conditions occurring during ARDS [192]. Also the expression of *IL10*, encoding the anti-inflammatory interleukin 10 with decreasing risk of ARDS development was not changed (Figure 3) [191].

Further, we analysed the expression of (*CHI3L1*) YKL-40 on RNA and protein levels (Figure 4 and S4). YKL-40 is a known mechanical stress marker [196] and its gene and protein expression were enhanced in our model, applying mechanical stress generated by CPAD on VA10 cells in ALI culture, supporting the evidence of YKL-40 as a marker for VILI and ARDS. Similar increased expression of *CHI3L1* was observed in BCi cells (Figure S3).

Interestingly, expression of genes encoding antimicrobial peptides: cathelicidin antimicrobial peptide LL-37 (*CAMP*) and β-defensin 2 (*HBD2*) produced by airway epithelia for sufficient host defence responses was increased in VA10 cells in ALI culture subjected to mechanical stress (Figure 3). Similar increased expression of *HBD2* was observed in BCi cells in ALI culture subjected to the mechanical stress (Figure S3). Apart from microbicidal activity antimicrobial peptides (AMPs) display immunomodulatory functions [36,37,42] that might affect the course of VILI and ARDS. AMPs are chemoattractant for neutrophils [36] and their massive influx to the alveolar space might contribute to the progression and severity of ARDS [21]. The high concentration of AMPs in the alveolar space released by macrophages, infiltrated neutrophils and lung epithelium might cause further tissue damage [47,197]. Thus, increased levels of LL-37 antimicrobial peptide and α-defensins were detected in bronchoalveolar lavage fluid (BALF) of ARDS patients that corresponded to the increased lung tissue injury [197]. The increased *CAMP* gene expression in differentiated VA10 cells subjected to mechanical stress generated by CPAD corresponded to the observed increased level of LL-37 in BALF of ARDS patients. However, this result is opposite of the previously described reduced *CAMP* gene expression in monolayer VA10 cells subjected to cyclical stretch only [169]. This difference highlighted the relevance of using the CPAD for *in vitro* research on VILI and ARDS.

There was no difference in expression of lipocalin 2 (*LCN*) on RNA level (Figure 4), but increased level of the protein was detected when cells were subjected to the highest pressure (Figure 4 and S5) and this phenotype was more pronounced in VA10 cells than BCi cells (Figure S5). The level of lipocalin 2 (also known as NGAL from neutrophil gelatinase-associated lipocalin) might be used as a clinical parameter for tissue damage [198] and in our system the increase of NGAL level could reflect epithelial damage observed in ARDS.

Mechanical stress generated by CPAD also induced expression of the pro-inflammatory genes *CXCL8* (Figure 4) and *TNF* (Figure 3) similar to the pronounced pro-inflammatory responses observed in VILI and ARDS. However, there was no further increase in IL-8 secreted to the cell culture medium (Figure 4) and the TNFα level was below detection. This might be the reason of the high volume of the culture medium volume used for the assembly of the CPAD and analyses of the protein markers would be advisable by different

methods, e.g. immunofluorescence staining. The induction of *HBD2* expression was supported by increased expression of pro-inflammatory cytokines. All these genes are regulated by NF-κB pathway responsible for activation of pro-inflammatory responses [199,200] typical for VILI and ARDS, indirectly pointing on activation of NF-κB pathway by mechanical stress [201].

This newly developed CPAD for mechanical stress of differentiated three-dimensional cultured human lung cells mimics VILI, contributing to ARDS development. The affected cell morphology and expression of epithelial and innate immunity biomarkers typical for VILI and ARDS warrant further utilization of CPAD for *in vitro* research, limiting the use of animals and overcoming the difficulties connected to obtain human lung tissue. The construction and characterization of the responses triggered by mechanical stress generated by CPAD enable its use in the drug testing for ARDS treatment.

Thus, as a continuation a pilot experiment was performed for analyzing if the aroylated phenylenediamine HO53 influences these responses in stressed differentiated VA10 cells (***Figure 11***). The aim of this pilot study was to evaluate if HO53 can counteract the injury mediated effects on lung epithelial cells by analysis of the expression of selected genes.

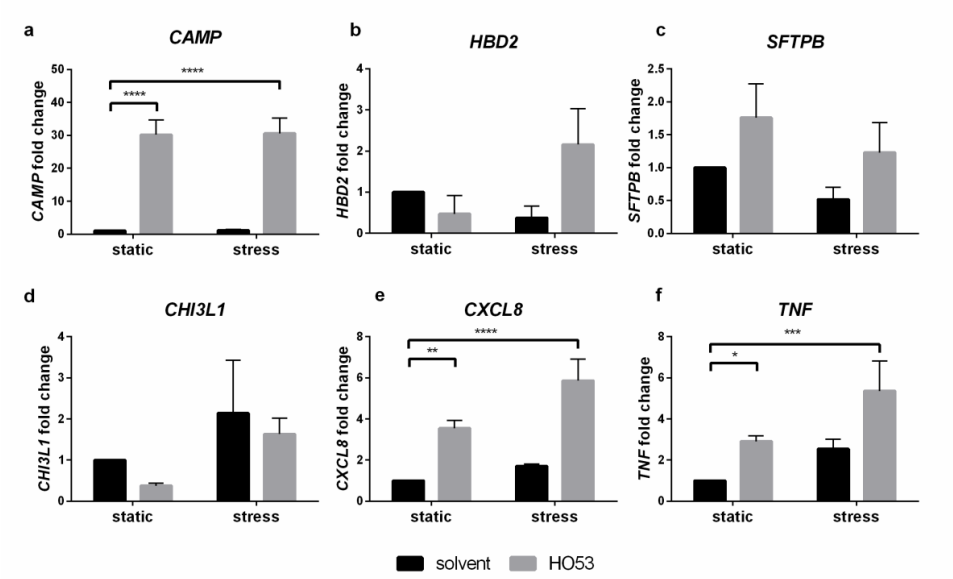


***Figure 11. Effect of HO53 treatment on differentiated VA10 cells mechanically stressed in Cyclical Pressure Air-liquid interface Device (CPAD).***
*Differentiated VA10 cells in air-liquid interphase culture were treated with HO53 (75 µM) for 2 days by addition of the compound to the lower chamber of ALI insert and then subjected to 27 cm $H_2O$ stress (day 21 of ALI culture) in the presence of HO53 for the next 24 h. Expression of* ***a)*** *CAMP,* ***b)*** *HBD2,* ***c)*** *SFTPB,* ***d)*** *CHI3L1,* ***e)*** *CXCL8,* ***f)*** *TNF genes was analysed by qPCR. Gene expression was normalized to GAPDH reference gene and presented as fold change of the expression compared to solvent treated cells in static conditions (solvent/static) set as 1. N=3 ± SD, two-way ANOVA with Dunnett´s multiple comparisons test. Only significant differences were marked, * p<0.05, *** p<0.001, **** p<0.0001.*

Among the selected innate immunity genes only expression of the *CAMP* gene was affected by HO53 and it was not dependent on mechanical stress. There was no significant difference in expression of the *HBD2* innate immunity gene, surfactant protein B (*SFTPB*) and a marker for mechanical stress *CHI3L1*. Treatment with HO53 led to induction of pro-inflammatory response in VA10 cells in ALI culture as showed by the increased levels of *CXCL8* and *TNF* expression and this pro-inflammatory response was further intensified by mechanical stress. This indicates that treatment with HO53 for 3 days of differentiated VA10 cells exacerbate pro-inflammatory responses induced by mechanical stress. Despite HO53 compound induces desirable responses for the treatment of infectious diseases, this pilot study indicates that HO53 does not appear to be a promising drug candidate for VILI and ARDS treatment. However, further experiment, evaluating the time of the HO53 compound administration would be beneficial, since the maximal exposition time to this compound in BCi cells to study induction of pro-inflammatory responses was 48 h (**Paper I**).

# 5 Conclusions

**Paper I**

- Aroylated phenylenediamine (APDs) compounds HO53 and HO56 are novel modulators of innate immunity, inducing the expression of antimicrobial peptides/proteins in lung epithelial cells, involving STAT3 signalling as demonstrated for HO53.

- The responses induced by APDs in lung epithelial cells were effective against *Pseudomonas aeruginosa* PAO1 infection, resulting in reduced number of intracellular bacteria.

- The selected APD compound HO53 enhances integrity of tight junction proteins and epithelial barrier function in differentiated polarized lung epithelial layers.

- The response to the treatment with APDs varies between cell types and depends on their differentiation status.

**Paper II**

- The selected APD compound HO53 promotes autophagy induction in differentiated polarized airway epithelial cells but had limited effect in the monolayer bronchial epithelial cells.

- The compound HO53 induces a broad response on the gene expression in differentiated bronchial epithelial cells including pathways, regulating autophagy induction.

- Treatment of differentiated bronchial epithelial cells with HO53 activates AMPK signalling cascade, affects mTOR pathway and activates TFEB, all known to activate autophagy.

- HO53 compound affects gene expression of histone modifying enzymes involved in regulation of autophagy by epigenetic mechanism, working on the chromatin level.

**Paper III**

- Mechanical stress generated by the cyclical pressure ALI device (CPAD) affects cell morphology and expression of genes previously indicated as markers for the risk of VILI and ARDS development.

- Expression of the innate immunity genes encoding antimicrobial effectors such as *CAMP*, *HBD1* and *SFTPB* was increased when mechanical stress generated by CPAD was applied.

- Mechanical stress generated by CPAD induces pronounced pro-inflammatory responses similar to the responses observed in VILI and ARDS.

- A preliminary study indicates that HO53 does not appear to be a promising drug candidate for VILI and ARDS treatment because HO53 treatment exacerbates the pro-inflammatory responses induced by mechanical stress in differentiated VA10 cells.

# 6 Future perspectives

The studies presented in this PhD thesis warrant further continuation of the research on novel APDs inducers. One approach would be to define additional molecular pathways involved in the responses to HO53 and study its effect in different cells, like gut epithelium or in macrophages, which has been partially done at Karolinska Institute [202]. Another interesting study would be detailed investigation of APDs responses depended on the cell differentiation status and the time of APDs exposition during the differentiation process. The broad picture about efficacy of APDs would need animal infection studies together with the pharmaco-kinetic profile and this work is ongoing with the support of Akthelia Pharmaceuticals. In respect to utilization of APDs for modulation of innate immunity and pro-inflammatory responses in VILI and ARDS, it would be worth to evaluate the effect of the APD compound HO56 or to synthesize a new library of APD compounds. Important future perspective in respect to studies on lung innate immunity would be the use of differentiated polarized cells in co-culture with endothelial and/or macrophages for better mimicking tissue environment as the access to lung tissue is limited. The limitation of the cell models used in these studies relates to the difficulty in the genetic manipulations, especially in differentiated cells in ALI culture. These limitations can be bypassed by using inhibitors or primary cells with defined genetic mutations. The establishment of efficient methods for genetic manipulations of lung cells, allowing them to maintain their differentiation potential would be beneficial for studies on the lung epithelial immunity.

# References


1. Gerard J. Tortora, Mark T. Nielsen (2012) *Principles of human anatomy*. John Wiley & Sons, Inc.

2. Zepp JA, Morrisey EE (2019) Cellular crosstalk in the development and regeneration of the respiratory system. *Nat Rev Mol Cell Biol* **20**: 551–566.

3. Reid L, Meyrick B, Antony VB, Chang LY, Crapo JD, Reynolds HY (2005) The mysterious pulmonary brush cell: A cell in search of a function. *Am J Respir Crit Care Med* **172**: 136–139.

4. Montoro DT, Haber AL, Biton M, Vinarsky V, Lin B, Birket SE, Yuan F, Chen S, Leung HM, Villoria J, et al. (2018) A revised airway epithelial hierarchy includes CFTR-expressing ionocytes. *Nature* **560**: 319–324.

5. Branchfield K, Nantie L, Verheyden JM, Sui P, Wienhold MD, Sun X (2016) Pulmonary neuroendocrine cells function as airway sensors to control lung immune response. *Science* **351**: 707–710.

6. Fahy J V, Dickey BF (2010) Airway mucus function and dysfunction. *N Engl J Med* **363**: 2233–2247.

7. Leiva-Juárez MM, Kolls JK, Evans SE (2018) Lung epithelial cells: therapeutically inducible effectors of antimicrobial defense. *Mucosal Immunol* **11**: 21–34.

8. Zihni C, Mills C, Matter K, Balda MS (2016) Tight junctions: From simple barriers to multifunctional molecular gates. *Nat Rev Mol Cell Biol* **17**: 564–580.

9. Han SH, Mallampalli RK (2015) The role of surfactant in lung disease and host defense against pulmonary infections. *Ann Am Thorac Soc* **12**: 765–774.

10. Georas SN, Rezaee F (2014) Epithelial barrier function: at the front line of asthma immunology and allergic airway inflammation. *J Allergy Clin Immunol* **134**: 509–520.

11. Zulianello L, Canard C, Köhler T, Caille D, Lacroix J-S, Meda P (2006) Rhamnolipids are virulence factors that promote early infiltration of primary human airway epithelia by Pseudomonas aeruginosa. *Infect Immun* **74**: 3134–3147.

12. Golovkine G, Faudry E, Bouillot S, Elsen S, Attrée I, Huber P (2016) Pseudomonas aeruginosa Transmigrates at Epithelial Cell-Cell Junctions, Exploiting Sites of Cell Division and Senescent Cell Extrusion. *PLoS Pathog* **12**: e1005377.

13. Matter K, Balda MS (2003) Signalling to and from tight junctions. *Nat Rev Mol Cell Biol* **4**: 225–236.

14. Roy MG, Livraghi-Butrico A, Fletcher AA, McElwee MM, Evans SE, Boerner RM, Alexander SN, Bellinghausen LK, Song AS, Petrova YM, et al. (2014) Muc5b is required for airway defence. *Nature* **505**: 412–416.

15. Kim YD, Bae CH, Song SY, Choi YS (2015) Effect of β-glucan on MUC4 and MUC5B expression in human airway epithelial cells. *Int Forum Allergy Rhinol* **5**: 708–715.

16. Fujisawa T, Chang MMJ, Velichko S, Thai P, Hung LY, Huang F, Phuong N, Chen Y, Wu R (2011) NF-κB mediates IL-1β- and IL-17A-induced MUC5B expression in airway epithelial cells. *Am J Respir Cell Mol Biol* **45**: 246–252.

17. Rada B, Gardina P, Myers TG, Leto TL (2011) Reactive oxygen species mediate inflammatory cytokine release and EGFR-dependent mucin secretion in airway epithelial cells exposed to Pseudomonas pyocyanin. *Mucosal Immunol* **4**: 158–171.

18. Atherton HC, Jones G, Danahay H, Dana H (2003) IL-13-induced changes in the goblet cell density of human bronchial epithelial cell cultures: MAP kinase and phosphatidylinositol 3-kinase regulation. *Am J Physiol Lung Cell Mol Physiol* **285**: 730–739.

19. Zhang Y, Zhu M, Yang Z, Pan X, Jiang Y, Sun C, Wang Q, Xiao W (2014) The human Cathelicidin LL-37 induces MUC5AC mucin production by airway epithelial cells via TACE-TGF-α-EGFR pathway. *Exp Lung Res* **40**: 333–342.

20. Knowles MR, Boucher RC (2002) Mucus clearance as a primary innate defense mechanism for mammalian airways. *J Clin Invest* **109**: 571–577.

21. Matthay MA, Zemans RL, Zimmerman GA, Arabi YM, Beitler JR, Mercat A, Herridge M, Randolph AG, Calfee CS (2019) Acute respiratory distress syndrome. *Nat Rev Dis Prim* **5**: 1–22.

22. Cheng G, Ueda T, Nakajima H, Nakajima A, Kinjyo S, Motojima S, Fukuda T (1998) Suppressive effects of SP-A on ionomycin-induced IL-8 production and release by eosinophils. *Int Arch Allergy Immunol* **117**: 59–62.

23. Barkauskas CE, Cronce MJ, Rackley CR, Bowie EJ, Keene DR, Stripp BR, Randell SH, Noble PW, Hogan BLM (2013) Type 2 alveolar cells are stem cells in adult lung. *J Clin Invest* **123**: 3025–3036.

24. Takeuchi O, Akira S (2010) Pattern Recognition Receptors and Inflammation. *Cell* **140**: 805–820.

25. De Nardo D (2015) Toll-like receptors: Activation, signalling and transcriptional modulation. *Cytokine* **74**: 181–189.

26. Brubaker SW, Bonham KS, Zanoni I, Kagan JC (2015) Innate Immune Pattern Recognition: A Cell Biological Perspective. *Annu Rev Immunol* **33**: 257–290.

27. Hosseinian N, Cho Y, Lockey RF, Kolliputi N (2015) The role of the NLRP3 inflammasome in pulmonary diseases. *Ther Adv Respir Dis* **9**: 188–197.

28. Thomas PG, Dash P, Aldridge JR, Ellebedy AH, Reynolds C, Funk AJ, Martin WJ, Lamkanfi M, Webby RJ, Boyd KL, et al. (2009) The Intracellular Sensor NLRP3 Mediates Key Innate and Healing Responses to Influenza A Virus via the Regulation of Caspase-1. *Immunity* **30**: 566–575.

29. Hise AG, Tomalka J, Ganesan S, Patel K, Hall BA, Brown GD, Fitzgerald KA (2009) An Essential Role for the NLRP3 Inflammasome in Host Defense against the Human Fungal Pathogen Candida albicans. *Cell Host Microbe* **5**: 487–497.

30. Kato H, Takeuchi O, Sato S, Yoneyama M, Yamamoto M, Matsui K, Uematsu S, Jung A, Kawai T, Ishii KJ, et al. (2006) Differential roles of MDA5 and RIG-I helicases in the recognition of RNA viruses. *Nature* **441**: 101–105.

31. Bhoj VG, Sun Q, Bhoj EJ, Somers C, Chen X, Torres JP, Mejias A, Gomez AM, Jafri H, Ramilo O, et al. (2008) MAVS and MyD88 are essential for innate immunity but not cytotoxic T lymphocyte response against respiratory syncytial virus. *Proc Natl Acad Sci U S A* **105**: 14046–14051.

32. Parker D, Prince A (2011) Type I interferon response to extracellular bacteria in the airway epithelium. *Trends Immunol* **32**: 582–588.

33. Chen Q, Sun L, Chen ZJ (2016) Regulation and function of the cGAS-STING pathway of cytosolic DNA sensing. *Nat Immunol* **17**: 1142–1149.

34. Heyl KA, Klassert TE, Heinrich A, Müller MM, Klaile E, Dienemann H, Grünewald C, Bals R, Singer BB, Slevogt H (2014) Dectin-1 is expressed in human lung and mediates the proinflammatory immune response to nontypeable Haemophilus influenzae. *MBio* **5**: e01492-14.

35. Werner JL, Metz AE, Horn D, Schoeb TR, Hewitt MM, Schwiebert LM, Faro-Trindade I, Brown GD, Steele C (2009) Requisite Role for the Dectin-1 β-Glucan Receptor in Pulmonary Defense against Aspergillus fumigatus. *J Immunol* **182**: 4938–4946.

36. Lai Y, Gallo RL (2009) AMPed up immunity: how antimicrobial peptides have multiple roles in immune defense. *Trends Immunol* **30**: 131–141.

37. Mansour SC, Pena OM, Hancock REW (2014) Host defense peptides: front-line immunomodulators. *Trends Immunol* **35**: 443–450.

38. Agerberth B, Gunne H, Odeberg J, Kogner P, Boman HG, Gudmundsson GH (1995) FALL-39, a putative human peptide antibiotic, is cysteine-free and expressed in bone marrow and testis. *Proc Natl Acad Sci U S A* **92**: 195–199.

39. Gudmundsson GH, Agerberth B, Odeberg J, Bergman T, Olsson B, Salcedo R (1996) The Human Gene FALL39 and Processing of the Cathelin Precursor to the Antibacterial Peptide LL-37 in Granulocytes. *Eur J Biochem* **238**: 325–332.

40. Zasloff M (2002) Antimicrobial peptides of multicellular organisms. *Nature* **415**: 389–395.

41. Selsted M (2005) θ-Defensins: Cyclic Antimicrobial Peptides Produced by Binary Ligation of Truncated α-Defensins. *Curr Protein Pept Sci* **5**: 365–371.

42. Mookherjee N, Anderson MA, Haagsman HP, Davidson DJ (2020) Antimicrobial host defence peptides: functions and clinical potential. *Nat Rev Drug Discov* **19**: 311–332.

43. Sass V, Schneider T, Wilmes M, Körner C, Tossi A, Novikova N, Shamova O, Sahl HG (2010) Human β-defensin 3 inhibits cell wall biosynthesis in staphylococci. *Infect Immun* **78**: 2793–2800.

44. Nizet V, Ohtake T, Lauth X, Trowbridge J, Rudisill J, Dorschner RA, Pestonjamasp V, Piraino J, Huttner K, Gallo RL (2001) Innate antimicrobial peptide protects the skin from invasive bacterial infection. *Nature* **414**: 454–457.

45. Salzman NH, Ghosh D, Huttner KM, Paterson Y, Bevins CL (2003) Protection against enteric salmonellosis in transgenic mice expressing a human intestinal defensin. *Nature* **422**: 522–526.

46. Ordonez SR, Amarullah IH, Wubbolts RW, Veldhuizen EJA, Haagsman HP (2014) Fungicidal mechanisms of cathelicidins LL-37 and CATH-2 revealed by live-cell imaging. *Antimicrob Agents Chemother* **58**: 2240–2248.

47. Ganz T (2003) Defensins: Antimicrobial peptides of innate immunity. *Nat Rev Immunol* **3**: 710–720.

48. Cullen TW, Schofield WB, Barry NA, Putnam EE, Rundell EA, Trent MS, Degnan PH, Booth CJ, Yu H, Goodman AL (2015) Antimicrobial peptide resistance mediates resilience of prominent gut commensals during inflammation. *Science* **347**: 170–175.

49. Bevins CL, Bäumler AJ (2015) What's one phosphate between friends (and foe)? *Cell Host Microbe* **17**: 1–3.

50. Niyonsaba F, Iwabuchi K, Matsuda H, Ogawa H, Nagaoka I (2002) Epithelial cell-derived human b-defensin-2 acts as a chemotaxin for mast cells through a pertussis toxin-sensitive and phospholipase C-dependent pathway. *Int Immunlogy* **14**: 421–426.

51. De Yang B, Chen Q, Schmidt AP, Anderson GM, Wang JM, Wooters J, Oppenheim JJ, Chertov O (2000) LL-37, the neutrophil granule- and epithelial cell-derived cathelicidin, utilizes formyl peptide receptor-like 1 (FPRL1) as a receptor to chemoattract human peripheral blood neutrophils, monocytes, and T cells. *J Exp Med* **192**: 1069–1074.

52. Scott MG, Davidson DJ, Gold MR, Bowdish D, Hancock REW (2002) The Human Antimicrobial Peptide LL-37 Is a Multifunctional Modulator of Innate Immune Responses. *J Immunol* **169**: 3883–3891.

53. Mookherjee N, Brown KL, Bowdish DME, Doria S, Falsafi R, Hokamp K, Roche FM, Mu R, Doho GH, Pistolic J, et al. (2006) Modulation of the TLR-Mediated

Inflammatory Response by the Endogenous Human Host Defense Peptide LL-37. *J Immunol* **176**: 2455–2464.

54. Koziel J, Bryzek D, Sroka A, Maresz K, Glowczyk I, Bielecka E, Kantyka T, Pyrć K, Svoboda P, Pohl J, et al. (2014) Citrullination Alters Immunomodulatory Function of LL-37 Essential for Prevention of Endotoxin-Induced Sepsis. *J Immunol* **192**: 5363–5372.

55. Wong A, Bryzek D, Dobosz E, Scavenius C, Svoboda P, Rapala-Kozik M, Lesner A, Frydrych I, Enghild J, Mydel P, et al. (2018) A Novel Biological Role for Peptidyl-Arginine Deiminases: Citrullination of Cathelicidin LL-37 Controls the Immunostimulatory Potential of Cell-Free DNA. *J Immunol* **200**: 2327–2340.

56. McHugh BJ, Wang R, Li H-N, Beaumont PE, Kells R, Stevens H, Young L, Rossi AG, Gray RD, Dorin JR, et al. (2019) Cathelicidin is a "fire alarm", generating protective NLRP3-dependent airway epithelial cell inflammatory responses during infection with Pseudomonas aeruginosa. *PLOS Pathog* **15**: e1007694.

57. Coorens M, Schneider VAF, de Groot AM, van Dijk A, Meijerink M, Wells JM, Scheenstra MR, Veldhuizen EJA, Haagsman HP (2017) Cathelicidins Inhibit Escherichia coli –Induced TLR2 and TLR4 Activation in a Viability-Dependent Manner. *J Immunol* **199**: 1418–1428.

58. Wu H, Santoni-Rugiu E, Ralfkiaer E, Porse BT, Moser C, Høiby N, Borregaard N, Cowland JB (2010) Lipocalin 2 is protective against E. coli pneumonia. *Respir Res* **11**: 96.

59. Cramer EP, Dahl SL, Rozell B, Knudsen KJ, Thomsen K, Moser C, Cowland JB, Borregaard N (2017) Lipocalin-2 from both myeloid cells and the epithelium combats Klebsiella pneumoniae lung infection in mice. *Blood* **129**: 2813–2817.

60. Williams SE, Brown TI, Roghanian A, Sallenave JM (2006) SLPI and elafin: One glove, many fingers. *Clin Sci* **110**: 21–35.

61. Hiemstra PS, Maassen RJ, Stolk J, Heinzel-Wieland R, Steffens GJ, Dijkman JH (1996) Antibacterial activity of antileukoprotease. *Infect Immun* **64**: 4520–4524.

62. Simpson AJ, Maxwell AI, Govan JRW, Haslett C, Sallenave JM (1999) Elafin (elastase-specific inhibitor) has anti-microbial activity against Gram-positive and Gram-negative respiratory pathogens. *FEBS Lett* **452**: 309–313.

63. Henriksen PA, Hitt M, Xing Z, Wang J, Haslett C, Riemersma RA, Webb DJ, Kotelevtsev Y V., Sallenave J-M (2004) Adenoviral Gene Delivery of Elafin and Secretory Leukocyte Protease Inhibitor Attenuates NF-κB-Dependent Inflammatory Responses of Human Endothelial Cells and Macrophages to Atherogenic Stimuli. *J Immunol* **172**: 4535–4544.

64. Chu HW, Thaikoottathil J, Rino JG, Zhang G, Wu Q, Moss T, Refaeli Y, Bowler R, Wenzel SE, Chen Z, et al. (2007) Function and Regulation of SPLUNC1 Protein in Mycoplasma Infection and Allergic Inflammation. *J Immunol* **179**: 3995–4002.

65. Cole AM, Ganz T, Liese AM, Burdick MD, Liu L, Strieter RM (2001) Cutting Edge: IFN-Inducible ELR − CXC Chemokines Display Defensin-Like Antimicrobial Activity. *J Immunol* **167**: 623–627.

66. Fischer H (2009) Mechanisms and function of DUOX in epithelia of the lung. *Antioxid Redox Signal* **11**: 2453–2465.

67. Ragupathy S, Esmaeili F, Paschoud S, Sublet E, Citi S, Borchard G (2014) Toll-like receptor 2 regulates the barrier function of human bronchial epithelial monolayers through atypical protein kinase C zeta, and an increase in expression of claudin-1. *Tissue Barriers* **2**: e29166.

68. Reddick LE, Alto NM (2014) Bacteria fighting back: How pathogens target and subvert the host innate immune system. *Mol Cell* **54**: 321–328.

69. Lauth X, von Köckritz-Blickwede M, McNamara CW, Myskowski S, Zinkernagel AS, Beall B, Ghosh P, Gallo RL, Nizet V (2009) M1 Protein Allows Group A Streptococcal Survival in Phagocyte Extracellular Traps through Cathelicidin Inhibition. *J Innate Immun* **1**: 202–214.

70. Islam D, Bandholtz L, Nilsson J, Wigzell H, Christensson B, Agerberth B, Gudmundsson GH (2001) Downregulation of bactericidal peptides in enteric infections: A novel immune escape mechanism with bacterial DNA as a potential regulator. *Nat Med* **7**: 180–185.

71. World Health Organization (WHO) (2014) *Summary of the World Health Organization report: Antimicrobial Resistance - global report on surveillance 2014. https://www.who.int/antimicrobial-resistance/publications/surveillancereport/en/*.

72. Laxminarayan R, Van Boeckel T, Frost I, Kariuki S, Khan EA, Limmathurotsakul D, Larsson DGJ, Levy-Hara G, Mendelson M, Outterson K, et al. (2020) The Lancet Infectious Diseases Commission on antimicrobial resistance: 6 years later. *Lancet Infect Dis* **20**: e51–e60.

73. Laxminarayan R, Van Boeckel T, Frost I, Kariuki S, Khan EA, Limmathurotsakul D, Larsson DGJ, Levy-Hara G, Mendelson M, Outterson K, et al. (2020) Correction to Lancet Infect Dis 2020; published online Feb 11. https://doi.org/10.1016/S1473-3099(20)30003-7. *Lancet Infect Dis* **20**: e50.

74. Rice LB (2008) Federal Funding for the Study of Antimicrobial Resistance in Nosocomial Pathogens: No ESKAPE. *J Infect Dis* **197**: 1079–1081.

75. Pogue JM, Kaye KS, Cohen DA, Marchaim D (2015) Appropriate antimicrobial therapy in the era of multidrug-resistant human pathogens. *Clin Microbiol Infect* **21**: 302–312.

76. Cassini A, Högberg LD, Plachouras D, Quattrocchi A, Hoxha A, Simonsen GS, Colomb-Cotinat M, Kretzschmar ME, Devleesschauwer B, Cecchini M, et al. (2019) Attributable deaths and disability-adjusted life-years caused by infections with antibiotic-resistant bacteria in the EU and the European Economic Area in 2015: a population-level modelling analysis. *Lancet Infect Dis* **19**: 56–66.

77. Lazzaro BP, Zasloff M, Rolff J (2020) Antimicrobial peptides: Application informed by evolution. *Science* **368**: eaau5480.

78. Andersson DI, Hughes D, Kubicek-Sutherland JZ (2016) Mechanisms and consequences of bacterial resistance to antimicrobial peptides. *Drug Resist Updat* **26**: 43–57.

79. Grönberg A, Mahlapuu M, Ståhle M, Whately-Smith C, Rollman O (2014) Treatment with LL-37 is safe and effective in enhancing healing of hard-to-heal venous leg ulcers: a randomized, placebo-controlled clinical trial. *Wound Repair Regen* **22**: 613–621.

80. Riool M, de Breij A, Drijfhout JW, Nibbering PH, Zaat SAJ (2017) Antimicrobial peptides in biomedical device manufacturing. *Front Chem* **5**: 63.

81. Niyonsaba F, Madera L, Afacan N, Okumura K, Ogawa H, Hancock REW (2013) The innate defense regulator peptides IDR-HH2, IDR-1002, and IDR-1018 modulate human neutrophil functions. *J Leukoc Biol* **94**: 159–170.

82. Hing TC, Ho S, Shih DQ, Ichikawa R, Cheng M, Chen J, Chen X, Law I, Najarian R, Kelly CP, et al. (2013) The antimicrobial peptide cathelicidin modulates Clostridium difficile-associated colitis and toxin A-mediated enteritis in mice. *Gut* **62**: 1295–1305.

83. Cuperus T, Van Dijk A, Matthijs MGR, Veldhuizen EJA, Haagsman HP (2016) Protective effect of in ovo treatment with the chicken cathelicidin analog D-CATH-2 against avian pathogenic E. coli. *Sci Rep* **6**: 26622.

84. Fan D, Coughlin LA, Neubauer MM, Kim J, Kim MS, Zhan X, Simms-Waldrip TR, Xie Y, Hooper L V, Koh AY (2015) Activation of HIF-1α and LL-37 by commensal bacteria inhibits Candida albicans colonization. *Nat Med* **21**: 808–814.

85. Sechet E, Telford E, Bonamy C, Sansonetti PJ, Sperandio B (2018) Natural molecules induce and synergize to boost expression of the human antimicrobial peptide β-defensin-3. *Proc Natl Acad Sci U S A* **115**: E9869–E9878.

86. Jatana S, Homer CR, Madajka M, Ponti AK, Kabi A, Papay F, McDonald C (2018) Pyrimidine synthesis inhibition enhances cutaneous defenses against antibiotic resistant bacteria through activation of NOD2 signaling. *Sci Rep* **8**: 8708.

87. Cederlund A, Kai-Larsen Y, Printz G, Yoshio H, Alvelius G, Lagercrantz H, Strömberg R, Jörnvall H, Gudmundsson GH, Agerberth B (2013) Lactose in Human Breast Milk an Inducer of Innate Immunity with Implications for a Role in Intestinal Homeostasis. *PLoS One* **8**: e53876.

88. Chen J, Zhai Z, Long H, Yang G, Deng B, Deng J (2020) Inducible expression of defensins and cathelicidins by nutrients and associated regulatory mechanisms. *Peptides* **123**: 170177.

89. Miraglia E, Nylén F, Johansson K, Arnér E, Cebula M, Farmand S, Ottosson H, Strömberg R, Gudmundsson GH, Agerberth B, et al. (2016) Entinostat up-regulates

the CAMP gene encoding LL-37 via activation of STAT3 and HIF-1α transcription factors. *Sci Rep* **6**: 33274.

90. Ottosson H, Nylén F, Sarker P, Miraglia E, Bergman P, Gudmundsson GH, Raqib R, Agerberth B, Strömberg R (2016) Potent Inducers of Endogenous Antimicrobial Peptides for Host Directed Therapy of Infections. *Sci Rep* **6**: 36692.

91. Hansdottir S, Monick MM (2011) Vitamin D Effects on Lung Immunity and Respiratory Diseases. *Vitam Horm* **86**: 217–237.

92. DeLuca HF (2016) Vitamin D: Historical Overview. *Vitam Horm* **100**: 1–20.

93. Neme A, Nurminen V, Seuter S, Carlberg C (2016) The vitamin D-dependent transcriptome of human monocytes. *J Steroid Biochem Mol Biol* **164**: 180–187.

94. Wang T-T, Nestel FP, Bourdeau V, Nagai Y, Wang Q, Liao J, Tavera-Mendoza L, Lin R, Hanrahan JW, Mader S, et al. (2004) Cutting edge: 1,25-dihydroxyvitamin D3 is a direct inducer of antimicrobial peptide gene expression. *J Immunol* **173**: 2909–2912.

95. Gombart AF, Borregaard N, Koeffler HP (2005) Human cathelicidin antimicrobial peptide (CAMP) gene is a direct target of the vitamin D receptor and is strongly up-regulated in myeloid cells by 1,25-dihydroxyvitamin D3. *FASEB J* **19**: 1067–1077.

96. Carlberg C (2017) Molecular endocrinology of vitamin D on the epigenome level. *Mol Cell Endocrinol* **453**: 14–21.

97. Termén S, Tollin M, Rodriguez E, Sveinsdóttir SH, Jóhannesson B, Cederlund A, Sjövall J, Agerberth B, Gudmundsson GH (2008) PU.1 and bacterial metabolites regulate the human gene CAMP encoding antimicrobial peptide LL-37 in colon epithelial cells. *Mol Immunol* **45**: 3947–3955.

98. Wei R, Dhawan P, Baiocchi RA, Kim KY, Christakos S (2019) PU.1 and epigenetic signals modulate 1,25-dihydroxyvitamin D 3 and C/EBPα regulation of the human cathelicidin antimicrobial peptide gene in lung epithelial cells. *J Cell Physiol* **234**: 10345–10359.

99. Liu PT, Stenger S, Li H, Wenzel L, Tan BH, Krutzik SR, Ochoa MT, Schauber J, Wu K, Meinken C, et al. (2006) Toll-like receptor triggering of a vitamin D-mediated human antimicrobial response. *Science* **311**: 1770–1773.

100. Yuk J-M, Shin D-M, Lee H-M, Yang C-S, Jin HS, Kim K-K, Lee Z-W, Lee S-H, Kim J-M, Jo E-K (2009) Vitamin D3 Induces Autophagy in Human Monocytes/Macrophages via Cathelicidin. *Cell Host Microbe* **6**: 231–243.

101. Shaykhiev R, Beißwenger C, Kändler K, Senske J, Püchner A, Damm T, Behr J, Bals R (2005) Human endogenous antibiotic LL-37 stimulates airway epithelial cell proliferation and wound closure. *Am J Physiol Lung Cell Mol Physiol* **289**: 842–848.

102. Gonzalez-Curiel I, Trujillo V, Montoya-Rosales A, Rincon K, Rivas-Calderon B, De Haro-Acosta J, Marin-Luevano P, Lozano-Lopez D, Enciso-Moreno JA, Rivas-

Santiago B (2014) 1,25-dihydroxyvitamin D3 induces LL-37 and HBD-2 production in keratinocytes from diabetic foot ulcers promoting wound healing: An in vitro model. *PLoS One* **9**: e111355.

103. Schögler A, Muster RJ, Kieninger E, Casaulta C, Tapparel C, Jung A, Moeller A, Geiser T, Regamey N, Alves MP (2016) Vitamin D represses rhinovirus replication in cystic fibrosis cells by inducing LL-37. *Eur Respir J* **47**: 520–530.

104. Brockman-Schneider RA, Pickles RJ, Gern JE (2014) Effects of vitamin D on airway epithelial cell morphology and rhinovirus replication. *PLoS One* **9**: e86755.

105. Steinmann J, Halldórsson S, Agerberth B, Gudmundsson GH (2009) Phenylbutyrate induces antimicrobial peptide expression. *Antimicrob Agents Chemother* **53**: 5127–5133.

106. Mily A, Rekha RS, Kamal SMM, Arifuzzaman ASM, Rahim Z, Khan L, Haq MA, Zaman K, Bergman P, Brighenti S, et al. (2015) Significant Effects of Oral Phenylbutyrate and Vitamin D3 Adjunctive Therapy in Pulmonary Tuberculosis: A Randomized Controlled Trial. *PLoS One* **10**: e0138340.

107. Bekele A, Gebreselassie N, Ashenafi S, Kassa E, Aseffa G, Amogne W, Getachew M, Aseffa A, Worku A, Raqib R, et al. (2018) Daily adjunctive therapy with vitamin D 3 and phenylbutyrate supports clinical recovery from pulmonary tuberculosis: a randomized controlled trial in Ethiopia. *J Intern Med* **284**: 292–306.

108. Bilotta AJ, Cong Y (2019) Gut microbiota metabolite regulation of host defenses at mucosal surfaces: implication in precision medicine. *Precis Clin Med* **2**: 110–119.

109. Liu H, Wang J, He T, Becker S, Zhang G, Li D, Ma X (2018) Butyrate: A double-edged sword for health? *Adv Nutr* **9**: 21–29.

110. Schauber J, Svanholm C, Termén S, Iffland K, Menzel T, Scheppach W, Melcher R, Agerberth B, Lührs H, Gudmundsson GH (2003) Expression of the cathelicidin LL-37 is modulated by short chain fatty acids in colonocytes: Relevance of signalling pathways. *Gut* **52**: 735–741.

111. Frank DN, St. Amand AL, Feldman RA, Boedeker EC, Harpaz N, Pace NR (2007) Molecular-phylogenetic characterization of microbial community imbalances in human inflammatory bowel diseases. *Proc Natl Acad Sci U S A* **104**: 13780–13785.

112. Lavelle A, Sokol H (2020) Gut microbiota-derived metabolites as key actors in inflammatory bowel disease. *Nat Rev Gastroenterol Hepatol* **17**: 223–237.

113. Fachi JL, Felipe J de S, Pral LP, da Silva BK, Corrêa RO, de Andrade MCP, da Fonseca DM, Basso PJ, Câmara NOS, de Sales e Souza ÉL, et al. (2019) Butyrate Protects Mice from Clostridium difficile-Induced Colitis through an HIF-1-Dependent Mechanism. *Cell Rep* **27**: 750-761.e7.

114. Schulthess J, Pandey S, Capitani M, Rue-Albrecht KC, Arnold I, Franchini F, Chomka A, Ilott NE, Johnston DGW, Pires E, et al. (2019) The Short Chain Fatty Acid Butyrate Imprints an Antimicrobial Program in Macrophages. *Immunity* **50**:

432-445.e7.

115. De Ruijter AJM, Van Gennip AH, Caron HN, Kemp S, Van Kuilenburg ABP (2003) Histone deacetylases (HDACs) : characterization of the classical HDAC family. *Biochem J* **370**: 737–749.

116. Sarker P, Ahmed S, Tiash S, Rekha RS, Stromberg R, Andersson J, Bergman P, Gudmundsson GH, Agerberth B, Raqib R (2011) Phenylbutyrate Counteracts Shigella Mediated Downregulation of Cathelicidin in Rabbit Lung and Intestinal Epithelia: A Potential Therapeutic Strategy. *PLoS One* **6**: e20637.

117. Jellbauer S, Lopez AP, Behnsen J, Gao N, Nguyen T, Murphy C, Edwards RA, Raffatellua M (2016) Beneficial effects of sodium phenylbutyrate administration during infection with salmonella enterica serovar typhimurium. *Infect Immun* **84**: 2639–2652.

118. Knipstein J, Gore L (2011) Entinostat for treatment of solid tumors and hematologic malignancies. *Expert Opin Investig Drugs* **20**: 1455–1467.

119. Ryan QC, Headlee D, Acharya M, Sparreboom A, Trepel JB, Ye J, Figg WD, Hwang K, Chung EJ, Murgo A, et al. (2005) Phase I and pharmacokinetic study of MS-275, a histone deacetylase inhibitor, in patients with advanced and refractory solid tumors or lymphoma. *J Clin Oncol* **23**: 3912–3922.

120. Cody JJ, Markert JM, Hurst DR (2014) Histone deacetylase inhibitors improve the replication of oncolytic herpes simplex virus in breast cancer cells. *PLoS One* **9**: e92919.

121. Nylén F, Miraglia E, Cederlund A, Ottosson H, Strömberg R, Gudmundsson GH, Agerberth B (2014) Boosting innate immunity: Development and validation of a cell-based screening assay to identify LL-37 inducers. *Innate Immun* **20**: 364–376.

122. Zhang YG, Wu S, Lu R, Zhou D, Zhou J, Carmeliet G, Petrof E, Claud EC, Sun J (2015) Tight junction CLDN2 gene is a direct target of the Vitamin D receptor. *Sci Rep* **5**: 10642.

123. Yan H, Ajuwon KM (2017) Butyrate modifies intestinal barrier function in IPEC-J2 cells through a selective upregulation of tight junction proteins and activation of the Akt signaling pathway. *PLoS One* **12**: e0179586.

124. Principi N, Blasi F, Esposito S (2015) Azithromycin use in patients with cystic fibrosis. *Eur J Clin Microbiol Infect Dis* **34**: 1071–1079.

125. Halldorsson S, Gudjonsson T, Gottfredsson M, Singh PK, Gudmundsson GH, Baldursson O (2010) Azithromycin Maintains Airway Epithelial Integrity during *Pseudomonas aeruginosa* Infection. *Am J Respir Cell Mol Biol* **42**: 62–68.

126. Arason AJ, Joelsson JP, Valdimarsdottir B, Sigurdsson S, Gudjonsson A, Halldorsson S, Johannsson F, Rolfsson O, Lehmann F, Ingthorsson S, et al. (2019) Azithromycin induces epidermal differentiation and multivesicular bodies in airway epithelia. *Respir Res* **20**: 129.

127. Deretic V (2014) Autophagy in tuberculosis. *Cold Spring Harb Perspect Med* **4**: a018481.

128. Kimmey JM, Stallings CL (2016) Bacterial Pathogens versus Autophagy: Implications for Therapeutic Interventions. *Trends Mol Med* **22**: 1060–1076.

129. Dikic I, Elazar Z (2018) Mechanism and medical implications of mammalian autophagy. *Nat Rev Mol Cell Biol* **19**: 349–364.

130. Yoshii SR, Mizushima N (2017) Monitoring and measuring autophagy. *Int J Mol Sci* **18**: 1865.

131. Mizushima N, Komatsu M (2011) Autophagy: renovation of cells and tissues. *Cell* **147**: 728–741.

132. Günther J, Seyfert HM (2018) The first line of defence: insights into mechanisms and relevance of phagocytosis in epithelial cells. *Semin Immunopathol* **40**: 555–565.

133. Kinsella RL, Nehls EM, Stallings CL (2018) Roles for Autophagy Proteins in Immunity and Host Defense. *Vet Pathol* **55**: 366–373.

134. Benjamin JL, Sumpter R, Levine B, Hooper L V. (2013) Intestinal epithelial autophagy is essential for host defense against invasive bacteria. *Cell Host Microbe* **13**: 723–734.

135. Junkins RD, Shen A, Rosen K, McCormick C, Lin TJ (2013) Autophagy Enhances Bacterial Clearance during P. aeruginosa Lung Infection. *PLoS One* **8**: e72263.

136. Capasso D, Pepe MV, Rossello J, Lepanto P, Arias P, Salzman V, Kierbel A (2016) Elimination of Pseudomonas aeruginosa through Efferocytosis upon Binding to Apoptotic Cells. *PLOS Pathog* **12**: e1006068.

137. Croft CA, Culibrk L, Moore MM, Tebbutt SJ (2016) Interactions of Aspergillus fumigatus Conidia with Airway Epithelial Cells: A Critical Review. *Front Microbiol* **7**: 472.

138. Luciani A, Villella VR, Esposito S, Brunetti-Pierri N, Medina D, Settembre C, Gavina M, Pulze L, Giardino I, Pettoello-Mantovani M, et al. (2010) Defective CFTR induces aggresome formation and lung inflammation in cystic fibrosis through ROS-mediated autophagy inhibition. *Nat Cell Biol* **12**: 863–875.

139. Shin D-M, Jeon B-Y, Lee H-M, Jin HS, Yuk J-M, Song C-H, Lee S-H, Lee Z-W, Cho S-N, Kim J-M, et al. (2010) Mycobacterium tuberculosis Eis Regulates Autophagy, Inflammation, and Cell Death through Redox-dependent Signaling. *PLoS Pathog* **6**: e1001230.

140. Chandra P, Ghanwat S, Matta SK, Yadav SS, Mehta M, Siddiqui Z, Singh A, Kumar D (2015) Mycobacterium tuberculosis Inhibits RAB7 Recruitment to Selectively Modulate Autophagy Flux in Macrophages. *Sci Rep* **5**: 1–10.

141. Kreibich S, Emmenlauer M, Fredlund J, Rämö P, Münz C, Dehio C, Enninga J,

Hardt WD (2015) Autophagy proteins promote repair of endosomal membranes damaged by the Salmonella type three secretion system 1. *Cell Host Microbe* **18**: 527–537.

142. Owen KA, Meyer CB, Bouton AH, Casanova JE (2014) Activation of Focal Adhesion Kinase by Salmonella Suppresses Autophagy via an Akt/mTOR Signaling Pathway and Promotes Bacterial Survival in Macrophages. *PLoS Pathog* **10**: e1004159.

143. Nahid P, Dorman SE, Alipanah N, Barry PM, Brozek JL, Cattamanchi A, Chaisson LH, Chaisson RE, Daley CL, Grzemska M, et al. (2016) Executive Summary: Official American Thoracic Society/Centers for Disease Control and Prevention/Infectious Diseases Society of America Clinical Practice Guidelines: Treatment of Drug-Susceptible Tuberculosis. *Clin Infect Dis* **63**: 853–867.

144. Torres-Juarez F, Cardenas-Vargas A, Montoya-Rosales A, González-Curiel I, Garcia-Hernandez MH, Enciso-Moreno JA, Hancock REW, Rivas-Santiago B (2015) LL-37 immunomodulatory activity during Mycobacterium tuberculosis infection in macrophages. *Infect Immun* **83**: 4495–4503.

145. Rekha RS, Rao Muvva SSVJ, Wan M, Raqib R, Bergman P, Brighenti S, Gudmundsson GH, Agerberth B (2015) Phenylbutyrate induces LL-37-dependent autophagy and intracellular killing of Mycobacterium tuberculosis in human macrophages. *Autophagy* **11**: 1688–1699.

146. Kim TS, Shin YH, Lee HM, Kim JK, Choe JH, Jang JC, Um S, Jin HS, Komatsu M, Cha GH, et al. (2017) Ohmyungsamycins promote antimicrobial responses through autophagy activation via AMP-Activated protein kinase pathway. *Sci Rep* **7**: 1–14.

147. Nagy TA, Quintana JLJ, Reens AL, Crooks AL, Detweiler CS (2019) Autophagy induction by a small molecule inhibits Salmonella survival in macrophages and mice. *Antimicrob Agents Chemother* **63**: e01536-19.

148. Al Azzaz J, Rieu A, Aires V, Delmas D, Chluba J, Winckler P, Bringer M-A, Lamarche J, Vervandier-Fasseur D, Dalle F, et al. (2019) Resveratrol-Induced Xenophagy Promotes Intracellular Bacteria Clearance in Intestinal Epithelial Cells and Macrophages. *Front Immunol* **9**: 3149.

149. American Thoracic Society. ATS Patient Education Series. (2017) Mechanical ventilation. *Am J Respir Crit Care Med* **196**: 3–4.

150. Yang CY, Chen CS, Yiang GT, Cheng YL, Yong SB, Wu MY, Li CJ (2018) New insights into the immune molecular regulation of the pathogenesis of acute respiratory distress syndrome. *Int J Mol Sci* **19**: 588.

151. WHO (2020) *Coronavirus disease 2019 (COVID-19) Situation Report –51*.

152. Fisher D, Heymann D (2020) Q&A: The novel coronavirus outbreak causing COVID-19. *BMC Med* **18**: 57.

153. Matthay MA, Aldrich JM, Gotts JE (2020) Treatment for severe acute respiratory

distress syndrome from COVID-19. *Lancet Respir Med* **8**: 433–434.

154. Matthay MA, Zemans RL (2011) The Acute Respiratory Distress Syndrome: Pathogenesis and Treatment. *Annu Rev Pathol Mech Dis* **6**: 147–163.

155. Zemans RL, Colgan SP, Downey GP (2009) Transepithelial migration of neutrophils: Mechanisms and implications for acute lung injury. *Am J Respir Cell Mol Biol* **40**: 519–535.

156. Högner K, Wolff T, Pleschka S, Plog S, Gruber AD, Kalinke U, Walmrath H-D, Bodner J, Gattenlöhner S, Lewe-Schlosser P, et al. (2013) Macrophage-expressed IFN-β Contributes to Apoptotic Alveolar Epithelial Cell Injury in Severe Influenza Virus Pneumonia. *PLoS Pathog* **9**: e1003188.

157. Gavard J (2009) Breaking the VE-cadherin bonds. *FEBS Lett* **583**: 1–6.

158. Schulte D, Küppers V, Dartsch N, Broermann A, Li H, Zarbock A, Kamenyeva O, Kiefer F, Khandoga A, Massberg S, et al. (2011) Stabilizing the VE-cadherin-catenin complex blocks leukocyte extravasation and vascular permeability. *EMBO J* **30**: 4157–4170.

159. Matthay MA, Ware LB, Zimmerman GA (2012) The acute respiratory distress syndrome. *J Clin Invest* **122**: 2731–2740.

160. Shaver CM, Wickersham N, McNeil JB, Nagata H, Miller A, Landstreet SR, Kuck JL, Diamond JM, Lederer DJ, Kawut SM, et al. (2018) Cell-free hemoglobin promotes primary graft dysfunction through oxidative lung endothelial injury. *JCI insight* **3**: e98546.

161. Beitler JR, Malhotra A, Thompson BT (2016) Ventilator-induced Lung Injury. *Clin Chest Med* **37**: 633–646.

162. Brower RG, Matthay MA, Morris A, Schoenfeld D, Thompson BT, Wheeler A (2000) Ventilation with lower tidal volumes as compared with traditional tidal volumes for acute lung injury and the acute respiratory distress syndrome. *N Engl J Med* **342**: 1301–1308.

163. Thompson BT, Chambers RC, Liu KD (2017) Acute Respiratory Distress Syndrome. *N Engl J Med* **377**: 562–572.

164. Matthay MA, McAuley DF, Ware LB (2017) Clinical trials in acute respiratory distress syndrome: challenges and opportunities. *Lancet Respir Med* **5**: 524–534.

165. Spragg RG, Lewis JF, Walmrath H-D, Johannigman J, Bellingan G, Laterre P-F, Witte MC, Richards GA, Rippin G, Rathgeb F, et al. (2004) Effect of Recombinant Surfactant Protein C–Based Surfactant on the Acute Respiratory Distress Syndrome. *N Engl J Med* **351**: 884–892.

166. Thille AW, Esteban A, Fernández-Segoviano P, Rodriguez JM, Aramburu JA, Peñuelas O, Cortés-Puch I, Cardinal-Fernández P, Lorente JA, Frutos-Vivar F (2013) Comparison of the berlin definition for acute respiratory distress syndrome

with autopsy. *Am J Respir Crit Care Med* **187**: 761–767.

167. Thille AW, Esteban A, Fernández-Segoviano P, Rodriguez JM, Aramburu JA, Vargas-Errázuriz P, Martín-Pellicer A, Lorente JA, Frutos-Vivar F (2013) Chronology of histological lesions in acute respiratory distress syndrome with diff use alveolar damage: A prospective cohort study of clinical autopsies. *Lancet Respir Med* **1**: 395–401.

168. Ressler B, Lee RT, Randell SH, Drazen JM, Kamm RD (2000) Molecular responses of rat tracheal epithelial cells to transmembrane pressure. *Am J Physiol - Lung Cell Mol Physiol* **278**: L1264-72.

169. Karadottir H, Kulkarni NN, Gudjonsson T, Karason S, Gudmundsson GH (2015) Cyclic mechanical stretch down-regulates cathelicidin antimicrobial peptide expression and activates a pro-inflammatory response in human bronchial epithelial cells. *PeerJ* **3**: e1483.

170. Walters MS, Gomi K, Ashbridge B, Moore M a S, Arbelaez V, Heldrich J, Ding B-S, Rafii S, Staudt MR, Crystal RG (2013) Generation of a human airway epithelium derived basal cell line with multipotent differentiation capacity. *Respir Res* **14**: 135.

171. Halldorsson S, Asgrimsson V, Axelsson I, Gudmundsson GH, Steinarsdottir M, Baldursson O, Gudjonsson T (2007) Differentiation potential of a basal epithelial cell line established from human bronchial explant. *Vitr Cell Dev Biol - Anim* **43**: 283–289.

172. Kulkarni NN, Yi Z, Huehnken C, Agerberth B, Gudmundsson GH (2015) Phenylbutyrate induces cathelicidin expression via the vitamin D receptor: Linkage to inflammatory and growth factor cytokines pathways. *Mol Immunol* **63**: 530–539.

173. Yoshio H, Tollin M, Gudmundsson GH, Lagercrantz H, Jörnvall H, Marchini G, Agerberth B (2003) Antimicrobial Polypeptides of Human Vernix Caseosa and Amniotic Fluid: Implications for Newborn Innate Defense. *Pediatr Res* **53**: 211–216.

174. Riquelme SA, Hopkins BD, Wolfe AL, DiMango E, Kitur K, Parsons R, Prince A (2017) Cystic Fibrosis Transmembrane Conductance Regulator Attaches Tumor Suppressor PTEN to the Membrane and Promotes Anti Pseudomonas aeruginosa Immunity. *Immunity* **47**: 1169-1181.e7.

175. Hawdon NA, Aval PS, Barnes RJ, Gravelle SK, Rosengren J, Khan S, Ciofu O, Johansen HK, Høiby N, Ulanova M (2010) Cellular responses of A549 alveolar epithelial cells to serially collected *Pseudomonas aeruginosa* from cystic fibrosis patients at different stages of pulmonary infection. *FEMS Immunol Med Microbiol* **59**: 207–220.

176. O'Grady EP, Mulcahy H, O'Callaghan J, Adams C, O'Gara F (2006) Pseudomonas aeruginosa infection of airway epithelial cells modulates expression of Kruppel-like factors 2 and 6 via RsmA-mediated regulation of type III exoenzymes S and Y. *Infect Immun* **74**: 5893–5902.

177. Bedi B, Maurice NM, Ciavatta VT, Lynn KS, Yuan Z, Molina SA, Joo M, Tyor WR, Goldberg JB, Koval M, et al. (2017) Peroxisome proliferator-activated receptor-γ agonists attenuate biofilm formation by Pseudomonas aeruginosa. *FASEB J* **31**: 3608–3621.

178. Wang Z, Li R, Tan J, Peng L, Wang P, Liu J, Xiong H, Jiang B, Chen Y (2015) Syndecan-1 Acts in Synergy with Tight Junction Through Stat3 Signaling to Maintain Intestinal Mucosal Barrier and Prevent Bacterial Translocation. *Inflamm Bowel Dis* **21**: 1894–1907.

179. Randow F, Münz C (2012) Autophagy in the regulation of pathogen replication and adaptive immunity. *Trends Immunol* **33**: 475–487.

180. Rubinsztein DC, Codogno P, Levine B (2012) Autophagy modulation as a potential therapeutic target for diverse diseases. *Nat Rev Drug Discov* **11**: 709–730.

181. Sanchez AMJ, Bernardi H, Py G, Candau RB (2014) Autophagy is essential to support skeletal muscle plasticity in response to endurance exercise. *Am J Physiol Integr Comp Physiol* **307**: R956–R969.

182. Losier TT, Akuma M, McKee-Muir OC, LeBlond ND, Suk Y, Alsaadi RM, Guo Z, Reshke R, Sad S, Campbell-Valois FX, et al. (2019) AMPK Promotes Xenophagy through Priming of Autophagic Kinases upon Detection of Bacterial Outer Membrane Vesicles. *Cell Rep* **26**: 2150-2165.e5.

183. You L, Wang Z, Li H, Shou J, Jing Z, Xie J, Sui X, Pan H, Han W (2015) The role of STAT3 in autophagy. *Autophagy* **11**: 729–739.

184. Hardie DG (2011) AMPK and autophagy get connected. *EMBO J* **30**: 634–635.

185. Jia J, Abudu YP, Claude-Taupin A, Gu Y, Kumar S, Choi SW, Peters R, Mudd MH, Allers L, Salemi M, et al. (2019) Galectins control MTOR and AMPK in response to lysosomal damage to induce autophagy. *Autophagy* **15**: 169–171.

186. Jia J, Abudu YP, Claude-Taupin A, Gu Y, Kumar S, Choi SW, Peters R, Mudd MH, Allers L, Salemi M, et al. (2018) Galectins Control mTOR in Response to Endomembrane Damage. *Mol Cell* **70**: 120-135.e8.

187. Napolitano G, Ballabio A (2016) TFEB at a glance. *J Cell Sci* **129**: 2475–2481.

188. Baek SH, Kim K Il (2017) Epigenetic Control of Autophagy: Nuclear Events Gain More Attention. *Mol Cell* **65**: 781–785.

189. Ricard JD, Dreyfuss D, Saumon G (2001) Production of inflammatory cytokines in ventilator-induced lung injury: A reappraisal. *Am J Respir Crit Care Med* **163**: 1176–1180.

190. Tremblay L, Valenza F, Ribeiro SP, Li J, Slutsky AS (1997) Injurious ventilatory strategies increase cytokines and c-fos m-RNA expression in an isolated rat lung model. *J Clin Invest* **99**: 944–952.

191. Meyer NJ, Christie JD (2013) Genetic heterogeneity and risk of acute respiratory distress syndrome. *Semin Respir Crit Care Med* **34**: 459–474.

192. Vohwinkel CU, Hoegl S, Eltzschig HK (2015) Hypoxia signaling during acute lung injury. *J Appl Physiol* **119**: 1157–1163.

193. Bersten AD, Hunt T, Nicholas TE, Doyle IR (2001) Elevated plasma surfactant protein-B predicts development of acute respiratory distress syndrome in patients with acute respiratory failure. *Am J Respir Crit Care Med* **164**: 648–652.

194. Abadie Y, Bregeon F, Papazian L, Lange F, Chailley-Heu B, Thomas P, Duvaldestin P, Adnot S, Maitre B, Delclaux C (2005) Decreased VEGF concentration in lung tissue and vascular injury during ARDS. *Eur Respir J* **25**: 139–146.

195. Thickett DR, Armstrong L, Christie SJ, Millar AB (2001) Vascular endothelial growth factor may contribute to increased vascular permeability in acute respiratory distress syndrome. *Am J Respir Crit Care Med* **164**: 1601–1605.

196. Park JA, Drazen JM, Tschumperlin DJ (2010) The chitinase-like protein YKL-40 is secreted by airway epithelial cells at base line and in response to compressive mechanical stress. *J Biol Chem* **285**: 29817–29825.

197. Potey PM, Rossi AG, Lucas CD, Dorward DA (2019) Neutrophils in the initiation and resolution of acute pulmonary inflammation: understanding biological function and therapeutic potential. *J Pathol* **247**: 672–685.

198. Xiao R, Chen R (2017) Neutrophil gelatinase-associated lipocalin as a potential novel biomarker for ventilator-associated lung injury. *Mol Med Rep* **15**: 3535–3540.

199. Schutte BC, McCray PB (2002) β-Defensins in Lung Host Defense. *Annu Rev Physiol* **64**: 709–748.

200. Liu T, Zhang L, Joo D, Sun SC (2017) NF-κB signaling in inflammation. *Signal Transduct Target Ther* **2**: 17023.

201. Lemarié CA, Esposito B, Tedgui A, Lehoux S (2003) Pressure-induced vascular activation of nuclear factor-κB: Role in cell survival. *Circ Res* **93**: 207–212.

202. Rekha RS, Karadottir H, Ahmed S, Gudmundsson GH, Agerberth B, Bergman P (2020) Innate Effector Systems in Primary Human Macrophages Sensitize Multidrug-Resistant Klebsiella pneumoniae to Antibiotics. *Infect Immun* **88**: e00186-20.

# Paper I

SCIENTIFIC REPORTS

OPEN

# Novel aroylated phenylenediamine compounds enhance antimicrobial defense and maintain airway epithelial barrier integrity

Received: 31 January 2019
Accepted: 18 April 2019
Published online: 08 May 2019

Iwona T. Myszor[1], Zahida Parveen[1], Håkan Ottosson[2], Peter Bergman[3], Birgitta Agerberth[3], Roger Strömberg[2] & Gudmundur H. Gudmundsson[1]

**Aroylated phenylenediamines (APDs) are novel inducers of innate immunity enhancing cathelicidin gene expression in human bronchial epithelial cell lines. Here we present two newly developed APDs and aimed at defining the response and signaling pathways for these compounds with reference to innate immunity and antimicrobial peptide (AMP) expression. Induction was initially defined with respect to dose and time and compared with the APD Entinostat (MS-275). The induction applies to several innate immunity effectors, indicating that APDs trigger a broad spectrum of antimicrobial responses. The bactericidal effect was shown in an infection model against *Pseudomonas aeruginosa* by estimating bacteria entering cells. Treatment with a selected APD counteracted *Pseudomonas* mediated disruption of epithelial integrity. This double action by inducing AMPs and enhancing epithelial integrity for one APD compound is unique and taken as a positive indication for host directed therapy (HDT). The APD effects are mediated through Signal transducer and activator of transcription 3 (STAT3) activation. Utilization of induced innate immunity to fight infections can reduce antibiotic usage, might be effective against multidrug resistant bacteria and is in line with improved stewardship in healthcare.**

The airway epithelium plays a critical role in the first line of defense against respiratory pathogens. The pseudostratified bronchial epithelial layer is composed of undifferentiated basal cells and mature cells tightly linked by adherent and tight junctions providing a stringent barrier between the host milieu and the environment[1,2]. Protection is also provided by the mucus layer at the apical surface of the airway epithelium, which is a complex mixture of different glycoproteins and defense components such as antimicrobial peptides (AMPs). Mucociliary clearance by beating cilia drives movements of the mucus layer for the removal of particles and microbes[1,3–5]. Multiple human AMPs have been identified, the major two families include the defensins (α- and β-defensins) and the cathelicidin-family with one dominant peptide LL-37[6–8]. AMPs on the airway epithelial surfaces are expressed constitutively and can be induced by activation of pattern recognition receptors (PRRs) on the epithelial cells, such as transmembrane Toll-like receptors and intracellular NOD-like receptors. Cytokines can also affect the AMPs expression, as confirmed for IL-17 and IL-22[1,9]. The crucial role of AMPs in the first line of defense against respiratory pathogens was confirmed by using β-defensin-1 and cathelicidin deficient mice that were more susceptible to infections[10,11]. Besides broad-spectrum direct microbicidal activity, AMPs display immunomodulatory functions such as chemotaxis[6,12]. Similar to the defensins, LL-37 can also be immunomodulatory, stimulating airway epithelial cell proliferation and wound healing[13,14]. Recently, it was shown that LL-37 activates autophagy and promotes killing of intracellular *M. tuberculosis*[15,16].

Human AMPs can be regarded as endogenous antibiotics because of their broad antimicrobial activity[14,17]. AMPs are important in host - pathogen interactions and could be utilized to fight infections, potentially including those caused by antibiotic resistant bacteria. Multidrug-resistant (MDR) pathogens are a serious threat for the society and healthcare as exemplified by growing number of infections with the ESKAPE pathogens (*Enterococcus faecium*, *Staphylococcus aureus*, *Klebsiella pneumoniae*, *Acinetobacter baumanni*, *Pseudomonas aeruginosa* and

[1]Biomedical Center, University of Iceland, Reykjavik, 101, Iceland. [2]Department of Biosciences and Nutrition, Karolinska Institutet, S-14183, Huddinge, Sweden. [3]Department of Laboratory Medicine, Clinical Microbiology, Karolinska Institutet, S-14186, Huddinge, Sweden. Correspondence and requests for materials should be addressed to G.H.G. (email: ghrafn@hi.is)

*Enterobacter spp*.), where some of these bacteria are opportunistic pathogens[18,19]. Specifically *P. aeruginosa* and *S. aureus* are pathogens causing respiratory tract infections that can be life-threatening for immunocompromised patients especially for those suffering from cystic fibrosis[20]. Therefore alternative therapies to treat infections are urgently needed[18,19]. The induction of endogenous AMPs could be an effective way of treating infections because many MDR strains are susceptible to different AMPs. Several different compounds inducing expression of AMPs to boost innate immunity have been shown effective in animal models and clinical trials for treatment of infectious diseases, e.g. pulmonary tuberculosis[21,22]. Vitamin D3 is a direct inducer of the *CAMP* gene expression, the gene encoding the antimicrobial peptide LL-37[23–25]. Another potent inducer is phenylbutyrate (PBA), a short chain fatty acid derivative and also a histone deacetylase inhibitor (HDACi)[26]. Interestingly, PBA treatment of *Shigella*-infected rabbits resulted in clearance of *Shigella* infection and counteracted the suppression of rabbit cathelicidin (CAP-18) in the gut and lung epithelium[27]. However, PBA has a fast turnover and is converted into phenylacetate by β-oxidation[28], therefore high doses of PBA are needed to induce AMPs expression *in vitro* and *in vivo*. Additional potent *CAMP* gene inducers described recently are Entinostat and derivatives designated aroylated phenylenediamines (APDs)[29,30]. It has been shown that Entinostat stimulates *CAMP* gene expression via activation of STAT3 and HIF-1α transcription factors in human colonic epithelial cells[29]. Moreover, oral treatment of *Shigella*- and *Vibrio cholera*- infected rabbits with Entinostat improved their survival and restored production of the rabbit cathelicidin CAP-18 in gut epithelial surfaces[30,31]. Entinostat is an HDACi undergoing clinical trials as adjunctive cancer therapy[32]. However, Entinostat has a documented cytotoxicity[33,34].

In this study we tested if new APDs, designated HO53 and HO56 could stimulate innate immunity responses in airway epithelial cells by enhancing the expression of endogenous AMPs and if that response was effective against the respiratory pathogen *Pseudomonas aeruginosa* PAO1 strain. We used bronchial epithelial cell lines, exhibiting a basal-like character and with the ability to differentiate towards polarized bronchial epithelium during air-liquid interface culture (ALI). In human bronchial epithelial cell lines, the new APDs markedly induced expression of the *CAMP* gene (encoding cathelicidin pro-LL-37/LL-37) both in monolayer and in ALI. The *CAMP* gene served as the reference, but also induction of other innate immunity genes involved in the defense against infections was observed. In the infection model with pretreatment of bronchial epithelial cells with the APDs significantly reduced the number of intracellular bacteria without exhibiting direct antibiotic properties. We could also demonstrate that treatment with one APD (HO53) of ALI cells counteracted the disruptive effect of *P. aeruginosa* conditioned medium by maintaining the epithelial barrier integrity. Utilizing a specific inhibitor, we showed that STAT3 transcription factor was involved in the HO53 mediated *CAMP* induction. Taken together, the current study might open up possibilities for using APDs as novel innate immunity modulators for host directed therapy (HDT) of infectious diseases.

## Results

### HO53 and HO56 induce *CAMP* gene expression in bronchial epithelial cell lines (BCi and VA10).

Entinostat has been confirmed as a potent inducer of AMPs, with effects against bacterial infections in animal models[30,31], but is known to possess cytotoxic properties[33,34] and has limited solubility in aqueous solutions. Based on the structure activity relations found in the first studies on APDs[30], we started to optimize the AMP-inducing aroylated phenylenediamines (APDs) by designing and synthesizing new alternative compounds. The criterion was to reduce toxicity, while retaining efficient induction of AMPs and the design was based on making more hydrophilic APDs. Using the previously described luciferase reporter HT29 colonic cell line for expression-analysis of the antimicrobial peptide LL-37[35], we identified, among the novel APDs, HO53 and HO56 (Fig. 1a; Supplementary Figs S1 and S2; Supplementary Methods) as interesting AMP-inducers with high activity but reduced toxicity.

The present study is focused on the effect of the two new compounds HO53 and HO56 (Fig. 1a) and with Entinostat as comparison. HO53 and HO56 enhanced *CAMP* gene expression in BCi-NS1.1 cells (BCi) at 24 h post treatment in a dose dependent way (Fig. 1b; Supplementary Fig. S3b and S3c). Entinostat also induced *CAMP* gene expression in BCi cells at 24 h but in contrast to HO53 and HO56, the induction was not dose dependent (Fig. 1b; Supplementary Fig. S3a). A similar pattern of induction with HO53 and HO56 was observed for the bronchial epithelial cell line VA10 (Supplementary Fig. S4). A broad range of HO53 and HO56 concentrations (2.5–250 μM) (Supplementary Fig. S3b and S3c) was tested and for further experiments we selected 75 μM for both compounds. These concentrations represented a low dose that significantly induced *CAMP* gene expression and had low effect on cytotoxicity and proliferation of BCi cells as compared to Entinostat, but comparable to PBA (Supplementary Fig. S5a and S5b). We used lower concentrations of Entinostat (2.5–50 μM) to keep the DMSO (solvent) concentration in the cell culture medium lower than 1% (v/v). However, there was no difference in the *CAMP* gene induction between the various concentrations of Entinostat in BCi cells and therefore we decided to use 10 μM in following experiments because of low cytotoxicity (Supplementary Fig. S5).

Next, we monitored *CAMP* gene expression over time (0–72 h) with the selected concentration of Entinostat (10 μM), HO53 and HO56 (both 75 μM) (Fig. 1c–e). Notably, the *CAMP* gene expression was increased significantly after 12 h and 24 h of treatment with HO56 and HO53, respectively and reached maximum expression at 24 h that was maintained up to 48 h post- treatment, but declined at 72 h. A similar effect was observed for Entinostat, where the maximal fold induction was after 24 h and lasted until 48 h, but declined at 72 h. Furthermore, we tested cooperation of HO53 and HO56 with the known *CAMP* gene inducers PBA (2 mM) and vitamin D3 (1α,25-dihydroxyvitamin D3; 100 nM) (Fig. 1f). We observed a synergistic effect between vitamin D3 and the two compounds at 24 h. However, no cooperation was observed upon treatment with PBA and HO53 or HO56 (Fig. 1f). Consistent with these findings, the synergistic effect after co-treatment with vitamin D3 was also reflected at the protein level by Western blot analyzes, where higher amount of pro-LL-37 was secreted to the cell culture medium (Fig. 1g). HO53 and HO56 separately and in combination with PBA did not affect the pro-LL-37

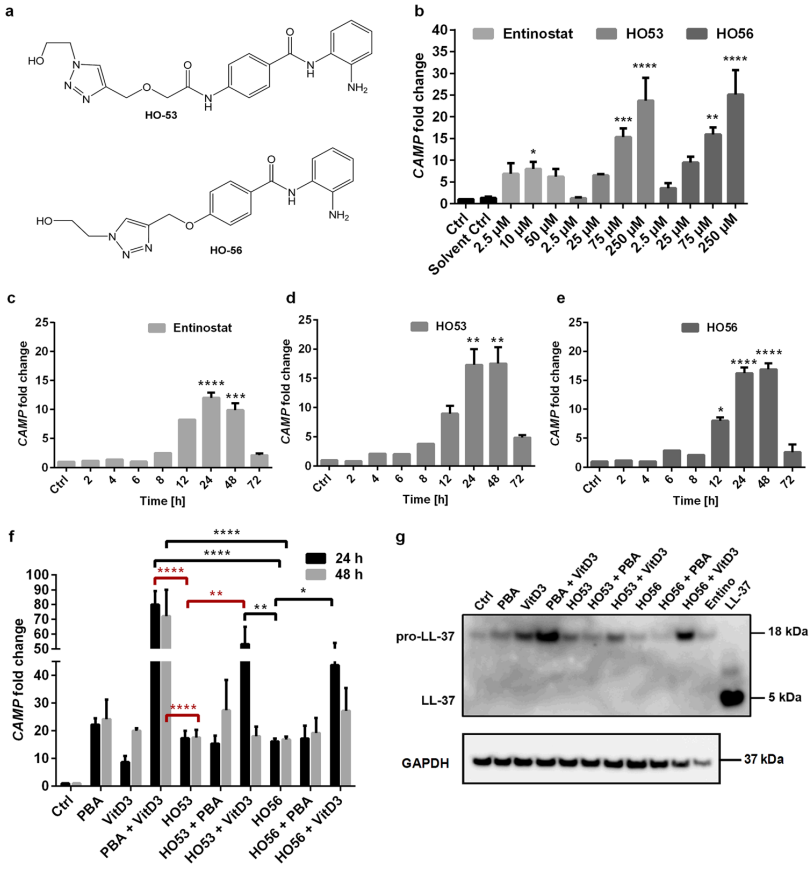


**Figure 1.** Enhanced induction of the *CAMP* gene by HO53 and HO56 in BCi cells. (**a**) Structure of the two novel aroylated phenylenediamine (APD) compounds investigated in this study, HO53 and HO56. (**b**) Induction of the *CAMP* gene with increasing concentration of Entinostat, HO53 and HO56 in BCi cells after 24 h post treatment. DMSO (final concentration lower than 1%) was used as a solvent control (Solvent Ctrl). Each bar represents mean value of 3 independent experiments ± SEM; statistical significance was calculated in comparison to control cells (Ctrl) using one-way ANOVA with Dunnett's multiple comparisons test. Time-dependent *CAMP* induction by (**c**) Entinostat (10 µM), (**d**) HO53 (75 µM) and (**e**) HO56 (75 µM) in BCi cells, respectively. Bars for 2–8 h (for HO53 and HO56) and bars for 2–12 h (for Entinostat) represent values from two technical repeats. Bars for 12–72 h (for HO53 and HO56) and bars for 24–72 h (for Entinostat) are mean values of 3 independent experiments ± SEM; statistical significance was calculated in comparison to control cells (Ctrl) using one-way ANOVA with Sidak's multiple comparisons test. (**f**) Cooperation of HO53 and HO56 (both at 75 µM) with sodium 4-phenylbutyrate (PBA; 2 mM) or 1α,25-dihyroxyvitamin D3 (VitD3; 100 nM) for the induction of the *CAMP* gene at 24 h and 48 h. Each bar represents mean value of 3 independent experiments ± SEM; statistical significance was calculated in comparison to HO53 (red) and HO56 (black) using two-way ANOVA with Dunnett's multiple comparisons test. (**g**) Concentrated culture medium after 24 h stimulation was used for Western blot analyses using monoclonal antibody against LL-37. Positive control included 2 ng of synthetic LL-37 peptide. GAPDH analyzed in cell lysates was used as a loading control. The representative Western blot is one of 3 independent experiments. The full-length blots are presented in Supplementary Figure S10a. For all qRT-PCR experiments the *CAMP* gene expression was normalized to *TUBB* (tubulin-β) reference gene and presented as fold change of the expression compared to control cells (Ctrl) set as 1. Symbols for statistical analysis indicate p-values *$p < 0.05$, **$p < 0.01$, ***$p < 0.001$, ****$p < 0.0001$.

secretion. Taken together, our findings showed that HO53 and HO56 are novel, low toxic inducers of the *CAMP* gene expression in bronchial epithelium, working in synergy with vitamin D3.

**HO53 and HO56 induce several antimicrobial effectors in a bronchial epithelial cell line (BCi).** Further, we analyzed expression of additional antimicrobial proteins/peptides. *LCN2* encoding lipocalin 2, a siderophore binding protein that inhibits bacterial growth in iron deficient environment[36]. After 48 h stimulation

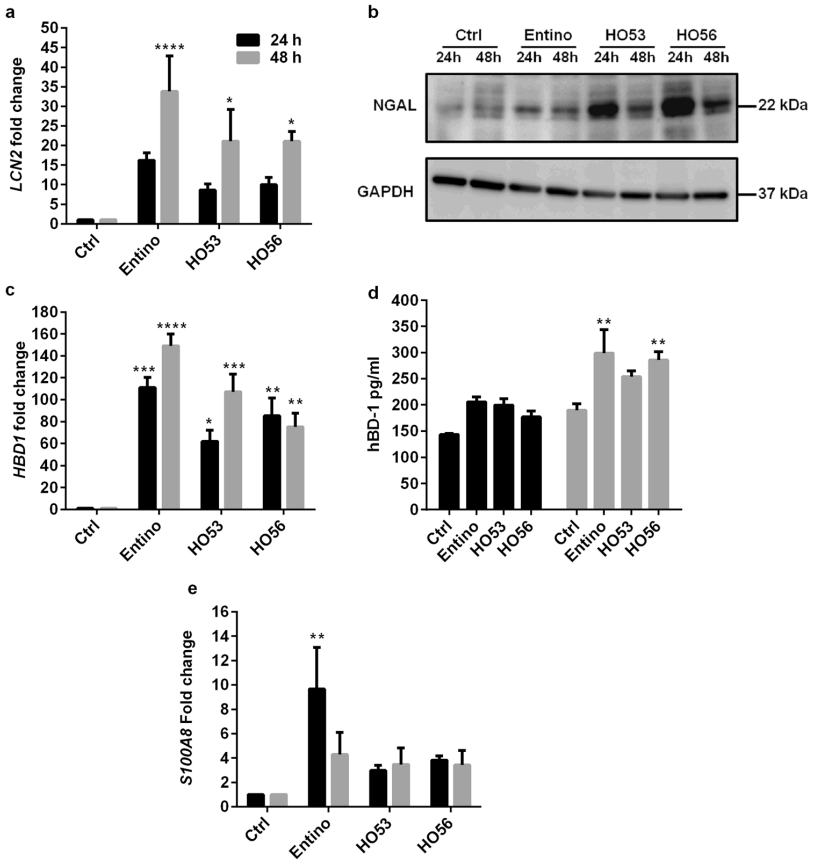


**Figure 2.** Enhanced expression of antimicrobial effectors by HO53 and HO56 stimulation in BCi cells. Samples were collected after 24 h (black bars) and 48 h (grey bars) post stimulation with Entinostat (10 μM), HO53 (75 μM) and HO56 (75 μM). Followed by expression analysis at mRNA and protein level by qRT-PCR and ELISA/Western blot, respectively. (**a**) Expression of *LCN2* (lipocalin 2) at mRNA and (**b**) protein (lipocalin 2, NGAL) level in cell lysates. The representative Western blot is selected from one of the 3 independent experiments. GAPDH was used as a loading control. Full-length blots are presented in Supplementary Figure S10b. (**c**) Fold change of *HBD1* (human β-defensin 1) mRNA in comparison to control (Ctrl) and (**d**) secretion of hBD-1 peptide measured by ELISA in cell culture supernatants. (**e**) *S100A8* expression was analyzed by qRT-PCR. *TUBB* (tubulin-β) was the reference gene in qRT-PCR. Each bar represents mean value of 3 independent experiments ± SEM; statistical significance was calculated in comparison to the control group using two-way ANOVA with Dunnett's multiple comparisons test; *$p < 0.05$, **$p < 0.01$, ***$p < 0.001$, ****$p < 0.0001$. Significant changes are highlighted.

with Entinostat, HO53 and HO56, the expression of *LCN2* at mRNA level was significantly increased (approximately 20–30 times) (Fig. 2a). The analyses at protein level revealed low induction of lipocalin 2 (also called Neutrophil gelatinase-associated lipocalin, NGAL) by Entinostat at 24 and 48 h and the representative relative NGAL/GAPDH ratio normalized to control was 1.85 and 1.45, respectively (Fig. 2b and Supplementary Table S2). In contrast to Entinostat, the induction of lipocalin 2 with HO53 and HO56 was prominent at 24 h (the representative relative NGAL/GAPDH ratio normalized to control was 6.56 and 6.98 respectively) and decreased at 48 h (2.24 and 2.23 for HO53 and HO56, respectively) (Fig. 2b and Supplementary Table S2). *HBD1* encoding the human β-defensin-1 antimicrobial peptide[37] was significantly induced by Entinostat, HO53 and HO56 at mRNA level (Fig. 2c). Significant induction of human β-defensin-1 antimicrobial peptide at the protein level analyzed by ELISA was observed at 48 h (Fig. 2d). In addition, the *S100A8* gene encoding a unit of calprotectin antimicrobial protein[38] was significantly induced by Entinostat (approximately 10 times) after 24 h stimulation, whereas induction with HO53 and HO56 was not significant (Fig. 2e). In contrast, the expression of lysozyme (*LYZ*), lactoferrin (*LTF*) and β-defensin 2 (*HBD2)* at mRNA levels was not detected in monolayer BCi cells. In summary the APD compounds affected multiple innate antimicrobial effectors in bronchial undifferentiated epithelial cells.

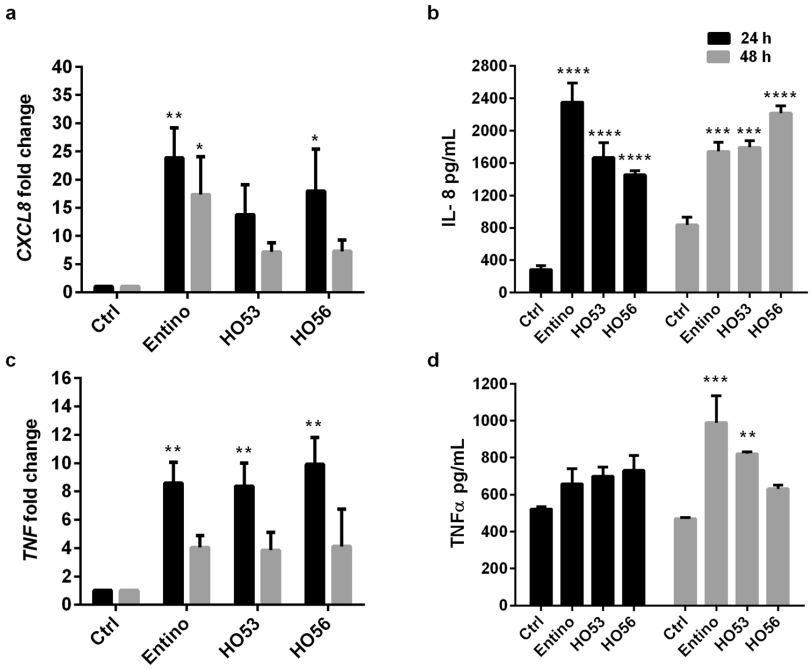


**Figure 3.** HO53 and HO56 alter expression of cytokines in BCi cells. Expression of (**a**) *CXCL8* and (**c**) *TNF* at mRNA level was analyzed by qRT-PCR and normalized to *TUBB* (tubulin-β) reference gene. The secretion of the proteins (**b**) IL8 (CXCL8) and (**d**) TNFα was evaluated by ELISA in corresponding cell culture medium. Analysis was performed at 24 h (black bars) and 48 h (grey bars) after stimulation with Entinostat (10 μM), HO53 (75 μM) and HO56 (75 μM). For all experiment each bar represents mean value of 3 independent experiments ± SEM; statistical significance was calculated in comparison to the untreated control cells (Ctrl) using two-way ANOVA with Dunnett's multiple comparisons test; *$p < 0.05$, **$p < 0.01$, ***$p < 0.001$, ****$p < 0.0001$. Significant changes are highlighted.

**HO53 and HO56 affect cytokine profiles in bronchial epithelial cell line (BCi).** We also evaluated the effect of Entinostat, HO53 and HO56 on the induction of the pro-inflammatory mediators IL-8 (CXCL8) and TNFα. Upon induction with Entinostat and HO56 a significant induction of mRNA for IL-8 was observed (Fig. 3a). However, at the protein level significantly increased secretion of IL-8 in cell supernatants was observed for the three inducing compounds (Fig. 3b). Induction of TNFα mRNA expression for three inducing compounds was observed only at 24 h (Fig. 3c) but at the protein level significant increased secretion was detected only in cell supernatants from Entinostat and HO53 stimulated culture at 48 h (Fig. 3d). In summary the APD compounds Entinostat, HO53 and HO56 affected the expression and release of specific cytokines and chemokines, indicating potent enhancement of innate immunity defenses in bronchial epithelial cells.

**HO53 and HO56 enhance antibacterial activity of the human bronchial epithelial cells (BCi).** We observed that HO53 and HO56 treatment enhanced production of AMPs and other innate immunity factors in human bronchial epithelial cells. Therefore, we tested if HO53 and HO56 treatment was effective in inducing a functional antimicrobial response in BCi cells against the respiratory pathogen *Pseudomonas aeruginosa* strain PAO1 (Fig. 4). BCi cells were treated for 24 h with HO53 and HO56, then infected for 1 h with multiplicity of infection (MOI) ~40, remaining extracellular bacteria were eliminated by treatment with gentamicin and the number of intracellular bacteria were enumerated as colony forming units (CFU). The number of intracellular PAO1 was significantly lower after HO53 (~75%) and HO56 (~60%) treatment in comparison to the PAO1 number in untreated control cells (100%; equal to ~$1.0 \times 10^4$ intracellular PAO1) (Fig. 4a). The treatment with low doses of gentamicin (0.5 μg/ml), a cell impermeable antibiotic, served as a positive control and reduced PAO1 entry to the cells about 50%. We performed an analogous experiment to the infection assay but in the absence of the BCi cells (Fig. 4b). After 1 h direct exposure of PAO1 to HO53 and HO56 in the cell culture medium, there was no significant differences in CFU counts (Fig. 4b). Furthermore, HO53 and HO56 did not inhibit PAO1 growth in Luria Bertani (LB) medium over time and did not kill bacteria after 2 h of direct exposure (Fig. 4c,d). To verify if the reduction of the intracellular PAO1 number was caused by induced antimicrobial polypeptides, we excluded additional antimicrobial effector systems that are involved in the defense of the epithelial surfaces, by analyzing the production of reactive oxygen species (ROS) (Supplementary Fig. S6a) and nitric oxide (NO) (Supplementary Fig. S6b, S6c)[39,40]. These findings indicated that the reduction of intracellular bacterial number

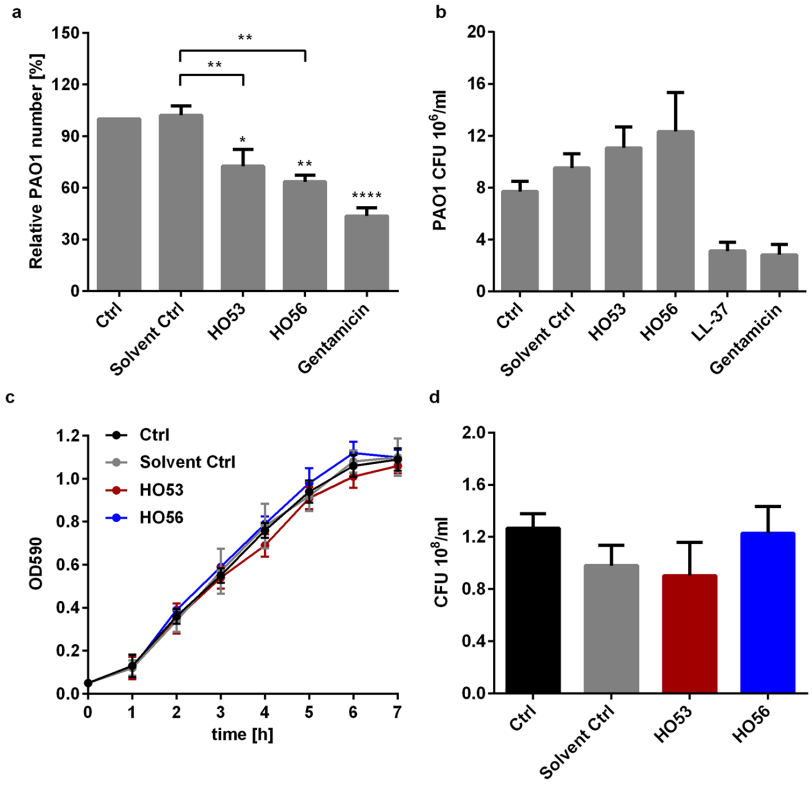


**Figure 4.** HO53 and HO56 enhance antimicrobial response in BCi cells but are not directly bactericidal. (**a**) Effect of APDs treatment on *Pseudomonas aeruginosa* PAO1 invasion of BCi cells. Cells were stimulated with HO53 and HO56 (both at 75 µM) for 24 h, then infected with PAO1 for 1 h and the remaining extracellular bacteria were eliminated with gentamicin (100 µg/ml) treatment for 20 min. Intracellular bacteria are presented as a percentage of colony forming units (CFU) from untreated cells (Ctrl) showed as relative PAO1 number [%]. Gentamicin at low concentration (0.5 µg/ml) was used as a positive control. (**b**) The direct effect of the two APDs on PAO1 in the cell culture medium (BEGM) in absence of BCi cells, presented as CFU after 1 h direct exposure. Gentamicin at low concentration (1 µg/ml) and synthetic LL-37 peptide (1 µg/ml) were used as positive controls. (**c**) *Pseudomonas aeruginosa* PAO1 growth and **d**) viability after 2 h co-incubation with the two APDs in Luria Bertani (LB) medium. Independent experiments of 3 ± SEM, for (**a**,**b** and **d**) statistical significance was calculated using one-way ANOVA with Dunnett's multiple comparisons test while comparing to untreated group (Ctrl) or with Sidak's multiple comparisons test while comparing to solvent control group. For (**c**) statistical significance was calculated using two-way ANOVA with Dunnett's multiple comparisons test, $^{*}p < 0.05$, $^{**}p < 0.01$, $^{****}p < 0.0001$. Significant changes are highlighted.

was due to induced antimicrobial responses in human bronchial epithelial cells, but not any direct activity of the two APD compounds.

**HO53 and HO56 induce several innate immunity genes in polarized bronchial epithelial cells.** In order to transfer our findings into a more clinically relevant context, we tested if HO53 and HO56 treatment was effective in stimulating antimicrobial responses in polarized mature epithelium, mimicking the human bronchi[41], we analyzed expression of AMPs in differentiated BCi cells. The mRNA levels of *LCN2* and *S100A8* were significantly higher compared to untreated cells, especially after 24 h post-treatment with HO56 (~4 and ~40 fold, respectively) (Fig. 5a,b). We also observed increased protein levels of lipocalin 2 (NGAL) and S100A8 after 24 and 48 h of treatment with HO53 and HO56. However, induction of lipocalin 2 was more pronounced after 48 h (Fig. 5c). Further, we analyzed the effects of HO53 and HO56 treatment on the expression of the genes *CAMP*, *HBD1* and *LYZ* in differentiated BCi cells (ALI). The *CAMP* gene expression was on a similar level as the cells in monolayer (upregulated about 15-times) but that effect was not observed after 48 h of treatment with HO53 and HO56 (Fig. 5d). The enhanced expression of *HBD1* (Fig. 5e) and *LYZ* (Fig. 5f) upon treatment with HO53 and HO56 was significantly higher (~10 times and 3 times, respectively). Furthermore, the expression of pro-inflammatory cytokines/chemokines was not significantly upregulated, except the expression of *IL1B* after

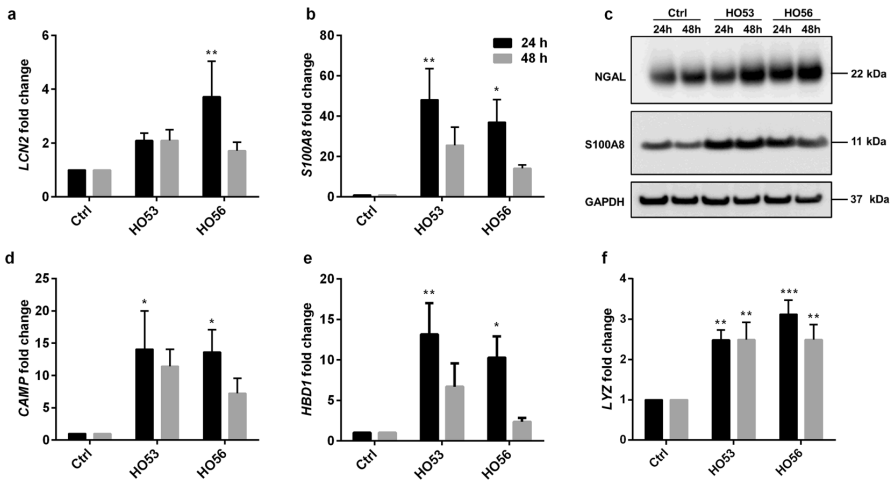


**Figure 5.** HO53 and HO56 enhance induction of additional innate immunity genes including cytokines in ALI differentiated BCi cells. Differentiated cells were used for experiments when TEER value reached approx. $\geq 1000\ \Omega \times cm^2$. Expression at mRNA level of (**a**) *LCN2*, (**b**) *S100A8* and (**c**) subsequent protein level expression of NGAL and S100A8 analyzed by Western blot. GAPDH was used as loading control. The Western blot analysis was performed n = 2 with similar results. Full-length blots are presented in Supplementary Figure S10c. The mRNA level of (**d**) *CAMP*, (**e**) *HBD1*, (**f**) *LYZ* after 24 h (black bars) and 48 h (grey bars) stimulation with HO53 and HO56 (both at 75 μM). Expression at mRNA level was analyzed by qRT-PCR and normalized to *TUBB* (tubulin-β) reference gene. Data is from n = 4 independent experiments ± SEM, statistical significance was calculated in comparison to untreated cells (Ctrl) using two-way ANOVA with Dunnett's multiple comparisons test, *$p < 0.05$, **$p < 0.01$, ***$p < 0.001$. Significant changes are indicated.

24 h of treatment with HO53 (Supplementary Fig. S7d). In contrast to monolayer cells, the expression of *TNF*/TNFα and *CXCL8*/IL-8 was not significant (Supplementary Fig. S7). In summary, we observed a different induction profile of antimicrobial effectors and cytokines/chemokines for differentiated cells in comparison to monolayer cells.

**HO53 counteracts disruptive effect of *P. aeruginosa* conditioned medium on airway epithelial integrity.** Pathogens exhibit different strategies to evade the host epithelial surfaces. *P. aeruginosa* can disintegrate the junctions between epithelial cells and enter tissue through the paracellular space[42]. Another strategy is the production of virulence factors that can be injected into the host cells or secreted by bacteria to the environment, e.g. rhamnolipids[43]. We have shown that *Pseudomonas aeruginosa* PAO1 conditioned medium can disrupt epithelial barrier integrity[44]. Here we investigated if the treatment with HO53 can counteract the disruptive effect of PAO1 conditioned medium (Fig. 6). BCi cells differentiated in ALI culture were pretreated with HO53 for three consecutive days and challenged with PAO1 conditioned medium applied on the apical side of ALI culture for 24 h. Azithromycin was used as a positive control (Supplementary Fig. S8). After 3 h exposure of control BCi cells to PAO1 conditioned medium, trans-epithelial electrical resistance (TEER) decreased from ~1200 $\Omega \times cm^2$ to ~200 $\Omega \times cm^2$ and the disruptive effect was also observed after 6 h of exposure (Fig. 6a). The recovery of the tight junctions (TJs) integrity was noted after 24 h post challenge. In contrast to the control cells, the pretreatment of the ALI culture with HO53 did not lead to a pronounced TEER drop (~1000 $\Omega \times cm^2$ to ~700 $\Omega \times cm^2$) and the epithelial barrier integrity was restored after 5 h. To illustrate counteraction of TJ disruption, we performed confocal microscopy after 6 h of PAO1 conditioned medium challenge. Consistent with the TEER results, the disruption of zonula occludens (ZO-1) and occludin was observed in the control group, while HO53 treated group maintained TJs integrity (Fig. 6b). We further analyzed levels of the tight junction proteins occludin and claudin-1 at selected time points (0, 3, 6, 24 h) by Western blot analysis (Fig. 6c). The band corresponding to the main occludin isoform was faintly detected after 3 and 6 h of PAO1 conditioned medium challenge in the control group (the western blot analyses shows the occludin degradation/processing product, Supplementary Fig. S9) and did not reach the same expression level after 24 h. However, in the cells pretreated with HO53 occludin was not degraded. After 3 h of challenge the occludin level was reduced, while after 6 h the expression was restored. Notably, induction of occludin expression was detected upon HO53 treatment, whereas there was no change in claudin-1 level (Fig. 6c). In conclusion, HO53 counteracted disruptive effect of PAO1 conditioned medium on respiratory epithelium via a novel mechanism affecting tight junctions.

**STAT3 activation is required for HO53 mediated *CAMP* gene induction.** It has been shown that Entinostat induces *CAMP* gene expression in gut epithelial cells *via* activation of STAT3 and HIF-1α transcription factors[29]. HO53 is structurally related to Entinostat and here we investigated if the molecular pathways

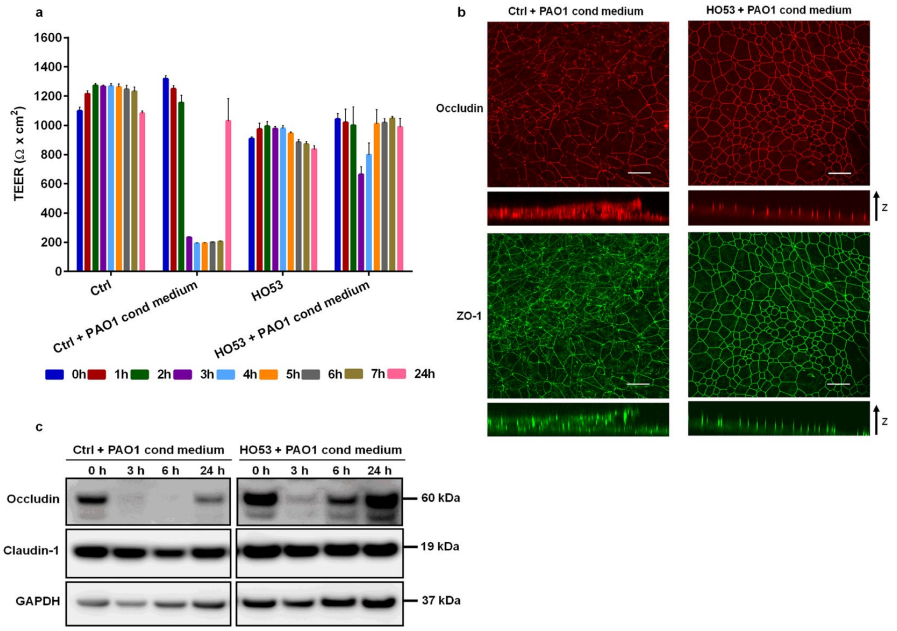


**Figure 6.** HO53 treatment counteracts the disruptive effect of *P. aeruginosa* PAO1 conditioned medium in ALI differentiated BCi cells. Differentiated BCi cells (trans epithelial electrical resistance, TEER $\geq 1000\ \Omega \times cm^2$) were treated with 75 µM HO53 in the lower chamber of transwell insert for 3 days and challenged with PAO1 conditioned medium (PAO1 cond medium) applied on the apical surface of the cells for the next 24 h. (**a**) TEER measurement after every hour from 0 to 7 h and after 24 h post PAO1 culture medium challenge. Data shown is representative of two experiment and showing mean values of four independent ALI filters at each time point ± SEM. Samples for confocal microscopy and Western blot were collected at selected time points in order to analyze tight junctions (TJ) integrity. (**b**) Confocal images showing disruption of occludin (red) and ZO-1 (green) after 6 h post PAO1 culture medium challenge of HO53 treated cells as compared to control cells (Ctrl), *Bar* = 10 µm. (**c**) Western blot analyses of occludin and claudin-1 after 0, 3, 6 and 24 h exposure to PAO1 culture medium. GAPDH was used as a loading control. The full-length blot for occludin is presented in Supplementary Figure S9 and for claudin-1 and GAPDH in Supplementary Figure S10d.

involved in the HO53 induced *CAMP* gene expression in bronchial epithelial cells follows similar pathways as described for the colon epithelial cell line HT-29[29]. For that, we examined the role of STAT3 by using the STAT3 inhibitor Stattic (Fig. 7a,b). BCi cells were pretreated with increasing doses of the Stattic inhibitor (5 µM, 10 µM, and 20 µM) for 30 min followed by stimulation with HO53 for 24 h. We observed significant dose-dependent Stattic mediated decrease in *CAMP* gene expression (Fig. 7a). Transcription factor HIF-1α expression was also decreased in a dose-dependent manner as for the *CAMP* gene (Fig. 7b). Furthermore, we investigated if HO53 treatment resulted in enhanced STAT3 expression or post-translational modifications (Fig. 7c). The expression level of STAT3 and phosphorylated-STAT3 was increased in a time dependent manner after treatment with HO53. The level of the phosphorylated STAT3 increased after 4 h and reached the maximum after 6 h of treatment with HO53. We did not observe any difference in the acetylation at Lys685 of STAT3 after treatment with HO53. However, modifications of other lysine residues of STAT3 cannot be excluded. HIF-1α expression level was gradually elevated at 4, 6 and 8 h and at 24 h there was a prominent enhanced level of HIF-1α. In summary, STAT3 is most likely a central regulator of the *CAMP* gene induction by HO53 although other STAT3 modifications need to be evaluated to explain the detailed mechanism of the inducing effect of HO53.

## Discussion

An increasing number of infections caused by antibiotic resistant pathogens contribute to higher morbidity/mortality rate and generate high costs for the health care system[45]. Therefore, development of alternative strategies to conventional antibiotic therapy is urgently needed. Host directed therapy (HDT) based on inducing innate immunity by enhancing expression of endogenous antimicrobial components or counteracting pathogen-mediated suppression of first line defenses could be an alternative[27]. HDT could limit the selection of antibiotic resistant strains and might be used against multidrug-resistant (MDR) bacteria.

Development of novel stable compounds for the induction of innate immunity would be beneficial. To approach this aim, a reporter cell line with the *CAMP* gene fused to the luciferase gene was established for screening induction of the *CAMP* gene expression[35]. Screening of compound libraries and selected HDAC inhibitors resulted in the identification of Entinostat, working against *Shigella* and *Vibrio* infections in rabbits[30,31]. Recently,

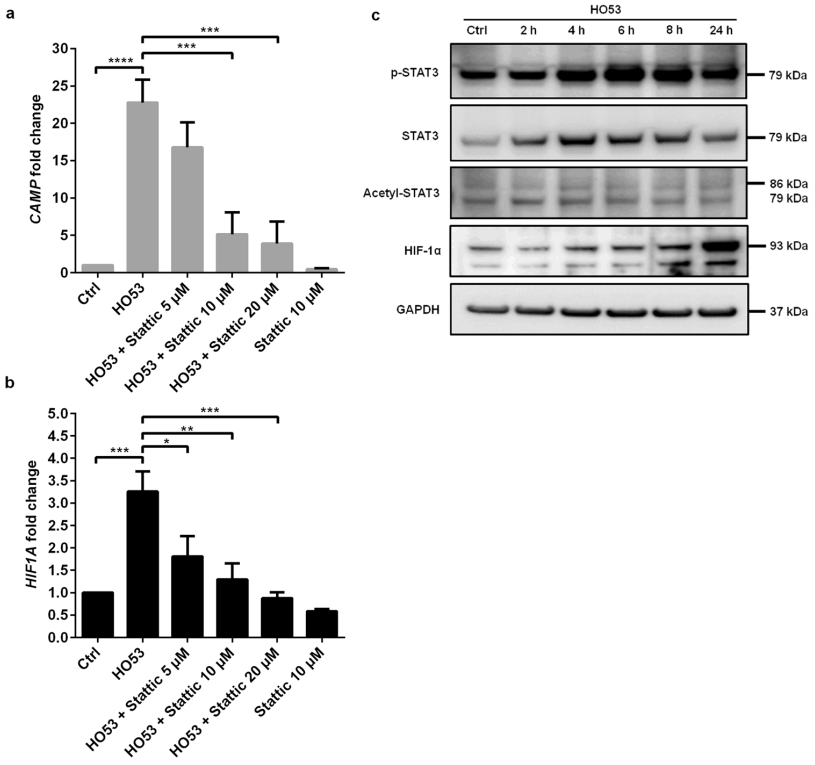


**Figure 7.** STAT3 and HIF-1α mediate *CAMP* gene induction by HO53 in BCi cells. The effect of the STAT3 inhibitor Stattic on (**a**) *CAMP* and (**b**) *HIF1A* expression in BCi cells. Cells were pretreated with 5, 10 and 20 µM of Stattic for 30 min and then stimulated with HO53 (75 µM) for 24 h. *CAMP* and *HIF1A* expression was analyzed by qRT-PCR and normalized to *TUBB* (tubulin-β) reference gene. The data (**a**,**b**) represent mean of n = 4 independent experiments ± SEM. Statistical significance for HO53 and Stattic 10 µM was calculated in comparison to control (Ctrl), while the inhibitory effect of Stattic refers to HO53 alone using one-way ANOVA with Sidak's multiple comparisons test, *$p < 0.05$, **$p < 0.01$, ***$p < 0.001$, ****$p < 0.0001$. Significant alterations are highlighted. (**c**) Effect of HO53 (75 µM) treatment of BCi cells on STAT3 phosphorylation (p-STAT3 at Tyr705), total STAT3, acetylation (Acetyl-STAT3 at Lys685) and HIF-1α expression after 2, 4, 6, 8 and 24 h was analyzed by Western blot. GAPDH served as a loading control. The experiment was performed n = 2 with similar results. Full-length blots are presented in Supplementary Figure S10e.

a similar strategy for identification of other innate immunity inducers was described based on the induction of the defensins genes *HBD2* and *HBD3*[46,47]. Another interesting approach was through the pattern recognition receptor NOD2 (Nucleotide Binding Oligomerization Domain Containing 2), when activation of this receptor by N-phosphonacetyl-L-aspartate (PALA), was identified as a potent inducer of innate immunity. Expression of *HBD2* and *CAMP* were induced by PALA and antimicrobial activity was demonstrated in skin explants against bacteria including methicillin-resistant *Staphylococcus aureus* (MRSA)[48].

In the current study we describe that the novel APD compounds HO53 and HO56 induced a broad spectrum of antimicrobial effectors in bronchial epithelium. Both compounds are developed as AMP inducers with increased water solubility, lower cytotoxicity and reduced effects on cell proliferation as compared to Entinostat. We mainly used the BCi-NS1.1 (BCi) cell line[41] but the induction of the *CAMP* gene expression was also confirmed in the VA10 cell line[49]. The gene induction profiles of HO53, HO56 and Entinostat were similar with reference to time but not with reference to the concentration. The dose studies utilizing BCi cells revealed a concentration dependent response for HO53 and HO56, but not for Entinostat (Fig. 1b; Supplementary Fig. S3) most likely due to higher cytotoxicity of the latter. Interestingly, when HO53 and HO56 were tested with the known innate immunity inducers vitamin D3 and PBA, a synergistic induction of the *CAMP* gene expression was noted with vitamin D3 but not with PBA. This suggests that APDs and PBA possibly act through the same signaling pathways. PBA and Entinostat are known HDAC inhibitors[28,32], however today this activity is referred to as lysine deacetylases inhibition (KDACi) because apart from histones also cytoplasmic signaling pathway proteins are affected[50]. Indeed, the suggested mechanism of Entinostat activity included acetylation of the cytoplasmic

signaling protein STAT3[29]. Therefore, possible KDAC inhibition by the novel APD compounds must be experimentally confirmed.

For both novel APDs we found induced antimicrobial activity in BCi cells against *Pseudomonas aeruginosa* (PAO1) and the disruptive effect of PAO1 on epithelial integrity was counteracted by HO53. This double effect of HO53 on the epithelial barrier might be potentially beneficial *in vivo* for fending off bacterial intruders and blocking bacterial translocation. Thus, HO53 would be an interesting candidate to treat and/or prevent infections. Interestingly, the antimicrobial activity was assessed against *Pseudomonas aeruginosa* that is prevalent in immune compromised lungs, including cystic fibrosis patients. The characteristics of the cellular response to treatment with HO53 suggest an effective HDT compound that might be beneficial for cystic fibrosis patients and used against MDR strains.

Induction of the *CAMP* gene expression served as a reference for the selection of HO53 and HO56 compounds. We selected additional genes encoding peptides/proteins with known defense functions at epithelial surfaces such as lipocalin 2, HBD1, S100A8, lysozyme and lactoferrin to verify whether the induced expression would mimic *in vivo* defenses. Significant induction of lipocalin 2, HBD1 and S100A8 expression was observed at mRNA and protein levels, indicating the APD compounds as powerful activators of a broad spectrum defense. Kinetics of mRNA and protein induction were not strictly correlated, where the most pronounced deviation was for *HBD1* expression with a fold change of mRNA from 50 to 100, while at protein level only approximately 2 times changed (Fig. 2c,d). Similar differences were also observed for lipocalin 2, indicating a regulation at translational level in the cells. However, the current overall expression profile shows a broad induction of multiple polypeptides. In addition, we estimated the influence of APDs on reactive oxygen species (ROS) and nitric oxide (NO) production. ROS was not affected but the expression of *NOS2* (encoding inducible nitric oxide synthase iNOS) was enhanced. However, this enhancement was not confirmed on effector level by the Griess method, measuring nitrate in solution probably due to low concentrations. The observed antimicrobial effect in our system is unlikely due to enhanced NO production. However, low induction of the iNOS protein may contribute to the antimicrobial effect *in vivo*. Thus, the main antibacterial activity in our model is most likely due to increased expression of antimicrobial proteins/peptides and could even be enhanced in the *in vivo* situation with complete processing of active components.

We analyzed the induction of different innate immunity effectors expression both in monolayer BCi cells and air liquid interphase (ALI), thereby comparing basal like cells with differentiated epithelial cells[41]. Several differences were observed: (1) the mRNA expression for lysozyme (*LYZ*) was not detected in monolayer but was inducible in differentiated cells (Fig. 5f), (2) induction of *S100A8* expression was more pronounced in ALI culture (S100A8 could not be detected in undifferentiated cells). (3) In contrast, the *HBD1* expression was more pronounced in undifferentiated cells. (4) The expression of pro-inflammatory effectors like, *TNF*/TNF-α and *CXCL8*/IL-8 was significantly enhanced in monolayer cells (Fig. 3) but not in ALI cultured cells, except *IL1B* expression (Supplementary Fig. S7). These differences indicate that the undifferentiated cells are more sensitive to external stimuli and trigger NF-kB regulated responses, which might be linked to their basal functions. The different responses can also reflect different transcription factors setup and chromatin accessibility in the basal cells versus polarized cells.

In the experiments for approaching molecular mechanism and epithelial integrity we selected HO53 because of lower cytotoxic effects on BCi cells, higher yields from the synthesis and better solubility than HO56. One suggested mechanism for induction of innate immunity by Entinostat included two steps: first, activation of STAT3 by acetylation and second, subsequent increase of HIF-1α[29]. Notably, the transcription factor HIF-1α has been confirmed important for transcription of innate immunity genes[51]. Because the new APDs are structurally related to Entinostat, we tested the effect of HO53 in relation to the STAT3 transcription factor using a specific inhibitor - Stattic. By blocking STAT3 we observed significant reduction of *CAMP* and *HIF1A* expression upon HO53 treatment. Furthermore, upon HO53 treatment there was a time dependent increase of the STAT3 protein and in particular a pronounced effect on the phosphorylation of STAT3, whereas the acetylation status at Lys685 was unchanged. Gradually increased expression of HIF-1α was detected with time after stimulation of the cells by HO53. In conclusion, STAT3 seems to be an important mediator of the APD response but more detailed studies on STAT3 modifications are needed that might define the cellular target of HO53.

In gut epithelia STAT3 mediated expression of occludin was shown to enhance tight junction function and prevent bacterial translocation[52]. HO53 treatment led to increased occludin expression (Fig. 6) that could be an explanation for limited disruption of tight junctions (TJs) caused by *Pseudomonas*. This type of counteraction was initially identified on polarized lung epithelium for the antibiotic azithromycin (AZM) by an unknown mechanism[44]. Here, we confirmed the effect by AZM (Supplementary Fig. S8), but interestingly the HO53 effect seemed to be more potent in rescuing the barrier integrity than AZM. Together all these effects of HO53 do not only underline the double action of the molecule but also highlights the importance of STAT3 in epithelial immunity[53,54].

Our results warrant continuation in animal infection models and motivate pharmacodynamics and pharmacokinetic studies. Usage of the APDs could re-establish the niche for the natural microbiota and avoid selection of resistant bacteria in line with improvement of stewardship in healthcare.

## Materials and Methods

**Reagents and materials.** Entinostat (SNDX-275), 1α,25-dihydroxyvitamin D3 (D1530), collagen from human placenta (C7521), Stattic inhibitor (S7947), LB broth (L3522), agar (05039-500G), gentamicin (G1914), methanol (34885-2.5L), menadione (M5625), the secondary antibodies conjugated with HRP for Western blotting (A5420 and A0545), DAPI (D9564) were purchased from Sigma. UltroserG (UG, 15950-017) was obtained from PALL Life Sciences and sodium 4-phenylbutyrate (2682) from Tocris Bioscience. Synthetic LL-37 peptide (SP-LL37) was bought from Innovagen and DMSO (sc-358801) from Santa Cruz. Azithromycin (Zitromax) of

500 mg was from Pfizer. The monoclonal anti-LL-37 antibody was generated by us and described in Yoshio *et al.*[55]. Anti-ZO-1 (#13663), anti-STAT3 (#9139), anti-acetyl-STAT3 (#2523), anti-phospho-STAT3 (#9145) and anti-GAPDH (#2118) antibodies were purchased from Cell Signaling Technology. Anti-lipocalin 2 (AF1757) antibody was obtained from R&D Systems, anti-HIF-1α (ab113642) antibody was from Abcam and anti-occludin (331500) and anti-claudin-1 (51-9000) antibodies from Thermo Scientific. Secondary antibodies for immunofluorescence staining were obtained from Thermo Scientific (A-11070 and A-11020). 2-Azidoethanol was synthesized according to a published procedure and distilled under reduced pressure[56]. All other synthesis reagents and solvents (analytical grade) were purchased from commercial sources and were used without further purification. The NMR spectra were collected on a Bruker DRX-400 spectrometer (400 MHz for 1H and 101 MHz for 13C) with the residual solvent signal as chemical shift reference. Mass spectra were recorded on a Micromass LCT (ESI-TOF) mass spectrometer.

**Cell cultures.** The human bronchial epithelial cell line BCi-NS1.1 (BCi) immortalized with retrovirus expressing human telomerase (hTERT) was from dr Matthew S. Walters, Weill Cornell Medical College, New York NY, USA[41]. An E6/E7 viral oncogene immortalized human bronchial epithelial cell line VA10 has been described previously[49]. Both cell lines were cultured in Bronchial/Tracheal Epithelial cell growth medium (BEGM) (Cell Applications, 511A-500) supplemented with retinoic acid (Cell Applications, 511-RA) and Penicillin-Streptomycin ((20 U/ml, 20 µg/ml, respectively) (Life Technologies, 15140122)) at 37 °C and 5% $CO_2$. The ALI (air-liquid interface) culture of BCi cells were maintained as described previously[41]. Cells in monolayer were treated with HO53 and HO56 by direct addition to the culture medium. Differentiated BCi cells were used for experiments when TEER value of $\geq$1000 $\Omega \times cm^2$ was reached and then HO53 and HO56 were added to the lower chamber for indicated period of time. Azithromycin was used as a control.

**Bacterial culture.** The overnight culture of *Pseudomonas aeruginosa* PAO1 strain was diluted in LB medium to $OD_{590} = 0.05$ and cultured at 37 °C with 180 rpm shaking until the bacterial subculture reached the mid-log phase.

**RNA analysis.** Total RNA was extracted using Nucleo Spin RNA kit (Machinery-Nagel, 740955.50). Total RNA of 1 µg was used to synthesize complementary DNA (cDNA) according to the manufacture's recommendations using the High Capacity cDNA reverse transcriptase kit (Applied Biosystems, 4368814). One µl of cDNA, 5 µl of PowerUp SYBR Green Master Mix (Applied Biosystems, A25742) and 0.5 µM primers enlisted in Supplementary Table S1 were used for qRT-PCRs. The qRT-PCRs were performed using LG 7500 Real Time PCR System (Applied Biosystems) with the following cycling conditions: (1) holding stage: 95 °C for 10 min, followed by 40 cycles of (2) denatured stage: 95 °C for 15 s and (3) annealed/extended stage: 60 °C for 1 min. The $2^{(-\Delta\Delta CT)}$ Livak method was utilized for calculating fold differences over untreated control[57].

**Immunoblotting.** Cells were washed with PBS and lysed in RIPA lysis buffer (Santa Cruz, sc-364162) supplemented with Halt Protease Inhibitor Cocktail (Thermo Scientific, 87786) on ice for 30 min. The cell culture media in the volume of 2 ml were concentrated as it has been described earlier[58]. The concentrated culture media or 10–30 µg of total protein content was separated using NuPAGE 4–12% Bis–Tris gradient gel (Life Technologies, NP0323), NuPAGE MES SDS Running Buffer (Life Technologies, NP0002) and the running conditions were 120 V and 275 mA. The proteins were transferred on to a PVDF membrane (0.2 µm pores) using XCell II™ Blot Module (Invitrogen, EI9051) and the membrane was blocked with 10% skimmed milk or 5% BSA in TBS-T buffer (50 mM Tris, 150 mM NaCl, 0.1% Tween-20) for 1 h at room temperature. Then, the membrane was incubated with primary antibodies overnight at 4 °C using a dilution recommended by the manufacturer's protocol. After washing with TBS-T buffer the membrane was incubated with horse radish peroxidase (HRP) conjugated secondary antibodies (1:10 000 dilution) in 5% skimmed milk or 5% BSA in TBS-T for at least 1.5 h at room temperature. Immunoblots were developed using Pierce ECL Plus Western blotting substrate (Thermo Scientific, #34095) or Western blotting Luminol reagent (Santa Cruz, sc-2048) and ImageQuant LAS 4000 system (GE Healthcare). Quantification of the band intensity was performed using ImageJ software.

**ELISA.** Sandwich enzyme-linked immunosorbent assays (ELISAs) were performed utilizing a human beta defensin-1 (hBD-1), interleukin 8 (CXCL8) and tumor necrosis factor alpha (TNFα) assay kit according to the manufacturer's instructions (Peprotech, UK). The results are represented from three independent experiments.

**Cytotoxicity and cell viability assays.** BCi cells (10,000) were seeded in 96-well plate chambers in 200 µl of BEGM. Once adhesion was verified, cells were incubated with different concentrations of Entinostat (2.5–50 µM), HO53 (2.5–250 µM) and HO56 (2.5–250 µM) along with the known *CAMP* inducer PBA (4 mM) for 24 h. Cytotoxicity and cell proliferation was determined using CytoTox 96® Non-Radioactive Cytotoxicity Assay (Promega, G1781) kit and Cell Proliferation Reagent WST-1 (Roche, 05015944001), respectively, according to the manufacturer's instructions. The results presented were from three independent experiments for cytotoxicity and two independent experiments for cell proliferation.

**Antimicrobial assays.** BCi cells in monolayer were treated for 24 h with APDs or low dose of gentamycin (0.5 µg/ml) used as a positive control and then infected with PAO1 using MOI ~40 for 1 h. Cells were then washed 3 times with PBS and incubated for 20 min with medium containing 100 µg/ml gentamicin (bacterial killing concentration). Cells were washed again, lysed in 0.1% Triton X-100/$H_2O$ (v/v) for 5 min, serially diluted in PBS and plated on LB agar plates. After overnight incubation at 37 °C, the PAO1 CFU (colony forming units) were enumerated.

**ROS detection.** The $H_2O_2$ level in the cell culture medium after 24 h of treatment with HO53 and HO56 (both at 75 µM) was measured using ROS-Glo™ $H_2O_2$ assay (Promega, G8820) according to the manufacture's protocol.

**Agarose gel electrophoresis.** Semi-quantitative PCR products were separated on 1.5% agarose gel containing ethidium bromide (0.5 µg/ml). Electrophoresis was run at 80 V for 30 min using 1x TAE (Tris-acetate-EDTA) buffer. β-tubulin was used as a control for the quantification of the band intensity using ImageJ software.

**Preparation of PAO1 conditioned medium and challenge of differentiated BCi cells.** Wild-type (WT) *P. aeruginosa* strain PAO1 was used to prepare bacterial conditioned medium. Shortly, the bacteria were cultured in Dulbecco's Modified Eagle Medium F-12 Nutrient Mixture (DMEM/F12) + 2% UltroserG (UG) at 30 °C and shaking was at 180 rpm for 5 days. Bacterial culture supernatants were collected, vortexed thoroughly, centrifuged, and filtered through 0.22 mm pore-size filter (GE Healthcare and Life Science, Whatman, Germany). BCi cells were cultured at the ALI for 3 weeks with medium changed every 2–3 days to get differentiated cells, followed by placing HO53 (75 µM diluted in DMEM/F12 + 2% UG) in the basal chamber of the transwell insert for 3 consecutive days, while Azithromycin was used as positive control as described previously[44]. Next, differentiated cells were challenged with PAO1 conditioned medium and TEER was measured after every hour. Samples for Western blot and confocal microscopy analyzes were collected at selected time points.

**Immunofluorescence staining and confocal microscopy.** BCi cells growing on ALI filters were fixed using chilled methanol at 4 °C overnight followed by chilled acetone. Briefly, staining was done as follows: filters were hydrated with IF buffer (PBS + 0.3% Triton X-100), blocked with 10% FBS, washed and incubated with a primary antibody overnight at 4 °C. The following primary antibodies were used: rabbit anti-occludin and mouse anti-ZO-1. Next day the filter was washed and incubated with a secondary antibody for 2 h. For immunofluorescence staining, isotype-specific Alexa Fluor secondary antibody conjugates were used and DAPI was used to stain nuclei. The filter was then washed with IF buffer and finally rinsed with water. Cell culture transwell filters were mounted in Fluoromount™ Aqueous Mounting Medium (F4680-Sigma) and coverslips were placed over the filters. Images were captured using Olympus fluoview Fv1200 confocal microscope at 30x magnification. Z-scans were performed by taking series of images at the same location with fixed focal intervals.

**Statistical analysis.** Results are presented as mean ± standard error of mean (SEM) from at least three independent experiments, otherwise it is indicated in the figure legends. One- or two-way ANOVA with post-hoc Dunnett's or Sidak's multiple comparisons test were used to determine significance of the data. *p* values are included in the figure legends. The statistical analysis were performed with GraphPad Prism 6 software (Graph Pad, USA). The Western blots are representative of at least two independent experiments.

## Data Availability

The data generated during and/or analysed during the current study are available from the corresponding author on reasonable request.

## References


1. Leiva-Juárez, M. M., Kolls, J. K. & Evans, S. E. Lung epithelial cells: therapeutically inducible effectors of antimicrobial defense. *Mucosal Immunol.* **11**, 21–34 (2018).
2. Hasan, S., Sebo, P. & Osicka, R. A guide to polarized airway epithelial models for studies of host-pathogen interactions. *FEBS J.* https://doi.org/10.1111/febs.14582 (2018).
3. Knowles, M. R. & Boucher, R. C. Mucus clearance as a primary innate defense mechanism for mammalian airways. *J. Clin. Invest.* **109**, 571–7 (2002).
4. Fahy, J. V. & Dickey, B. F. Airway mucus function and dysfunction. *N. Engl. J. Med.* **363**, 2233–47 (2010).
5. Bansil, R. & Turner, B. S. The biology of mucus: Composition, synthesis and organization. *Adv. Drug Deliv. Rev.* **124**, 3–15 (2018).
6. Mansour, S. C., Pena, O. M. & Hancock, R. E. W. Host defense peptides: front-line immunomodulators. *Trends Immunol.* **35**, 443–450 (2014).
7. Agerberth, B. *et al*. FALL-39, a putative human peptide antibiotic, is cysteine-free and expressed in bone marrow and testis. *Proc. Natl. Acad. Sci. USA* **92**, 195–9 (1995).
8. Gudmundsson, G. H. *et al*. The Human Gene FALL39 and Processing of the Cathelin Precursor to the Antibacterial Peptide LL-37 in Granulocytes. *Eur. J. Biochem.* **238**, 325–332 (1996).
9. Kolls, J. K., McCray, P. B., Chan, Y. R. & Chan, Y. R. Cytokine-mediated regulation of antimicrobial proteins. *Nat. Rev. Immunol.* **8**, 829–35 (2008).
10. Moser, C. *et al*. beta-Defensin 1 contributes to pulmonary innate immunity in mice. *Infect. Immun.* **70**, 3068–72 (2002).
11. Kovach, M. A. *et al*. Cathelicidin-related antimicrobial peptide is required for effective lung mucosal immunity in Gram-negative bacterial pneumonia. *J. Immunol.* **189**, 304–11 (2012).
12. Lai, Y. & Gallo, R. L. AMPed up immunity: how antimicrobial peptides have multiple roles in immune defense. *Trends Immunol.* **30**, 131–141 (2009).
13. Torres-Juarez, F. *et al*. LL-37 immunomodulatory activity during Mycobacterium tuberculosis infection in macrophages. *Infect. Immun.* **83**, 4495–503 (2015).
14. Shaykhiev, R. *et al*. Human endogenous antibiotic LL-37 stimulates airway epithelial cell proliferation and wound closure. *Am. J. Physiol. Cell. Mol. Physiol.* **289**, L842–L848 (2005).
15. Yuk, J.-M. *et al*. Vitamin D3 Induces Autophagy in Human Monocytes/Macrophages via Cathelicidin. *Cell Host Microbe* **6**, 231–243 (2009).
16. Rekha, R. S. *et al*. Phenylbutyrate induces LL-37-dependent autophagy and intracellular killing of Mycobacterium tuberculosis in human macrophages. *Autophagy* **11**, 1688–99 (2015).
17. Zasloff, M. Antimicrobial peptides of multicellular organisms. *Nature* **415**, 389–395 (2002).
18. Rice, L. B. Federal Funding for the Study of Antimicrobial Resistance in Nosocomial Pathogens: No ESKAPE. *J. Infect. Dis.* **197**, 1079–1081 (2008).
19. Pogue, J. M., Kaye, K. S., Cohen, D. A. & Marchaim, D. Appropriate antimicrobial therapy in the era of multidrug-resistant human pathogens. *Clin. Microbiol. Infect.* **21**, 302–312 (2015).

20. Cohen, T. S. & Prince, A. Cystic fibrosis: a mucosal immunodeficiency syndrome. *Nat. Med.* **18**, 509–519 (2012).
21. Mily, A. *et al*. Significant Effects of Oral Phenylbutyrate and Vitamin D3 Adjunctive Therapy in Pulmonary Tuberculosis: A Randomized Controlled Trial. *PLoS One* **10**, e0138340 (2015).
22. Bekele, A. *et al*. Daily adjunctive therapy with vitamin D $_3$ and phenylbutyrate supports clinical recovery from pulmonary tuberculosis: a randomized controlled trial in Ethiopia. *J. Intern. Med.* https://doi.org/10.1111/joim.12767 (2018).
23. Wang, T.-T. *et al*. Cutting edge: 1,25-dihydroxyvitamin D3 is a direct inducer of antimicrobial peptide gene expression. *J. Immunol.* **173**, 2909–12 (2004).
24. Weber, G. *et al*. Vitamin D Induces the Antimicrobial Protein hCAP18 in Human Skin. *J. Invest. Dermatol.* **124**, 1080–1082 (2005).
25. Gombart, A. F., Borregaard, N. & Koeffler, H. P. Human cathelicidin antimicrobial peptide (CAMP) gene is a direct target of the vitamin D receptor and is strongly up-regulated in myeloid cells by 1,25-dihydroxyvitamin D $_3$. *FASEB J.* **19**, 1067–1077 (2005).
26. Steinmann, J., Halldórsson, S., Agerberth, B. & Gudmundsson, G. H. Phenylbutyrate induces antimicrobial peptide expression. *Antimicrob. Agents Chemother.* **53**, 5127–33 (2009).
27. Sarker, P. *et al*. Phenylbutyrate Counteracts Shigella Mediated Downregulation of Cathelicidin in Rabbit Lung and Intestinal Epithelia: A Potential Therapeutic Strategy. *PLoS One* **6**, e20637 (2011).
28. Iannitti, T. & Palmieri, B. Clinical and experimental applications of sodium phenylbutyrate. *Drugs R. D.* **11**, 227–49 (2011).
29. Miraglia, E. *et al*. Entinostat up-regulates the CAMP gene encoding LL-37 via activation of STAT3 and HIF-1$\alpha$ transcription factors. *Sci. Rep.* **6**, 1–12 (2016).
30. Ottosson, H. *et al*. Potent Inducers of Endogenous Antimicrobial Peptides for Host Directed Therapy of Infections. *Sci. Rep.* **6**, 1–11 (2016).
31. Sarker, P. *et al*. Treatment with Entinostat Heals Experimental Cholera by Affecting Physical and Chemical Barrier Functions of Intestinal Epithelia. *Antimicrob. Agents Chemother.* **61**, e02570–16 (2017).
32. Knipstein, J. & Gore, L. Entinostat for treatment of solid tumors and hematologic malignancies. *Expert Opin. Investig. Drugs* **20**, 1455–1467 (2011).
33. Ryan, Q. C. *et al*. Phase I and pharmacokinetic study of MS-275, a histone deacetylase inhibitor, in patients with advanced and refractory solid tumors or lymphoma. *J. Clin. Oncol.* **23**, 3912–22 (2005).
34. Cody, J. J., Markert, J. M. & Hurst, D. R. Histone deacetylase inhibitors improve the replication of oncolytic herpes simplex virus in breast cancer cells. *PLoS One* **9**, e92919 (2014).
35. Nylén, F. *et al*. Boosting innate immunity: Development and validation of a cell-based screening assay to identify LL-37 inducers. *Innate Immun.* **20**, 364–376 (2014).
36. Wu, H. *et al*. Lipocalin 2 is protective against E. coli pneumonia. *Respir. Res.* **11**, 96 (2010).
37. Schutte, B. C. & McCray, P. B. β-Defensins in Lung Host Defense. *Annu. Rev. Physiol.* **64**, 709–748 (2002).
38. Nisapakultorn, K., Ross, K. F. & Herzberg, M. C. Calprotectin expression inhibits bacterial binding to mucosal epithelial cells. *Infect. Immun.* **69**, 3692–6 (2001).
39. Ganesan, S., Comstock, A. T. & Sajjan, U. S. Barrier function of airway tract epithelium. *Tissue barriers* **1**, e24997 (2013).
40. Bogdan, C. Nitric oxide synthase in innate and adaptive immunity: an update. *Trends Immunol.* **36**, 161–178 (2015).
41. Walters, M. S. *et al*. Generation of a human airway epithelium derived basal cell line with multipotent differentiation capacity. *Respir. Res.* **14**, 135 (2013).
42. Golovkine, G. *et al*. Pseudomonas aeruginosa Transmigrates at Epithelial Cell-Cell Junctions, Exploiting Sites of Cell Division and Senescent Cell Extrusion. *PLoS Pathog.* **12**, e1005377 (2016).
43. Zulianello, L. *et al*. Rhamnolipids are virulence factors that promote early infiltration of primary human airway epithelia by Pseudomonas aeruginosa. *Infect. Immun.* **74**, 3134–47 (2006).
44. Halldorsson, S. *et al*. Azithromycin Maintains Airway Epithelial Integrity during *Pseudomonas aeruginosa* Infection. *Am. J. Respir. Cell Mol. Biol.* **42**, 62–68 (2010).
45. CDC. *Antibiotic Resistance Threats in the United States, 2013. Centers for Disease Control and Prevention, U.S. Department of Health and Human Services* (2013).
46. Fischer, N. *et al*. Histone deacetylase inhibition enhances antimicrobial peptide but not inflammatory cytokine expression upon bacterial challenge. *Proc. Natl. Acad. Sci. USA* **113**, E2993–3001 (2016).
47. Sechet, E., Telford, E., Bonamy, C., Sansonetti, P. J. & Sperandio, B. Natural molecules induce and synergize to boost expression of the human antimicrobial peptide β-defensin-3. *Proc. Natl. Acad. Sci. USA* **115**, E9869–E9878 (2018).
48. Jatana, S. *et al*. Pyrimidine synthesis inhibition enhances cutaneous defenses against antibiotic resistant bacteria through activation of NOD2 signaling. *Sci. Rep.* **8**, 8708 (2018).
49. Halldorsson, S. *et al*. Differentiation potential of a basal epithelial cell line established from human bronchial explant. *Vitr. Cell. Dev. Biol. - Anim.* **43**, 283–289 (2007).
50. Menzies, K. J., Zhang, H., Katsyuba, E. & Auwerx, J. Protein acetylation in metabolism — metabolites and cofactors. *Nat. Rev. Endocrinol.* **12**, 43–60 (2016).
51. Palazon, A., Goldrath, A. W., Nizet, V. & Johnson, R. S. HIF transcription factors, inflammation, and immunity. *Immunity* **41**, 518–28 (2014).
52. Wang, Z. *et al*. Syndecan-1 Acts in Synergy with Tight Junction Through Stat3 Signaling to Maintain Intestinal Mucosal Barrier and Prevent Bacterial Translocation. *Inflamm. Bowel Dis.* **21**, 1894–1907 (2015).
53. Quinton, L. J. & Mizgerd, J. P. NF-κB and STAT3 signaling hubs for lung innate immunity. *Cell Tissue Res.* **343**, 153–165 (2011).
54. Ching, C. B. *et al*. Interleukin-6/Stat3 signaling has an essential role in the host antimicrobial response to urinary tract infection. *Kidney Int.* **93**, 1320–1329 (2018).
55. Yoshio, H. *et al*. Antimicrobial Polypeptides of Human Vernix Caseosa and Amniotic Fluid: Implications for Newborn Innate Defense. *Pediatr. Res.* **53**, 211–216 (2003).
56. Smith, R. H., Mehl, A. F., Shantz, D. L., Chmurny, G. N. & Michejda, C. J. Novel cross-linking alkylating agents, 1-(2-chloroethyl)-3-methyl-3-acyltriazenes. *J. Org. Chem.* **53**, 1467–1471 (1988).
57. Livak, K. J. & Schmittgen, T. D. Analysis of Relative Gene Expression Data Using Real-Time Quantitative PCR and the $2-\Delta\Delta CT$ Method. *Methods* **25**, 402–408 (2001).
58. Kulkarni, N. N., Yi, Z., Huehnken, C., Agerberth, B. & Gudmundsson, G. H. Phenylbutyrate induces cathelicidin expression via the vitamin D receptor: Linkage to inflammatory and growth factor cytokines pathways. *Mol. Immunol.* **63**, 530–539 (2015).


## Acknowledgements

Icelandic Center for Research (RANNÍS) and University of Iceland research fund are acknowledged for support. Bryndís Valdimarsdóttir for advises on preparation of conditioned media and cell culture. Kristín Elísabet Alansdóttir for help with confocal microscopy and ImageJ analyses. Thanks to Náttúruverndarsjóður Pálma Jónssonar for early support of this project. We acknowledge Prof. Ronald G. Crystal and collaborators for generously providing us with the BCi-NS1.1 cell line. We thank Snæbjörn Pálsson for advices on statistical analysis.

## Author Contributions

G.H.G., I.T.M. and Z.P. designed and performed experiments, analyzed data, wrote and edited the manuscript. R.S. and H.O. performed chemical synthesis and analyses. B.A., P.B. and R.S. provided experimental advises and edited the manuscript. All authors reviewed and approved the final manuscript.

## Additional Information

**Supplementary information** accompanies this paper at https://doi.org/10.1038/s41598-019-43350-z.

**Competing Interests:** I.T.M., Z.P. and H.O. declare no competing interests. G.H.G., B.A. and R.S. are founders and stockholders in Akthelia Pharmaceuticals that hold a patent on APD compounds, Patent No. US 9,957,226 B2. P.B. is a stockholder in Akthelia Pharmaceuticals.

**Publisher's note:** Springer Nature remains neutral with regard to jurisdictional claims in published maps and institutional affiliations.

# Supplementary Information for

## Novel aroylated phenylenediamine compounds enhance antimicrobial defense and maintain airway epithelial barrier integrity

**Iwona T. Myszor[1], Zahida Parveen[1], Håkan Ottosson[2], Peter Bergman[3], Birgitta Agerberth[3], Roger Strömberg[2], Gudmundur H. Gudmundsson[1]**

[1] Biomedical Center; University of Iceland; Reykjavik 101; Iceland

[2] Department of Biosciences and Nutrition; Karolinska Institutet; S-14183 Huddinge; Sweden

[3] Department of Laboratory Medicine; Clinical Microbiology; Karolinska Institutet; S-14186 Huddinge; Sweden

Correspondence and requests for materials should be addressed to G. H. G.; address: Biomedical Center, University of Iceland, Vatnsmyrarvegur 16, Reykjavik 101, Iceland; phone: +354 525 5276; email: ghrafn@hi.is

**This PDF file includes:**

**Supplementary Figure S1.** Synthesis scheme for the APD HO53 (*N*-(2-aminophenyl)-4-(2-{[1-(2-hydroxyethyl)-1H-1,2,3-triazol-4-yl]methoxy}-acetamido)benzamide)

**Supplementary Figure S2.** Synthesis scheme for the APD HO56 (*N*-(2-aminophenyl)-4-{[1-(2-hydroxyethyl)-1H-1,2,3-triazol-4-yl]methoxy}benzamide)

**Supplementary Methods**

**Synthesis for the APD HO53** (*N*-(2-aminophenyl)-4-(2-{[1-(2-hydroxyethyl)-1H-1,2,3-triazol-4-yl]methoxy}-acetamido)benzamide)

**Synthesis for the APD HO56** (*N*-(2-aminophenyl)-4-{[1-(2-hydroxyethyl)-1H-1,2,3-triazol-4-yl]methoxy}benzamide)

**Supplementary Figure S3.** Dose dependent induction of the *CAMP* gene in BCi cells by Entinostat, HO53 and HO56

**Supplementary Figure S4.** Dose dependent induction of the *CAMP* gene in VA10 cells by Entinostat, HO53 and HO56

**Supplementary Figure S5.** Cytotoxicity and proliferation of BCi cells after 24 h exposure to Entinostat, HO53 and HO56

**Supplementary Figure S6.** Effect of APDs treatment on reactive oxygen species (ROS) production and inducible nitric oxide synthase (*NOS2*) in BCi cells

**Supplementary Figure S7.** Expression of cytokines in ALI differentiated BCi cells upon treatment with HO53 and HO56

**Supplementary Figure S8.** Azithromycin treatment counteracts disruptive effect of *P. aeruginosa* PAO1 conditioned medium in airway epithelium in ALI culture of BCi cells

**Supplementary Figure S9.** Changes in occludin pattern in control and HO53 treated airway epithelial BCi cells upon PAO1 conditioned medium challenge

**Supplementary Figure S10.** Display of full-length blots presented in the article.

**Supplementary Table S1.** List of primers used in this study

**Supplementary Table S2.** Quantification of lipocalin 2 expression.

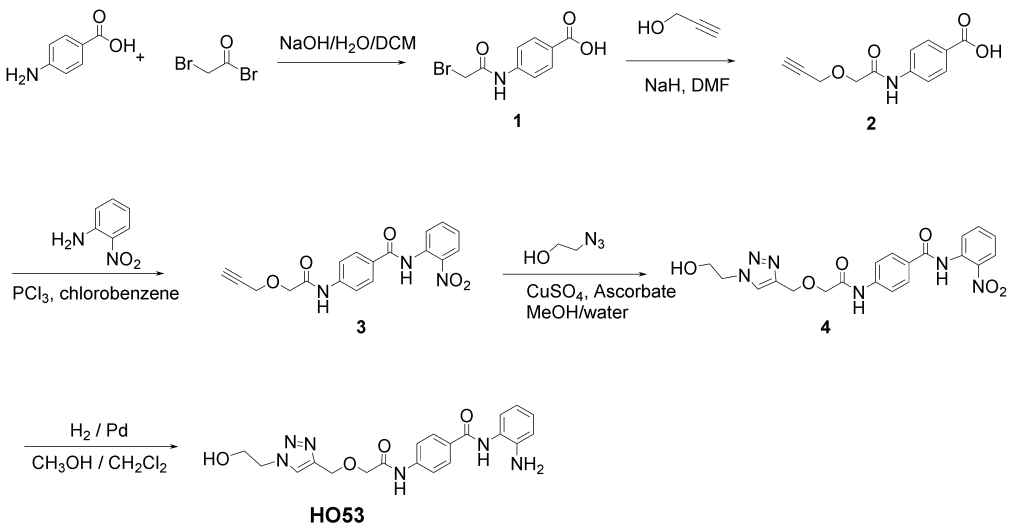


**Supplementary Figure S1. Synthesis scheme for the APD HO53** (*N*-(2-aminophenyl)-4-(2-{[1-(2-hydroxyethyl)-1H-1,2,3-triazol-4-yl]methoxy}-acetamido)benzamide). Detailed description of synthesis of the intermediate compounds **1-4** and the final product **HO53** is presented below in Supplementary Methods.

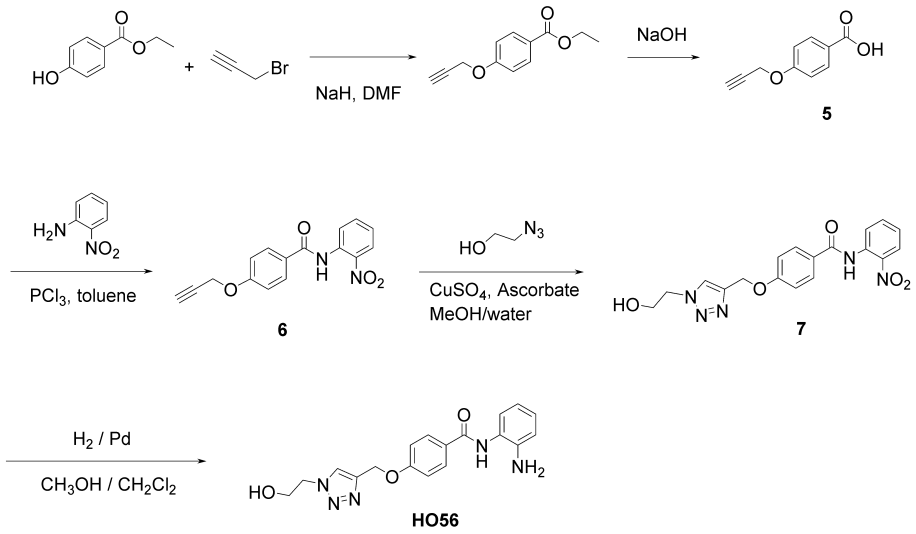


**Supplementary Figure S2. Synthesis scheme for the APD HO56** (*N*-(2-aminophenyl)-4-{[1-(2-hydroxyethyl)-1H-1,2,3-triazol-4-yl]methoxy}benzamide). Detailed description of synthesis of the intermediate compounds **5-7** and the final product **HO56** is presented below in Supplementary Methods.

**Supplementary Methods**

**Synthesis for the APD HO53** (*N*-(2-aminophenyl)-4-(2-{[1-(2-hydroxyethyl)-1H-1,2,3-triazol-4-yl]methoxy}-acetamido)benzamide)

*4-(2-bromoacetamido)benzoic acid (**1**).*

Bromoacetyl chloride (5.23 mL, 60.0 mmol) in dichloromethane (15 mL) was added dropwise over 30 min to a solution of 4-aminobenzoic acid (5.49 g, 40.0 mmol) and sodium hydroxide (3.59 g, 89.8 mmol) in water (90 mL) on an ice-salt bath. The precipitate formed was filtered off after ca 3 h (pH ~5). The collected precipitate was washed with water, methanol and dried under reduced pressure. A second precipitate was collected after the filtrate was left overnight and 2.4 mL HCl (conc. *aq*) was added. The second precipitate was washed with water and dried under reduced pressure. The two collected precipitates amounted to 9.3 g (90%) of product which was used as is in the next step. $^{1}$H NMR (400 MHz, DMSO-d6) δ ppm: 11.92 - 13.67 (m, 1 H), 10.67 (s, 1 H), 7.92 (d, J=9.06 Hz, 2 H), 7.70 (d, J=8.56 Hz, 2 H), 4.07 (s, 2 H). $^{13}$C NMR (101 MHz, DMSO-d6) δ ppm: 166.83, 165.30, 142.57, 130.49, 130.49, 125.74, 118.57, 118.57, 30.29.

*4-{2-[(prop-2-yn-1-yl)oxy]acetamido}benzoic acid (**2**).*

Sodium hydride (60% suspension in oil, 3.25 g, 81.2 mmol) was weighed into a flask which was kept under nitrogen. Dry DMF (5 mL) was added. Propargyl alcohol (5.83 mL, 100 mmol) and 4-(2-bromoacetamido) benzoic acid (5.164 g, 20.0 mmol) in dry DMF (40 mL) was added dropwise at 0 °C. As the reaction got thicker more DMF was added in several portions to a total volume of 250 mL. The reaction was then left at room temperature overnight. The reaction mixture was diluted with dichloromethane. Water was added as well as HCl (6 mL, conc. *aq*). After partitioning additional extraction of the water phase with dichloromethane was done. The combined organic layers were collected pooled and dried over sodium sulfate. The drying agent was filtered off and the solvent was evaporated under reduced pressure to give 4.2 g (90%) of product after drying and that could be used directly in the next step. $^{1}$H NMR (400 MHz, DMSO-d6) δ ppm: 7.89 (m, J=8.56 Hz, 2 H), 7.76 (m, J=9.06 Hz, 2 H), 4.27 - 4.33 (m, 2 H), 4.14 - 4.19 (m, 2 H), 3.53 (t, J=2.27 Hz, 1 H), 10.12 (s, 1 H). $^{13}$C NMR (101 MHz, DMSO-d6) δ ppm: 168.06, 166.89, 142.46, 130.29, 130.29, 125.46, 118.90, 118.90, 79.57, 78.04, 68.46, 57.92.

*N-(2-nitrophenyl)-4-{2-[(prop-2-yn-1-yl)oxy]acetamido}benzamide (**3**).*

4-{2-[(prop-2-yn-1-yl)oxy]acetamido}benzoic acid (174 mg, 0.746 mmol) and 2-nitroaniline (156 mg, 1.132 mmol) was dissolved in chlorobenzene (10 mL). $PCl_3$ (33 µL, 0.378 mmol) was added and the reaction was heated for 2 h at 130 °C and then left at room temperature overnight. The mixture was diluted with dichloromethane and water was added. After partitioning the organic layer was washed with 0-1 M HCl and dried with sodium sulfate. After removal of the solvent under reduced pressure the residue was recrystallized from ethanol (two crops) to yield the product as a light yellow solid (133 mg, 50%). $^1$H NMR (400 MHz, DMSO-d6) δ ppm: 10.68 (s, 1 H), 10.17 (s, 1 H), 8.01 (dd, J=8.10, 1.51 Hz, 1 H), 7.94 (d, J=8.56 Hz, 2 H), 7.78 - 7.86 (m, 3 H), 7.75 (td, J=7.80, 1.51 Hz, 1 H), 7.41 (ddd, J=8.50, 7.00, 1.50 Hz, 1 H), 4.32 (d, J=2.52 Hz, 2 H), 4.16 - 4.21 (m, 2 H), 3.56 (t, J=2.52 Hz, 1 H). $^{13}$C NMR (101 MHz, DMSO-d6) δ ppm: 168.13, 164.70, 142.06, 134.05, 131.77, 128.72, 128.72, 125.77, 125.36, 125.00, 119.05, 119.05, 79.60, 78.11, 68.48, 57.97.

*4-(2-{[1-(2-hydroxyethyl)-1H-1,2,3-triazol-4-yl]methoxy}acetamido)-N-(2-nitrophenyl)-benzamide (**4**).*

N-(2-nitrophenyl)-4-{2-[(prop-2-yn-1-yl)oxy]acetamido}benzamide (71 mg, 0.201 mmol) and 2-azidoethanol (73 µL, 1.00 mmol) was mixed with methanol (46 mL) and water (4 mL). the mixture was then heated to dissolve the reagents. $CuSO_4$*$5H_2O$ (50 mg, 0.200 mmol) and ascorbic acid (142 mg, 0.800 mmol) were added while the mixture was still warm. The mixture became cloudy after a few minutes and was kept overnight at room temperature. EDTA (95 mg) was added and the mixture was then diluted with dichloromethane. Partitioning of the dichloromethane solution with water (with approx. 1/5 brine). The dichloromethane phase was washed with water containing 1/5 brine and EDTA (ca 100 mg). The collected organic layer was dried with $Na_2SO_4$, filtered and concentrated under reduced pressure. The resulting yellow solid was recrystallized from ethanol to yield 59 mg (67 %) of product as a yellow solid. $^1$H NMR (400 MHz, DMSO-d6) δ ppm: 10.68 (s, 1 H), 10.14 (s, 1 H), 8.15 (s, 1 H), 8.01 (dd, J=8.06, 1.51 Hz, 1 H), 7.89 - 7.98 (m, 2 H), 7.84 (d, J=8.56 Hz, 2 H), 7.80 (d, J=8.06 Hz, 1 H), 7.75 (ddd, J=8.20, 7.00, 1.50 Hz, 1 H), 7.41 (ddd, J=8.10, 7.00, 1.51 Hz, 1 H), 5.05 (t, J=5.29 Hz, 1 H), 4.70 (s, 2 H), 4.41 (t, J=5.40 Hz, 2 H), 4.17 (s, 2 H), 3.78 (q, J=5.40 Hz, 2 H). $^{13}$C NMR (101 MHz, DMSO-d6) δ ppm: 168.55, 164.69, 143.04, 142.71, 142.07, 134.04, 131.76, 128.70, 128.70, 128.10, 125.77, 125.37, 124.99, 124.74, 119.03, 119.03, 69.13, 63.82, 59.87, 52.18.

*N-(2-aminophenyl)-4-(2-{[1-(2-hydroxyethyl)-1H-1,2,3-triazol-4-yl]methoxy}-acetamido)-benzamide* (**HO53**).

To a solution of 4-(2-{[1-(2-hydroxyethyl)-1H-1,2,3-triazol-4-yl]methoxy}acetamido)-N-(2-nitrophenyl)benzamide (39 mg, 0.0886 mmol) in MeOH (4 mL) and DCM (4 mL), activated palladium on carbon (~10% by weight, 21 mg) was added. The flask was fitted with a rubber septum and the mixture was flushed with $N_2$ (g) via a needle twice. A balloon filled with $H_2$ (g) was connected and the mixture was stirred for 2.5 h at room temperature. After flushing, with nitrogen the solution was filtered through silica and evaporated under reduced pressure to give 31 mg (86 %) of product. 1H NMR (400 MHz, MeOH) δ ppm: 8.07 (s, 1 H), 7.97 (m, J=8.56 Hz, 2 H), 7.79 (m, J=8.56 Hz, 2 H), 7.16 - 7.21 (m, 1 H), 7.04 - 7.11 (m, 1 H), 6.90 (d, J=7.55 Hz, 1 H), 6.77 (t, J=7.55 Hz, 1 H), 4.78 (s, 2 H), 4.50 (t, J=5.04 Hz, 2 H), 4.11 - 4.21 (m, 2 H), 3.93 (t, J=5.29 Hz, 2 H). 13C NMR (101 MHz, DMSO-d6) δ ppm: 170.86, 168.34, 144.94, 143.96, 142.58, 131.14, 129.89, 129.89, 128.67. MS (ESI-TOF) m/z: $[M^-H]^-$: calcd. for $C_{20}H_{21}N_6O_4$, 409.2, found, 409.1. m/z: $[M^+H]^+$: calcd. for $C_{20}H_{23}N_6O_4$, 411.2, found, 411.2.

**Synthesis for the APD HO56** (*N*-(2-aminophenyl)-4-{[1-(2-hydroxyethyl)-1H-1,2,3-triazol-4-yl]methoxy}benzamide).

*4-[(prop-2-yn-1-yl)oxy] benzoic acid (**5**).*

Ethyl 4-hydroxybenzoate (8.308 g, 50.0 mmol) in DMF (20 mL) was added dropwise to sodium hydride (2.278 g, 57.0 mmol) in DMF (15 mL) at 0 °C followed by dropwise addition of propargyl bromide (80% in toluene, 6.465 mL, 60.0 mmol) in DMF (10 mL). After reaching room temperature the reaction mixture was left stirring overnight. Water (10 mL) was added and then sodium hydroxide (2.15 g, 53.7 mmol). The mixture was washed with dichloromethane and the water layer was acidified with HCl to give a precipitate that after drying under reduced pressure amounted to 3.28 g (37%) of the desired product. $^1$H NMR (400 MHz, DMSO-d6) δ ppm: 7.91 (d, J=8.56 Hz, 2 H), 7.07 (d, J=8.56 Hz, 2 H), 4.88 (d, J=2.52 Hz, 2 H), 3.60 (t, J=2.27 Hz, 1 H). $^{13}$C NMR (101 MHz, DMSO-d6) δ ppm: 166.92, 160.74, 131.28, 131.28, 123.70, 114.67, 114.67, 78.76, 78.64, 55.66.

*N-(2-nitrophenyl)-4-[(prop-2-yn-1-yl)oxy]benzamide (**6**).*

A mixture of 4-[(prop-2-yn-1-yl)oxy] benzoic acid (353 mg, 2.0 mmol) and 2-nitroaniline (415 mg, 3.0 mmol) in toluene (30 mL) was heated to boiling. After some cooling, phosphorus trichloride (87 µL, 1.0 mmol) was added. The mixture was reflux for 2 h, cooled to room temperature, diluted with dichloromethane. Partitioning was the done between the dichloromethane solution and an added 0.1 M HCl (*aq*) phase. The organic phase was washed with 0.1 M HCl, water and aqueous sodium bicarbonate. The organic layer then collected,

dried with sodium sulfate, and concentrated under reduced pressure. The resulting solid was recrystallized from ethanol to give a yellow powder (365 mg, 61%). $^{1}$H NMR (400 MHz, DMSO-d6) δ ppm: 10.66 (s, 1 H), 8.01 (dd, J=8.31, 1.26 Hz, 1 H), 7.95 (d, J=9.06 Hz, 1 H), 7.78 (td, J=8.06, 1.51 Hz, 1 H), 7.73 (dd, J=8.06, 1.50 Hz, 1 H), 7.40 (ddd, J=8.06, 7.05, 1.51 Hz, 1 H), 7.15 (d, J=9.06 Hz, 1 H), 4.92 (d, J=2.52 Hz, 1 H), 3.63 (t, J=2.52 Hz, 1 H). $^{13}$C NMR (101 MHz, DMSO-d6) δ ppm: 164.77, 160.34, 142.78, 134.10, 131.83, 129.74, 129.74, 126.36, 125.83, 125.40, 125.05, 114.86, 114.86, 78.84, 78.76, 55.74.

*4-{[1-(2-hydroxyoethyl)-1H-1,2,3-triazol-4-yl]methoxy}-N-(2-nitrophenyl)benzamide (**7**).*

N-(2-nitrophenyl)-4-[(prop-2-yn-1-yl)oxy]benzamide (503.6 mg, 1.70 mmol) and 2-azidoethanol (370 µL, 5.10 mmol) was mixed with methanol (225 mL) and water (25 mL). The mixture was then heated to dissolve the reagents. $CuSO_4$*$5H_2O$ (213 mg, 0.85 mmol) and ascorbic acid (1.20 g, 6.82 mmol) were added at 50 - 60 ºC. The reaction was left overnight at room temperature. EDTA was added and the mixture was then diluted with dichloromethane. Partitioning of the dichloromethane solution with water (with approx. 1/5 brine). The dichloromethane phase was washed with water containing 1/5 brine and EDTA (ca 100 mg). The water layer was extracted with ethyl acetate and the collected organic layers were dried with $Na_2SO_4$, filtered and concentrated under reduced pressure. The resulting yellow solid was recrystallized from ethanol to yield 364 mg (56 %) of product as a yellow solid. $^{1}$H NMR (400 MHz, DMSO-d6) δ ppm 10.64 (s, 3 H), 8.24 (s, 4 H), 8.01 (dd, J=8.06, 1.51 Hz, 1 H), 7.92 - 7.98 (m, 2 H), 7.81 (dd, J=8.31, 1.26 Hz, 1 H), 7.75 (td, J=7.55, 1.50 Hz, 1 H), 7.40 (ddd, J=8.00, 7.80, 1.50 Hz, 1 H), 7.22 (d, J=8.56 Hz, 8 H), 5.26 (s, 2 H), 5.07 (t, J=5.29 Hz, 3 H), 4.42 (t, J=5.29 Hz, 8 H), 3.79 (q, J=5.54 Hz, 8 H). $^{13}$C NMR (101 MHz, DMSO-d6) δ ppm 165.27, 161.62, 142.90, 136.34, 136.08, 129.31, 129.31, 126.53, 125.81, 124.33, 123.17, 122.03, 121.95, 114.91, 114.91, 61.73, 60.46, 52.69.

*N-(2-aminophenyl)-4-{[1-(2-hydroxyethyl)-1H-1,2,3-triazol-4-yl]methoxy}benzamide* (**HO56**).

To a solution of N-(2-aminophenyl)-4-{[1-(2-hydroxyethyl)-1H-1,2,3-triazol-4-yl]methoxy}benzamide (23.9 mg, 0.062 mmol) in methanol (10 mL) and dichloromethane (5 mL), activated palladium on carbon (~10% by weight, 10 mg) was added. The flask was fitted with a rubber septum and the mixture was flushed with $N_2$ (g) via a needle twice. A balloon of H2 gas was introduced at room temperature with stirring. A balloon filled with $H_2$ (g) was connected and the mixture was stirred for 2 h at room temperature. After flushing with nitrogen the solution was filtered through Celite and evaporated under reduced pressure to give an off-

white powder (21 mg, 0,060 mmol, 96%). $^{1}$H NMR (400 MHz, DMSO-d6) δ ppm: 9.57 (s, 1 H), 8.23 (s, 1 H), 7.97 (d, J=8.06 Hz, 2 H), 7.15 (d, J=7.05 Hz, 4 H), 6.96 (s, 1 H), 6.77 (d, J=8.06 Hz, 1 H), 6.59 (s, 1 H), 5.23 (s, 2 H), 5.08 (t, J=5.04 Hz, 1 H), 4.88 (br. s., 2 H), 4.42 (t, J=5.29 Hz, 2 H), 3.75 - 3.84 (m, 2 H). $^{13}$C NMR (101 MHz, DMSO-d6) δ ppm: 164.70, 160.55, 143.21, 142.05, 129.67, 129.67, 127.00, 126.74, 126.36, 125.19, 123.54, 116.26, 116.14, 114.21, 114.21, 61.23, 59.83, 52.25. MS (ESI-TOF) m/z: $[M^{-}H]^{-}$: calcd. for $C_{20}H_{21}N_6O_4$, 252.1, found, 252.0. m/z: $[M^{+}H]^{+}$: calcd. for $C_{20}H_{23}N_6O_4$, 354.16, found, 354.1.

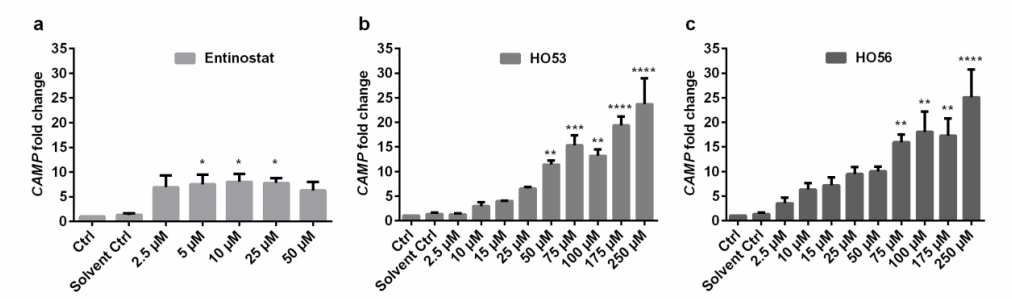


**Supplementary Figure S3. Dose dependent induction of the *CAMP* gene in BCi cells by Entinostat, HO53 and HO56.** Cells were stimulated for 24 h with increasing doses of **a)** Entinostat, **b)** HO53 and **c)** HO56. DMSO (final concentration lower than 1%) was used as a solvent control (Solvent Ctrl). The *CAMP* gene expression was normalized to *TUBB* (tubulin-β) reference gene and presented as fold change of the expression in comparison to control cells (Ctrl). Each bar represents mean value of 3 independent experiments ± SEM; statistical significance was calculated in comparison to control cells using one-way ANOVA with Dunnett´s multiple comparisons test; * $p<0.05$, ** $p<0.01$, *** $p<0.001$, **** $p<0.0001$. All tested concentrations are shown and selected concentrations are presented in figure 1b.

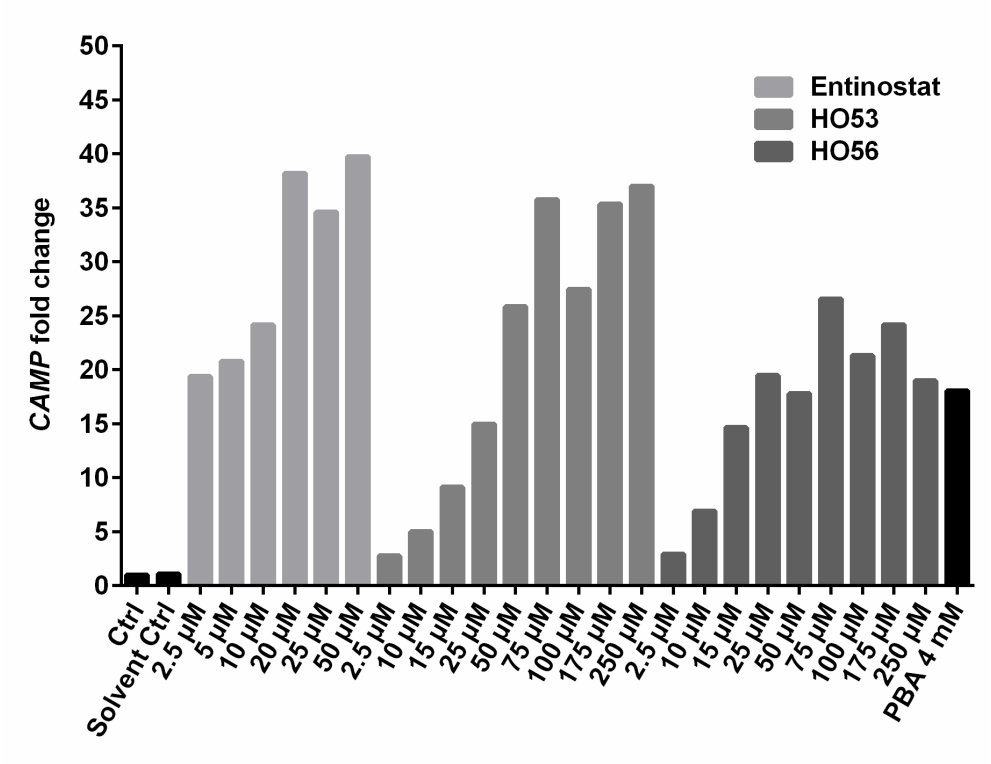


**Supplementary Figure S4. Dose dependent induction of the *CAMP* gene in VA10 cells by Entinostat, HO53 and HO56.** Cells were stimulated for 24 h with increasing doses of Entinostat (2.5-50 µM), HO53 and HO56 (both at 2.5-250 µM). DMSO (final concentration lower than 1%) and PBA (4 mM) were used as a solvent control (Solvent Ctrl) and positive control, respectively. The *CAMP* gene expression was normalised to *TUBB* (tubulin-β) reference gene and presented as fold change of the expression in comparison to control cells (Ctrl). Each bar is representative of technical duplicates.

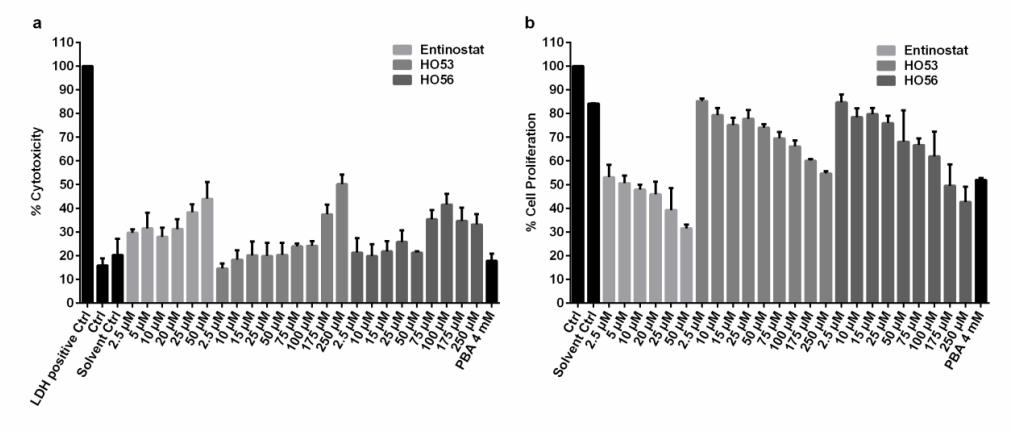


**Supplementary Figure S5. Cytotoxicity and proliferation of BCi cells after 24 h exposure to Entinostat, HO53 and HO56. a)** Cytotoxic effect of Entinostat (2.5-50 μM), HO53 (2.5-250 μM) and HO56 (2.5-250 μM) on BCi cells was determined by the LDH assay. Cytotoxicity was measured as a percentage of the LDH positive control. Each bar is the mean value of 3 independent experiments ± SEM. Using unpaired student t-test *p value* of selected concentration 75 μM HO53 and HO56 in comparison to solvent control is 0.237 and 0.027, respectively. **b)** Effect of Entinostat, HO53 and HO56 on cell proliferation was determined by WST-1 assay. Data shown as percentage of the control cells and presented as a mean value of 2 independent experiments ± SEM. Using unpaired student t-test *p value* of selected concentration 75 μM HO53 and HO56 in comparison to solvent control is 0.0437 and 0. 0336, respectively.

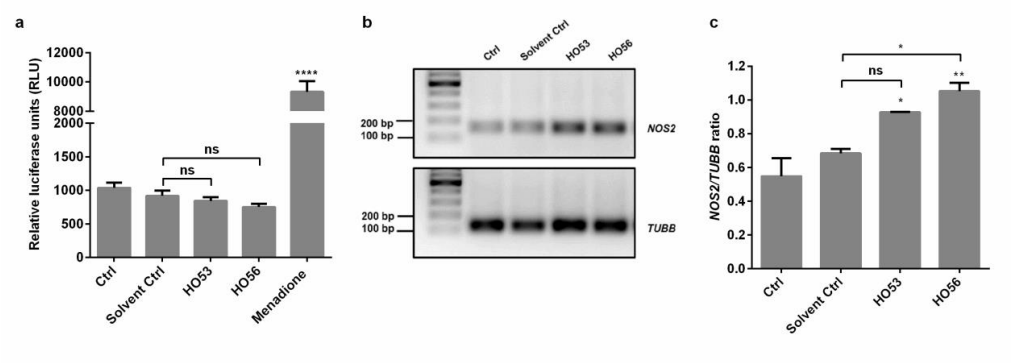


**Supplementary Figure S6. Effect of HO53 and HO56 treatment on reactive oxygen species (ROS) production and inducible nitric oxide synthase (*NOS2*) in BCi cells. a)** The $H_2O_2$ level in cell culture medium was measured in relative luciferase units (RLU) after 24 h of induction with HO53 and HO56 (both at 75 µM). Menadione (50 µM) treatment for 90 min served as a positive control. Data is representative of n=3 independent experiments ± SEM, statistical significance was calculated using one-way ANOVA with Dunnett´s multiple comparisons test while comparing to control (Ctrl) or with Sidak´s multiple comparisons test while comparing HO53 and HO56 to solvent control (Solvent Ctrl). **b)** *NOS2* expression accessed by semi-quantitative PCR (representative of 2 independent experiments). **c)** Quantification of *NOS2/TUBB* ratio of 2 independent experiments ± SEM, statistical significance was calculated using one-way ANOVA with Dunnett´s multiple comparisons test while comparing to control (Ctrl) or with Sidak´s multiple comparisons test while comparing HO53 and HO56 to solvent control (Solvent Ctrl). * $p<0.05$, ** $p<0.01$, **** $p<0.0001$, ns indicates non-significant.

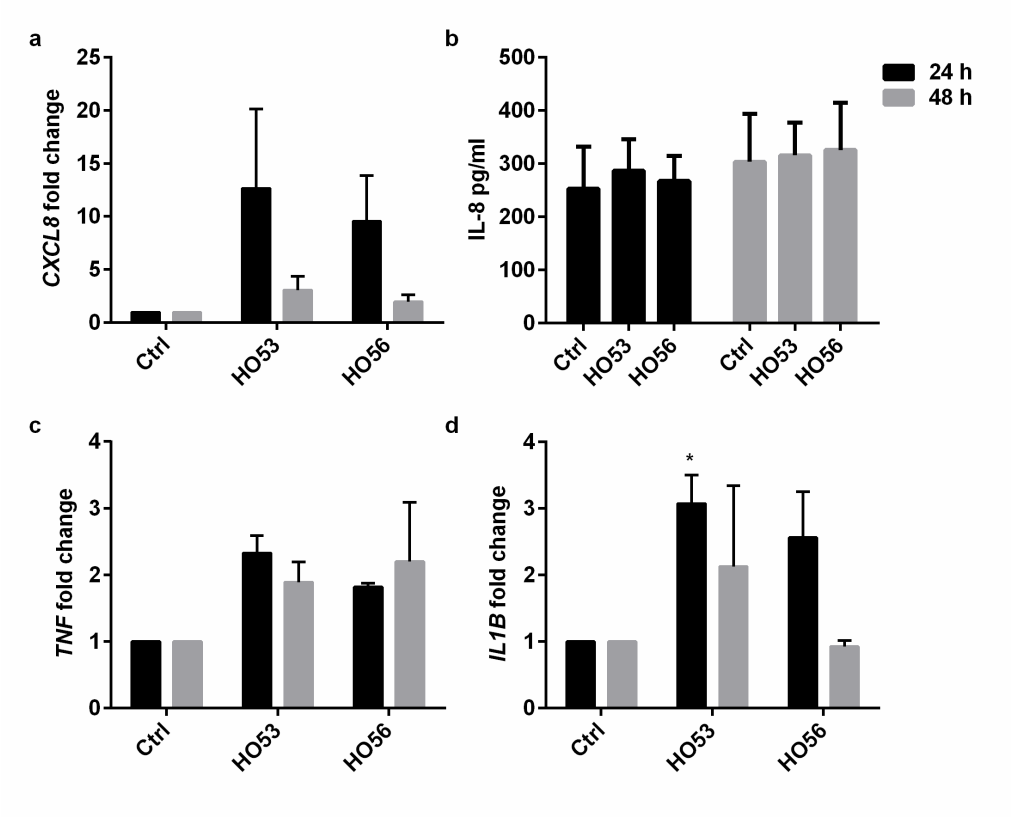


**Supplementary Figure S7. Expression of cytokines in ALI differentiated BCi cells upon treatment with HO53 and HO56.** mRNA expression of **a)** *CXCL8*, **c)** *TNF* and **d)** *IL1B* measured by qRT-PCR and normalized to *TUBB* (tubulin-β) reference gene. Data is from n=4 independent experiments ± SEM. **b)** Protein level of IL-8 was accessed by ELISA. Data is representative of n=2 independent experiments ± SEM. Statistical significance was calculated in comparison to untreated cells (Ctrl) using two-way ANOVA with Dunnett´s multiple comparisons test, * $p<0.05$, only significant changes were highlighted.

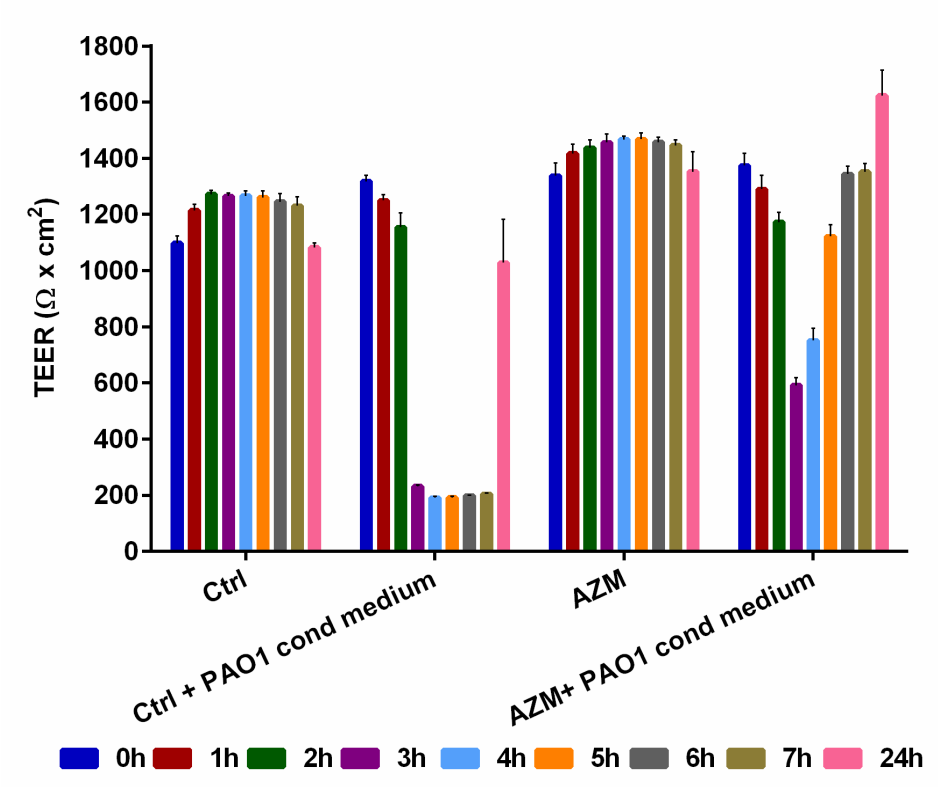


**Supplementary Figure S8. Azithromycin treatment counteracts disruptive effect of *P. aeruginosa* PAO1 conditioned medium in airway epithelium in ALI culture of BCi cells.** Differentiated BCi cells (TEER ≥1000 Ω×cm$^2$) were treated with 40 µg/mL Azithromycin in the lower chamber of transwell insert for 3 days and challenged with PAO1 conditioned medium applied on the apical surface of the cells. TEER (Trans epithelial electrical resistance) measurement after every hour from 0 to 7 h and after 24 h post PAO1 culture medium challenge with and without Azithromycin basal treatment. Data shown is representative of two experiments, showing mean values of four independent ALI filters at each time point ± SEM.

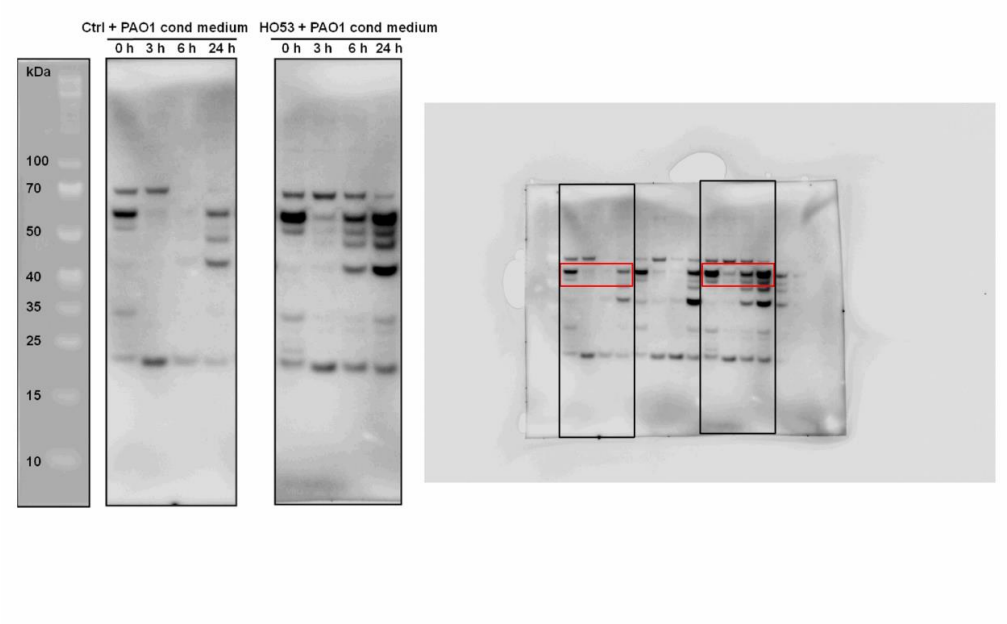


**Supplementary Figure S9. Changes in occludin pattern in control and HO53 treated airway epithelial BCi cells upon PAO1 conditioned medium challenge.** The main occludin isoform is the ~ 60 kDa band and it is presented in Figure 6c. The uncropped immunoblot is presented on the right.

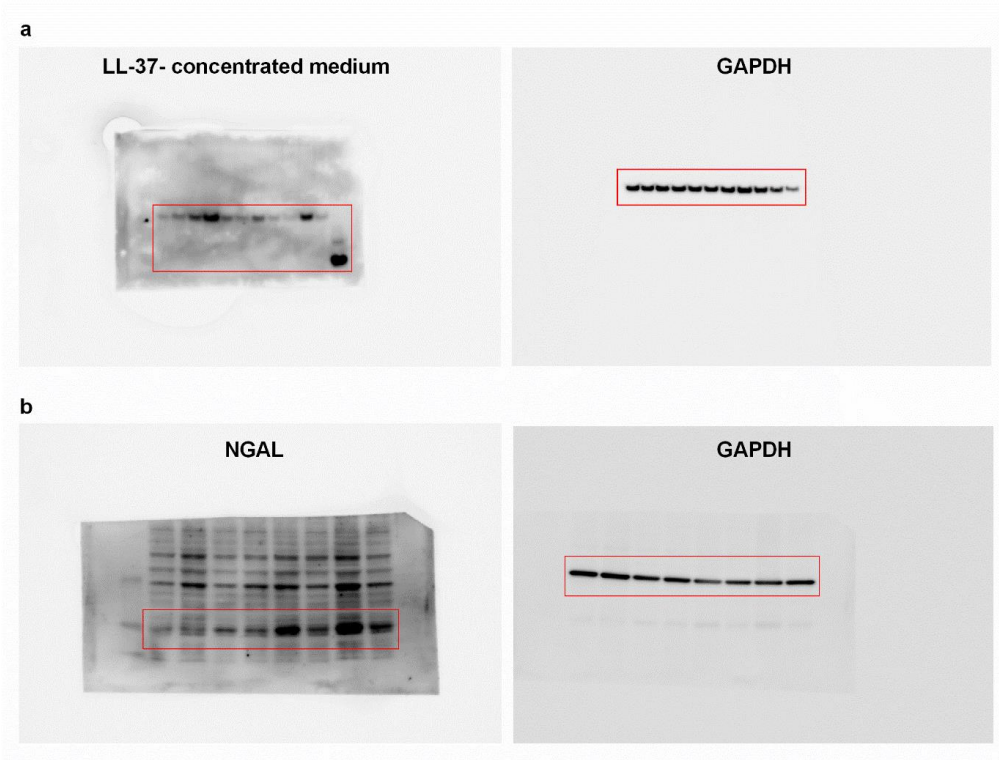
a
LL-37- concentrated medium
GAPDH
b
NGAL
GAPDH

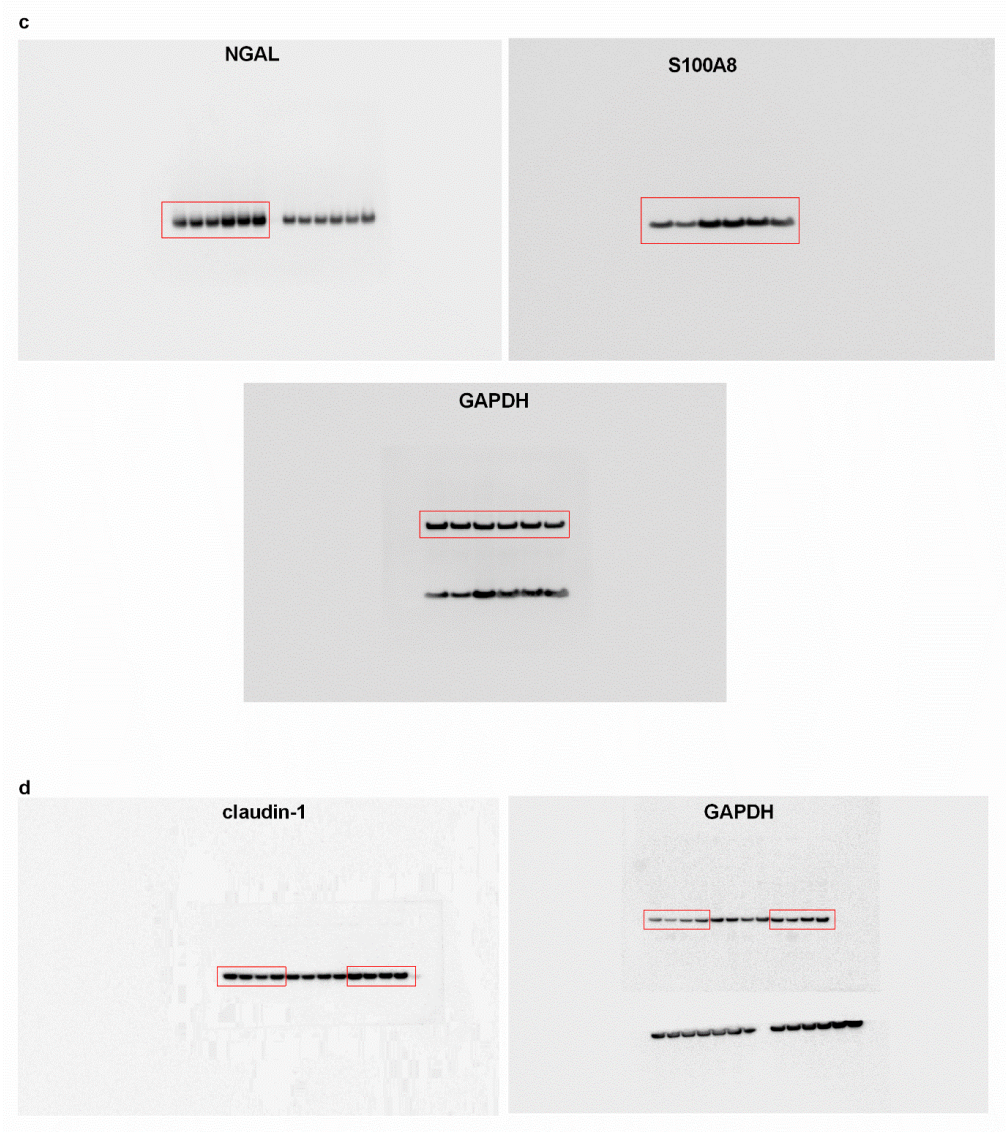
c
NGAL
S100A8
GAPDH
d
claudin-1
GAPDH

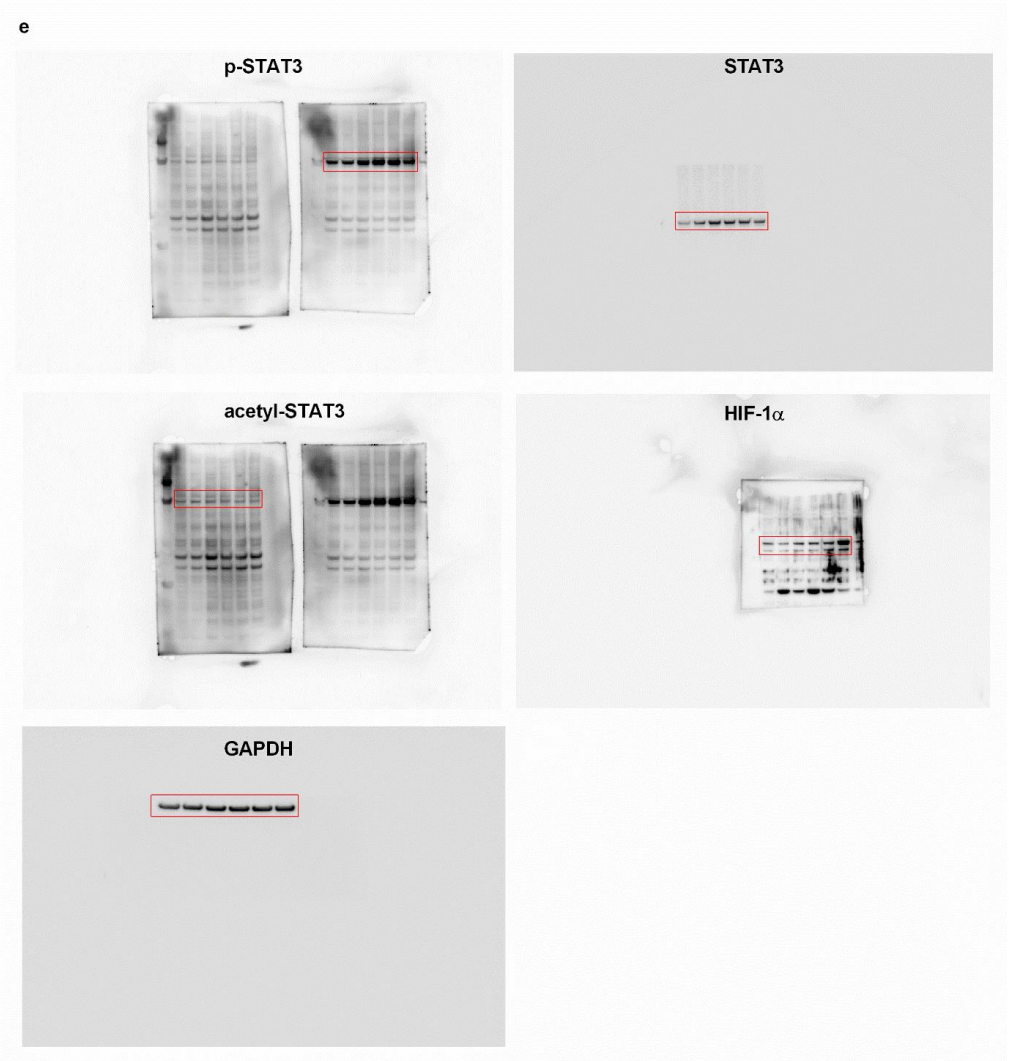


**Supplementary Figure S10. Display of full-length blots presented in the article.** Uncropped immunoblots showing: **a)** pro-LL-37 in the concentrated medium and synthetic LL-37 together with GAPDH loading control (presented in Fig. 1g), **b)** NGAL and GAPDH (presented in Fig. 2b), **c)** NGAL, S100A8 and GAPDH (presented in Fig. 5c), **d)** claudin-1 and GAPDH (presented in Fig. 6c), **e)** p-STAT3, STAT3, acetyl-STAT3, HIF-1α, GAPDH (presented in Fig. 7c).

**Supplementary Table S1. List of primers used in this study**

| Gene | RefSeq number | Forward Primer (5´→3´) | Reverse Primer (5´→3´) |
|---|---|---|---|
| ***CAMP*** | NM_004345.4 | GCACACTGTCTCCTTCACTG | CTAACCTCTACCGCCTCCT |
| ***HBD1*** | NM_005218.3 | CCAGTCGCCATGAGAACTTCC | GTGAGAAAGTTACCACCTGAGGC |
| ***LCN2*** | NM_005564.4 | AACTTCATCCGCTTCTCCAA | TCTCCCAGCTCCCTCAATG |
| ***LYZ*** | NM_000239.2 | AGATAACATCGCTGATGCTGTAG | CTCCACAACCTTGAACATACTGA |
| ***LTF*** | NM_001321122.1 | TGTATCCAGGCCATTGCG | ATAGTGAGTTCGTGGCTGTC |
| ***S100A8*** | NM_002964.4 | TCTACCACAAGTACTCCCTGAT | TCCAACTCTTTGAACCAGACG |
| ***CXCL8*** | NM_000584.3 | CTGTCTGGACCCCAAGGAA | CTGGCATCTTCACTGATTCTTG |
| ***IL1B*** | NM_000576.2 | CAGCCAATCTTCATTGCTCAAG | GAACAAGTCATCCTCATTGCC |
| ***TNF*** | NM_000594.3 | CCTCTCTCTAATCAGCCCTC | CCTCAGCTTGAGGGTTTGC |
| ***NOS2*** | NM_000625.4 | AATGAATACCGGTCCCGTGG | CATGGGTTTTCCAGGCCTCT |
| ***HIF1A*** | NM_001530 | CCATTAGAAAGCAGTTCCGC | TGGGTAGGAGATGGAGATGC |
| ***TUBB*** | NM_178014.3 | GCCAGATCTTTAGACCAGACAA | CCTCCTTCCGTACCACATC |

**Supplementary Table S2. Quantification of lipocalin 2 expression.** The representative relative quantification of NGAL/GAPDH ratio normalized to control from Western blotting presented in Fig. 2b.

| Lane | Treatment | NGAL | GAPDH | NGAL/GAPDH ratio | Relative NGAL/GAPDH ratio normalized to control |
|---|---|---|---|---|---|
| 1 | ctrl-24h | 8336.347 | 36005.47 | 0.23153 | 1.00 |
| 2 | ctrl-48h | 14835.2 | 38151.83 | 0.388846 | 1.00 |
| 3 | Entinostat-24h | 10763.47 | 25078.3 | 0.429195 | 1.85 |
| 4 | Entinostat-48h | 15800.42 | 28032.13 | 0.563654 | 1.45 |
| 5 | HO53-24h | 31168 | 20517 | 1.51913 | 6.56 |
| 6 | HO53-48h | 20721.81 | 23823 | 0.869824 | 2.24 |
| 7 | HO56-24h | 38882.83 | 24053.71 | 1.6165 | 6.98 |
| 8 | HO56-48h | 24374.05 | 28127.25 | 0.866564 | 2.23 |

# Paper II

# Novel inducer of innate immunity HO53 stimulates autophagy in human airway epithelial cells

Iwona T. Myszor[1], Snaevar Sigurdsson[1], Alexia Ros Viktorsdottir[1], Birgitta Agerberth[2], Eeva-Liisa Eskelinen[3,4], Margret Helga Ogmundsdottir[5], Gudmundur H. Gudmundsson[1,2]

[1] Life and Environmental Sciences, Biomedical Center, University of Iceland, Reykjavik, Iceland

[2] Department of Laboratory Medicine, Clinical Microbiology, Karolinska Institutet, Huddinge, Sweden

[3] Institute of Biomedicine, University of Turku, Turku, Finland

[4] Molecular and Integrative Biosciences Research Programme, University of Helsinki, Helsinki, Finland

[5] Department of Anatomy, Biomedical Center, Faculty of Medicine, University of Iceland, Reykjavik, Iceland.

Correspondence and requests for materials should be addressed to G. H. G.; address: Biomedical Center, University of Iceland, Vatnsmyrarvegur 16, Reykjavik 101, Iceland; phone: +354 525 5276; email: ghrafn@hi.is

**Abstract**

Aroylated phenylenediamines are novel modulators of innate immunity with respect to enhancing antimicrobial peptides expression and maintaining epithelial barrier integrity. Here we present a new study on induction of autophagy in human lung epithelial cells by aroylated phenylenediamine HO53. Interestingly, HO53 affected autophagy in a dose dependent manner only in mature polarized bronchial epithelial cells. The induction of autophagy in differentiated lung epithelial cells was demonstrated by increased LC3B processing, presence of LC3B puncta indicating formation of autophagosomes visualized by TEM. The phenotypic changes indicating autophagy induction were associated with activation of AMPK kinase pathway, nuclear translocation of transcription factor TFEB and changes in expression of autophagy related genes. The kinetics of the explored signaling pathways revealed first, activation of AMPK followed by the nuclear translocation of TFEB. Moreover, our data suggest that HO53 modulates epigenetic changes related to induction of autophagy manifested by transcriptional regulation of histone modifying enzymes. These changes were reflected by decreased ubiquitination of H2BK120 that has been associated with autophagy induction. Taken together, HO53 modulates autophagy, a part of the host defense system through a complex mechanism involving several signaling pathways and epigenetic events.

**Keywords**

airway epithelium, AMPK, aroylated phenylenediamine, autophagy, epigenetics, RNAseq

## Introduction

Autophagy is the essential adaptive process promoting cell survival and maintaining cell homeostasis in response to different stimuli from constantly changing environment. The prominent function of autophagy is to provide nutrients and energy for cellular processes during starvation. It is also cytoprotective in stress conditions like hypoxia, shortage of growth factors, accumulation of misfolded proteins and damaged organelles [1,2]. Moreover, autophagy is considered as selective process for innate and adaptive immunity as a cell autonomous defense system protecting the host from pathogens [3]. Interestingly, autophagy impairment is also related to the autoimmune and inflammatory diseases such as inflammatory bowel diseases, e.g. Crohn´s disease [4,5] implicating autophagy as a vital process with precise regulation [1,4].

The epithelial layer in the human respiratory tract is the first line of defense providing an important protective barrier for pathogens [6]. The initial active shield for the host consists of the mucus layer composed of different glycoproteins and antimicrobial peptides (AMPs) accompanied by mucociliary clearance by beating cilia [7,8]. However, when the first line of defense fails and bacteria enter the epithelial cells, autophagy is a crucial process for protecting the host from invading pathogens [9,10]. Dynamics of the autophagy process varies depending on the cell type. The clearance of pathogens is more rapid in phagocytic cells such as macrophages than in non-phagocytic bronchial epithelial cells for instance [11]. Importantly, airway epithelial cells can effectively eliminate pathogens like *Pseudomonas aeruginosa* [12,13] or conidia of *Aspergillus fumigatus* [14]. Moreover, pathogens utilize a variety of virulence factors that allow them for effective replication, e.g. *Mycobacterium tuberculosis* (Mtb) blocks autophagosome maturation in infected macrophages [15]. Therefore, modulation of the autophagy pathways can be an effective strategy to eliminate pathogens and to avoid/limit use of antibiotics, thereby reducing the selection of multidrug resistant bacteria strains [16].

Several different agents including inducers of AMPs production have been shown effective in bacterial killing through autophagy [16,17]. Among them, vitamin D3 and phenylbutyrate (PBA) gave positive outcome in the clinical trials for the treatment of pulmonary tuberculosis [18,19]. Moreover, phenylbutyrate induces autophagy and promotes intracellular killing of Mtb in human macrophages [20]. The short chain fatty acid (SCFA) butyrate imprints an antimicrobial program in macrophages including activation of autophagy [21]. Another example of autophagy activating

compounds is resveratrol [22], previously described as an inducer of cathelicidin expression in keratinocytes [23]. Recently, we reported on a compound from the novel group of aroylated phenelynediamines (APDs), HO53 that induced expression of several antimicrobial effectors, enhanced tight junctions and was efficient against *P. aeruginosa* infection [24].

In this study, we analyzed if HO53 induced autophagy in human airway epithelial cells and investigated molecular mechanisms behind autophagy induction by HO53. We found that HO53 stimulates autophagy in human bronchial epithelial cell lines BCi-NS1.1 (hereafter BCi) and VA10. Both cell lines retain basal-like character and are able to differentiate towards polarized epithelium approaching mature epithelial cells [25,26]. For differentiated BCi cells in air-liquid interphase (ALI) culture, autophagy induction with HO53 was monitored by analysis of microtubule-associated proteins 1A/1B light chain 3B (LC3B) processing and shown dose dependent. The LC3B processing was pronounced only in the mature polarized cells but not in the undifferentiated monolayer cells. Therefore, we used differentiated BCi cells in further experiments. We observed presence of LC3B puncta and these observations were supplemented by transmission electron microscopy (TEM) showing autophagosome formation. To define cell signaling pathway/s responsible for HO53 induced autophagy in ALI cultured BCi cells, we performed RNAseq analysis and further we confirmed increased phosphorylation level of AMPK. We observed that HO53 enhances TFEB nuclear translocation and affects expression of autophagy related genes. Furthermore, we show that HO53 affects gene expression of histone modifying enzymes, ubiquitin specific peptidase 44 (*USP44*) and enhancer of zeste homolog 2 (*EZH2*). Changes in expression of *USP44* were reflected by decreased ubiquitination status of H2BK120, indicating epigenetic regulation of autophagy by HO53. Taken together, HO53 promotes autophagy in human airway epithelial cells through a complex mechanism involving several signaling pathways and epigenetic events.

## Materials and methods

### Reagents and materials

Collagen from human placenta (C7521), the secondary antibody conjugated with HRP for Western blotting (A0545), DAPI (D9564) and all chemicals were purchased from Sigma. UltroserG (UG, 15950-017) was obtained from PALL Life Sciences and DMSO (sc-358801), Bafilomycin A1 (sc-201550) and Rapamycin (sc-3504) from Santa Cruz. Secondary antibodies for immunofluorescence staining were obtained from Thermo Scientific (A-11070, A-11020 and A-21244). HO53 was synthesized as was described previously [24].

### Cell cultures

The human bronchial epithelial cell line BCi-NS1.1 (BCi) immortalized with retrovirus expressing human telomerase (hTERT) was from dr Matthew S. Walters, Weill Cornell Medical College, New York NY, USA [26]. An E6/E7 viral oncogene immortalized human bronchial epithelial cell line VA10 has been described previously [25]. Both cell lines were cultured in Bronchial/Tracheal Epithelial cell growth medium (BEGM) (Cell Applications, 511A-500) supplemented with retinoic acid (Cell Applications, 511-RA) and Penicillin-Streptomycin ((20 U/ml, 20 µg/ml, respectively) (Life Technologies, 15140122)) at 37°C and 5% $CO_2$. The ALI (air-liquid interface) culture of BCi and VA10 cells were maintained as described previously [25,26]. Cells in monolayer were treated by direct addition of the compound to the culture medium. Differentiated cells were used for experiments at least after 21 days of ALI culture and then the treatment compound was added to the lower chamber for indicated period of time.

### Immunoblotting

Cells were washed with PBS and lysed in RIPA lysis buffer (Santa Cruz, sc-364162) supplemented with Halt protease inhibitor cocktail (Thermo Scientific, 87786) and phosphatase inhibitor cocktail (Cell Signal., 5870) on ice for 30 min. Histone extracts were obtained from ~$5\times10^5$ differentiated cells lysed in 80 µl of PBS with 0.5% Triton X-100 supplemented with protease and phosphatase inhibitors cocktail for 10 min on ice followed by overnight histones acid extraction (in 0.2 N HCl) from cell pellets. Acid extracts containing histones were neutralized by addition of 2 M NaOH (1/10 of final volume). The total protein of 10-20 µg and 2.5 µg of purified histone extracts were separated using NuPAGE 4–12% Bis–Tris gradient gels

(Life Technologies, NP0323) and NuPAGE MES SDS Running Buffer (Life Technologies, NP0002) or polyacrylamide gel electrophoresis (SDS-PAGE) and SDS-Tris-Glycine buffer (25 mM Tris, 250 mM glycine, 0.5% SDS) with the running conditions 120 V and 275 mA. The proteins were transferred on to a PVDF membrane (0.2 µm pores) using XCell II™ Blot Module (Invitrogen, EI9051) and the membrane was blocked with 10% skimmed milk or 10% BSA in TBS-T buffer (50 mM Tris, 150 mM NaCl, 0.1% Tween-20) for 1 h at room temperature. Then, the membrane was incubated with primary antibodies overnight at 4°C using a dilution recommended by the manufacturer´s protocol (List of primary antibodies in the Supplementary Table S1). After washing with TBS-T buffer the membrane was incubated with horse radish peroxidase (HRP) conjugated secondary antibodies (1:10 000 dilution) in 5% skimmed milk or 5% BSA in TBS-T for at least 1.5 h at room temperature. Immunoblots were developed using Pierce ECL Plus Western blotting substrate (Thermo Scientific, #34095) or Western blotting Luminol reagent (Santa Cruz, sc-2048) and ImageQuant LAS 4000 system (GE Healthcare). Quantification of the band intensity was performed using ImageJ software.

**Immunofluorescence**

Cells growing on ALI filters were fixed using pre-chilled methanol at 4°C overnight and then by pre-chilled acetone. Fixed cells on ALI filters were stained as follows: hydratation step was performed using IF buffer (PBS + 0.3% Triton X-100), the cells on the ALI filters were incubated with the blocking buffer (10% FBS in IF buffer) and incubated with primary antibodies overnight at 4°C using concentration recommended by the manufacturer´s protocol (Supplementary Table S1). The next day filters were washed and incubated with DAPI (1:5000) and secondary antibodies Alexa Fluor 488 (A-11070) and/or Alexa Fluor 594 (A-11020) for 2 h. Cells growing on ALI filters were mounted in Fluoromount™ Aqueous Mounting Medium (F4680-Sigma) and coverslips were placed over the filters. Images were taken using Olympus fluoview Fv1200 confocal microscope at 30x and 60x magnification. Z-scans were performed by taking series of images at the same location with fixed focal intervals. Nuclear translocation of TFEB was evaluated by using 'Colocalisation' function of the Olympus fluoview Fv1200 confocal microscope software. The threshold was adjusted to value of 1250 showing signal only from colocalized TFEB/nuclei (pink) extracted from merged images followed by quantification of

pixel intensity by ImageJ software. The same parameters of image acquisition and threshold were used for all images.

**Transmission electron microscopy (TEM)**

BCi-NS1.1 cells growing on trans-well inserts in ALI conditions were fixed with 2.5% glutaraldehyde (Ted Pella, Inc.) by addition of fixative to the upper and lower chamber. Next, cells were washed in phosphate buffer (0.075 M with 0.15 M sucrose) twice for 2 min and post fixed in 2% osmium tetroxide (J. B. EM Services Inc.) for 30 min followed by washing twice for 3 min. Cells were dehydrated in increasing concentrations of ethanol: 25%, 50% and 70% for 2 min each. Then, alcohol was replaced with 4% uranyl acetate in 70% ethanol (J. B. EM Services Inc.) for 7 min, followed by 2 min incubations in 80%, 90%, 96% solutions of ethanol and at the end in pure ethanol for 5 minutes and twice for 7 minutes. Then, the trans-well filters were placed on the coverslips with a drop of resin (Spurr Resin-Ted Pella, Inc.) and cells were embedded by adding a few drops of resin on top of the cell layer and incubated for 2 h at room temperature. Gelatin capsules were filled with resin and placed upside down on top of the coverslips to create a block and incubated overnight at 70°C. Afterwards, resin blocks and filters were separated from coverslips by submerging them for few seconds in liquid nitrogen. After that plastic filters were broken away which created round shape resin disks. Ultra-thin (100 nm) sections were cut with diamond knife (45° Diatome) on an Ultramicrotome (Leica EM UC7) and placed on copper grids (Ted Pella, Inc.). Sections on grids were stained for 1 minute with lead citrate (3% Ultrostain 2, Leica) and imaged using a JEM-1400PLUS PL Transmission Electron Microscope at various magnifications.

**RNA analysis**

Total RNA was extracted using NucleoSpin RNA kit (Machinery-Nagel, 740955.50). Total RNA of 1 µg was used to synthesize complementary DNA (cDNA) according to the manufacture´s recommendations using the High Capacity cDNA reverse transcriptase kit (Applied Biosystems, 4368814). One µl of cDNA, 5 µl of PowerUp SYBR Green Master Mix (Applied Biosystems, A25742) and 0.5 µM primers enlisted in Supplementary Table S2 were used for qRT-PCRs. The qRT-PCRs were performed using LG 7500 Real Time PCR System (Applied Biosystems) with the following cycling conditions: (1) holding stage: 95°C for 10 min, followed by 40 cycles of (2)

denatured stage: 95°C for 15 s and (3) annealed/extended stage: 60°C for 1 min. The $2^{(-\Delta\Delta CT)}$ Livak method was utilized for calculating fold differences over untreated control [27].

**Preparation of Poly-A cDNA sequencing libraries**

The quality (RIN score) and quantity of isolated total RNA samples was assessed using the DNA 5K/RNA chip for the LabChip GX (Perkin-Elmer). cDNA libraries derived from Poly-A mRNA were generated using Illumina´s TruSeq RNA v2 Sample Prep Kit. Briefly, Poly-A mRNA was isolated from total RNA samples (0.2–1 μg input) using hybridization to Poly-T beads. The Poly-A mRNA was fragmented at 94°C, and first-strand cDNA was prepared using random hexamers and the SuperScript II reverse transcriptase (Invitrogen). Following second-strand cDNA synthesis, end repair, addition of a single A base, indexed adaptor ligation, AMPure bead purification, and PCR amplification, the resulting cDNA sequencing libraries were measured on the LabChip GX, diluted to 3 nM and stored at -20 °C.

**RNA sequencing and gene expression analysis**

Samples were pooled and sequenced on NovaSeq 6000 (24 samples/pool/lane) using on-board clustering. Paired-end sequencing (2x125 cycles) was performed using S4 flowcells, following the XP workflow. We quantified the RNA transcript expression with Kallisto version 0.45.0 [28] using the Homo Sapiens GRCh38 reference transcriptome [29]. Gene expression estimates were computed with the sleuth R package v0.30 [30]. The gene set enrichment analysis (GSEA) version 3.0 developed by Broad Institute [31] was used for Gene Ontology (GO) analysis. The differentially expressed genes were ranked on the list based on the expression (b-estimate) and q value. Next, the ranked lists of differentially expressed genes were analyzed by GSEA software using the 'hallmark gene sets' database of biological processes and the customized list of autophagy-lysosome genes [32] as reference with following parameters: 1. Number of permutations: 1000, 2. Enrichment statistic: classic, 3. Gene sets larger than 5000 and smaller than 15 were excluded from the analysis. Among positively and negatively enriched gene sets autophagy related pathways with false discovery rate FDR<0.05 were presented. Heatmaps showing significant ($p$<0.05) gene expression presented as log2 fold change were created in R studio software.

## Statistical analysis

Results are presented as mean ± standard error of mean (SEM) from at least three independent experiments. One-, two-way ANOVA and student *t*-test were used to determine significance of the data; *p* values and corrections for multiple comparisons are indicated in the figure legends. The statistical analysis was performed with GraphPad Prism 6 software (Graph Pad, USA). Except Supplementary figure S3A, Western blots are representative of at least three independent experiments.

## Results

### HO53 induces autophagy in mature human lung epithelial cells

Several markers are utilized to monitor autophagy induction. The most common is autophagosomal marker LC3B-I processed to LC3B-II that informs about formation of autophagosomes. Further, degradation of p62 and Bafilomycin A1, an inhibitor of autophagosome-lysosome fusion, are used to evaluate lysosomal degradation of autophagosomal cargo described as autophagy flux [33]. To assess the effect of aroylated phenylenediamine compound HO53 on autophagy induction in human bronchial epithelial cells BCi and VA10, we analyzed LC3B processing, presence of LC3B puncta and occurrence of autophagosomes using transmission electron microscopy (TEM). The human bronchial epithelial cell lines used in this study have basal-like character and can be used as undifferentiated monolayer cells and mature differentiated in air-liquid interphase (ALI) cultures forming polarized epithelial layer of different cell types [25,26]. First, we analyzed effect of HO53 on autophagy induction by analysis of LC3B processing in both ALI and undifferentiated cells (Fig. 1A and 1B). Treatment with increasing doses of HO53 for 24 hours led to dose dependent accumulation of LC3B-II in ALI BCi (Fig. 1A) but not in undifferentiated cells (Fig. 1B), indicating potent autophagy induction only in the mature polarized BCi cells. Further, in co-treatment with Bafilomycin A1, these changes were significant also in undifferentiated cells for 75 µM HO53 (Fig. 1B) but in ALI cells only at 150 µM (Fig. 1A). These results indicate that autophagy is induced in the mature polarized BCi cells. However, when comparing HO53 treatment without and in co-treatment with Bafilomycin A1, the autophagy flux does not seem to be increased. Similar phenotype of autophagy induction by HO53 linked to cell differentiation status was observed in VA10 cells (Supplementary Fig. S1), where autophagy induction was identified only in mature cells

(Supplementary Fig. S1A and S1B). We observed low expression level of p62 protein, an additional autophagy flux indicator in both human lung epithelial cells VA10 and BCi, that remain unchanged upon treatment with HO53 (Supplementary Fig. S1A-D). Considering pronounced effect of HO53 on LC3B processing in BCi ALI cells, we continued our studies with ALI cells resembling *in vivo* environment. Based on the processing of LC3B and our previous studies [24], we selected 75 μM HO53 concentration for further studies. By using confocal imaging, fluorescent LC3B puncta are commonly used as an indicator for autophagosomes [33]. The treatment with HO53 appears to increase number of LC3B puncta in ALI cells co-stained with occludin, a tight junction protein serving as a marker for differentiated cells (Fig. 1C). Interestingly, the LC3B puncta were mainly clustered in small groups, therefore making them difficult to quantify but suggesting that autophagy possibly occurs in the specific cell types of ALI differentiated cell layers. Therefore, we next co-stained LC3B with mucin 5AC (MUC5AC), a marker for mucous cells and acetylated (at K40) tubulin α A4 (TUBA4A acetyl K40), a marker for ciliated cells, both occurring in ALI differentiated cell layers (Supplementary Fig. S1E and S1F). We observed only co-localization of LC3B and MUC5AC in specific areas but occurrence of LC3B puncta clusters was not exclusively restricted to mucous cells (Supplementary Fig. S1E). Next, autophagy induction was supported by transmission electron microscopy images of ALI cells treated with HO53 and Bafilomycin A1, showing formation of autophagosomes visible as double membrane vesicles (Fig. 1D). Taken together, our findings show that HO53, an innate immunity modulator, stimulates autophagy induction in mature human lung epithelial cells. In this work, we refer to "autophagy induction/stimulation" as HO53 affects the early phase of autophagy when autophagosomes are formed, without further changes in autophagy flux.

**HO53 treatment alters autophagy related pathways in mature human bronchial epithelial cells (BCi)**

To resolve the mechanism behind induction of autophagy by HO53 in ALI BCi cells, we performed RNA sequencing analysis of the transcriptome at different time points. Based on our previous studies, where we observed HO53 affecting innate immunity and epithelial barrier integrity [24], we selected 4 h, 8 h and 24 h time points of HO53 treatment. Analysis of the transcriptome of ALI BCi cells treated with HO53 revealed a broad response at RNA level that was observed at 4 h post treatment and expanded within time (Fig. 2 and S2A). The gene set

enrichment analyses (GSEA) revealed that several gene sets are affected by HO53 (Supplementary Fig. S2B) and among them are pathways directly related to autophagy [34–41] (Fig. 2). After 4 h of treatment with HO53, we observed molecular signature for the following autophagy related pathways that were positively correlated to the gene set enrichment (upregulated): 1) reactive oxygen species (ROS), 2) xenobiotic metabolism, 3) glycolysis, 4) IL6-JAK-STAT3, 5) peroxisome, 6) fatty acid metabolism. Moreover, the negatively correlated pathways (downregulated) were the following: 7) PI3K-AKT-mTOR, 8) mTORC1 and 9) oxidative phosphorylation (Fig. 2A). With time the molecular signatures were altered, ROS and peroxisome pathways were not enriched in the GSEA categories at 8 and 24 h (Fig. 2B and 2C). Furthermore, pathway linked to fatty acid metabolism was negatively correlated after 8 h (Fig. 2B). We observed only four negatively correlated pathways linked to mTOR/mTORC1 signaling, fatty acid metabolism and oxidative phosphorylation after 24 h (Fig. 2C). Importantly mTOR/mTORC1 signaling and oxidative phosphorylation pathways were negatively enriched for all time points. Overall, a broad effect of HO53 on the gene expression in human lung epithelial BCi cells shows molecular signature for pathways involved in autophagy regulation.

**HO53 enhances autophagy through activation of AMPK pathway**

In our previous studies we demonstrated that HO53 increases phosphorylation of STAT3 in monolayer BCi and the STAT3 pathway has been shown involved in the autophagy process [24]. Therefore, we first analyzed if HO53 has the same effect on post-translational modifications of STAT3 in ALI BCi cells and if these changes contribute to autophagy induction. We excluded the possibility that HO53 affects post-translational modifications of STAT3 related to autophagy induction in differentiated BCi cells (Supplementary Fig. S3A). Recently, it has been shown that galectins can control mTOR and AMPK to induce autophagy upon endolysosomal membrane damage [42,43]. Interestingly, analyses of the RNAseq data revealed enhanced expression of genes encoding galectins, e.g. *LGALS4*, *LGALS9B/C*, *LGALS7* (Fig. 3A) and other genes encoding key proteins involved in the mechanism of autophagy induction described by Jia *et al.* [42] (Fig. 3A). Notably, expression pattern of *LGALS9B/C* encoding galectin 9 observed in RNAseq data was confirmed by qPCR demonstrating significant increase after 8 h (Fig. 3B). However, these changes were not reflected by galectin 9 protein level (Supplementary Fig. S3B). Furthermore, we observed remarkably high expression of *PRKAA2* encoding catalytic subunit α2

of AMPK for all time points of HO53 treatment (Fig. 3A). We confirmed this observation by qPCR, noting 4-, 15- and 33-fold increase in *PRKAA2* gene expression at 4 h, 8 h and 24 h, respectively (Fig. 3C). To test whether these transcriptional changes caused by HO53 contribute to the activation of AMPK and inhibition of mTOR/mTORC1 indicated in the pathway analysis, we examined phosphorylation status of AMPK (Thr172) (Fig. 3D) and the downstream target of mTOR, S6K1 kinase (Thr389) (Fig. 3E). We measured p-AMPK/AMPK and p-S6K1/S6K1 ratio at 2, 4, 6, 8 and 24 hours of treatment with HO53 and found increased phosphorylation level of AMPK at 8 h and decreased but not significant phosphorylation level of S6K1 at 4 h and 6 h (Fig. 3E). These results indicate activation of AMPK and possibly inhibition of mTOR activity, respectively. Together, these results suggest that HO53 induces autophagy through a complex mechanism involving many cellular pathways linked to AMPK and possibly mTOR signaling.

**HO53 treatment leads to TFEB nuclear translocation and augments expression of autophagy-associated genes**

We next monitored TFEB nuclear translocation responsible for transcriptional regulation of autophagy and lysosomal gene expression. Moreover, RNAseq analysis indicated that HO53 affected mTOR pathway, well-known from negative regulation of TFEB translocation [44,45]. We observed increased nuclear localization of TFEB at 24 h of treatment with HO53 (Fig. 4A). Only weak nuclear signal for TFEB was detected at earlier time points 4 and 8 h (Supplementary Fig. S4), suggesting that TFEB nuclear translocation is a late event of HO53 induced signaling cascade leading to autophagy induction. We also assessed whether HO53 treatment of mature BCi cells led to the differential expression of autophagy related genes. By using the list of autophagy related genes (HGNC Group ID 1022; root symbol ATG) [46] from HGNC database (HUGO Gene Nomenclature Committee) [47,48] as a reference, we analyzed their expression in the RNAseq data (Fig. 4B) and confirmed expression of selected genes by qPCR (Fig. 4C-G). Interestingly, HO53 compound enhanced expression of the genes encoding LC3 isoforms, especially *MAP1LC3A* encoding LC3A at 24 h (Fig. 4C) and *MAP1LC3C* encoding LC3C at 8 h and 24 h (Fig. 4D). Next, we analyzed expression of *ATG4B* encoding protease responsible for processing and delipidation/deconjugation of ATG8 family proteins such as LC3 proteins necessary for the elongation of the autophagic membrane and maturation of autophagosomes [49]. We observed increased expression of *ATG4B* over time in RNAseq data (Fig. 4B) and the

similar trend was observed in qPCR, where *ATG4B* expression was downregulated at early time points and then increased after 24 h reaching similar level like in untreated cells (Fig. 4E). Further, HO53 treatment affected expression of *ATG16L* genes in differentiated BCi cells, encoding a component of E3-like complex, that couples ATG8 family proteins to phosphatidylethanolamine and contributes to the elongation of autophagosome [1]. Interestingly, the expression of *ATG16L1* decreased with time but the expression of its homolog *ATG16L2* was increased in analyzed RNAseq data (Fig. 4B). The same expression pattern for *ATG16L1* and *ATG16L2* was reconfirmed by qPCR, where expression of *ATG16L1* was downregulated during the HO53 treatment (Fig. 4F) and *ATG16L2* was upregulated after 24 h (Fig. 4G). These results indicate that HO53 affects nuclear translocation of TFEB and induces expression of selected autophagy related genes associated with formation of autophagosomes at early phase of autophagy. Of note, several autophagy related genes were downregulated (Fig. 4B). To evaluate if expression of lysosomal genes was affected by HO53, we performed gene set enrichment analysis for the set of autophagy-lysosomal genes at 24 h (Fig. 4H) [32]. The enrichment plot for autophagy-lysosomal genes was negatively correlated indicating that other mechanisms partially interacting with the effect of TFEB might be involved. Moreover, the modulated expression of autophagy genes at 4 h and 8 h would not depend on TFEB nuclear translocation, supporting the hypothesis that other mechanisms are involved.

**HO53 modulates epigenetic changes involved in autophagy induction**

Treatment with HO53 induces a broad response in gene expression and affects several autophagy related pathways in differentiated human lung epithelial cells. Therefore, we hypothesized that HO53 modulates epigenetic events such as histone modifications leading to autophagy induction. It has been shown that epigenetic enzymes like histone deacetylases (HDACs), methyltransferases and ubiquitinases can affect regulatory pathways for autophagy [50,51]. We analyzed if HO53 can modulate expression of histone modifying enzymes. Interestingly, *USP44* expression encoding a key enzyme contributing to enhanced autophagy by deubiquitination of lysine residue on histone 2B (H2BK120Ub) [52], was strongly upregulated after 8 h and 24 h of HO53 treatment (Fig. 5A). The enhanced expression of *USP44* was reconfirmed by qPCR (Fig. 5B). Moreover, expression of *EHMT2* encoding euchromatic histone lysine methyltransferase 2 (G9a), responsible for dimethylation of lysine residue on histone 3 (H3K9me2) that results in

inhibition of autophagy [53] was downregulated to a different extent at all analyzed time points of HO53 treatment (Fig. 5A). This was in agreement with expression of *EHMT2* analyzed by qPCR (Fig. 5C) and could promote autophagy by suppressing the inhibitory effect. Another enzyme repressing autophagy by trimethylation of lysine residue on histone3 (H3K27me3) is EZH2 [51]. Based on RNAseq data, the expression of *EZH2* was downregulated at the beginning of HO53 treatment and then enhanced after 24 h (Fig. 5A). This suppression of *EZH2* expression was confirmed at 4 h and 8 h by qPCR and reached similar level like in untreated BCi cells after 24 h (Fig. 5D). The kinetics of transcriptional changes for *EZH2* was reflected in expression of *TSC2* encoding tuberin, a downstream target gene of EZH2 (Fig. 5E). Expression of *TSC2*, a negative regulator of mTOR, is regulated by EZH2 that binds to the *TSC2* promoter and silences *TSC2* transcription leading to activation of mTOR pathway and inhibition of autophagy [51]. Unlike *EZH2*, expression of *TSC2* was gradually decreased with time of HO53 treatment (Fig. 5E). In the continuation, we verified if histones modification status reflects transcriptional changes in expression of key epigenetic enzymes regulating autophagy. Consequently, we analyzed ubiquitination status of H2BK120 and trimethylation of H3K27 over time of HO53 treatment (Fig. 5F and S5). Interestingly, in bronchial epithelial cells we observed reduced level of ubiquitinated H2BK120 at 8 h as a result of HO53 treatment indicating autophagy induction (Fig. 5F). The level of trimethylated H3K27 in BCi cells remained unchanged upon treatment with HO53 at all analyzed time points (Supplementary Fig. S5). In summary, these results indicate that HO53 affects expression of histone modifying enzymes, precisely controlling epigenetic machinery responsible for the balance between induction and inhibition of autophagy.

## Discussion

Autophagy as an integral part of innate immunity is recognized as one of the main host defense systems controlling invading pathogens (xenophagy). In response to the host defense mechanisms, several pathogens have evolved variety of different strategies to escape from autophagy clearance. Therefore, development of novel autophagy activating molecules for the enhancement of the innate immunity defense system against intruding pathogens would be a beneficial therapeutic approach to treat infections.

Here, we present a novel innate immunity inducer, HO53 from the class of aroylated phenylediamine (APD) compounds in relation to autophagy in human airway epithelial cells. Treatment with HO53 of mature bronchial epithelial cells cultured in air-liquid interphase model, resembling the *in vivo* situation, led to increased LC3B-II accumulation together with the presence of LC3B puncta and autophagosomes visualized by TEM images. Based on these, we conclude that HO53 stimulates autophagy by promoting autophagosome formation in mature bronchial epithelial cells. The co-treatment with Bafilomycin A1 and p62 marker indicate no changes in autophagy flux suggesting that additional trigger might be needed to complete autophagy clearance. Another possibility is that cells in this model reached maximum rate of autophagy flux or do not have all components to complete this process and to confirm that, further investigation would be needed. The effect of HO53 on autophagy in our model seems to be similar to the mechanism of AMPK, promoting autophagy by priming autophagy kinases upon detection bacterial outer membrane vesicles independently on bacterial invasion [54]. This mechanism prepares cells for the fast response in case of the bacterial invasion and facilitates rapid autophagy clearance of invading pathogens. Importantly, we showed previously, that HO53 can induce production of innate immunity antimicrobial effectors and enhance epithelial barrier integrity [24]. This, together with induction of autophagy could provide prevention and/or treatment of infectious diseases, especially caused by pathogens affecting initiation of autophagosome formation.

Further, to exploit molecular mechanisms behind observed induction of autophagy we performed RNAseq analysis of mature bronchial epithelial cells treated with HO53 at different time points. The early response to HO53 resulted in enrichment of following pathways directly related to autophagy: 1) reactive oxygen species (ROS), 2) xenobiotic metabolism, 3) glycolysis, 4) IL6-JAK-STAT3, 5) peroxisome, 6) fatty acid metabolism, 7) PI3K-AKT-mTOR, 8) mTORC1 and 9) oxidative phosphorylation. We observed enrichment in IL6-JAK-STAT3 pathway at early time points, however, unlike in monolayer BCi cells, we did not observe any changes in phosphorylation of STAT3 at Y705 in mature BCi cells [24]. By using non-phosphorylated $STAT3^{Y705F}$ mutant and STAT3 inhibitors, it was shown that phosphorylation of STAT3 at Y705 is considered as stimuli for autophagy induction. Phosphorylation of STAT3 at Y705 blocked direct interaction of STAT3 with catalytic domain of EIF2AK2 and consequently allows for phosphorylation EIF2A and activation of autophagy [38,55]. Our results suggest that activation

of STAT3 pathway by HO53 depends on the cell differentiation status and STAT3 pathway is not involved in the autophagy induction in mature bronchial epithelial cells.

Moreover, HO53 treatment of mature BCi cells affected ROS pathway that could contribute to further autophagy induction because ROS are known autophagy mediators in response to oxidative stress or in infection with *Salmonella enterica* serovar Typhimurium [37,56]. In addition to ROS pathway, we also observed enrichment in peroxisome pathway at early time point of the response to HO53 treatment. Recently, Kim et al. have demonstrated an essential role of peroxisome proliferator-activated receptor α (PPAR-α) in innate host defense against Mtb [40]. They have shown that stimulation of PPAR-α led to activation of TFEB and increased lipid catabolism depriving bacteria from the lipid source necessary for creation of intracellular niche for Mtb replication [40]. Therefore, the interesting effect of HO53 on bronchial epithelium connected to enrichment in ROS and peroxisome pathways warrants further research on exploring APD compounds as potential modulators of PPARs. This concept gains further support as HO53 affected fatty acid metabolism pathway that in turn, can regulate PPARs controlling lipid metabolism and inflammation [34]. The role of nuclear receptors like PPARs or xenobiotic nuclear receptor PXR (pregnane X receptor) linked to drug metabolism has been shown to modulate the antimicrobial response against Mtb [36,39]. In our model, HO53 affected xenobiotic metabolism pathway in mature BCi cells which could be linked directly to the HO53 administration but also to the observed promotion of autophagy.

Importantly, we demonstrated that HO53 activated AMPK pathway together with enrichment in positively correlated glycolysis and negatively correlated oxidative phosphorylation (OXPHOS) pathways. Activation of AMPK can stimulate glycolysis in response to the energetic deficit in the cell and directly inhibits mTOR pathway [37]. Interestingly, HO53 treatment led to activation of AMPK, enhancement of glycolysis pathway and inhibition of mTORC1 after 8 h, that can explain the signaling cascade leading to autophagy induction at later time point. Thus, the enzyme catalyzing the first reaction of glycolysis, hexokinase-II can directly bind and inhibit mTORC1 leading to autophagy induction [35]. This might explain inhibition of mTORC1 pathway without enrichment in glycolysis pathway observed after 24 h. Moreover, it has been demonstrated that activation of AMPK, enhanced expression of peroxisome proliferator-activated receptor-gamma, coactivator 1α (PPARGC1A) contribute to the autophagic clearance of Mtb and

induced expression of genes involved in the oxidative phosphorylation [36]. In our model we observed inhibition of oxidative phosphorylation during treatment with HO53, that might indicate on other regulatory mechanisms than AMPK-PPARGC1A pathway.

We observed activation of AMPK signaling cascade and indication of mTOR inhibition by HO53 in airway epithelial cells followed by investigation of TFEB nuclear translocation. Transcription factor EB (TFEB) is a key regulator of host innate immunity response to infections [57]. It has been shown to be responsible for the defense response against *Staphylococcus aureus* infections in mouse and in *Caenorhabditis elegans* by its orthologue HLH-30 [57]. In our model, translocation of TFEB to the nucleus is a rather late event linked to potential mechanism of autophagy induction by HO53 in mature bronchial epithelial cells. Despite of non-significant decrease in phosphorylation of S6K1, transcriptome analysis and the cellular localization of TFEB suggest mTOR inhibition that might contribute to the alterations in expression of autophagy related *ATG* and *MAP1LC3* genes. These genes encode proteins involved in formation of autophagosomes and their enhanced expression corresponds with increased formation of autophagosomes observed by TEM and analysis of LC3B marker. Moreover, several autophagy related genes were downregulated and the enrichment plot for autophagy-lysosomal genes was negatively correlated indicating no further increase of autophagy flux, as it was demonstrated by using co-treatment with Bafilomycin A1 and p62 marker. Since TFEB translocated to the nucleus between 8 and 24 h and we observed changes in the expression of autophagy related genes at earlier time points (4 h and 8 h), we conclude that additional regulatory mechanisms might be involved in induction of autophagy by HO53.

Administration of HO53 led to a broad response and caused pronounced transcriptional changes in BCi cells. Moreover, the structure of HO53 compound is related to the structure of the parental compound Entinostat [58,59], a well-known HDAC inhibitor [60], what led us to the hypothesis that other mechanisms related to the epigenetic regulation of the chromatin state could be involved in the HO53 induced autophagy. It has been shown that several histone modifying epigenetic enzymes, e.g. G9a, EZH2, USP44 or CARM1 are important for modulation of autophagy [51]. Interestingly, in our model the most affected gene expression by HO53 was for G9a - H3K9 methyltransferase, EZH2 - H3K27 methyltransferase and USP44 - H2BK120 deubiquitinase. We suspect that changes in the expression of histone modifying enzymes might

contribute to autophagy induction by decreased H2BK120Ub status as a result of increased *USP44* expression and reduced H3K27me3 status caused by downregulation of *EZH2* expression. However, we observed decrease in ubiquitination of H2BK120 at 8 h followed by increased expression of *USP44* at 24 h of HO53 treatment. Despite of changes in expression of *EZH2*, we did not observe any changes in H3K27me3 status. In our ALI cultured BCi cell model, reported epigenetic changes of histone modification and expression of histone modifying enzymes are rather late events, considering the fact, that regulation of chromatin state is recognized as a dynamic process and we would expect these changes to happen at early time points.

When we look at the overall picture of molecular signaling caused by HO53, we can see that these two regulatory mechanisms are intersecting mainly at 8 h and 24 h time points. Therefore, we suggest mechanism for induction of autophagy by HO53 in mature bronchial epithelial cells as follows, HO53 treatment causes activation of AMPK (at 8 h) concomitant with decreased expression of *EZH2* and decreased ubiquitination of H2BK120, followed by nuclear translocation of TFEB and increased expression of *USP44* at 24 h. Overall, the mechanism of HO53 induced autophagy in mature human airway epithelial cells present a complex picture that drew more attention to the nuclear events that interplay with the defined autophagy related pathways like mTOR or AMPK. It is also important to keep in mind that this could be simplified version of HO53 mechanism and there might be other effectors involved in the signaling cascade leading to autophagy induction what requires further investigation.

In summary, our results present a new effect of a drug candidate HO53, the representative of APD compounds, that could be used as a novel inducer of autophagy in mature bronchial epithelial cells. Together with previously shown properties of enhancing epithelial barrier integrity and production of AMPs, use of HO53 might have implications for prevention and/or treatment of infectious diseases, that can limit use of antibiotics and help reduce selection of antibiotic resistant strains.

**Acknowledgements**

We acknowledge deCODE genetics for the RNA sequencing and Arnar Pálsson for the help with designing the experiment. Sævar Ingþórsson and Jón Pétur Jóelsson for help with confocal microscopy and ImageJ analyses. Thanks to Paulina Cherek and Jóhann Arnfinnsson for sample

preparation and image acquisition by transmission electron microscopy. We acknowledge Prof. Ronald G. Crystal and collaborators for generously providing us with the BCi-NS1.1 cell line. We thank Roger Strömberg and Hakan Ottosson for providing HO53 compound for initial experiments. This work was supported by the Icelandic Center for Research (RANNÍS) and University of Iceland research fund.

**Declaration of interest statement**

G.H.G. and B.A. are founders and stockholders in Akthelia Pharmaceuticals that hold a patent on APD compounds, Patent No. US 9,957,226 B2.

**References**

1. Dikic I, Elazar Z (2018) Mechanism and medical implications of mammalian autophagy. *Nat Rev Mol Cell Biol* **19**: 349–364.
2. Levine B, Kroemer G (2008) Autophagy in the Pathogenesis of Disease. *Cell* **132**: 27–42.
3. Randow F, Münz C (2012) Autophagy in the regulation of pathogen replication and adaptive immunity. *Trends Immunol* **33**: 475–487.
4. Kinsella RL, Nehls EM, Stallings CL (2018) Roles for Autophagy Proteins in Immunity and Host Defense. *Vet Pathol* **55**: 366–373.
5. Saitoh T, Fujita N, Jang MH, Uematsu S, Yang B-G, Satoh T, Omori H, Noda T, Yamamoto N, Komatsu M, et al. (2008) Loss of the autophagy protein Atg16L1 enhances endotoxin-induced IL-1β production. *Nature* **456**: 264–268.
6. Leiva-Juárez MM, Kolls JK, Evans SE (2018) Lung epithelial cells: therapeutically inducible effectors of antimicrobial defense. *Mucosal Immunol* **11**: 21–34.
7. Bansil R, Turner BS (2018) The biology of mucus: Composition, synthesis and organization. *Adv Drug Deliv Rev* **124**: 3–15.
8. Knowles MR, Boucher RC (2002) Mucus clearance as a primary innate defense mechanism for mammalian airways. *J Clin Invest* **109**: 571–577.
9. Nakagawa I, Amano A, Mizushima N, Yamamoto A, Yamaguchi H, Kamimoto T, Nara A, Funao J, Nakata M, Tsuda K, et al. (2004) Autophagy defends cells against invading group A Streptococcus. *Science* **306**: 1037–1040.
10. Gomes LC, Dikic I (2014) Autophagy in antimicrobial immunity. *Mol Cell* **54**: 224–233.
11. Günther J, Seyfert HM (2018) The first line of defence: insights into mechanisms and relevance of phagocytosis in epithelial cells. *Semin Immunopathol* **40**: 555–565.
12. Junkins RD, Shen A, Rosen K, McCormick C, Lin TJ (2013) Autophagy Enhances

Bacterial Clearance during P. aeruginosa Lung Infection. *PLoS One* **8**: e72263.

13. Capasso D, Pepe MV, Rossello J, Lepanto P, Arias P, Salzman V, Kierbel A (2016) Elimination of Pseudomonas aeruginosa through Efferocytosis upon Binding to Apoptotic Cells. *PLOS Pathog* **12**: e1006068.

14. Croft CA, Culibrk L, Moore MM, Tebbutt SJ (2016) Interactions of Aspergillus fumigatus Conidia with Airway Epithelial Cells: A Critical Review. *Front Microbiol* **7**: 472.

15. Vergne I, Chua J, Deretic V (2003) Tuberculosis toxin blocking phagosome maturation inhibits a novel Ca2+/calmodulin-PI3K hVPS34 cascade. *J Exp Med* **198**: 653–659.

16. Kim YS, Silwal P, Kim SY, Yoshimori T, Jo EK (2019) Autophagy-activating strategies to promote innate defense against mycobacteria. *Exp Mol Med* **51**: 151.

17. Rubinsztein DC, Codogno P, Levine B (2012) Autophagy modulation as a potential therapeutic target for diverse diseases. *Nat Rev Drug Discov* **11**: 709–730.

18. Mily A, Rekha RS, Kamal SMM, Arifuzzaman ASM, Rahim Z, Khan L, Haq MA, Zaman K, Bergman P, Brighenti S, et al. (2015) Significant Effects of Oral Phenylbutyrate and Vitamin D3 Adjunctive Therapy in Pulmonary Tuberculosis: A Randomized Controlled Trial. *PLoS One* **10**: e0138340.

19. Bekele A, Gebreselassie N, Ashenafi S, Kassa E, Aseffa G, Amogne W, Getachew M, Aseffa A, Worku A, Raqib R, et al. (2018) Daily adjunctive therapy with vitamin D 3 and phenylbutyrate supports clinical recovery from pulmonary tuberculosis: a randomized controlled trial in Ethiopia. *J Intern Med* **284**: 292–306.

20. Rekha RS, Rao Muvva SSVJ, Wan M, Raqib R, Bergman P, Brighenti S, Gudmundsson GH, Agerberth B (2015) Phenylbutyrate induces LL-37-dependent autophagy and intracellular killing of Mycobacterium tuberculosis in human macrophages. *Autophagy* **11**: 1688–1699.

21. Schulthess J, Pandey S, Capitani M, Rue-Albrecht KC, Arnold I, Franchini F, Chomka A, Ilott NE, Johnston DGW, Pires E, et al. (2019) The Short Chain Fatty Acid Butyrate Imprints an Antimicrobial Program in Macrophages. *Immunity* **50**: 432-445.e7.

22. Kim SY, Yang C-S, Lee H-M, Kim JK, Kim Y-S, Kim Y-R, Kim J-S, Kim TS, Yuk J-M, Dufour CR, et al. (2018) ESRRA (estrogen-related receptor α) is a key coordinator of transcriptional and post-translational activation of autophagy to promote innate host defense. *Autophagy* **14**: 152–168.

23. Park K, Elias PM, Hupe M, Borkowski AW, Gallo RL, Shin KO, Lee YM, Holleran WM, Uchida Y (2013) Resveratrol stimulates sphingosine-1-phosphate signaling of cathelicidin production. *J Invest Dermatol* **133**: 1942–1949.

24. Myszor IT, Parveen Z, Ottosson H, Bergman P, Agerberth B, Strömberg R, Gudmundsson GH (2019) Novel aroylated phenylenediamine compounds enhance antimicrobial defense and maintain airway epithelial barrier integrity. *Sci Rep* **9**: 7114.

25. Halldorsson S, Asgrimsson V, Axelsson I, Gudmundsson GH, Steinarsdottir M, Baldursson O, Gudjonsson T (2007) Differentiation potential of a basal epithelial cell line

established from human bronchial explant. *Vitr Cell Dev Biol - Anim* **43**: 283–289.

26. Walters MS, Gomi K, Ashbridge B, Moore M a S, Arbelaez V, Heldrich J, Ding B-S, Rafii S, Staudt MR, Crystal RG (2013) Generation of a human airway epithelium derived basal cell line with multipotent differentiation capacity. *Respir Res* **14**: 135.

27. Livak KJ, Schmittgen TD (2001) Analysis of Relative Gene Expression Data Using Real-Time Quantitative PCR and the 2−ΔΔCT Method. *Methods* **25**: 402–408.

28. Bray NL, Pimentel H, Melsted P, Pachter L (2016) Near-optimal probabilistic RNA-seq quantification. *Nat Biotechnol* **34**: 525–527.

29. Yates A, Akanni W, Amode MR, Barrell D, Billis K, Carvalho-Silva D, Cummins C, Clapham P, Fitzgerald S, Gil L, et al. (2016) Ensembl 2016. *Nucleic Acids Res* **44**: D710–D716.

30. Pimentel H, Bray NL, Puente S, Melsted P, Pachter L (2017) Differential analysis of RNA-seq incorporating quantification uncertainty. *Nat Methods* **14**: 687–690.

31. Subramanian A, Tamayo P, Mootha VK, Mukherjee S, Ebert BL, Gillette MA, Paulovich A, Pomeroy SL, Golub TR, Lander ES, et al. (2005) Gene set enrichment analysis: a knowledge-based approach for interpreting genome-wide expression profiles. *Proc Natl Acad Sci U S A* **102**: 15545–15550.

32. Möller K, Sigurbjornsdottir S, Arnthorsson AO, Pogenberg V, Dilshat R, Fock V, Brynjolfsdottir SH, Bindesboll C, Bessadottir M, Ogmundsdottir HM, et al. (2019) MITF has a central role in regulating starvation-induced autophagy in melanoma. *Sci Rep* **9**: 1–12.

33. Yoshii SR, Mizushima N (2017) Monitoring and measuring autophagy. *Int J Mol Sci* **18**: 1865.

34. Varga T, Czimmerer Z, Nagy L (2011) PPARs are a unique set of fatty acid regulated transcription factors controlling both lipid metabolism and inflammation. *Biochim Biophys Acta - Mol Basis Dis* **1812**: 1007–1022.

35. Roberts DJ, Tan-Sah VP, Ding EY, Smith JM, Miyamoto S (2014) Hexokinase-II Positively Regulates Glucose Starvation-Induced Autophagy through TORC1 Inhibition. *Mol Cell* **53**: 521–533.

36. Yang CS, Kim JJ, Lee HM, Jin HS, Lee SH, Park JH, Kim SJ, Kim JM, Han YM, Lee MS, et al. (2014) The AMPK-PPARGC1A pathway is required for antimicrobial host defense through activation of autophagy. *Autophagy* **10**: 785–802.

37. Filomeni G, De Zio D, Cecconi F (2015) Oxidative stress and autophagy: The clash between damage and metabolic needs. *Cell Death Differ* **22**: 377–388.

38. You L, Wang Z, Li H, Shou J, Jing Z, Xie J, Sui X, Pan H, Han W (2015) The role of STAT3 in autophagy. *Autophagy* **11**: 729–739.

39. Bhagyaraj E, Nanduri R, Saini A, Dkhar HK, Ahuja N, Chandra V, Mahajan S, Kalra R, Tiwari D, Sharma C, et al. (2016) Human Xenobiotic Nuclear Receptor PXR Augments Mycobacterium tuberculosis Survival . *J Immunol* **197**: 244–255.

40. Kim YS, Lee H-M, Kim JK, Yang C-S, Kim TS, Jung M, Jin HS, Kim S, Jang J, Oh GT, et al. (2017) PPAR-α Activation Mediates Innate Host Defense through Induction of TFEB and Lipid Catabolism. *J Immunol* **198**: 3283–3295.

41. Sabatini DM (2017) Twenty-five years of mTOR: Uncovering the link from nutrients to growth. *Proc Natl Acad Sci U S A* **114**: 11818–11825.

42. Jia J, Abudu YP, Claude-Taupin A, Gu Y, Kumar S, Choi SW, Peters R, Mudd MH, Allers L, Salemi M, et al. (2018) Galectins Control mTOR in Response to Endomembrane Damage. *Mol Cell* **70**: 120-135.e8.

43. Jia J, Abudu YP, Claude-Taupin A, Gu Y, Kumar S, Choi SW, Peters R, Mudd MH, Allers L, Salemi M, et al. (2019) Galectins control MTOR and AMPK in response to lysosomal damage to induce autophagy. *Autophagy* **15**: 169–171.

44. Roczniak-Ferguson A, Petit CS, Froehlich F, Qian S, Ky J, Angarola B, Walther TC, Ferguson SM (2012) The transcription factor TFEB links mTORC1 signaling to transcriptional control of lysosome homeostasis. *Sci Signal* **5**: ra42.

45. Irazoqui JE (2020) Key Roles of MiT Transcription Factors in Innate Immunity and Inflammation. *Trends Immunol* **41**: 157–171.

46. Klionsky DJ, Cregg JM, Dunn WA, Emr SD (2003) A unified nomenclature for yeast autophagy-related genes. *Dev Cell* **5**: 539–545.

47. Yates B, Braschi B, Gray KA, Seal RL, Tweedie S, Bruford EA (2017) Genenames.org: The HGNC and VGNC resources in 2017. *Nucleic Acids Res* **45**: D619–D625.

48. HUGO Gene Nomenclature Committee (HGNC), European Molecular Biology Laboratory, European Bioinformatics Institute (EMBL-EBI), Wellcome Genome Campus, Hinxton, Cambridge CB10 1SD, United Kingdom. Data retrieved in October 2019.

49. Maruyama T, Noda NN (2018) Autophagy-regulating protease Atg4: Structure, function, regulation and inhibition. *J Antibiot (Tokyo)* **71**: 72–78.

50. Gammoh N, Marks PA, Jiang X (2012) Curbing autophagy and histone deacetylases to kill cancer cells. *Autophagy* **8**: 1521–1522.

51. Baek SH, Kim K Il (2017) Epigenetic Control of Autophagy: Nuclear Events Gain More Attention. *Mol Cell* **65**: 781–785.

52. Chen S, Jing Y, Kang X, Yang L, Wang DL, Zhang W, Zhang L, Chen P, Chang JF, Yang XM, et al. (2017) Histone H2B monoubiquitination is a critical epigenetic switch for the regulation of autophagy. *Nucleic Acids Res* **45**: 1144–1158.

53. Artal-Martinez de Narvajas A, Gomez TS, Zhang J-S, Mann AO, Taoda Y, Gorman JA, Herreros-Villanueva M, Gress TM, Ellenrieder V, Bujanda L, et al. (2013) Epigenetic Regulation of Autophagy by the Methyltransferase G9a. *Mol Cell Biol* **33**: 3983–3993.

54. Losier TT, Akuma M, McKee-Muir OC, LeBlond ND, Suk Y, Alsaadi RM, Guo Z, Reshke R, Sad S, Campbell-Valois FX, et al. (2019) AMPK Promotes Xenophagy through Priming of Autophagic Kinases upon Detection of Bacterial Outer Membrane Vesicles. *Cell Rep* **26**: 2150-2165.e5.

55. Shen S, Niso-Santano M, Adjemian S, Takehara T, Malik SA, Minoux H, Souquere S, Mariño G, Lachkar S, Senovilla L, et al. (2012) Cytoplasmic STAT3 Represses Autophagy by Inhibiting PKR Activity. *Mol Cell* **48**: 667–680.

56. Huang J, Canadien V, Lam GY, Steinberg BE, Dinauer MC, Magalhaes MAO, Glogauer M, Grinstein S, Brumell JH (2009) Activation of antibacterial autophagy by NADPH oxidases. *Proc Natl Acad Sci U S A* **106**: 6226–6231.

57. Visvikis O, Ihuegbu N, Labed SA, Luhachack LG, Alves AMF, Wollenberg AC, Stuart LM, Stormo GD, Irazoqui JE (2014) Innate host defense requires TFEB-mediated transcription of cytoprotective and antimicrobial genes. *Immunity* **40**: 896–909.

58. Ottosson H, Nylén F, Sarker P, Miraglia E, Bergman P, Gudmundsson GH, Raqib R, Agerberth B, Strömberg R (2016) Potent Inducers of Endogenous Antimicrobial Peptides for Host Directed Therapy of Infections. *Sci Rep* **6**: 1–11.

59. Miraglia E, Nylén F, Johansson K, Arnér E, Cebula M, Farmand S, Ottosson H, Strömberg R, Gudmundsson GH, Agerberth B, et al. (2016) Entinostat up-regulates the CAMP gene encoding LL-37 via activation of STAT3 and HIF-1α transcription factors. *Sci Rep* **6**: 1–12.

60. Knipstein J, Gore L (2011) Entinostat for treatment of solid tumors and hematologic malignancies. *Expert Opin Investig Drugs* **20**: 1455–1467.

**Figure 1**

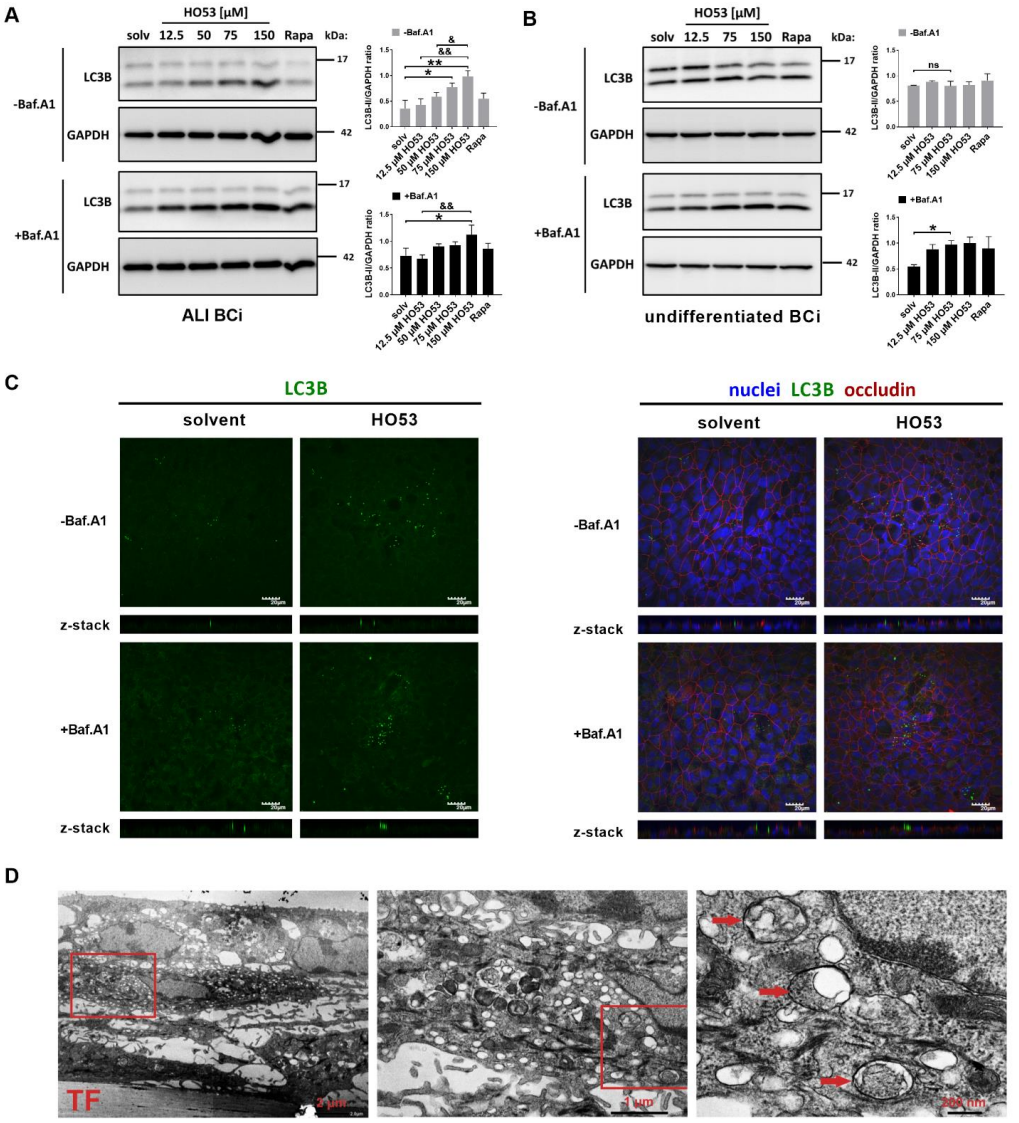


**Fig. 1. HO53 treatment induces autophagy in human airway epithelial cells.** BCi cells were stimulated for 24 h with different doses of HO53, 250 nM rapamycin (Rapa) used as a positive control for autophagy induction and DMSO (final concentration of 0.3%) used as a solvent control (solv), all in combination with (+Baf.A1) or without (-Baf.A1) Bafilomycin A1 (100 nM).

Treatment of differentiated BCi cells was performed by addition of the compound to the lower chamber of the trans-well insert. Induction of autophagy in **A)** air-liquid interphase (ALI) cultured and **B)** undifferentiated BCi was evaluated by analysis of LC3B processing on Western blotting. The processing of LC3B-I to LC3B-II was quantified by measurement of the LC3B-II band intensity vs GAPDH loading control and presented as LC3B-II/GAPDH ratio. Data present average values ± SEM from n=3 independent experiments analyzed by one-way ANOVA with Sidak post-hoc test, where * $p<0.05$, ** $p<0.01$ and ns – non significant versus solvent control, & $p<0.05$ versus 50 µM HO53, && $p<0.01$ versus 12.5 µM HO53. **C)** Analysis of the autophagy induction by HO53 (75 µM) in ALI cultured BCi cells by immunostaining of LC3B puncta (green), nuclei (blue) and occludin (red), a tight junction protein characteristic for the differentiated in ALI culture BCi cells. The scale bar is 20 µm. **D)** Transmission electron microscopy (TEM) analysis of autophagosome formation (red arrows) in differentiated BCi cells treated with HO53 (75 µM) and Bafilomycin A1 (100 nm) for 24 h; TF-trans-well filter/insert; red squares indicate magnified area with scale bars for images as indicated (from left to right) 2 µm, 1 µm and 200 nm. Representative images of n=4 trans-well inserts from 2 independent experiments.

**Figure 2**

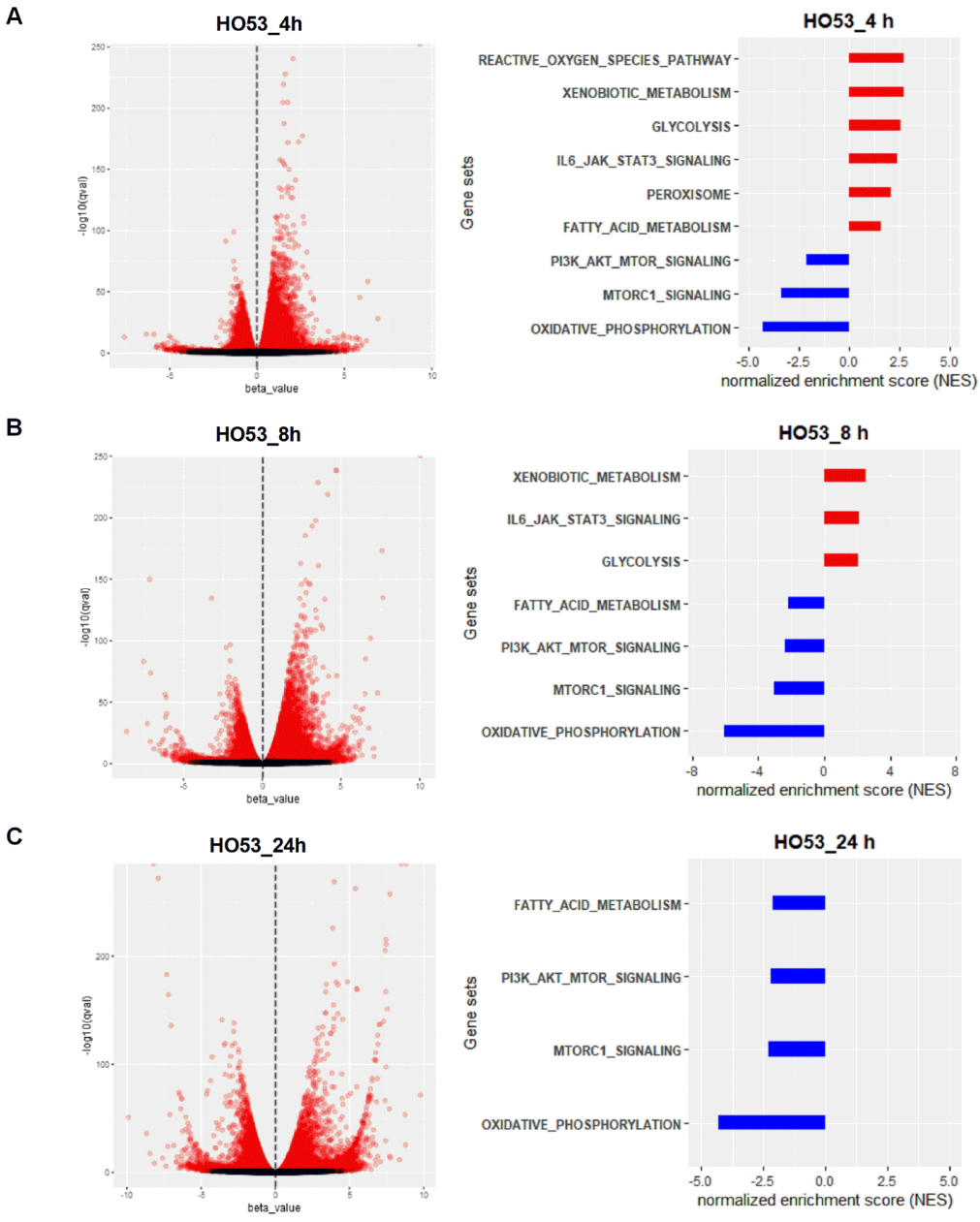
A
HO53_4h
-log10(qval)
beta_value
HO53_4 h
REACTIVE_OXYGEN_SPECIES_PATHWAY
XENOBIOTIC_METABOLISM
GLYCOLYSIS
IL6_JAK_STAT3_SIGNALING
PEROXISOME
FATTY_ACID_METABOLISM
PI3K_AKT_MTOR_SIGNALING
MTORC1_SIGNALING
OXIDATIVE_PHOSPHORYLATION
Gene sets
normalized enrichment score (NES)
B
HO53_8h
-log10(qval)
beta_value
HO53_8 h
XENOBIOTIC_METABOLISM
IL6_JAK_STAT3_SIGNALING
GLYCOLYSIS
FATTY_ACID_METABOLISM
PI3K_AKT_MTOR_SIGNALING
MTORC1_SIGNALING
OXIDATIVE_PHOSPHORYLATION
Gene sets
normalized enrichment score (NES)
C
HO53_24h
-log10(qval)
beta_value
HO53_24 h
FATTY_ACID_METABOLISM
PI3K_AKT_MTOR_SIGNALING
MTORC1_SIGNALING
OXIDATIVE_PHOSPHORYLATION
Gene sets
normalized enrichment score (NES)

**Fig. 2. HO53 affects autophagy related pathways in mature human bronchial epithelial cells (BCi).** Volcano plots with differentially expressed transcripts and gene set enrichments analysis (GSEA) of the expression data from BCi cells differentiated in air-liquid interphase culture after **A)** 4 h, **B)** 8 h and **C)** 24 h of treatment with HO53 (75 μM). Volcano plots represent b-estimate (expression) versus log of significance [–log10(q)] from Kallisto/sleuth Wald test. Significant differentially expressed genes were marked in red based on $q \leq 0.05$. In pathway analysis (GSEA), autophagy related gene sets were presented as positively correlated gene sets (red, NES > 0) and negatively correlated gene sets (blue, NES < 0) with FDR ≤ 0.05. NES – normalized enrichment score; FDR/ q-value – false discovery rate; NOM p – nominal p value.

**Figure 3**

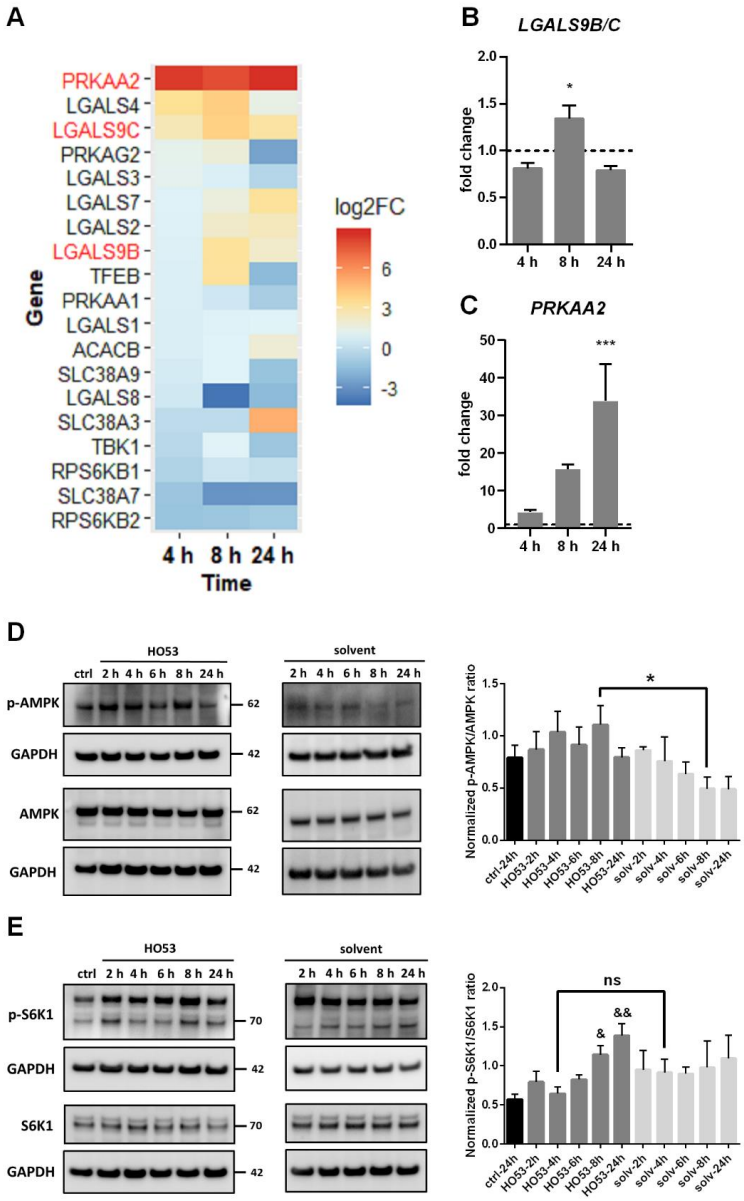


**Fig. 3. HO53 activates AMPK signaling cascade in differentiated BCi cells.** Differentiated in air-liquid interphase culture BCi cells were treated with HO53 (75 µM) for 4 h, 8 h and 24 h. **A)**

A heatmap showing changes in expression as $log_2$ fold change (log2FC) of genes related to mTOR/AMPK pathway at 4 h, 8 h and 24 h of treatment with HO53. The heatmap shows significantly differentially expressed genes in comparison to untreated cells collected at the same time points ($p<0.05$). Genes selected for further analysis were marked in red. Non-significant differentially expressed genes have arbitrary value 0. Expression level of **B)** *LGALS9B/C* and **C)** *PRKAA2* genes analyzed by qRT-PCR. Gene expression was represented as a fold change in comparison to the control cells (value 1, dashed line) collected at the same time point as treated cells and normalized to *EEF2* reference gene. n=3 trans-well inserts from 3 independent experiments ± SEM. * $p<0.05$, *** $p<0.001$ versus control cells analyzed by one-way ANOVA with Dunnett post-hoc test. **D) and E)** Activation of mTOR and AMPK signaling pathways analyzed by Western blotting of AMPKα (Thr172) and phosphorylated S6K1 (Thr389) at different time points of HO53 treatment. Quantification of Western blots was performed in two steps: first, by measurements of bands intensity and normalization to GAPDH (loading control) and then, by calculation of normalized ratio for phospho-S6K1 (Thr389) to total S6K1 and phospho-AMPKα (Thr172) to total AMPKα. The representative Western blot of n=4 independent experiments. Statistical analysis was performed by one-way ANOVA with Sidak post-hoc test when two indicated groups were compared * $p<0.05$, ns-non significant and with Dunnett post-hoc test when all treatment groups were compared to control untreated cells (ctrl-24h) where & $p<0.05$ and && $p<0.01$.

## Figure 4

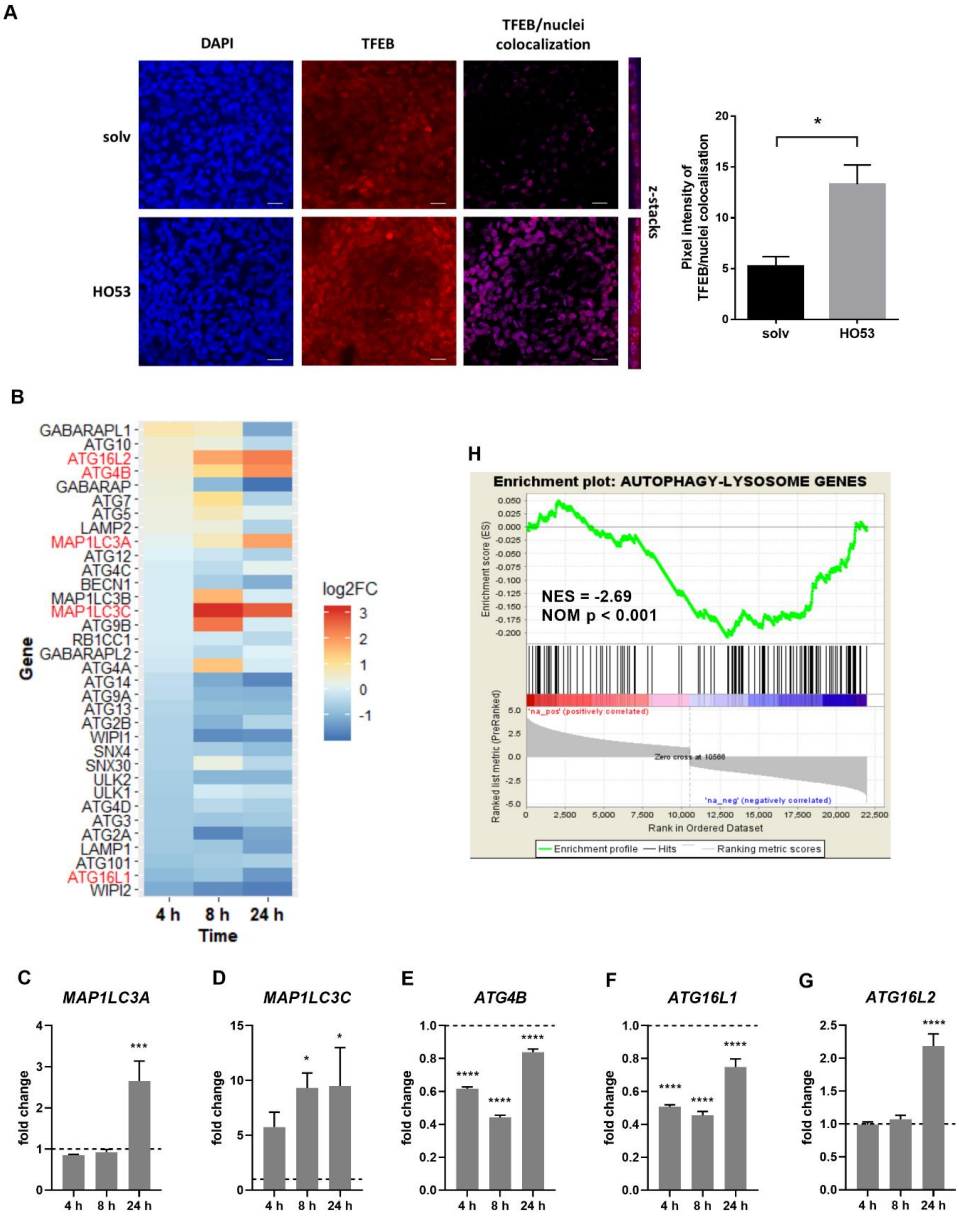
A
DAPI
TFEB
TFEB/nuclei colocalization
solv
HO53
z-stacks
Pixel intensity of TFEB/nuclei colocalisation
solv
HO53
B
Gene
log2FC
Time
4 h
8 h
24 h
H
Enrichment plot: AUTOPHAGY-LYSOSOME GENES
NES = -2.69
NOM p < 0.001
Enrichment score (ES)
Ranked list metric (PreRanked)
Rank in Ordered Dataset
Enrichment profile
Hits
Ranking metric scores
C
MAP1LC3A
D
MAP1LC3C
E
ATG4B
F
ATG16L1
G
ATG16L2
fold change

**Fig. 4. HO53 treatment leads to nuclear translocation of TFEB and augments expression of autophagy related genes in differentiated BCi cells. A)** Analysis of TFEB nuclear translocation upon treatment with 75 µM HO53 after 24 h by confocal imaging of nuclei (blue, DAPI), TFEB (red) and extracted signal from co-localized TFEB/nuclei (pink) from merged channels with scale bar 20 µm. The representative images from at least 3 different areas of ALI filter from n=3 independent experiments ± SEM with quantification of pixel intensity for signal from co-localized TFEB/nuclei (pink) extracted from merged DAPI/TFEB images. Statistical analysis was performed by using unpaired t-test with Welch´s correction, * $p<0.05$. Changes in autophagy related genes expression in differentiated (ALI) BCi cells at 4 h, 8 h and 24 h of treatment with HO53. **B)** A heatmap showing expression level represented as a $\log_2$ fold change (log2FC) of significantly differentially expressed genes in comparison to untreated cells collected at the same time points ($p<0.05$). Genes selected for further analysis were marked in red. Non-significant differentially expressed genes have arbitrary value 0. Expression level of selected autophagy related genes: **C)** *MAP1LC3A*, **D)** *MAP1LC3C*, **E)** *ATG4B*, **F)** *ATG16L1* and **G)** *ATG16L2* analyzed by qRT-PCR. Gene expression was represented as a fold change in comparison to the control cells (value 1, dashed line) collected at the same time point as treated cells and normalized to *EEF2* reference gene. n=3 trans-well inserts from 3 independent experiments ± SEM. * $p<0.05$, *** $p<0.001$, **** $p<0.0001$ versus control cells analyzed by one-way ANOVA with Dunnett post-hoc test. **H)** Enrichment plot for autophagy-lysosomal genes obtained from gene set enrichments analysis (GSEA) of the expression data from differentiated in air-liquid interphase culture BCi cells after 24 h of treatment with HO53. Normalized enrichment score (NES) and nominal p value (NOM) are indicated on the plot.

**Figure 5**

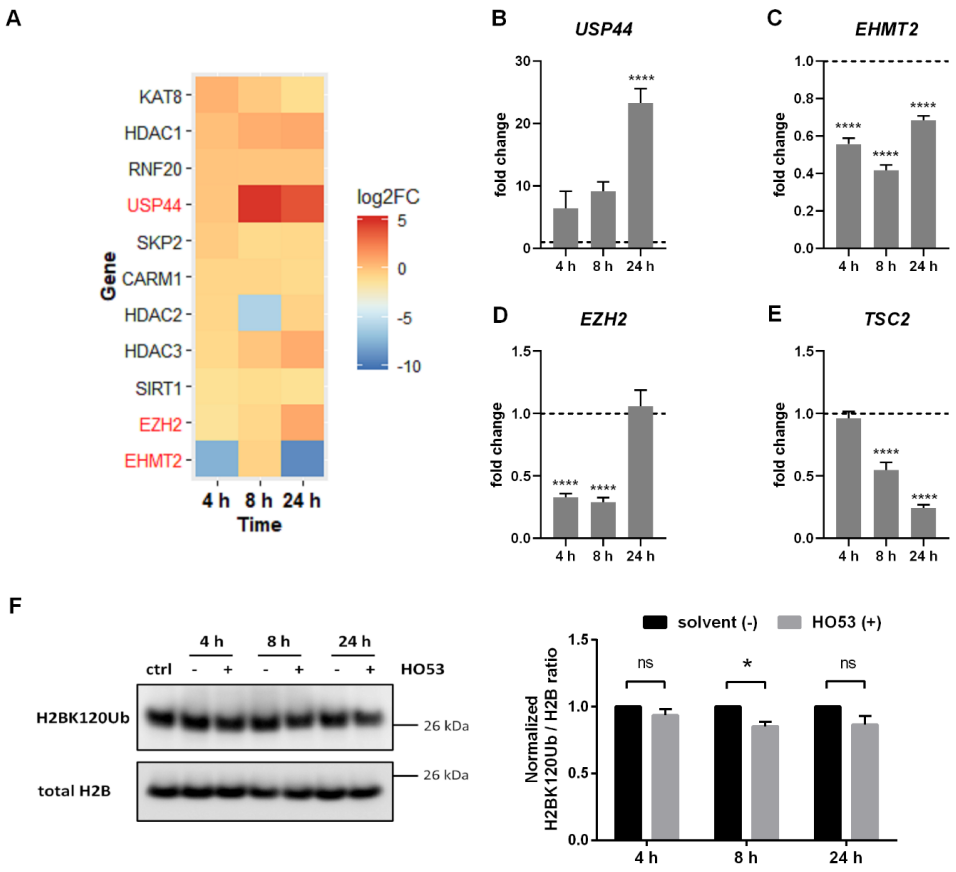


**Fig. 5. HO53 treatment modulates epigenetic regulation of autophagy in air-liquid interphase cultured BCi cells.** Air-liquid interphase culture BCi cells were treated with HO53 (75 µM) for 4 h, 8 h and 24 h. **A)** A heatmap showing changes in expression of genes encoding epigenetic enzymes involved in regulation of autophagy presented as $\log_2$ fold change (log2FC) at 4 h, 8 h and 24 h of treatment with HO53. The heatmap shows significantly differentially expressed genes in comparison to untreated cells collected at the same time points ($p$<0.05). Genes selected for further analysis were marked in red. Non-significant differentially expressed genes have arbitrary value 0. Expression level analyzed by qRT-PCR for the genes **B)** *USP44*, **C)** *EHMT2*, **D)** *EZH2* and **E)** *TSC2*, a downstream target of the EZH2 protein. Gene expression was represented as a fold

change in comparison to the control cells (value 1, dashed line) collected at the same time points as treated cells and normalized to *EEF2* reference gene. n=3 trans-well inserts from 3 independent experiments ± SEM. **** $p<0.0001$ versus control cells analyzed by one-way ANOVA with Dunnett post-hoc test. **F**) The representative Western blot of H2BK120 ubiquitination and total H2B level (loading control) analyzed by Western blotting in untreated (ctrl) and treated with solvent (-) and 75 µM HO53 (+) ALI BCi cells at indicated time points. DMSO at final concentration of 0.3% was used as a solvent control. The Western blot band intensity was quantified as ratio of H2BK120Ub to total H2B and normalized to solvent control (value 1) based on n=3 independent experiments ± SEM. Statistical analysis was performed by two-way ANOVA with Bonferroni´s multiple comparisons test, * $p<0.05$.

**Supplementary information to the manuscript**

# Novel inducer of innate immunity HO53 stimulates autophagy in human airway epithelial cells

Iwona T. Myszor[1], Snaevar Sigurdsson[1], Alexia Ros Viktorsdottir[1], Birgitta Agerberth[2], Eeva-Liisa Eskelinen[3,4], Margret Helga Ogmundsdottir[5], Gudmundur H. Gudmundsson[1,2]

**Abbreviations:**

APDs - aroylated phenylenediamines

ALI – air-liquid interphase

mTOR – mechanistic target of rapamycin kinase

AMPK – AMP-activated protein kinase

RNAseq – RNA sequencing

AMPs – antimicrobial peptides

Mtb – *Mycobacterium tuberculosis*

GSEA – Gene Set Enrichment Analysis

LC3B – microtubule-associated proteins 1A/1B light chain 3B

p62 – Sequestosome 1 (also SQSTM1)

TEM – transmission electron microscopy

ROS – reactive oxygen species

IL-6 – interleukin 6

JAK – Janus kinase

STAT3 – Signal transducer and activator of transcription 3

PI3K – phosphoinositide 3-kinase

AKT – protein kinase B (PKB)

mTORC1 – mechanistic target of rapamycin kinase complex 1

*LGALS* genes – genes encode galectins

*PRKAA2* – gene encodes protein kinase AMP-activated catalytic subunit alpha 2

S6K1 – ribosomal protein S6 kinase B1

TFEB – transcription factor EB

HGNC Database – HUGO Gene Nomenclature Committee

*MAP1LC3A* – gene encodes microtubule-associated proteins 1A/1B light chain 3A

*MAP1LC3C* – gene encodes microtubule-associated proteins 1A/1B light chain 3C

*ATG* genes – genes encode autophagy related proteins

HDACs – histone deacetylases

USP44 – ubiquitin specific peptidase 44

EZH2 – enhancer of zeste homolog 2

*EHMT2* – gene encodes euchromatic histone lysine methyltransferase 2

G9a – euchromatic histone lysine methyltransferase 2

TSC2 – tuberin

H3 – histone 3

H2B – histone 2B

H3K9me2 – dimethylation of histone 3 at lysine 9 residue

H3K27me3 – trimethylation of histone 3 at lysine 27 residue

H2BK120Ub – ubiquitination of histone 2B at lysine 120 residue

PPARs – peroxisome proliferator-activated receptors

**Supplementary Figure S1**

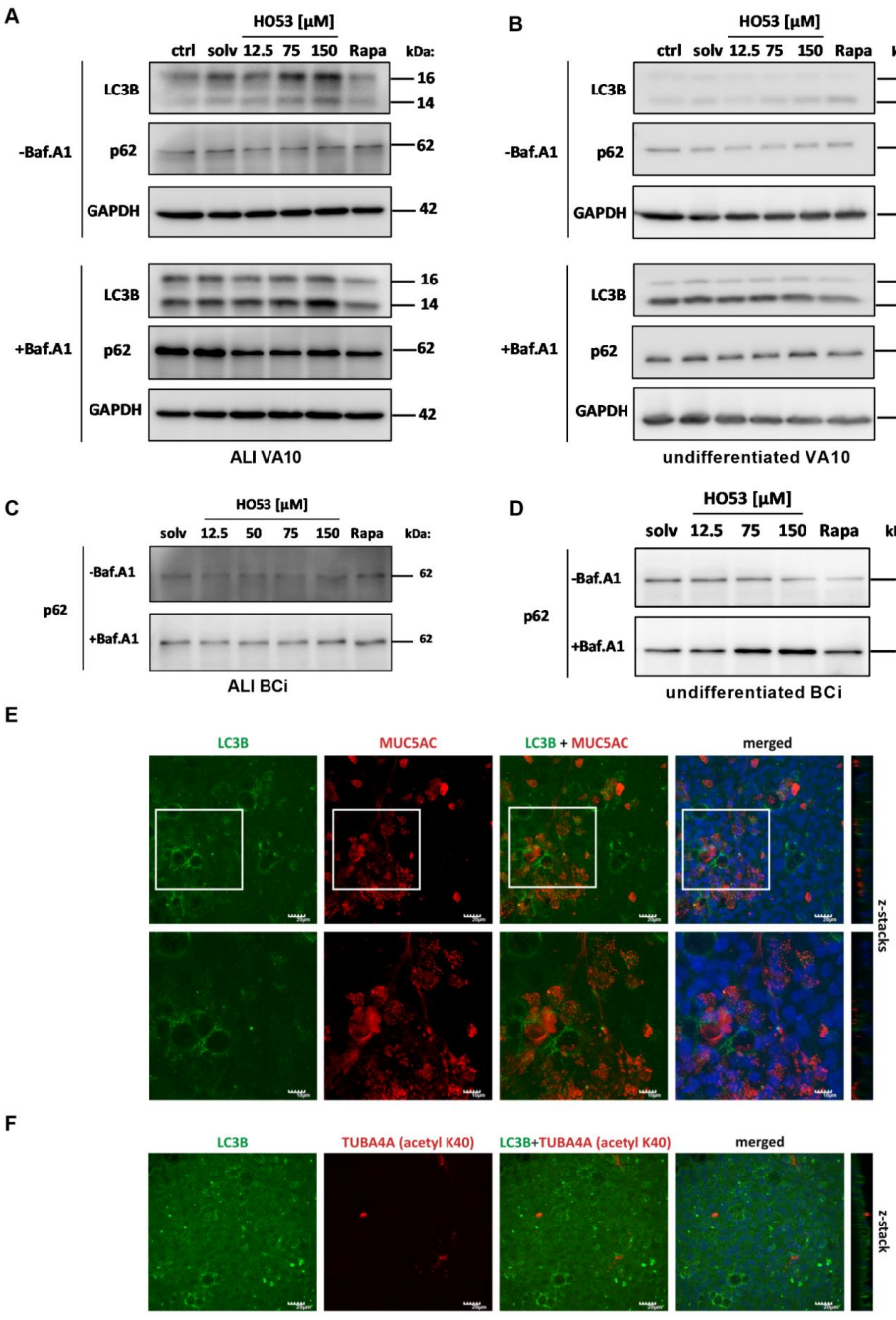

**Fig. S1. Effect of HO53 treatment on induction of autophagy in VA10 cells and different cell populations of differentiated BCi cells.** BCi and VA10 cells were stimulated for 24 h with different doses of HO53, 250 nM rapamycin (Rapa) used as a positive control and DMSO (final concentration of 0.3%) used as a solvent control (solv) in combination with (+Baf.A1) or without (-Baf.A1) Bafilomycin A1 (100 nM). Treatment of differentiated VA10 and BCi cells was performed by addition of the compound to the lower chamber of the trans-well insert. The level of both autophagy markers LC3B and p62 in **A)** air-liquid interphase cultured VA10 and **B)** undifferentiated VA10, and p62 marker in **C)** air-liquid interphase cultured BCi and **D)** undifferentiated BCi was evaluated by Western blotting. Representative pictures of n=3 independent experiments where GAPDH was used as a loading control. Co-localization of LC3B puncta clusters (green) with **E)** mucous cells stained with antibodies against mucin 5AC (MUC5AC, mucous cells marker; red) and **F)** ciliated cells stained with antibodies against acetylated (K40) α-tubulin (TUBA4A, ciliated cells marker; red) in differentiated bronchial epithelial BCi cell layer treated with HO53 (75 µM) and Bafilomycin A1 (100 nM) for 24 h. Representative pictures of one experiment with scale bar 20 µm and 10 µm for magnified area in white frame.

**Supplementary Figure S2**

**A**

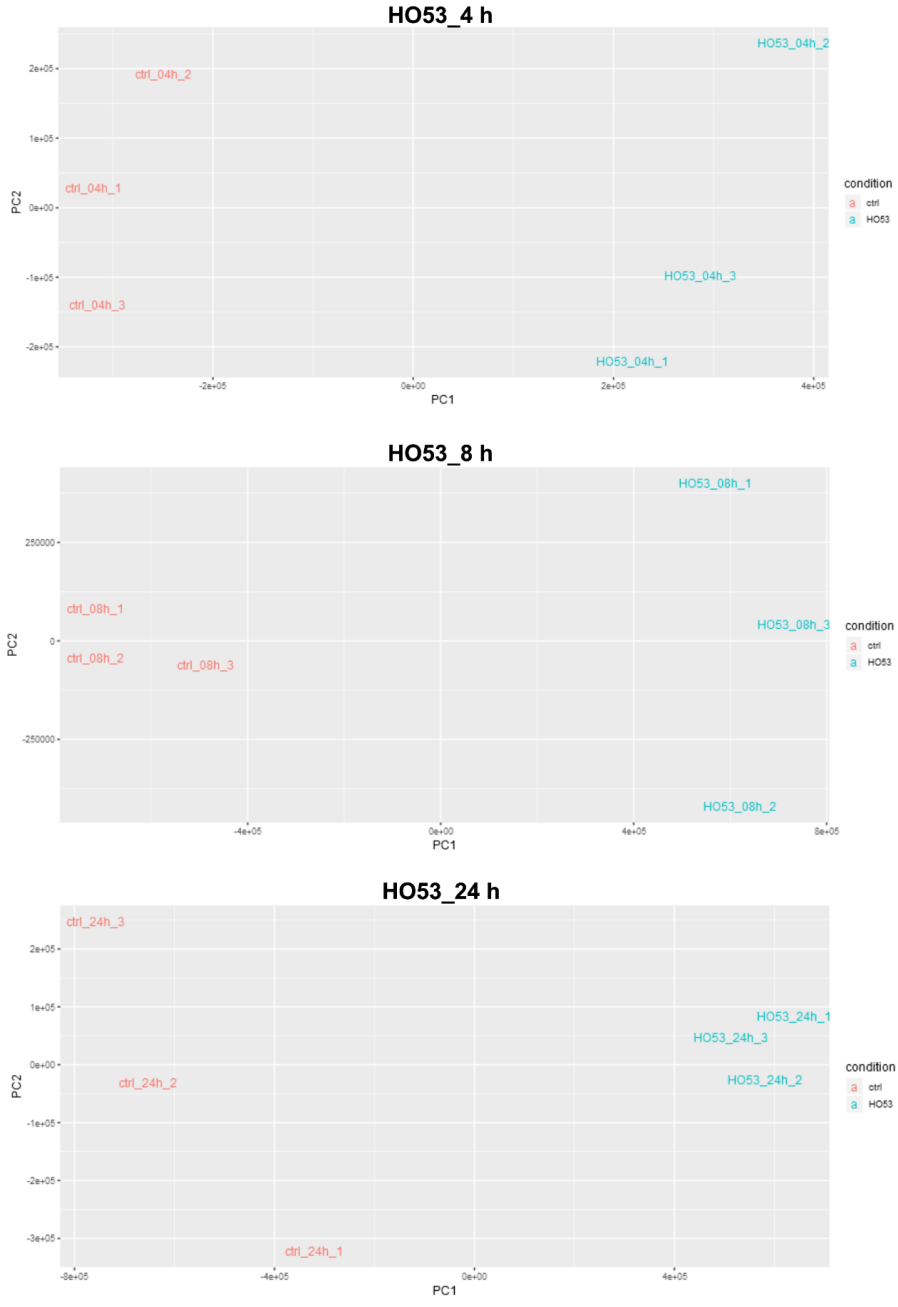

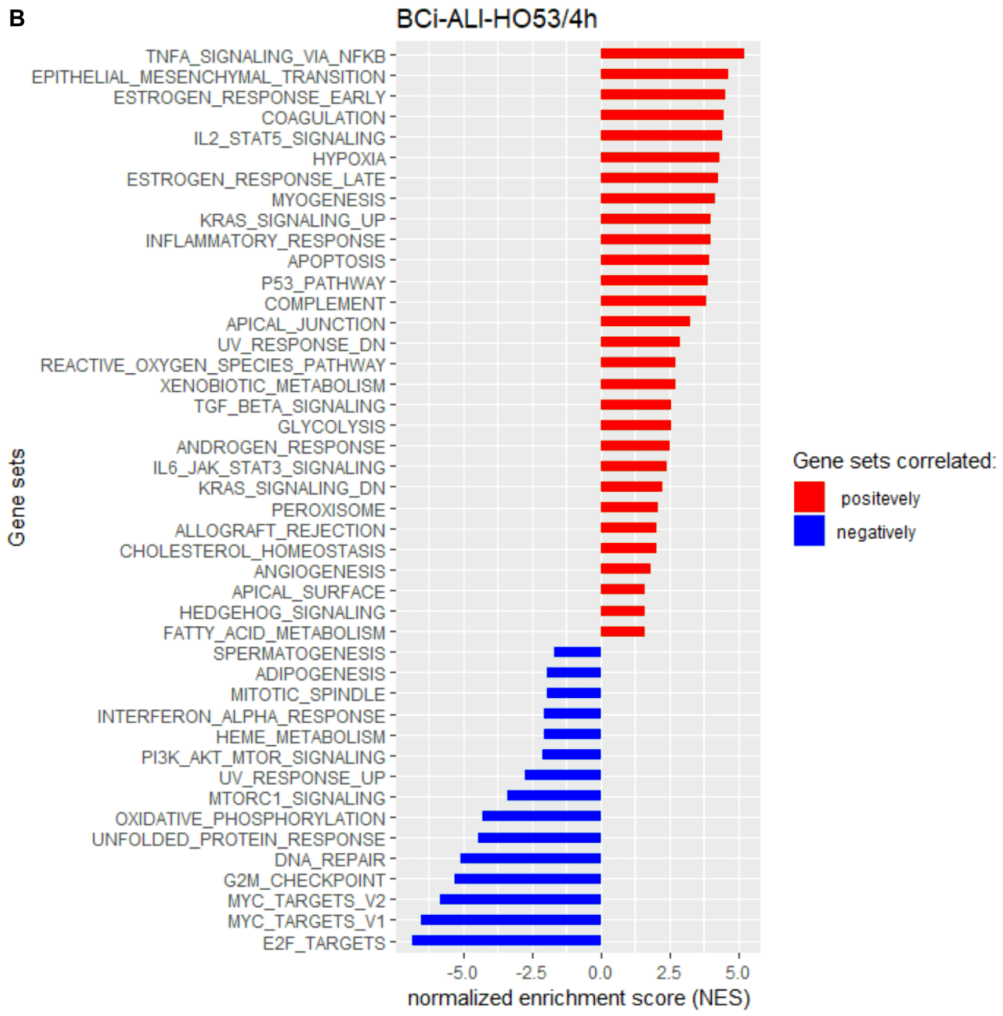
B
BCi-ALI-HO53/4h
TNFA_SIGNALING_VIA_NFKB
EPITHELIAL_MESENCHYMAL_TRANSITION
ESTROGEN_RESPONSE_EARLY
COAGULATION
IL2_STAT5_SIGNALING
HYPOXIA
ESTROGEN_RESPONSE_LATE
MYOGENESIS
KRAS_SIGNALING_UP
INFLAMMATORY_RESPONSE
APOPTOSIS
P53_PATHWAY
COMPLEMENT
APICAL_JUNCTION
UV_RESPONSE_DN
REACTIVE_OXYGEN_SPECIES_PATHWAY
XENOBIOTIC_METABOLISM
TGF_BETA_SIGNALING
GLYCOLYSIS
ANDROGEN_RESPONSE
IL6_JAK_STAT3_SIGNALING
KRAS_SIGNALING_DN
PEROXISOME
ALLOGRAFT_REJECTION
CHOLESTEROL_HOMEOSTASIS
ANGIOGENESIS
APICAL_SURFACE
HEDGEHOG_SIGNALING
FATTY_ACID_METABOLISM
SPERMATOGENESIS
ADIPOGENESIS
MITOTIC_SPINDLE
INTERFERON_ALPHA_RESPONSE
HEME_METABOLISM
PI3K_AKT_MTOR_SIGNALING
UV_RESPONSE_UP
MTORC1_SIGNALING
OXIDATIVE_PHOSPHORYLATION
UNFOLDED_PROTEIN_RESPONSE
DNA_REPAIR
G2M_CHECKPOINT
MYC_TARGETS_V2
MYC_TARGETS_V1
E2F_TARGETS
Gene sets
-5.0
-2.5
0.0
2.5
5.0
normalized enrichment score (NES)
Gene sets correlated:
positevely
negatively

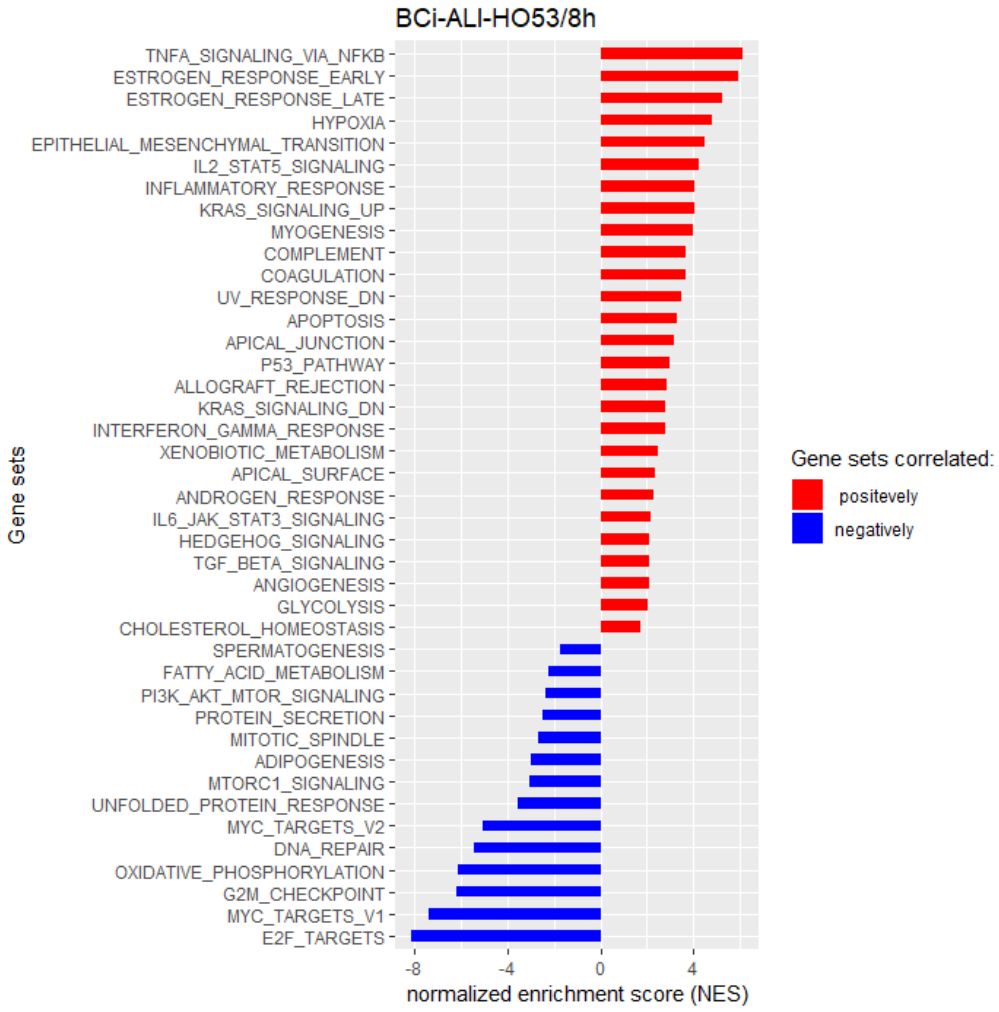
BCi-ALI-HO53/8h
TNFA_SIGNALING_VIA_NFKB
ESTROGEN_RESPONSE_EARLY
ESTROGEN_RESPONSE_LATE
HYPOXIA
EPITHELIAL_MESENCHYMAL_TRANSITION
IL2_STAT5_SIGNALING
INFLAMMATORY_RESPONSE
KRAS_SIGNALING_UP
MYOGENESIS
COMPLEMENT
COAGULATION
UV_RESPONSE_DN
APOPTOSIS
APICAL_JUNCTION
P53_PATHWAY
ALLOGRAFT_REJECTION
KRAS_SIGNALING_DN
INTERFERON_GAMMA_RESPONSE
XENOBIOTIC_METABOLISM
APICAL_SURFACE
ANDROGEN_RESPONSE
IL6_JAK_STAT3_SIGNALING
HEDGEHOG_SIGNALING
TGF_BETA_SIGNALING
ANGIOGENESIS
GLYCOLYSIS
CHOLESTEROL_HOMEOSTASIS
SPERMATOGENESIS
FATTY_ACID_METABOLISM
PI3K_AKT_MTOR_SIGNALING
PROTEIN_SECRETION
MITOTIC_SPINDLE
ADIPOGENESIS
MTORC1_SIGNALING
UNFOLDED_PROTEIN_RESPONSE
MYC_TARGETS_V2
DNA_REPAIR
OXIDATIVE_PHOSPHORYLATION
G2M_CHECKPOINT
MYC_TARGETS_V1
E2F_TARGETS
Gene sets
-8
-4
0
4
normalized enrichment score (NES)
Gene sets correlated:
positevely
negatively

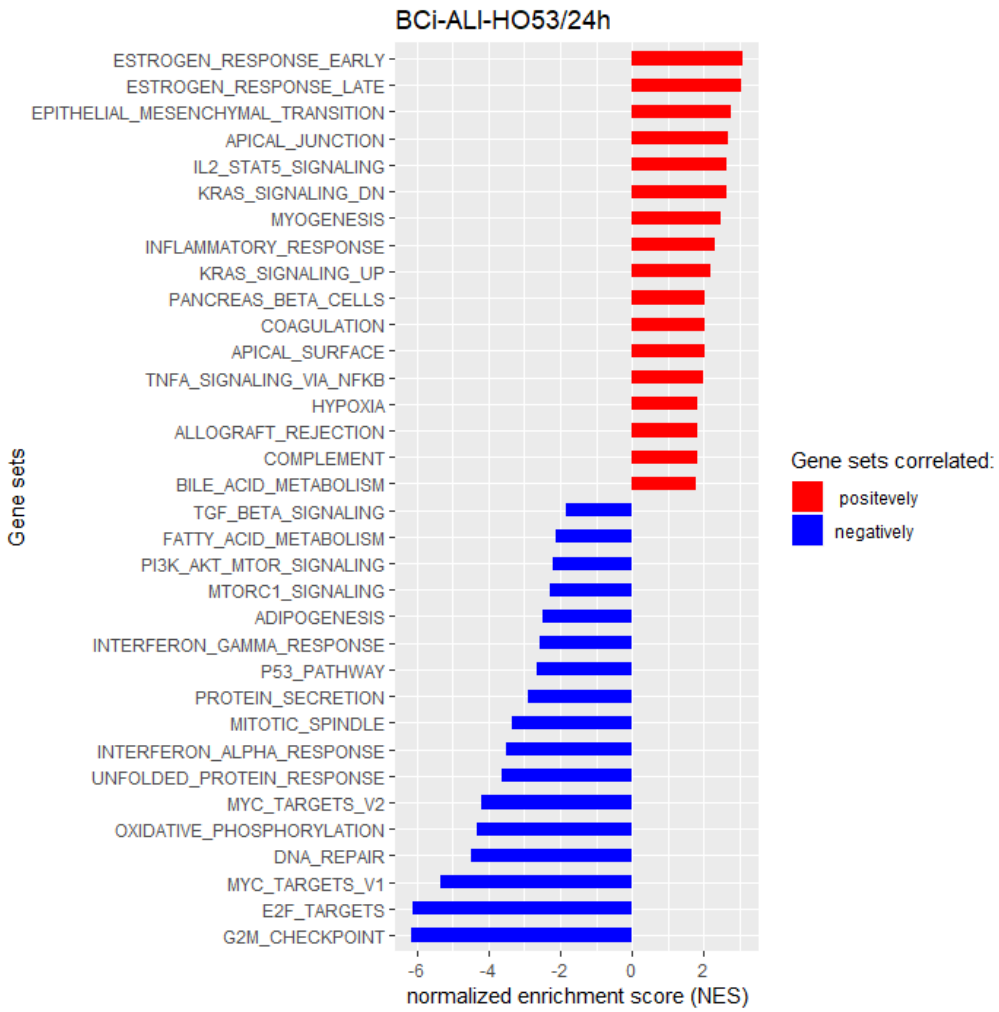


**Fig. S2. Transcriptome analysis of HO53 treated differentiated BCi cells. A)** Principal component analysis (PCA) of Kallisto/sleuth output data for triplicates from control and HO53 treated groups. PCA plots present clustering of triplicates from the control group in comparison to triplicates from HO53 treated groups for each time point 4 h (HO53/ctrl-4h-1/2/3), 8 h (HO53/ctrl-8h-1/2/3) and 24 h (HO53/ctrl-24h-1/2/3) treatment. Estimated counts were used as a unit of principal component analysis. **B)** Gene set enrichments analysis (GSEA) of the expression data from differentiated in air-liquid interphase culture BCi cells after 4 h, 8 h and 24 h of treatment with HO53. All affected gene sets by HO53 for each time point were presented as positively

correlated gene sets (red, NES > 0) and negatively correlated gene sets (blue, NES < 0) with FDR ≤ 0.05. NES – normalized enrichment score; FDR/ q-value – false discovery rate; NOM p – nominal p value.

**Supplementary Figure S3**

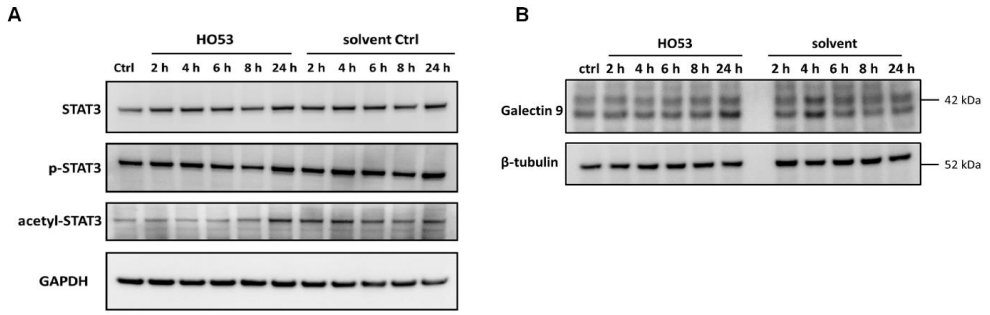


**Fig. S3. Induction of autophagy by HO53 in differentiated BCi cells is not mediated by STAT3 and galectin 9. A)** Changes in STAT3 phosphorylation (Tyr705) and STAT3 acetylation (Lys685) analysed by Western blot after 2, 4, 6, 8 and 24 h of treatment with HO53 (75 µM) and solvent control (solvent Ctrl; 0.3% final concentration of DMSO). GAPDH served as a loading control and the experiment was performed n=1. **B)** Expression level of galectin 9 at different time points of HO53 and solvent control treatment analyzed by Western blotting. β-tubulin was used as a loading control. The representative Western blot of n=3 independent experiments.

**Supplementary Figure S4**

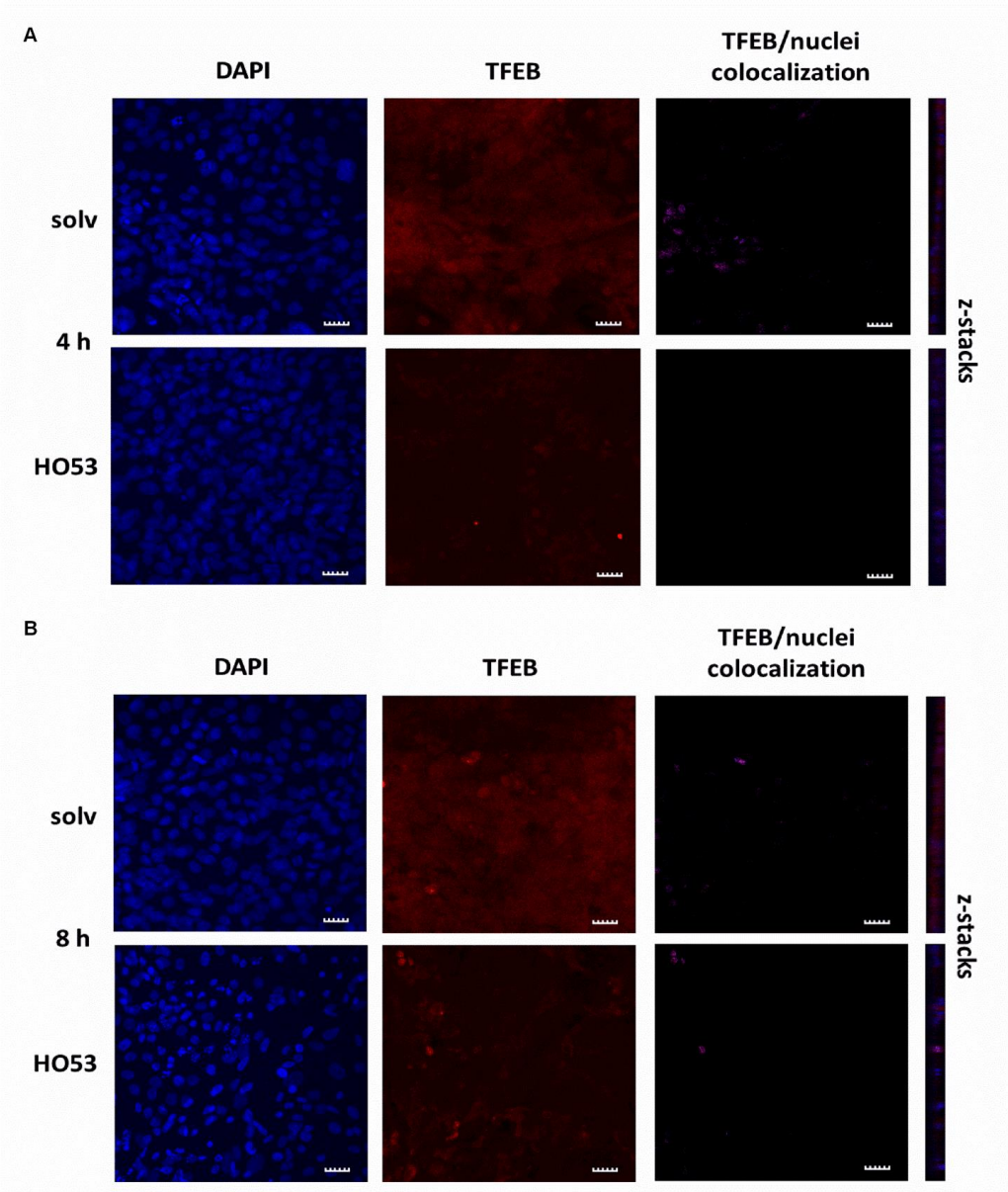


**Fig. S4. Nuclear translocation of TFEB in differentiated BCi cells upon HO53 treatment at different time points.** Analysis of TFEB nuclear translocation upon treatment with 75 µM HO53

after 4 h and 8 h by confocal imaging of nuclei (blue, DAPI), TFEB (red) and extracted signal from co-localized TFEB/nuclei (pink) from merged channels with scale bar 20 µm. The representative images from at least 3 different areas of ALI filter from n=3 independent experiments.

**Supplementary Figure S5**

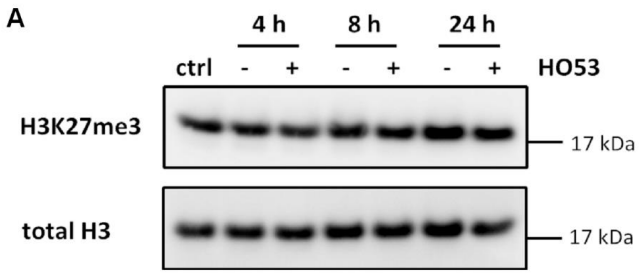


**Fig. S5. Treatment with HO53 does not affect H3K27 trimethylation level.** The representative Western blot of H3K27 trimethylation and total H3 level (loading control) analyzed by Western blotting in untreated (ctrl) and treated with solvent (-) and 75 µM HO53 (+) ALI BCi cells at indicated time points. DMSO at final concentration of 0.3% was used as a solvent control. The representative Western blot of n=3 independent experiments.

**Supplementary Table S1. List of primary antibodies used in this study**

| Antibodies | Source | Identifier |
|---|---|---|
| Rabbit acetyl-Stat3 (Lys685) | Cell Signalling Technology | #2523 |
| Mouse AMPKα (F6) | Cell Signalling Technology | #2793 |
| Rabbit GAPDH (14C10) | Cell Signalling Technology | #2118 |
| Rabbit LC3B | Cell Signalling Technology | #2775 |
| Rabbit SQSTM1/p62 (D1Q5S) | Cell Signalling Technology | #39749 |
| Rabbit phospho-AMPKα (Thr172) (D4D6D) | Cell Signalling Technology | #50081 |
| Mouse phospho-p70 S6 kinase (Thr389) (1A5) | Cell Signalling Technology | #9206 |
| Rabbit phospho-Stat3 (Tyr705) (D3A7) | Cell Signalling Technology | #9145 |
| Rabbit p70 S6 kinase (49D7) | Cell Signalling Technology | #2708 |

| | | |
|---|---|---|
| Mouse Stat3 (124H6) | Cell Signalling Technology | #9139 |
| Rabbit TFEB | Cell Signalling Technology | #4240 |
| Rabbit Galectin-9 | Cell Signalling Technology | #54330 |
| Rabbit β-Tubulin | Cell Signalling Technology | #2128 |
| Rabbit Tri-Methyl-Histone H3 (Lys27) | Cell Signalling Technology | #9733 |
| Mouse Ubiquityl-Histone H2B (Lys120) | Cell Signalling Technology | #5546 |
| Mouse Histone H3 | Cell Signalling Technology | #3638 |
| Rabbit Histone H2B | Cell Signalling Technology | #8135 |
| Mouse Occludin (OC-3F10) | Invitrogen | #33-1500 |
| Mouse Mucin 5AC | Abcam | ab3649 |
| Mouse alpha Tubulin (acetyl K40) | Abcam | ab24610 |

**Supplementary Table S2. List of primers used in this study**

| Gene | Forward Primer (5′→3′) | Reverse Primer (5′→3′) |
|---|---|---|
| ***LGALS9B/C*** | CGTCCCCTTTTCTGGGACTA | CGTGTTGCACACCACATACC |
| ***PRKAA2*** | GCTATGAAGCAGCTGGATTTTGA | GCTGAGGTGTTGAGGAACCA |
| ***MAP1LC3A*** | TGAACTGAGCTGCCTCTACC | GAGGGACAACCCTAACACG |
| ***MAP1LC3C*** | GAGGAAGTTGCTGGAATCCG | GTAAAAGGCTTCCGTGGCTC |
| ***ATG4B*** | GGACATCAACGAGGCCTAC | CAACGTAGCCGATGAAGTAGT |
| ***ATG16L1*** | GCACCAAGAGGAACTGACTGA | AAAGCTTAGTGCGCAGGTCT |
| ***ATG16L2*** | CTTCGGGACCGTACGCAA | GACCAGTGATGGGACTTGGT |
| ***USP44*** | CCTGATGGAAACTGGGCGA | CATGTTTGCACGTATCCATTGC |
| ***EHMT2*** | CTCCGACGTGTGGTTTGC | GACACAGGGAATGGGCAC |
| ***EZH2*** | TGCTTCCTACATCGTAAGTGC | TGGGGTCTTTATCCGCTCAG |
| ***TSC2*** | TTGATGACACCCCCGAGAAG | CGGACCACATGTTCAGACAC |
| ***EEF2*** | GACATCACCAAGGGTGTGCAG | GCGGTCAGCACACTGGCATA |

## Display of full-length Western blot pictures

Figure 1A

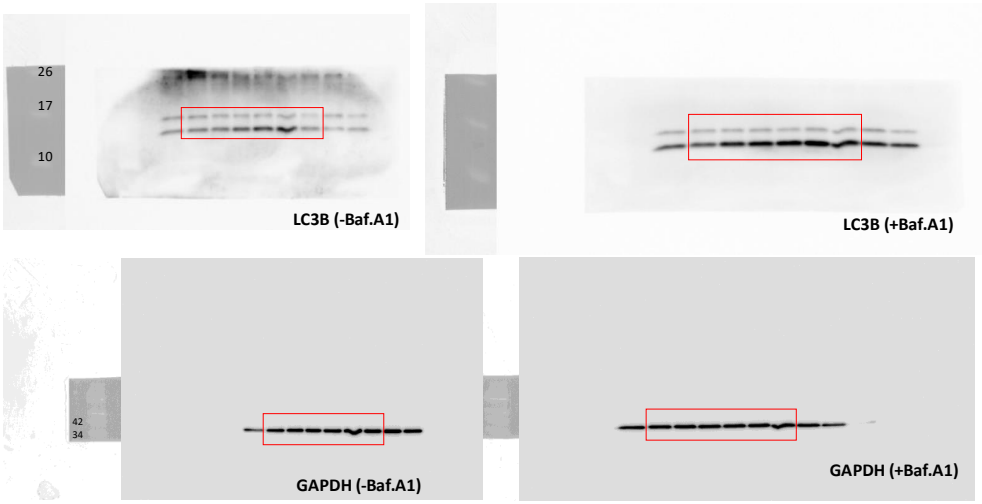


Figure 1B

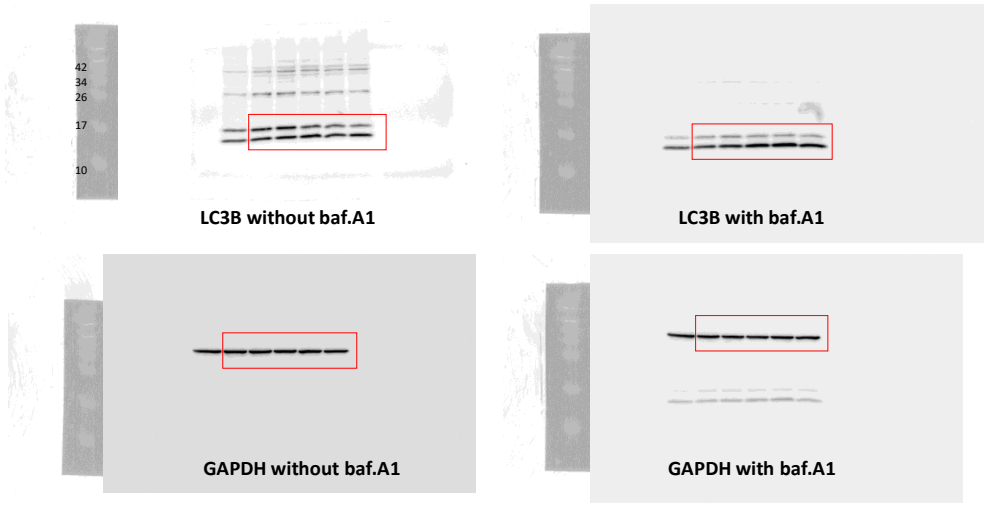

Figure S1A

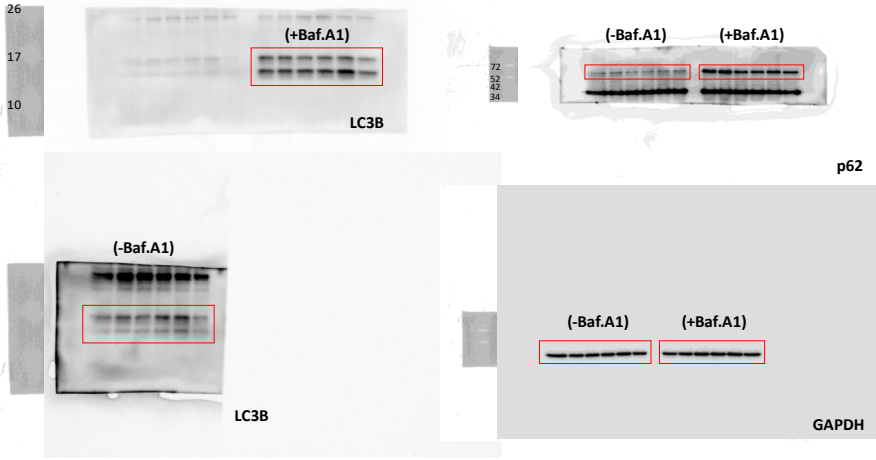


Figure S1B

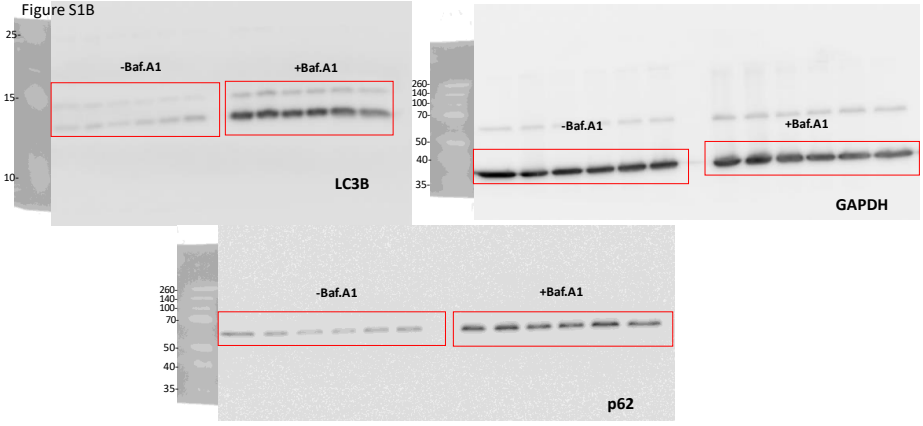

Figure S1C

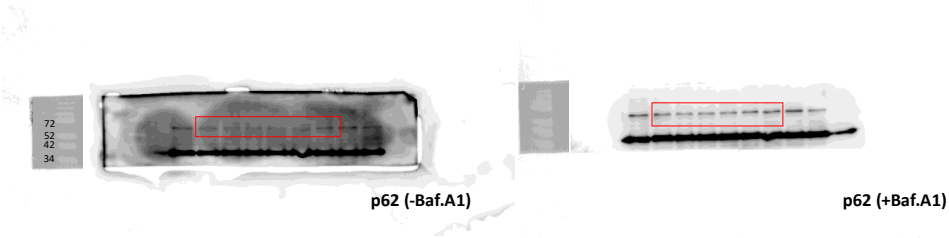


Figure S1D

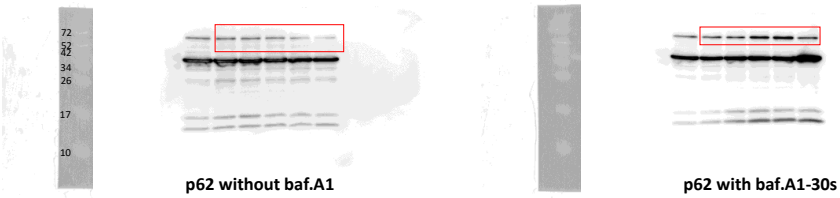

Figure 3D

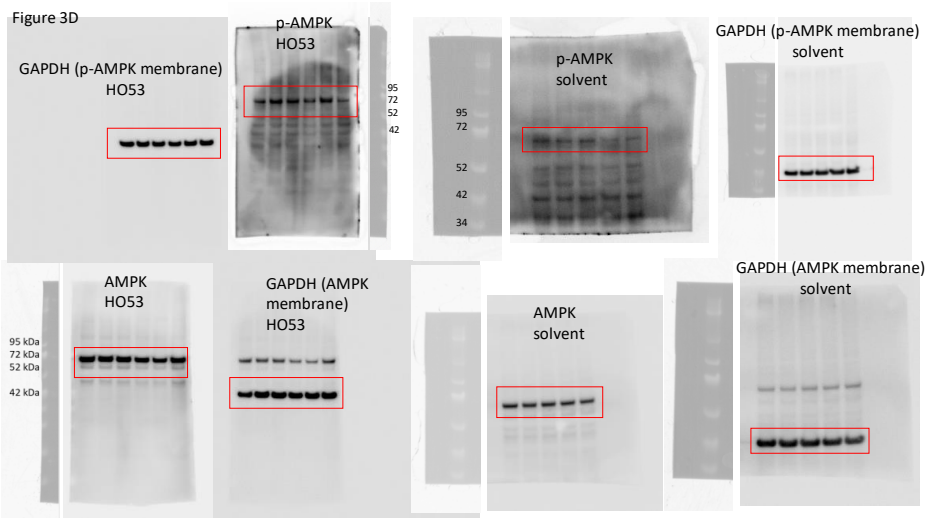


Figure 3E

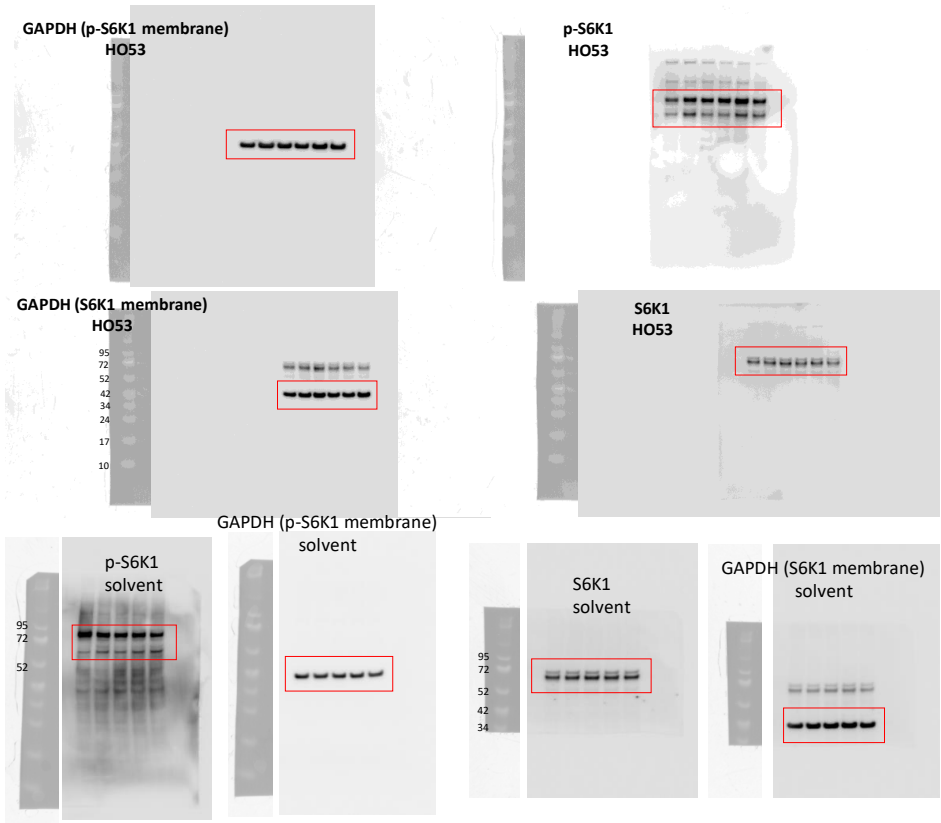

Figure S3A

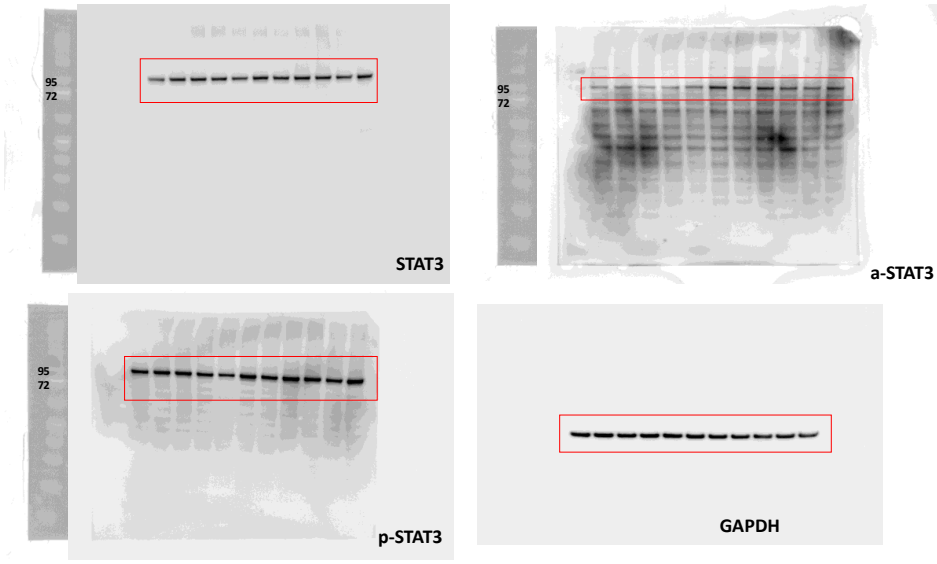


Figure S3B

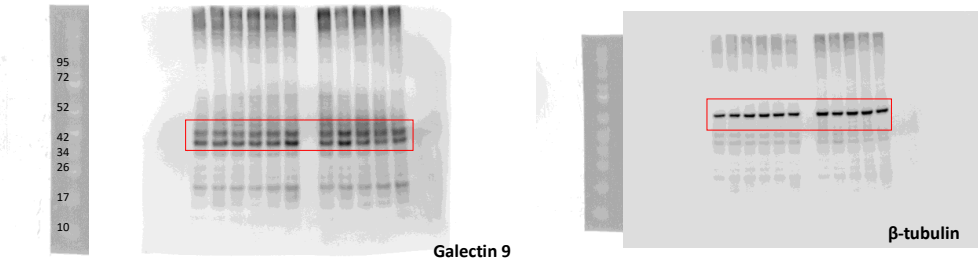

Figure 5F

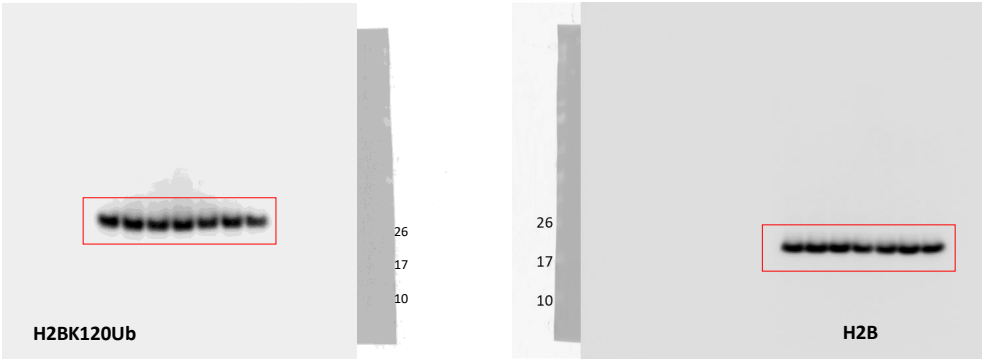


Figure S5

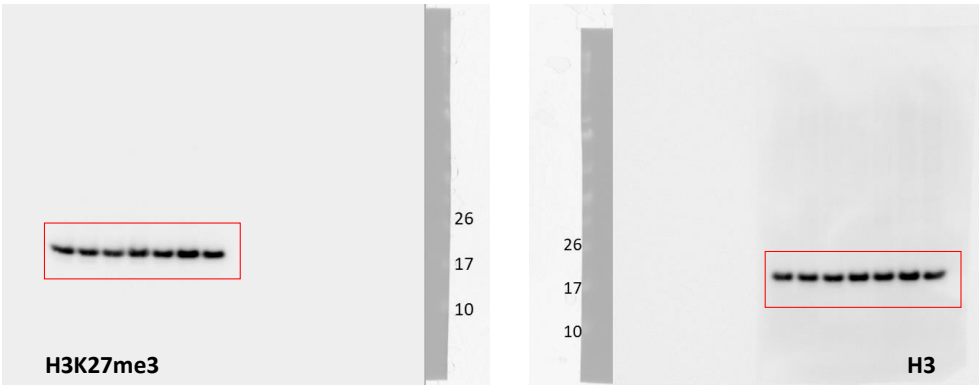

# Paper III

Research Article

# Innovative *In Vitro* Method to Study Ventilator Induced Lung Injury

*Jon P. Joelsson[1,2], Iwona T. Myszor[3], Ari J. Arason[1,2], Saevar Ingthorsson[1,2], Paulina Cherek[1], Gabriel S. Windels[1], Kristjan Leosson[5], Gudmundur H. Gudmundsson[3], Thorarinn Gudjonsson[1,2] and Sigurbergur Karason[1,4]*

[1]Stem Cell Research Unit, BioMedical Centre, School of Health Sciences, University of Iceland, Reykjavík, Iceland; [2]Department of Laboratory Hematology, Landspitali-University Hospital, Reykjavík, Iceland; [3]Life and Environmental Sciences, BioMedical Centre, University of Iceland, Reykjavík, Iceland; [4]Intensive Care Unit, Landspitali-University Hospital, Reykjavík, Iceland; [5]Innovation Centre Iceland, Reykjavík, Iceland

**Abstract**

Mechanical ventilation is a life-saving therapy for critically ill patients, alleviating the work of breathing and supporting adequate gas exchange. However, mechanical ventilation can cause ventilator induced lung injury (VILI) by baro/volu- and atelectrauma, lead to acute respiratory distress syndrome (ARDS), and substantially increase mortality. There is a need for specific biomarkers and novel research platforms for VILI/ARDS research to study these detrimental disorders and seek ways to avoid or prevent them. Previous *in vitro* studies on bronchial epithelium, cultured in air-liquid interface (ALI) conditions, have generally utilized static or constant pressure. We have developed a Cyclical Pressure ALI Device (CPAD) that enables cyclical stress on ALI cultured human bronchial cells with the aim of mimicking the effects of mechanical ventilation. Using CPAD we were able to analyze differentially expressed VILI/ARDS and innate immunity associated genes along with increased expression of associated proteins. CPAD provides an easy and accessible way to analyze functional and phenotypic changes that occur during VILI and may provide a platform for future drug testing.

## 1 Introduction

Mechanical ventilation is life-saving for patients suffering from respiratory failure. Unfortunately, mechanical ventilation can be injurious to lung tissues by mechanical stress through baro/volu- and atelectrauma and by oxidative stress through the high fraction of oxygen in inspired air, collectively called ventilator induced lung injury (VILI), which is a well-known risk of mechanical ventilation (Slutsky, 2005).

During normal inspiration, negative pressure is created inside the thorax through contraction of the diaphragm and intercostal muscles and air flows gently in. During mechanical ventilation the opposite happens: Air is pushed into the lungs with positive pressure that can have aberrant effects on the epithelium in the lungs due to mechanical distortion. The alveoli are heterogeneous in a diseased lung, some are open and others collapse at the end of expiration. During inspiration the open ones can be subjected to harm by overdistension termed volu/barotrauma, while the collapsed ones are vulnerable to shear stress through forced re-opening, termed atelectrauma. These injuries, along with oxidative stress, may lead to activation of resident immune cells in the distal lungs to secrete inflammatory mediators resulting in edema and fibrosis, collectively referred to as biotrauma (Beitler et al., 2016).

All mechanically ventilated patients are at risk for VILI, especially when it becomes challenging to ventilate the patient due to pathology in the lungs, as in acute respiratory distress syndrome (ARDS) (Carrasco Loza et al., 2015). VILI can cause, or augment substantially, damage of lung tissue in ARDS while being a necessary part of its treatment. The onset of ARDS is associated with the activation of the resident alveolar macrophages as a response to an insult or injury. The ensuing secretion of inflammatory mediators attracts neutrophils and monocytes from nearby capillaries, which secrete mediators harmful to endothelium and alveolar epithelium, causing increased permeability of the alveolar-capillary membrane, facilitating edema in the interstitium and air spaces. The following collapse of alveoli, increased dead space, worsening gas exchange and reduced lung compliance necessitate mechanical ventilation (Slutsky and Ranieri, 2013). ARDS is a common and lethal or disabling syndrome that 10% of

Received January 18, 2019; Accepted June 4, 2019;
Epub June 5, 2019; © The Authors, 2019
**ALTEX 36(4), 634-642.** doi:10.14573/altex.1901182

Correspondence: Sigurbergur Kárason, MD, PhD
Landspitali – University Hospital, Department of Anesthesiology,
Intensive Care Unit, Hringbraut 101
101 Reykjavík, Iceland
(skarason@landspitali.is)

all patients admitted to the intensive care unit (ICU) and 23% of all mechanically ventilated patients develop. The mortality of patients with severe ARDS is 46% and patients that survive are at high risk for cognitive decline, depression, post-traumatic stress disorder, and persistent skeletal muscle weakness (Thompson et al., 2017). It is therefore of high importance to explore methods to avoid or hamper the mechanisms of VILI.

It has been suggested that the lack of specific biomarkers for ARDS/VILI is one of the most important tasks facing researchers and clinicians in this field (Villar and Slutsky, 2017). However, studying VILI can be challenging as lung tissue is not readily available from VILI patients and obtaining a patient sample can be risky. As a result, there is still a limited connection between candidate genes and the susceptibility to VILI.

Most research on the pathogenesis of VILI has been performed in animal models (Hegeman et al., 2013). *In vitro* systems exploring VILI also have provided valuable information on the subject. These methods include applying static pressure on air-liquid interphase (ALI) cultured lung cells (Ressler et al., 2000; Shiomi et al., 2011) or cyclical stress on monolayered cells (Karadottir et al., 2015; Yu and Li, 2017; Zhao et al., 2014). There is also great potential in using lung-on-a-chip for VILI research, although this system has yet to see common use (Huh, 2015). Cellular adaptation to static pressure on ALI cultured cells is a concern and using cyclical stress on monolayered cells is limited to using less differentiated/polarized cells and fails to represent the more specialized cells of the distal bronchi. Using the best of these two systems would generate an *in vitro* system capable of cyclically stressing ALI cultured cells. Such a system could be a platform for finding genetic or biochemical biomarkers for ARDS/VILI. It could also be utilized for inducing VILI for the purpose of drug screening for drugs counteracting VILI and would thus have the potential of facilitating drug discovery and research.

For this purpose, we constructed a Cyclical Pressure ALI Device (CPAD), a novel *in vitro* pressure system capable of challenging ALI cultured lung cells with cyclical hyperbaric pressure. The cell lines used in this research are VA10 and BCi-NS1.1 (Halldorsson et al., 2007; Walters et al., 2013). Both cell lines project a basal cell phenotype, are derived from human lungs and have the potential of forming a pseudostratified-like epithelial layer when grown in ALI conditions. They are of bronchial origin but bronchial cells are, along with alveolar cells, subjected to mechanical strain in the distal and terminal bronchi during mechanical ventilation (Beitler et al., 2016). The A549 adenocarcinoma alveolar cell line has been used extensively in lung research, but it does not produce high TEER (i.e., does not produce tight junctions of high integrity) when grown in ALI conditions (Foster et al., 1998), which is an essential part of establishing the CPAD system.

In this study we used ARDS/VILI associated biomarkers to validate our novel pressure system. Additional markers were tested, including the mechanically sensitive CHI3L and innate immunity markers.

In patients, lung protective ventilation with lower tidal volumes (6 ml/kg), higher positive end-expiratory pressure (PEEP) and a peak inspiratory pressure below 30 cm $H_2O$ are used to limit VILI. These settings are generally adjusted according to individual patients based on bodyweight, severity of injury, lung size and other relevant factors. Two peak inspiratory pressure levels were selected for this study, i.e., 22 and 27 cm $H_2O$, to reflect a possible gradual increase of VILI with increasing mechanical strain. The frequency was set at 0.27 Hz (16 bpm). For our experiments, positive end-expiratory pressure (PEEP) was set as 5 cm $H_2O$. These pressure values create driving pressures, i.e., the difference between PEEP and the peak pressure, that are above recommended driving pressure, i.e., 14 cm $H_2O$, which is associated with increased risk of death in ventilated patients (Amato et al., 2015).

There are to our best knowledge no other mechanical models in use applying cyclical pressure on ALI cultures; therefore the CPAD may provide a novel approach to study VILI.

## 2 Materials and methods

*3D printed material*

3D printed transwell holders were printed with polylactic acid (PLA) and fitted with FKM (Fleuroelastomer) Viton 75Sha O-rings. These were sterilized before each run of the CPA by bathing them in 96% ethanol for 1 h and left to dry in a laminar flow hood. PLA was chosen as this is a known biocompatible material for *in vitro* studies (Ramot et al., 2016).

*Cell culture*

The E6/E7 viral oncogene immortalized human bronchial epithelial cell line VA10 was cultured in Bronchial/Tracheal Epithelial cell growth medium (Cell Applications, 511A-500) supplemented with retinoic acid (Cell Applications, 511-RA) and penicillin-streptomycin (20 U/ml, 20 µg/ml, respectively, Life Technologies, 15140122) at 37°C and 5% $CO_2$ (Halldorsson et al., 2007). The other cell line used was BCi-NS1.1, a human airway bronchial cell line immortalized via hTERT expression (Walters et al., 2013). Both cell lines have basal like characteristics and are able to differentiate towards polarized epithelium, generating high transepithelial electrical resistance (TEER). Cells were seeded at passage 10-15. For passaging, cells were trypsinized and spun down in PBS with 10% FBS. PBS/FBS was aspirated and the cell pellet resuspended in medium. All cell cultures were screened bi-monthly for *Mycoplasma* contamination (all negative). Oxygen fraction used in the CPAD experiments was 21%, the same as in the atmosphere. Medium was constantly monitored for color changes, indicating pH level changes, with no coloration changes observed.

In order to establish an ALI culture, VA10 or BCi-NS1.1 cells were seeded onto 12 mm diameter transwell inserts (Corning, Costar) pre-coated with collagen IV from human placenta (Sigma, C7521). Approximately $2.5\times10^5$ cells were seeded onto each transwell insert. After 2 days, medium was replaced with Dulbecco's Modified Eagle Medium F-12 Nutrient Mixture (DMEM/F12, Thermo Fisher Scientific) supplemented with penicillin/streptomycin (20 U/ml and 20 µg/ml, respectively) and 10% fetal bovine serum (FBS), (ThermoFisher Scientific). The next day (3 days after seeding), medium was replaced

with DMEMF/F12 with added penicillin/streptomycin and 2% Ultroser G (PALL Corporation). ALI was established (day 0) by aspirating media from the upper chamber. Medium was changed every other day and TEER was measured. All ALI control samples were maintained at normal air pressure.

*Reverse transcription – qPCR*

Total RNA was extracted using TRIzol reagent (Invitrogen, Thermo Fisher Scientific) according to the manufacturer's protocol. One µg of RNA was reverse-transcribed to cDNA using 1 µl random primers, 1 µl dNTP mix (Life technologies) and up to 14 µl sterile $dH_2O$. Using a PCR machine (MJ Research, Peltier Thermal Cycler, PTC-225), the sample was heated to 65°C for 5 min, put on ice for 1 min, and 4 µl 5xSSIV buffer was added along with 1 µl 0.1 MDTT and 1 µl superscript IV (SSIV) (ThermoFisher Scientific). Samples were mixed gently and placed in the PCR machine for 10 min at 23°C, 10 min at 50°C and 10 min at 80°C. One µl of cDNA (50 ng/µl), PowerUp SYBR Green Master Mix (Applied Biosystems, A25742) and 0.5 µM primers listed in Table S1[1] were used for qRT-PCR. qRT-PCR was performed using the LG 7500 Real Time PCR System (Applied Biosystems) with the following cycling conditions: (1) holding stage: 95°C for 10 min, followed by 40 cycles of (2) denatured stage: 95°C for 15 s and (3) annealed/extended stage: 60°C for 1 min. The $2(^{-\Delta\Delta CT})$ Livak method was utilized to calculate fold differences over untreated control (Livak and Schmittgen, 2001).

*Live cell imaging – proliferation assay*

Cells were incubated in the Incucyte (Incucyte ZOOM, Essen BioScience) for live cell imaging and cell proliferation assay.

*Transmission electron microscopy*

VA10 or BCi-NS1.1 cells were grown as monolayers on coverslips and under ALI conditions, and prepared for electron microscopy. Medium was removed and cells were washed with PBS. Cells were fixed with 2.5% glutaraldehyde (Ted Pella, Inc.) for 20 min. For ALI transwell filters, glutaraldehyde was as added on top of the cells and also to the bottom of the well. Fixative was removed and cells washed in phosphate buffer (0.075 M with 0.15 M sucrose) twice for 2 min. Fixed coverslips/filters were postfixed in 2% osmium tetroxide (J. B. EM Services, Inc.) for 30 min, followed by a phosphate buffer rinse twice for 3 min. Cells were dehydrated in series with ethanol: 25% ethanol for 2 min, 50% ethanol for 2 min and 70% ethanol for 2 min. Alcohol was replaced with 4% uranyl acetate in 70% ethanol (J. B. EM Services, Inc.) for 7 min, followed by 80% ethanol for 2 min, 90% ethanol for 2 min and 96% ethanol for 2 min and again for 5 min and twice for 7 min. For transwell filters, glass coverslips were placed on a plastic petri dish with a drop of resin (Spurr Resin – Ted Pella, Inc.) on top of them. Coverslips were kept in the plastic petri dish. After the last change of ethanol, the filter was removed from the well and placed on the drop of resin on the coverslip. A few drops of resin were poured on top of cells and left for 30 min. For monolayers of cells, ethanol was removed and a drop of resin was put on the coverslip and left for 30 min. A gelatin capsule was filled with resin and placed upside down on top of the coverslip to create a block. Coverslip/filters were then incubated at 70°C overnight. When capsules were separated from coverslips, ultra-thin (100 nm) sections were cut on an Ultramicrotome (Leica EM UC7) and placed on copper grids (Ted Pella, Inc.). Sections on grids were stained for 10 min with lead citrate (3% J. T. Baker Chemical Co.) and imaged using a JEM-1400PLUS PL Transmission Electron Microscope at different magnifications.

*Confocal imaging*

Immunofluorescence was captured and visualized using an Olympus FV1200 confocal microscope (Olympus, Tokyo, Japan). Cells were fixed in formalin for 20 min before staining. Antibodies used were host Ac-tubulin (Abcam) and EGFR (Abcam). Alexa Fluor phalloidin (ThermoFisher Scientific) was used to stain for filamentous actin. Counterstaining was done using DAPI (Sigma-Aldrich).

*Immunoblotting*

Cells were washed with PBS and lysed in RIPA lysis buffer supplemented with Halt Protease and Phosphatase Inhibitor Cocktails (ThermoFisher Scientific) on ice for 30 min. 15-20 µg of total protein was separated using NuPAGE 4-12% Bis-Tris gradient gel (Life Technologies, NP0323) and NuPAGE NuPAGE MES SDS Running Buffer (Life Technologies, NP0002), and the running conditions were 120 V and 275 mA. The proteins were transferred on to a PVDF membrane (0.2 µm pores) using XCell II™ Blot Module (Invirogen, EI9051) and the membrane was blocked with 10% skimmed milk or 5% BSA (Sigma) in TBS-T buffer (50 mM Tris, 150 mM NaCl, 0.1% Tween-20) for 1 h at RT. Then, the membrane was incubated with primary antibodies: mouse anti-chitinase-3-like protein 1 (YKL-40) (Millipore, MABC196); goat anti-lipocalin 2/NGAL antibody (R&D Systems, AF1757); rabbit anti-surfactant protein B (Abcam, ab40876); rabbit anti-GAPDH (Cell Signaling Technology, 2118) and rabbit anti-β-tubulin (Cell Signaling Technology, 2128) overnight at 4°C using a dilution recommended in the manufacturer's protocol. After washing with TBS-T buffer the membrane was incubated with horse radish peroxidase (HRP) conjugated secondary antibodies (Sigma, A5420 and A0545; Millipore, AP181P) diluted 1:10,000 in 5% skimmed milk or 5% BSA in TBS-T for at least 1.5 h at RT. Immunoblots were developed using Pierce ECL Plus Western blotting substrate (Thermo Scientific, #34095) or Western blotting Luminol reagent (Santa Cruz, sc-2048) and ImageQuant LAS 4000 system (GE Healthcare).

*ELISA*

Cell culture conditioned medium was analyzed by sandwich enzyme-linked immunosorbent assays (ELISAs) utilizing a human beta defensin-1 (hBD-1), interleukin 8 (*IL-8*), and *TNFα* assay kit according to the manufacturer's instructions (Peprotech, UK).

[1] doi:10.14573/altex.1901182s

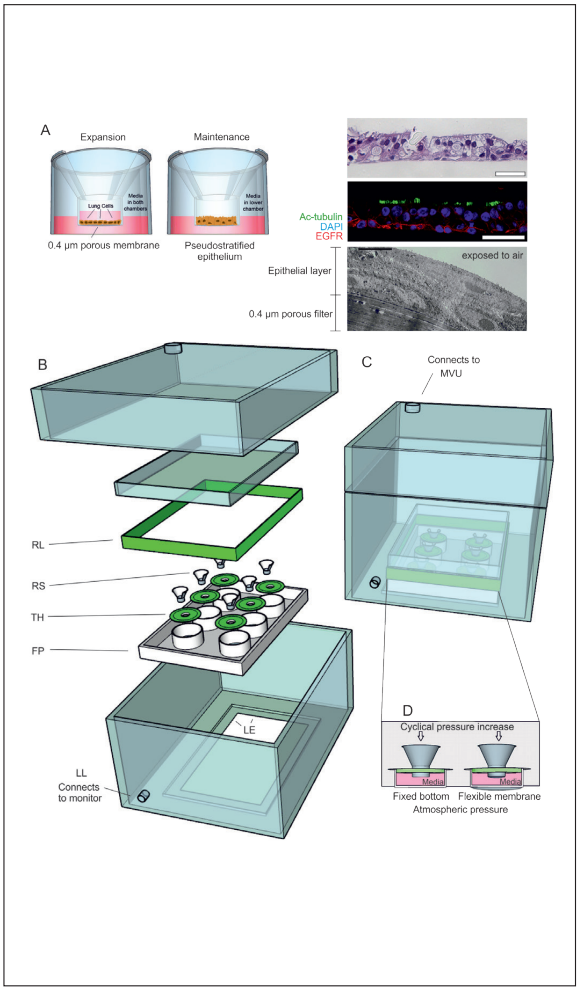


**Fig. 1: Construction of ventilator-attached cyclical pressure ALI device (CPAD)**
A, Bronchial epithelial cell lines are seeded onto transwell filters. For 2 days they are expanded with medium in the top and bottom chambers. Then the medium is removed from the top chamber and cells are subjected to ALI culture conditions for 21 days with medium being changed every other day. From top to bottom, hematoxylin and eosin staining, scale bar is 50 $\mu$m, confocal (Ac-Tubulin and EGFR, counterstained with DAPI), scale bar is 50 $\mu$m and electron microscope imaging of cross sectional 21-day ALI cultures (VA10) show the pseudostratified cell layer on top of the 0.4 $\mu$m porous filter. Electron microscope image scale bar is 5.0 $\mu$m. B, CPAD consists of a lid, which connects to a mechanical ventilation unit (MVU). The bottom part of the pressure chamber has a luer lock outlet (LL), which connects to a monitor where pressure increases can be monitored as well as cycles/sec. The bottom part of the CPAD has an opening with a lowered edge (LE), where a cell culture plate snugly fits. The plate used is a Flexcell plate (FP) with 6 wells and a flexible bottom in each well. The transwell holder is a specifically 3D printed unit that fits inside the well of the Flexcell plate. Transwell filters with differentiated lung cells are moved, under sterile conditions, into a 3D printed transwell holder (TH). The well is filled with appropriate medium. The transwell holder with inserted transwell filter is placed in a well on the Flexcell plates. As transwell filters have raised shoulders (RS), the lid of the Flexcell plate needs to be raised (RL). This is done with a 3D printed scaffold, which is inserted between plate and lid. C, The assembled CPAD is placed into an incubator and connected to a mechanical ventilator unit (MVU) and monitor (LL). D, Flexcell plates have flexible bottoms, therefore the increase in pressure inside the CPAD results in displacement of transwell filters towards the media, which in turn results in displacement of the medium and a slight displacement of the flexible membrane underneath the Flexcell plate towards atmospheric pressure (right). If the cells were placed in plates with a fixed bottom, the cells would be exposed to hydrostatic pressure change and due to the incompressibility of the cells and the medium, less physical deformation would take place (left).

*Statistical analysis*
As pressure values (22 and 27 cm $H_2O$) were compared to the same control, Student's t-test was used for statistical analysis. GraphPad Prism 7.04 was used to calculate significance. Values are given as mean ±SD.

## 3 Results

### 3.1 Construction of Cyclical Pressure ALI Device (CPAD)

To simulate cyclical stress seen *in vivo* during mechanical ventilation and to address the lack of a cyclical stress inducing system of ALI cultures, we designed an airtight chamber for culture plates that connects to a mechanical ventilator. This enables positive pressure cyclical stress of ALI cultured cells.

A two-piece chamber was designed. The bottom part has an opening at its base and an insulated groove to fit a Flexcell culture plate. The top part consists of a lid with a connector to a mechanical ventilator. Locking mechanisms on the sides of the chamber and insulation between the bottom part of the chamber and the lid ensures air-tight conditions in the chamber once the cell culture plate is inserted (Fig. 1A,B). BioFlex 6-well culture plates with flexible, silicone membranes in the bottom (Dunn Labortechnik GmbH) were used. Transwell insert holders were 3D printed to fit into the wells of the BioFlex plates. They were lined with O-rings on the outside to tightly fit into the wells and on the inside to ensure full sealing of inserts (Fig. 1B).

Cells were cultured on transwell inserts (Corning, Costar) in ALI culture conditions for 21 days to allow differentiation of the airway epithelium (Fig. 1A). Transwell ALI culture inserts were

subsequently placed in the 3D printed transwell holders and inserted into BioFlex plates containing medium. A printed 3D scaffold to raise the BioFlex plate lid was placed on the plate, which was necessary because of the height of the transwell inserts in the holders. The BioFlex plate was then placed into the groove in the base of the CPAD (Fig. 1B). The CPAD was sealed off, connected to a mechanical ventilator (Elisée™ 150, ResMed) and placed in a standard cell incubator (Fig. 1C). Internal chamber pressure was monitored with a separate sensor and monitor.

The cells were mechanically influenced by the pressure change resulting from the pressure difference between the inside of the chamber and atmospheric pressure. The flexible membranes under the wells extend downwards toward atmospheric pressure once pressure is increased inside the chamber during inspiration. The medium on top of the flexible membrane is pushed towards atmospheric pressure and so is the transwell filter (Fig. 1D, right panel). This creates increased stress on the epithelium, whereas if there was no flexible membrane (Fig. 1D, left panel), the cells would mostly experience a change in hydrostatic pressure due to the incompressibility of the cells and the medium; we hypothesized that in that case less physical deformation would take place. In our model the cells were therefore simultaneously subjected to apical pressure from above and lateral stretch on the semipermeable transwell filter.

The transwell holders were 3D printed using polylactic acid (PLA) and fitted with FKM viton O-rings in order to seal better when the transwell holder, with the fitted transwell filter, is inserted into the Flexcell plate well. Even though PLA is the most commonly used biodegradable polymer in clinical use (Da Silva et al., 2018), we performed proliferation studies to test the biocompatibility of the 3D printed components. Cells were incubated in the presence of sterilized PLA and sterilized FKM Viton O-ring, separately and combined (Fig. S1A[1]). No difference in proliferation was observed and all samples reached full confluency (Fig. S1B[1]).

### 3.2 Phenotypic alterations of airway epithelium *in vitro* subsequent to cyclical pressure

The airway epithelial cells were differentiated in ALI culture for 21 days and subsequently challenged with cyclical hyperbaric stress. Figure 2A shows a representative graph from 4 different ALI cultures with VA10 cell lines; these values are comparable to published TEER values for differentiated VA10 cell line at day 21 (Halldorsson et al., 2007). When TEER values were measured before and after cyclical hyperbaric stress, no consistent trend was observed, as TEER would increase or decrease after stressing the cells.

We observed phenotypic alterations as a result of cyclical strain as shown by confocal and electron microscope (EM) imaging (Fig. 2B,C). Actin stress fiber expression was increased and aggregates were observed indicating increased tensional stress when cultures were subjected to 27 cm $H_2O$ cyclical pressure for 24 h (Fig. 2B). Cross sectional EM images show the difference between cultures subjected to 27 cm $H_2O$ pressure for 24 h and controls, where stressed cell layers show a disrupted phenotype when compared to the more uniform control cell lay-

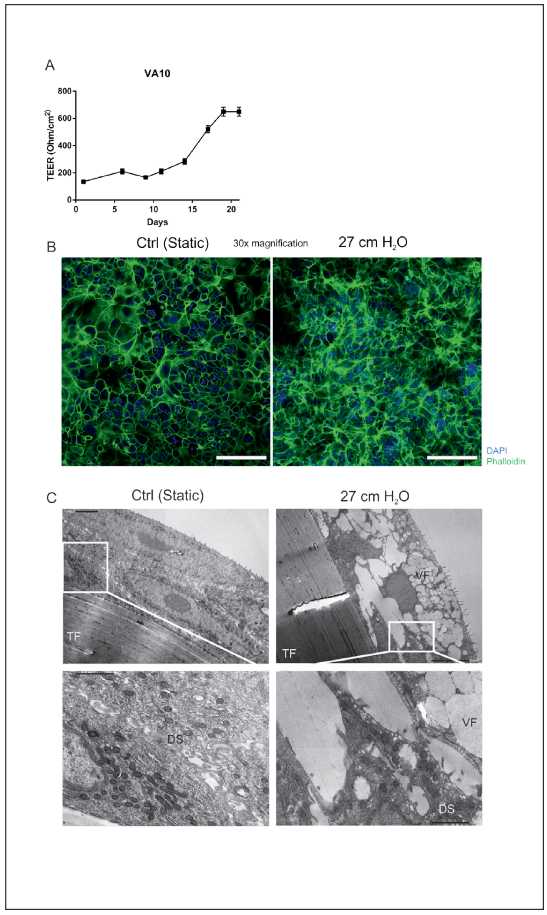


**Fig. 2: Phenotypic alterations of *in vitro* airway epithelium subsequent to cyclical pressure**

A, TEER is measured regularly during 3 weeks of differentiation. The graph represents results from four different 3-week ALI cultures (N = 4). B, Confocal microscope analyses using phalloidin staining of actin, counterstained with DAPI. Control cell layer (left, no pressure) and cells after 24 h cyclical stress with 27 cm $H_2O$ pressure (right). Images shown are representative of 3 different experiments (N = 3). Scale bar is 100 $\mu$m. C, Electron microscope analyses. The control cell layer presents differentiated lung epithelial cells with visible desmosomes and tight junctions (left). Image on right shows cell layer subsequent to 24 h cyclical stress with 27 cm $H_2O$ pressure. Images shown are representative of 3 different experiments (N = 3). Shown are desmosomes (DS), vesicle formations (VF) and transwell filter membrane (TF). The top left image scale bar is 2 $\mu$m, top right scale bar is 5 $\mu$m and lower image scale bars are 1 $\mu$m.

er (Fig. 2C). These phenotypic changes were also observed in BCi-NS1.1 derived airway epithelium (Fig. S2[1]).

In summary, mechanical stress generated by our pressure system affects cell morphology.

### 3.3 Cyclical pressure applied to airway epithelium *in vitro* induces differential mRNA expression of VILI/ARDS and innate immunity associated markers

Although ARDS or VILI do not have a definite clinically suitable biomarker that predicts their onset and clinical outcome, there are a number of biomarkers that are associated with ARDS/VILI (Blondonnet et al., 2016; Meyer and Christie, 2013). Table S2[1] summarizes biomarkers selected for this research. Using the CPAD to cyclically increase and decrease pressure over ALI cultured lung cells (VA10) for 24 hours using our aforementioned pressure values of 22 cm $H_2O$ and 27 cm $H_2O$, respectively, showed that expression of ARDS associated biomarkers was affected. Vascular endothelial growth factor A (*VEGFA*) and hypoxia-inducible factor 1-alpha (*HIF1A*) were increased in a pressure-dependent manner (Fig. 3A), However, only *VEGFA* showed a significant increase. Receptor for advanced glycation endproducts (*RAGE*) was significantly suppressed and surfactant protein B (*SFPB*) showed a significant upregulation at the 22 cm $H_2O$ pressure range and lower upregulation trend at 27 cm $H_2O$ (Fig. 3A).

Because the innate immunity components are closely associated with ARDS/VILI, we selected markers of innate immunity that might have implications in ARDS/VILI, i.e., β-defensin 2 (*HBD2*), cathelicidin antimicrobial peptide LL-37 (*CAMP*), interleukin 10 (*IL-10*), and tumor necrosis factor alpha (*TNFα*) (Fig. 3B). With the exception of *IL-10*, an induced expression was apparent for all of these markers upon cyclical stress of ALI cultured cells (Fig. 3B). Similar results were observed when using the BCi-NS1.1 cell line (Fig. S3[1]).

Our findings provide evidence that mechanical stress generated by our pressure system affects the gene expression profile of ARDS/VILI associated biomarkers and innate immunity genes.

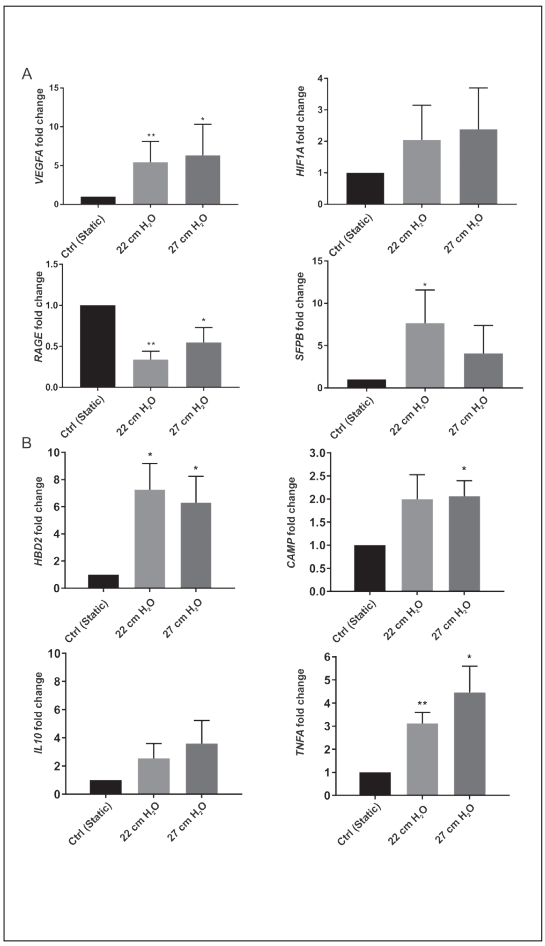


**Fig. 3: Cyclical pressure applied to *in vitro* airway epithelium shows differential expression of VILI/ARDS and innate immunity associated markers**

A, Expression of ARDS/VILI associated biomarkers *VEGFA*, *HIF1A*, *RAGE*, and *SFPB* by qRT-PCR, N = 5, P ≤ 0.05 = * and P ≤ 0.01 = **. B, Expression of innate immunity genes *HBD2*, *CAMP*, *IL10*, and *TNFα* analyzed in the novel pressure system. N = 5, P ≤ 0.05 = * and P ≤ 0.01 = **.

### 3.4 Cyclical pressure applied to ALI cultures affects expression of mechanically sensitive biomarker YKL-40 (*CHI3L*) and innate immunity markers IL-8 (*IL8*) and NGAL (*LCN2*)

Chitinase-like protein YKL-40, encoded by the *CHI3L* gene, has been shown to be upregulated in ALI cultured bronchial epithelial cells when they are mechanically stressed by 30 cm $H_2O$ static compressive stress (Park et al., 2010). Therefore, we analyzed the effect on *CHI3L* gene expression and the YKL-40 protein in our system. Cyclically stressing the cells (VA10) for 24 h at 22 and 27 cm $H_2O$, respectively, resulted in over 2-fold upregulation of *CHI3L* expression (Fig. 4A). YKL-40 expression was significantly increased (Fig. 4B; Fig. S4[1]).

Interleukin 8 (*IL-8*) is an innate immunity associated biomarker and when we tested the gene expression of *IL-8*, we saw a significant upregulation at both pressure values (Fig. 4C). However, changes at the protein level of IL-8 measured by ELISA were not significant (Fig. 4D). We also analyzed expression level of neutrophil gelatinase-associated lipocalin (*NGAL*) as it is a suggested biomarker for VILI (Xiao and Chen, 2017). We did not detect a significant alteration of NGAL (*LCN2*) expression in our model for VA10 and BCi-NS1.1 cell lines (Fig. 4E; Fig. S3[1]) although there was a tendency towards increased protein expression for VA10 cells (Fig. 4F; Fig. S5A[1]), but not for BCi-NS1.1 (Fig. S5B[1]).

In summary, using the novel pressure system on bronchial epithelial cell layers affects expression of candidate biomarkers.

## 4 Discussion

ALI culture is an *in vitro* approach used by many researchers as a way to induce and capture *in vivo*-like differentiation of airway epithelial cells towards a pseudostratified/polarized epithelial layer. In order to address responses to cyclical pressure in mature bronchial epithelium, a novel pressure chamber (CPAD) was designed. We have previously utilized the Flexcell 5000 tension system (Karadottir et al., 2015) to study cyclic stretch on monolayer (undifferentiated) cells. However, it was not possible to apply that system to study cyclical hyperbaric stress on ALI cultured cells. Ressler and coworkers (2000) used static stress to address tension caused by pressure in ALI cultured cells. The CPAD was developed to combine the two approaches. While using established components like transwell inserts and Flexcell 5000 tension system culture plates, we also designed and 3D printed components as complements (Fig. 1). Transwell filter membranes were observed to displace downward towards the media in a pressure-dependent manner. Transwell membranes were frequently seen to detach from transwell inserts when using pressure values over 30 cm $H_2O$.

Through a series of experiments we validated the CPAD as a novel platform for VILI research. VA10 and BCi-NS1.1 cell lines used in this research form polarized, differentiated epithelial layers in ALI culture (Halldorsson et al., 2007, 2010; Karadottir et al., 2015; Walters et al., 2013). We showed that the unaffected airway epithelium presented organized actin structures, (Fig. 2B, left panel), but when challenged by cyclical stress, the actin fibers showed a marked increase, disassociation and bundling, without apparent loss of cells as seen when the cell layer was counterstained with DAPI (Fig. 2B, right panel). VILI is characterized by epithelial barrier disruption (Carrasco Loza et al., 2015). By electron microscopy we confirmed that the *in vitro* airway epithelium exposed to 27 cm $H_2O$ cyclical stress shows a disrupted phenotype as compared to the static control (Fig. 2C). The affected cell layer shows a stressed phenotype with a disrupted barrier. Cells appear to separate without completely disassociating the epithelial layer. Along with this disruption, vesicle formation was observed in the stressed cell layers. This is an apparent stress response which could be linked to selective differentiation of the basal cells in the cell layer. Park and colleagues (2012) recently reported that compressive stress of bronchial cells induces tissue factor-bearing exosomes, which could be a possible explanation for the vesicle formation in our pressure system.

As a proof of principle, we wanted to test if known ARDS/VILI associated biomarkers (Blondonnet et al., 2016; Meyer and Christie, 2013) are modulated in the CPAD. As a reference gene, we used GAPDH, which is considered a relatively unaffected gene in cyclical mechanical stress (Pinhu et al., 2008). We compared B2M, UBC, and GAPDH as control genes and found GAPDH to be the most stable. Although there were consistently slightly higher CT values (difference of approx. 1.5) of GAPDH in the pressurized samples, this could not explain the differences observed in our qPCRs. This was confirmed in the YKL-40 Western blots, where β-tubulin was used as a reference protein and there was a clear increase in protein expression which was observed to be approximately the same as the gene level increase determined where GAPDH was used.

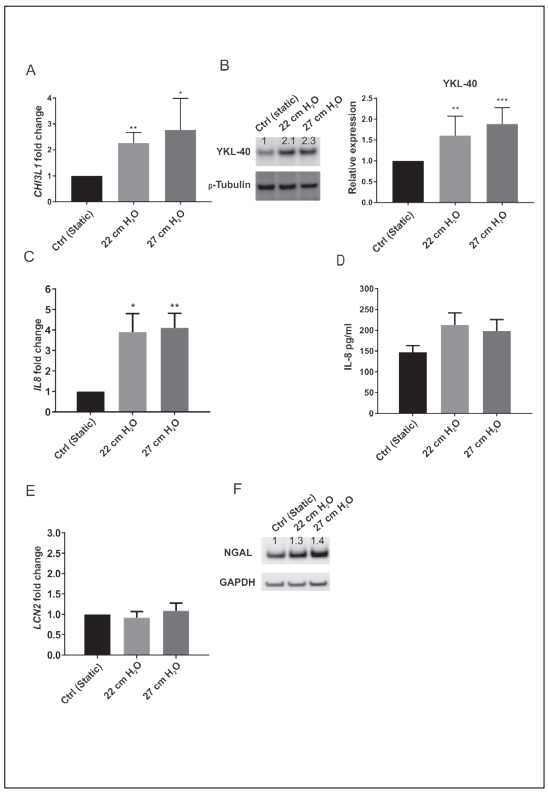


**Fig. 4: Cyclical pressure applied to ALI cultures affects expression of mechanically sensitive biomarker YKL-40 (*CHI3L*) and innate immunity markers IL-8 (*IL8*) and NGAL (*LCN2*)**

A, Expression of CHI3L analyzed by qRT-PCR at 22 cm and 27 cm $H_2O$ pressure values. N = 5, P ≤ 0.05 = * and P ≤ 0.01 = **. B, Western blot of YKL-40 at 22 cm and 27 cm $H_2O$ pressure values and quantification. N = 5, P ≤ 0.05 = *, P ≤ 0.01 = ** P ≤ 0.001 = ***. C, Expression of IL-8 at 22 cm and 27 cm $H_2O$ pressure values. N = 5, P ≤ 0.05 = * and P ≤ 0.01 = **. D, IL-8 ELISA at 22 cm and 27 cm $H_2O$ pressure values. E, Expression of LCN2 at 22 cm and 27 cm $H_2O$ pressure values. F, Western blot of NGAL at 22 cm and 27 cm $H_2O$ pressure values.

We selected *VEGFA*, *HIF1A*, *RAGE*, and *SFPB*. *VEGFA* and *HIF1A* responded in a stepwise pressure-dependent manner; the *SFPB* response was most prominent at the 22 cm $H_2O$ pressure value. This suggests that a careful selection of the pressure value is of importance and might indicate different lung responses to an individual degree of pressure insult. Furthermore, *RAGE* was significantly downregulated. *RAGE* is an ARDS associated biomarker (Jabaudon et al., 2018) and downregulation of

*RAGE* has been associated with pulmonary fibrosis (Queisser et al., 2008).

To see if selected innate immunity associated genes are affected by the cyclical stress of the CPAD, we selected initially *HBD2* and *CAMP*, both established innate immunity markers (Cederlund et al., 2011). A clear upregulation was seen in *HBD2* (Fig. 3B), an NF-κB regulated antimicrobial peptide. The cathelicidin (*CAMP*) response was not as pronounced but still significant when 27 cm $H_2O$ was applied, while the same trend was observed for the 22 cm $H_2O$ pressure value (Fig. 3B). *IL-10* and *TNFα* were also analyzed but only *TNFα* showed a significant response in a pressure-dependent manner (Fig. 3B).

Next we evaluated if YKL-40 (*CHI3L1*), a known mechanical stress biomarker (Park et al., 2010), is affected by the CPA unit. We observed a significant response (Fig. 4A), which was confirmed on protein level where cyclical stress was shown to significantly increase expression of YKL-40 (Fig. 4B). Innate immunity marker *IL-8* showed a clear upregulation in stressed cell layers on the gene expression level, however on the protein level, there was no significant difference (Fig. 4C, D). NGAL (*LCN2*) expression was not significantly altered, possibly due to pressure value selection (Fig. 4 E, F). Western blot analysis with SFPB showed no clear protein expression trend (Fig. S6[1]).

Pro-inflammatory chemokines/cytokines IL-8, TNFα and also human β-defensin 2 antimicrobial peptide are components regulated by the NF-κB pathway (Schutte and McCray, 2002; Liu et al., 2017). NF-κB induction by pressure has been shown (Lemarie et al., 2003). Interestingly, the observed expression increases in *IL-8*, *HBD2*, and *TNFα* in a pressure-dependent manner could indicate activation of the NF-κB pathway in our model.

An interesting next step for this system would be the co-culturing of macrophages and/or fibroblasts and bronchial/alveolar cell lines before introducing them to the CPAD. Kletting et al. (2018) showed that co-culturing macrophages and a newly developed alveolar type I cell line is a viable option. Another interesting venue would be to mimic normal breathing in the control cells, that is to introduce low cyclical pressure increases on the control cells.

We have constructed a pressure chamber that can cyclically stress ALI cultured cells and induce a VILI-like phenotype while expression of ARDS/VILI and other innate immunity and mechanically sensitive genes and proteins are significantly affected. This novel *in vitro* system can be a powerful tool in ARDS/VILI research and as a potential drug discovery platform. The fact that *in vitro* lung models are gaining popularity among researchers that are increasingly avoiding animal testing, and the difficulty in gaining human samples for lung research make this pressure system a very relevant tool for use in lung and drug testing research.

## References


Amato, M. B., Meade, M. O., Slutsky, A. S. et al. (2015). Driving pressure and survival in the acute respiratory distress syndrome. *N Engl J Med 372*, 747-755. doi:10.1056/NEJMsa1410639

Beitler, J. R., Malhotra, A. and Thompson, B. T. (2016). Ventilator-induced lung injury. *Clin Chest Med 37*, 633-646. doi:10.1016/j.ccm.2016.07.004

Blondonnet, R., Constantin, J. M., Sapin, V. et al. (2016). A pathophysiologic approach to biomarkers in acute respiratory distress syndrome. *Dis Markers 2016*, 3501373. doi:10.1155/2016/3501373

Carrasco Loza, R., Villamizar Rodriguez, G. and Medel Fernandez, N. (2015). Ventilator-induced lung injury (VILI) in acute respiratory distress syndrome (ARDS): Volutrauma and molecular effects. *Open Respir Med J 9*, 112-119. doi:10.2174/1874306401509010112

Cederlund, A., Gudmundsson, G. H. and Agerberth, B. (2011). Antimicrobial peptides important in innate immunity. *FEBS J 278*, 3942-3951. doi:10.1111/j.1742-4658.2011.08302.x

Da Silva, D., Kaduri, M., Poley, M. et al. (2018). Biocompatibility, biodegradation and excretion of polylactic acid (PLA) in medical implants and theranostic systems. *Chem Eng J 340*, 9-14. doi:10.1016/j.cej.2018.01.010

Foster, K. A., Oster, C. G., Mayer, M. M. et al. (1998). Characterization of the A549 cell line as a type II pulmonary epithelial cell model for drug metabolism. *Exp Cell Res 243*, 359-366. doi:10.1006/excr.1998.4172

Halldorsson, S., Asgrimsson, V., Axelsson, I. et al. (2007). Differentiation potential of a basal epithelial cell line established from human bronchial explant. *In Vitro Cell Dev Biol Anim 43*, 283-289. doi:10.1007/s11626-007-9050-4

Halldorsson, S., Gudjonsson, T., Gottfredsson, M. et al. (2010). Azithromycin maintains airway epithelial integrity during Pseudomonas aeruginosa infection. *Am J Respir Cell Mol Biol 42*, 62-68. doi:10.1165/rcmb.2008-0357OC

Hegeman, M. A., Hemmes, S. N., Kuipers, M. T. et al. (2013). The extent of ventilator-induced lung injury in mice partly depends on duration of mechanical ventilation. *Crit Care Res Pract 2013*, 435236. doi:10.1155/2013/435236

Huh, D. D. (2015). A human breathing lung-on-a-chip. *Ann Am Thorac Soc 12, Suppl 1*, S42-44. doi:10.1513/AnnalsATS.201410-442MG

Jabaudon, M., Berthelin, P., Pranal, T. et al. (2018). Receptor for advanced glycation end-products and ARDS prediction: A multicentre observational study. *Sci Rep 8*, 2603. doi:10.1038/s41598-018-20994-x

Karadottir, H., Kulkarni, N. N., Gudjonsson, T. et al. (2015). Cyclic mechanical stretch down-regulates cathelicidin antimicrobial peptide expression and activates a pro-inflammatory response in human bronchial epithelial cells. *PeerJ 3*, e1483. doi:10.7717/peerj.1483

Kletting, S., Barthold, S., Repnik, U. et al. (2018). Co-culture of human alveolar epithelial (hAELVI) and macrophage (THP-1) cell lines. *ALTEX 35*, 211-222. doi:10.14573/altex.1607191

Lemarie, C. A., Esposito, B., Tedgui, A. and Lehoux, S. (2003). Pressure-induced vascular activation of nuclear factor-κB: Role in cell survival. *Circ Res 93*, 207-212. doi:10.1161/01.RES.0000086942.13523.88

Liu, T., Zhang, L., Joo, D. and Sun, S. C. (2017). NF-κB sig-

naling in inflammation. *Signal Transduct Target Ther 2*, doi:10.1038/sigtrans.2017.23

Livak, K. J. and Schmittgen, T. D. (2001). Analysis of relative gene expression data using real-time quantitative PCR and the $2^{-\Delta\Delta C(T)}$ method. *Methods 25*, 402-408. doi:10.1006/meth.2001.1262

Meyer, N. J. and Christie, J. D. (2013). Genetic heterogeneity and risk of acute respiratory distress syndrome. *Semin Respir Crit Care Med 34*, 459-474. doi:10.1055/s-0033-1351121

Park, J. A., Drazen, J. M. and Tschumperlin, D. J. (2010). The chitinase-like protein YKL-40 is secreted by airway epithelial cells at base line and in response to compressive mechanical stress. *J Biol Chem 285*, 29817-29825. doi:10.1074/jbc.M110.103416

Park, J. A., Sharif, A. S., Tschumperlin, D. J. et al. (2012). Tissue factor-bearing exosome secretion from human mechanically stimulated bronchial epithelial cells in vitro and in vivo. *J Allergy Clin Immunol 130*, 1375-1383. doi:10.1016/j.jaci.2012.05.031

Pinhu, L., Park, J. E., Yao, W. and Griffiths, M. J. (2008). Reference gene selection for real-time polymerase chain reaction in human lung cells subjected to cyclic mechanical strain. *Respirology 13*, 990-999. doi:10.1111/j.1440-1843.2008.01396.x

Queisser, M. A., Kouri, F. M., Konigshoff, M. et al. (2008). Loss of RAGE in pulmonary fibrosis: Molecular relations to functional changes in pulmonary cell types. *Am J Respir Cell Mol Biol 39*, 337-345. doi:10.1165/rcmb.2007-0244OC

Ramot, Y., Haim-Zada, M., Domb, A. J. and Nyska, A. (2016). Biocompatibility and safety of PLA and its copolymers. *Adv Drug Deliv Rev 107*, 153-162. doi:10.1016/j.addr.2016.03.012

Ressler, B., Lee, R. T., Randell, S. H. et al. (2000). Molecular responses of rat tracheal epithelial cells to transmembrane pressure. *Am J Physiol Lung Cell Mol Physiol 278*, L1264-1272. doi:10.1152/ajplung.2000.278.6.L1264

Schutte, B. C. and McCray, P. B., Jr. (2002). β-defensins in lung host defense. *Annu Rev Physiol 64*, 709-748. doi:10.1146/annurev.physiol.64.081501.134340

Shiomi, T., Tschumperlin, D. J., Park, J. A. et al. (2011). TNF-α-converting enzyme/a disintegrin and metalloprotease-17 mediates mechanotransduction in murine tracheal epithelial cells. *Am J Respir Cell Mol Biol 45*, 376-385. doi:10.1165/rcmb.2010-0234OC

Slutsky, A. S. (2005). Ventilator-induced lung injury: From barotrauma to biotrauma. *Respir Care 50*, 646-659.

Slutsky, A. S. and Ranieri, V. M. (2013). Ventilator-induced lung injury. *N Engl J Med 369*, 2126-2136. doi:10.1056/NEJMra1208707

Thompson, B. T., Chambers, R. C. and Liu, K. D. (2017). Acute respiratory distress syndrome. *N Engl J Med 377*, 562-572. doi:10.1056/NEJMra1608077

Villar, J. and Slutsky, A. S. (2017). GOLDEN anniversary of the acute respiratory distress syndrome: Still much work to do! *Curr Opin Crit Care 23*, 4-9. doi:10.1097/MCC.0000000000000378

Walters, M. S., Gomi, K., Ashbridge, B. et al. (2013). Generation of a human airway epithelium derived basal cell line with multipotent differentiation capacity. *Respir Res 14*, 135. doi:10.1186/1465-9921-14-135

Xiao, R. and Chen, R. (2017). Neutrophil gelatinaseassociated lipocalin as a potential novel biomarker for ventilatorassociated lung injury. *Mol Med Rep 15*, 3535-3540. doi:10.3892/mmr.2017.6442

Yu, Q. and Li, M. (2017). Effects of transient receptor potential canonical 1 (TRPC1) on the mechanical stretch-induced expression of airway remodeling-associated factors in human bronchial epithelioid cells. *J Biomech 51*, 89-96. doi:10.1016/j.jbiomech.2016.12.002

Zhao, T., Liu, M., Gu, C. et al. (2014). Activation of c-Src tyrosine kinase mediated the degradation of occludin in ventilator-induced lung injury. *Respir Res 15*, 158. doi:10.1186/s12931-014-0158-2

## Conflict of interest

The authors declare no conflict of interest regarding the publication of this article.

## Acknowledgments

Technology development fund – Icelandic research council; University of Iceland, Research fund (Grant #163757); Landspitali, University Hospital, Science fund. We want to acknowledge Prof. Ronald G. Crystal and collaborators for generously providing us with the BCi-NS1.1 cell line.

*Joelsson et al.:*

# Innovative *In Vitro* Method to Study Ventilator Induced Lung Injury

## Supplementary Data

**Tab. S1: Primers used in this study**

| Gene | RefSeq number |
|---|---|
| ***CAMP*** | NM_004345.4 |
| ***HBD2*** | NM_004942.3 |
| ***LCN2*** | NM_005564.4 |
| ***CXCL8*** | NM_000584.3 |
| ***TNFα*** | NM_000594.3 |
| ***VEGFA*** | NM_001033756(18) |
| ***HIF1A*** | NM_001530(3) |
| ***SFPB*** | NM_000542(1) |
| ***RAGE*** | NM_001206966(10) |
| ***CHI3L*** | NM_001276(1) |
| ***IL-10*** | NM_000572.3 |
| ***GAPDH*** | NM_002046(1) |

**Tab. S2: Biomarkers**

| Biomarkers | Literature – relevance to VILI/ARDS or innate immunity |
|---|---|
| *VEGFA* | Abadie et al., 2005; International HapMap et al., 2010; Desai and Cardoso, 2002; Maitre et al., 2001; Medford et al., 2009; Meyer et al., 2012; Shibuya, 2013; Thickett et al., 2001; Ware et al., 2005 |
| *HIF1A* | N/A |
| *RAGE* | Jabaudon et al., 2015; Neeper et al., 1992; Shirasawa et al., 2004 |
| *SFPB* | Agrawal et al., 2012; Cheng et al., 2003; Lin et al., 2000 |
| *IL-8* | Baughman et al., 1996; Hildebrand et al., 2007; McClintock et al., 2008; Schutte et al., 1996 |
| *IL-10* | Armstrong and Millar, 1997; Fiorentino et al., 1991; Hindorff et al., 2009; Meyer et al., 2012; Parsons et al., 2005; Schroeder et al., 2008 |
| *HBD2* | Cederlund et al., 2011 |
| *TNFα* | Cross and Matthay, 2011; Dada and Sznajder, 2007; Gong et al., 2005; Park et al., 2001; Piguet et al., 1990; Postlethwaite and Seyer, 1990; Roten et al., 1991 |
| *CAMP* | Cederlund et al., 2011 |
| *YKL-40* | Park et al., 2010 |

doi:10.14573/altex.1901182s

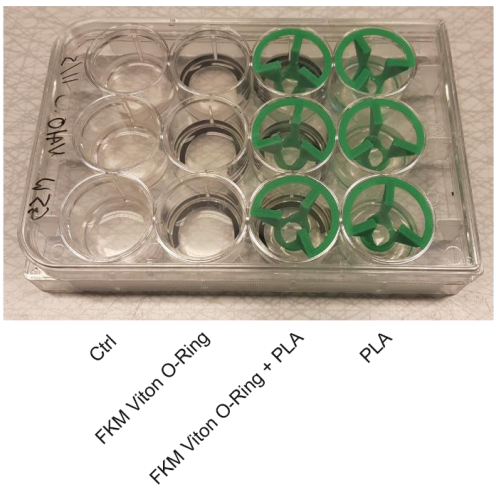


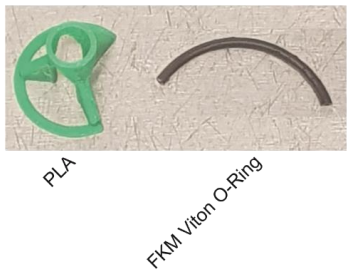


B

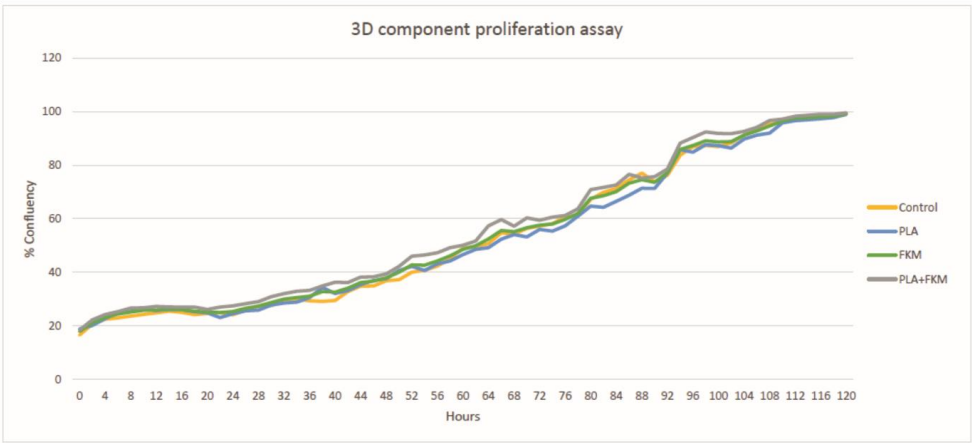


**Fig. S1: 3D printed components and O-rings used in this research (Biocompatibility assay)**
A, Polylactic acid (PLA), used for 3D printed components, along with FKM (Fleuroelastomer) Viton O-rings were tested for biocompatibility. Cells were grown in the presence of these components separately and together. B, Analyses of effects on proliferation in incucyte.

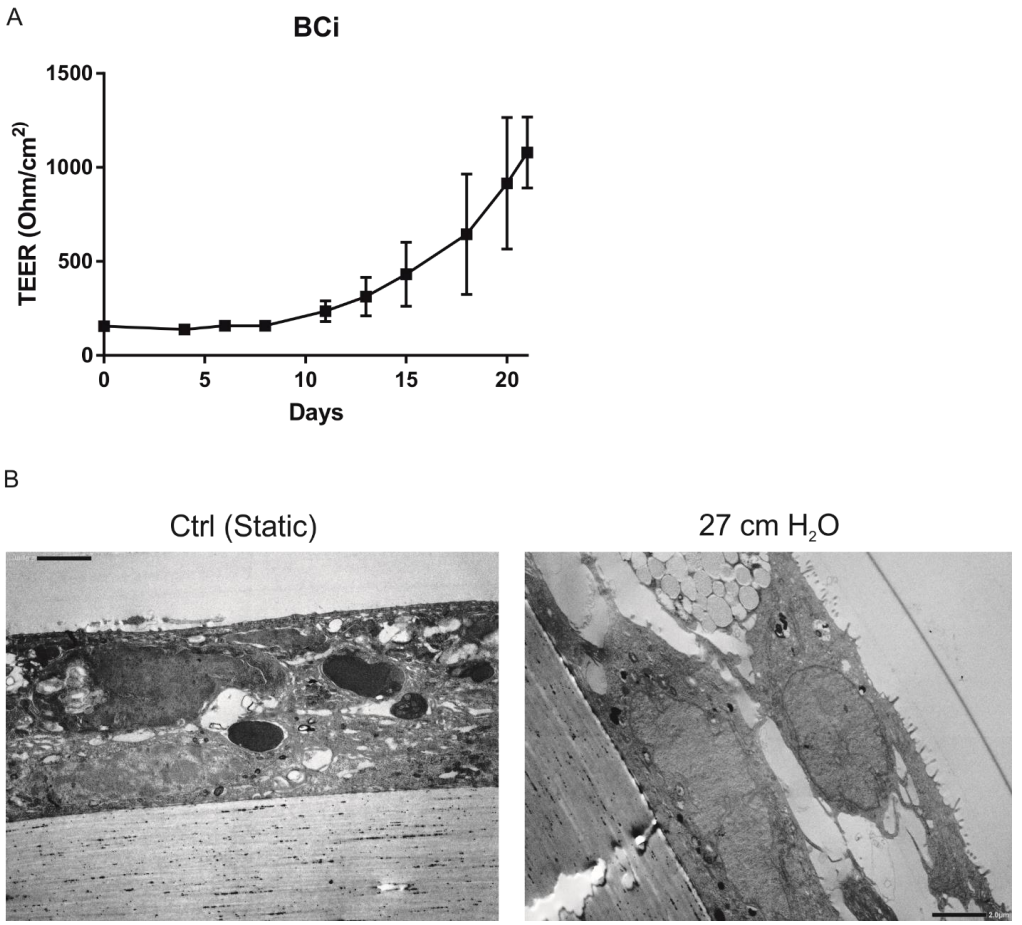


**Fig. S2: Cyclical pressure induces similar phenotypical changes in BCi-NS1.1 as seen in VA10**
A, TEER measurement of BCi ALI cultured cells. Graph represents results from four different 3-week ALI cultures (N = 4). B, Differentiated cell layer (left) and cells after cyclical stress (27 cm $H_2O$ for 24 h) (right). Scale bars are 2 µm.

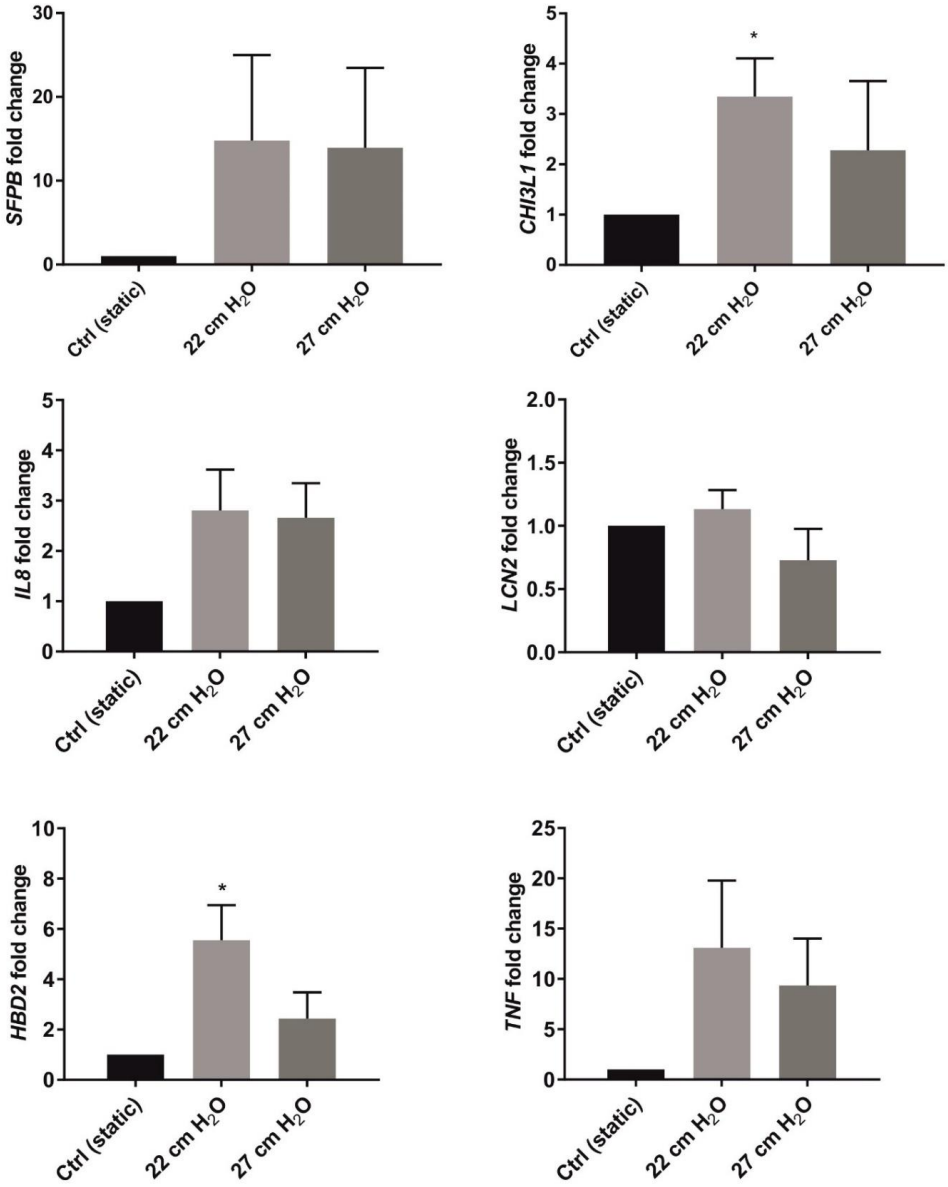


**Fig. S3: Cyclical pressure applied to *in vitro* airway epithelium shows differential expression of VILI/ARDS and innate immunity associated markers**

Expression of ARDS/VILI and innate immunity associated biomarkers *SFPB*, *CHI3L1*, *IL8*, *LCN2*, *HBD2*, *and TNFb* by qRT-PCR, N = 3, P ≤ 0.05 = *.

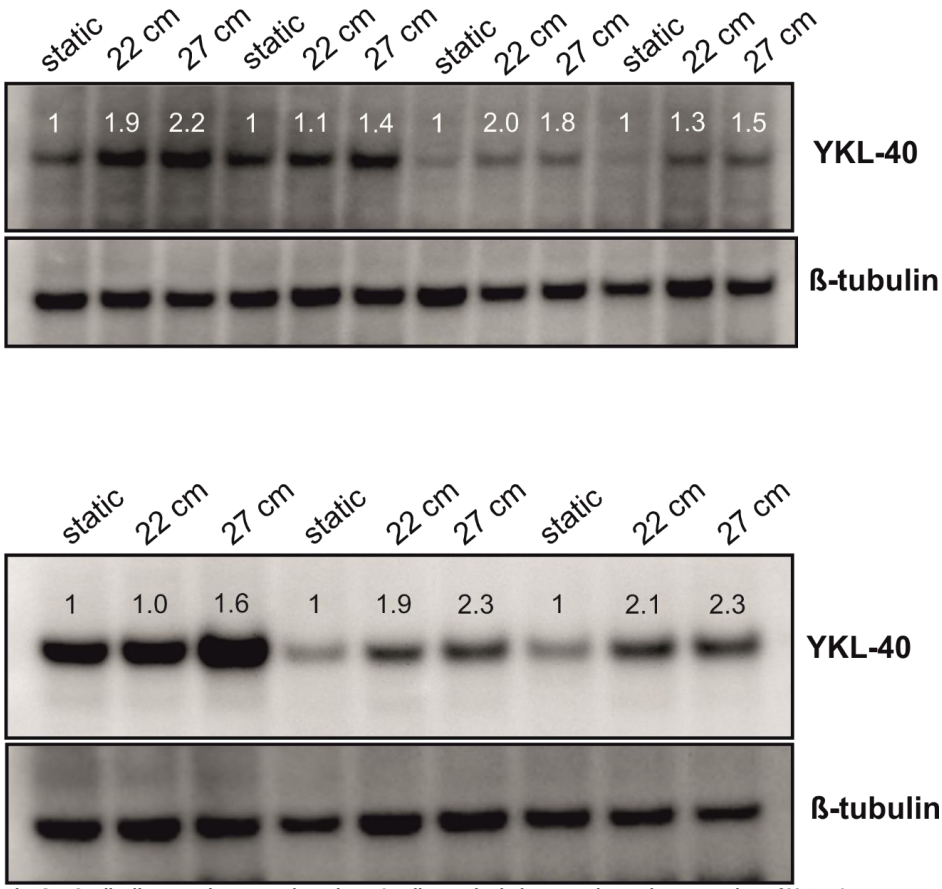


**Fig. S4: Cyclically stressing ALI cultured VA10 cells results in increased protein expression of YKL-40**
Western blots of YKL-40 from 7 experiments show an increase in protein expression when cells are cyclically stressed for 24 h in pressure chamber. Pressure values are 22 and 27 cm $H_2O$.

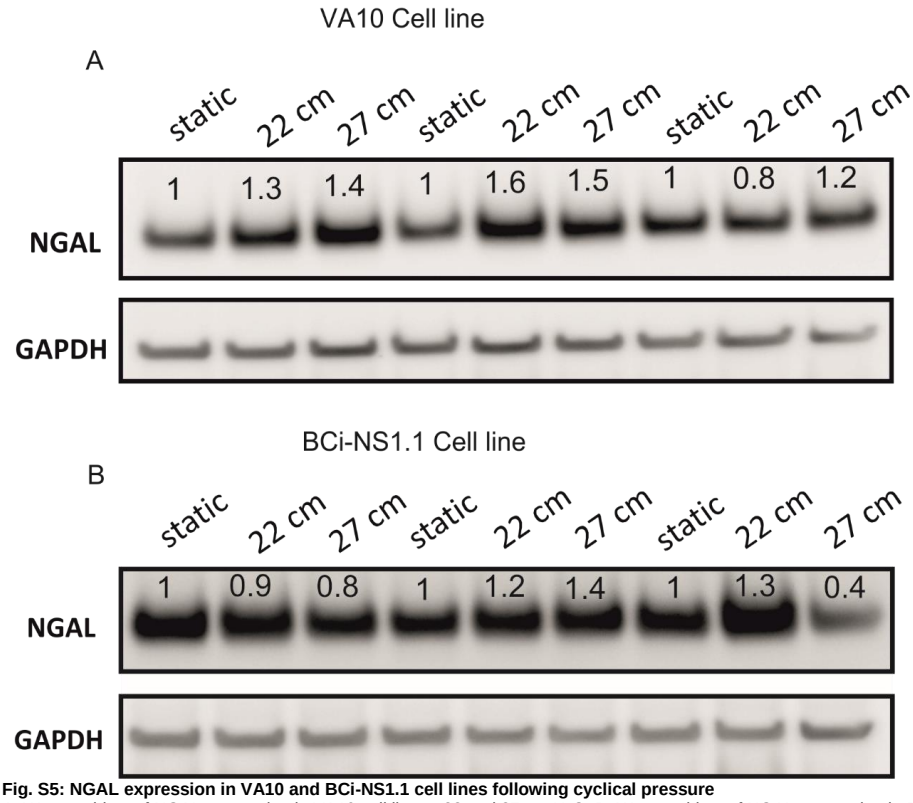


**Fig. S5: NGAL expression in VA10 and BCi-NS1.1 cell lines following cyclical pressure**
A, Western blots of NGAL expression in VA10 cell line at 22 and 27 cm $H_2O$. B, Western blots of NGAL expression in BCi cell line at 22 and 27 cm $H_2O$.

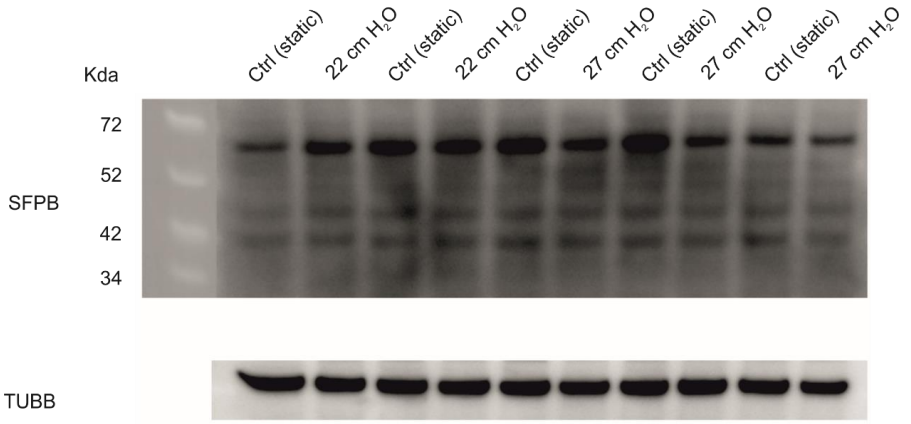


**Fig. S6: SFPB expression in VA10 cell line following cyclical hyperbaric pressure**
Western blots of SFPB expression in VA10 cell line at 22 and 27 cm $H_2O$.

**References**


Abadie, Y., Bregeon, F., Papazian, L. et al. (2005). Decreased vegf concentration in lung tissue and vascular injury during ards. *Eur Respir J 25*, 139-146. doi:10.1183/09031936.04.00065504

Agrawal, A., Zhuo, H., Brady, S. et al. (2012). Pathogenetic and predictive value of biomarkers in patients with ALI and lower severity of illness: Results from two clinical trials. *Am J Physiol Lung Cell Mol Physiol 303*, L634-639. doi:10.1152/ajplung.00195.2012

Armstrong, L. and Millar, A. B. (1997). Relative production of tumour necrosis factor alpha and interleukin 10 in adult respiratory distress syndrome. *Thorax 52*, 442-446.

Baughman, R. P., Gunther, K. L., Rashkin, M. C. et al. (1996). Changes in the inflammatory response of the lung during acute respiratory distress syndrome: Prognostic indicators. *Am J Respir Crit Care Med 154*, 76-81. doi:10.1164/ajrccm.154.1.8680703

Cederlund, A., Gudmundsson, G. H. and Agerberth, B. (2011). Antimicrobial peptides important in innate immunity. *FEBS J 278*, 3942-3951. doi:10.1111/j.1742-4658.2011.08302.x

Cheng, I. W., Ware, L. B., Greene, K. E. et al. (2003). Prognostic value of surfactant proteins A and D in patients with acute lung injury. *Crit Care Med 31*, 20-27. doi:10.1097/01.CCM.0000045028.46623.C2

Cross, L. J. and Matthay, M. A. (2011). Biomarkers in acute lung injury: Insights into the pathogenesis of acute lung injury. *Crit Care Clin 27*, 355-377. doi:10.1016/j.ccc.2010.12.005

Dada, L. A. and Sznajder, J. I. (2007). Hypoxic inhibition of alveolar fluid reabsorption. *Adv Exp Med Biol 618*, 159-168.

Desai, T. J. and Cardoso, W. V. (2002). Growth factors in lung development and disease: Friends or foe? *Respir Res 3*, 2.

Fiorentino, D. F., Zlotnik, A., Mosmann, T. R. et al. (1991). Il-10 inhibits cytokine production by activated macrophages. *J Immunol 147*, 3815-3822.

Gong, M. N., Zhou, W., Williams, P. L. et al. (2005). -308GA and TNFB polymorphisms in acute respiratory distress syndrome. *Eur Respir J 26*, 382-389. doi:10.1183/09031936.05.00000505

Hildebrand, F., Stuhrmann, M., van Griensven, M. et al. (2007). Association of IL-8-251A/T polymorphism with incidence of acute respiratory distress syndrome (ARDS) and IL-8 synthesis after multiple trauma. *Cytokine 37*, 192-199. doi:10.1016/j.cyto.2007.03.008

Hindorff, L. A., Sethupathy, P., Junkins, H. A. et al. (2009). Potential etiologic and functional implications of genome-wide association loci for human diseases and traits. *Proc Natl Acad Sci U S A 106*, 9362-9367. doi:10.1073/pnas.0903103106

International HapMap, C., Altshuler, D. M., Gibbs, R. A. et al. (2010). Integrating common and rare genetic variation in diverse human populations. *Nature 467*, 52-58. doi:10.1038/nature09298

Jabaudon, M., Futier, E., Roszyk, L. et al. (2015). Association between intraoperative ventilator settings and plasma levels of soluble receptor for advanced glycation end-products in patients without pre-existing lung injury. *Respirology 20*, 1131-1138. doi:10.1111/resp.12583

Lin, Z., Pearson, C., Chinchilli, V. et al. (2000). Polymorphisms of human SP-A, SP-B, and SP-D genes: Association of SP-B THR131Ile with ARDS. *Clin Genet 58*, 181-191.

Maitre, B., Boussat, S., Jean, D. et al. (2001). Vascular endothelial growth factor synthesis in the acute phase of experimental and clinical lung injury. *Eur Respir J 18*, 100-106.

McClintock, D., Zhuo, H., Wickersham, N. et al. (2008). Biomarkers of inflammation, coagulation and fibrinolysis predict mortality in acute lung injury. *Crit Care 12*, R41. doi:10.1186/cc6846

Medford, A. R. L., Godinho, S. I. H., Keen, L. J. et al. (2009). Relationship between vascular endothelial growth factor + 936 genotype and plasma/epithelial lining fluid vascular endothelial growth factor protein levels in patients with and at risk for ards. *Chest 136*, 457-464. doi:10.1378/chest.09-0383

Meyer, N. J., Daye, Z. J., Rushefski, M. et al. (2012). SNP-set analysis replicates acute lung injury genetic risk factors. *BMC Med Genet 13*, 52. doi:10.1186/1471-2350-13-52

Neeper, M., Schmidt, A. M., Brett, J. et al. (1992). Cloning and expression of a cell surface receptor for advanced glycosylation end products of proteins. *J Biol Chem 267*, 14998-15004.

Park, J. A., Drazen, J. M. and Tschumperlin, D. J. (2010). The chitinase-like protein YKL-40 is secreted by airway epithelial cells at base line and in response to compressive mechanical stress. *J Biol Chem 285*, 29817-29825. doi:10.1074/jbc.M110.103416

Park, W. Y., Goodman, R. B., Steinberg, K. P. et al. (2001). Cytokine balance in the lungs of patients with acute respiratory distress syndrome. *Am J Respir Crit Care Med 164*, 1896-1903. doi:10.1164/ajrccm.164.10.2104013

Parsons, P. E., Eisner, M. D., Thompson, B. T. et al. (2005). Lower tidal volume ventilation and plasma cytokine markers of inflammation in patients with acute lung injury. *Crit Care Med 33*, 1-6; discussion 230-232.

Piguet, P. F., Collart, M. A., Grau, G. E. et al. (1990). Requirement of tumour necrosis factor for development of silica-induced pulmonary fibrosis. *Nature 344*, 245-247. doi:10.1038/344245a0

Postlethwaite, A. E. and Seyer, J. M. (1990). Stimulation of fibroblast chemotaxis by human recombinant tumor necrosis factor alpha (TNF-alpha) and a synthetic tnf-alpha 31-68 peptide. *J Exp Med 172*, 1749-1756.

Roten, R., Markert, M., Feihl, F. et al. (1991). Plasma levels of tumor necrosis factor in the adult respiratory distress syndrome. *Am Rev Respir Dis 143*, 590-592. doi:10.1164/ajrccm/143.3.590
Schroeder, O., Schulte, K. M., Schroeder, J. et al. (2008). The -1082 interleukin-10 polymorphism is associated with acute respiratory failure after major trauma: A prospective cohort study. *Surgery 143*, 233-242. doi:10.1016/j.surg.2007.07.040
Schutte, H., Lohmeyer, J., Rosseau, S. et al. (1996). Bronchoalveolar and systemic cytokine profiles in patients with ards, severe pneumonia and cardiogenic pulmonary oedema. *Eur Respir J 9*, 1858-1867.
Shibuya, M. (2013). Vascular endothelial growth factor and its receptor system: Physiological functions in angiogenesis and pathological roles in various diseases. *J Biochem 153*, 13-19. doi:10.1093/jb/mvs136
Shirasawa, M., Fujiwara, N., Hirabayashi, S. et al. (2004). Receptor for advanced glycation end-products is a marker of type I lung alveolar cells. *Genes Cells 9*, 165-174.
Thickett, D. R., Armstrong, L., Christie, S. J. et al. (2001). Vascular endothelial growth factor may contribute to increased vascular permeability in acute respiratory distress syndrome. *Am J Respir Crit Care Med 164*, 1601-1605. doi:10.1164/ajrccm.164.9.2011071
Ware, L. B., Kaner, R. J., Crystal, R. G. et al. (2005). VEGF levels in the alveolar compartment do not distinguish between ARDS and hydrostatic pulmonary oedema. *Eur Respir J 26*, 101-105. doi:10.1183/09031936.05.00106604